

**QUANTIFYING THE ROLE OF
MICROPHYTOBENTHOS IN TEMPERATE
INTERTIDAL ECOSYSTEMS USING OPTICAL
REMOTE SENSING**

Tisja Daggers

This dissertation has been approved by:

Supervisors

prof. dr. D. van der Wal

prof. dr. P.M.J. Herman

Cover design: Job Duim and Tisja Daggars (painting)

Printed by: ITC Printing Department

Lay-out: Tisja Daggars

ISBN: 978-90-365-5124-3

DOI: 10.3990/1.9789036551243

This research was carried out at NIOZ Royal Netherlands Institute for Sea Research and financially supported by the ‘User Support Programme Space Research’ of the Netherlands Organisation for Scientific Research.

© 2021 Tisja Dorine Daggars/ NIOZ, The Netherlands. All rights reserved. No parts of this thesis may be reproduced, stored in a retrieval system or transmitted in any form or by any means without permission of the author. Alle rechten voorbehouden. Niets uit deze uitgave mag worden vermenigvuldigd, in enige vorm of op enige wijze, zonder voorafgaande schriftelijke toestemming van de auteur.

**QUANTIFYING THE ROLE OF
MICROPHYTOBENTHOS IN TEMPERATE
INTERTIDAL ECOSYSTEMS USING OPTICAL
REMOTE SENSING**

DISSERTATION

to obtain
the degree of doctor at the Universiteit Twente,
on the authority of the rector magnificus,
prof. dr. ir. A. Veldkamp,
on account of the decision of the Doctorate Board
to be publicly defended
on Thursday 25 February 2021 at 14.45 hours

by

Tisja Dorine Daggers

born on the 13th of June, 1990
in Leersum, The Netherlands

Graduation Committee:

Chair / secretary:

prof.dr. F.D. van der Meer

Supervisors:

prof.dr. D. van der Wal

prof.dr. P.M.J. Herman

Committee Members:

prof. dr. ir. A. Stein

dr. ir. C.M.M. Mannaerts

prof. dr. ir. C.J.M. Philippart

prof. dr. K. Sabbe

dr. V. Meleder-Tard

Acknowledgements

Many people have contributed to the completion of this PhD. To them I would like to express my sincere gratitude.

I would like to thank my promoter prof. dr. Daphne van der Wal for her advice and encouragement. Even though she had a busy schedule, there was always time for constructive discussions. With patience she gave detailed feedback on a large number of manuscripts. I have learnt a great deal from Daphne on all aspects of setting up and conducting scientific research.

I would like to thank my co-promotor prof. dr. Peter Herman for his useful feedback on several research set-ups, data analyses and manuscripts, even after he changed jobs.

My gratitude also goes to dr. Jacco Kromkamp, advisor in this project, for the pleasant cooperation on Chapter 2, considering the measurement of primary production rates of microphytobenthos. This was the first project I performed and I learnt from Jacco how to deal with knowledge gaps and uncertainties in field and lab measurements.

I also would like to thank prof. dr. Tjeerd Bouma, advisor in this project, for providing me the opportunity to join a large field campaign, in which we performed defaunation experiments on several locations (Chapter 4). By combining forces, it was possible to carry out a diverse range of measurements for several Phd and postdoc projects, of which Chapter 4 is one. I would like to thank Tjeerd for his useful feedback on this manuscript.

My gratitude also goes to the people of NIOZ-Yerseke. It has been a pleasure to work and study here, and being surrounded by so many inspiring people was invaluable. There are too many people to thank individually, but everyone has in a way contributed to the completion of this work. I would like to especially thank Annette Wielemaker for her contribution to the processing of satellite imagery and valuable discussions on image analyses. Many thanks to Brenda Walles, Dick van Oevelen, Eric Boschker, Laura Soissons, Lodewijk de Vet, Sven Ihnken, Tom Ysebaert, Bas Oteman and Jim van Belzen for valuable discussions and their contributions to papers. I would like to thank Lennart van IJzerloo, Jeroen van Dalen and Daniel Blok for their contributions to several field campaigns. I would also like to acknowledge Anke Engelberts, Angela Dekker, Frank Brouwer and Daniel Blok for their help with the identification of macrofauna and Anke for her help with the identification of macroalgae species. Many thanks to Jan Sinke and Joeri

Minderhoud for chlorophyll-*a* analyses and Jetta Vlaming for performance of the ^{14}C incubations.

Many fellow scientists and students were invaluable by providing field assistance, including Joost Hamoen, Joeri Minderhoud, Roeland van de Vijzel and Clara Cardoso.

Also many thanks in particular to all the young scientists I have met during my stay in Yerseke, for all the stimulating discussions we had and who made living in The Keete very pleasant.

I would never have completed this PhD without the support and encouragement of my friends and family. Many thanks to my friends from school, university and the rowing club for distracting me from science and sharing many happy moments. Special thanks to Jantien and Marjolein, with whom I could share PhD struggles. I would also like to express my gratitude to my parents and sister, for always having faith in me. And lastly, I would like to express my deepest gratitude to Lars for his support and patience during the final stage of the PhD.

Table of Contents

Acknowledgements	i
Chapter 1 Introduction	1
Chapter 2 A model to assess microphytobenthic primary production in tidal systems using satellite remote sensing	13
Chapter 3 Spatial variability in macrofaunal diet composition and grazing pressure on microphytobenthos in intertidal areas	53
Chapter 4 The influence of macrofauna on biomass and spatial heterogeneity of intertidal microphytobenthos under varying hydrodynamic conditions: an experimental approach	81
Chapter 5 Seasonal and spatial variability in patchiness of microphytobenthos on intertidal flats from Sentinel-2 satellite imagery	113
Chapter 6 Synthesis	137
Supplementary information	147
Bibliography	179
Summary	191
Samenvatting	195
Curriculum Vitae	199

Chapter 1 Introduction

1.1 Estuaries and tidal flats

Estuaries are semi-enclosed coastal water bodies, which are connected to the open sea. Estuaries contain sea water that is measurably diluted with fresh water originating from land drainage (Pritchard, 1967). In most cases, estuaries are situated where rivers flow into the open sea. Estuaries are common in low relief coastal regions such as the east coast of North America, Asia and Europe and are much less common along elevated coastlines, such as the Pacific edge of North and South America (Day, 1990; Murray et al., 2019). Estuaries are often narrow upstream and become wider towards the mouth (Day, 1990). Sediment enters estuaries via rivers and marine sources and may accrete forming tidal flats (Figure 1), depending on local environmental conditions such as tides, waves and fluvial processes (Dalrymple, 1992). Tidal flats are characterized by being submerged by water during high tide and being emerged during low tide. An analysis of over 700,000 satellite images demonstrated that the total surface area of tidal flats (sand, rock and mud flats) worldwide is at least 127,921 km² (Murray et al., 2019).

For a long time, estuaries have been important to mankind as harbors, fishing grounds and locations for towns and cities. Estuaries are highly productive ecosystems and are among the most economically valuable ecosystems worldwide (Costanza et al., 1997; Heip et al., 1995; Schelske and Odum, 1962). However, nowadays, estuaries are heavily exploited and among the most threatened ecosystems globally, mainly due to industrial activities such as dredging for ship navigation and extraction of sand resources (Simonini et al., 2007; Borja et al., 2010) and agricultural activities (Galbraith et al., 2002; Lotze et al., 2006; Worm et al., 2006). As a result, >90% of the species originally living in estuaries have been lost (Lotze et al., 2006). Estuarine intertidal zones are also an important focus of concern with respect to the potential impacts of climate change (Harley et al., 2006). The observed and projected climate trends include changes in air and sea temperature, sea level, tidal range, river discharge and turbidity, wind fields and storm frequency and intensity (Bates et al., 2008). The total area of tidal flats has declined by approximately 16% over the period 1984-2016 (Murray et al., 2019). The combined effects of degradation due to coastal development, reduced sediment input from rivers, increased coastal erosion and sea level rise are expected to lead to a continued decline of tidal flat ecosystems worldwide (Murray et al., 2019).



Figure 1. The Oosterschelde and Westerschelde estuary, The Netherlands, containing emerged tidal flats. Source image: Copernicus Sentinel-2 MSI, 12 March 2016.

1.2 Abiotic gradients on tidal flats

Tidal flats form a highly variable habitat due to the presence of tides, waves and seasonal as well as short-term weather variations. The tides lead to constantly varying water depths, which results in strong environmental gradients in the cross-shore direction (Le Hir et al., 2000). A cross-shore gradient that affects biota includes for example emersion duration, with higher areas being exposed to air and solar irradiation longer than low lying areas. The exposure to air may lead to increased sediment surface temperatures, depending on weather conditions, time of day and the total emersion duration. In summer, intertidal sediment temperatures can easily increase up to 10–15°C during an emersion period (Blanchard et al., 1997; Vieira et al., 2013). The increased temperatures may benefit growth of photosynthetic organisms such as algae and saltmarsh plants on tidal flats (Vieira et al., 2013), but may on the other hand also lead to thermal stress on biota (Bertness and Leonard, 1997; Vogt et al., 2014). Depending on water turbidity, light availability on intertidal sediments may be limited (Colijn, 1982) and the photosynthetic period on intertidal sediments may be closely linked to emersion duration. In

addition, drainage of porewater will occur for a longer period in high intertidal areas compared to low intertidal areas, possibly leading to desiccation stress on biota (Thompson et al., 2004). Maximum current velocities generally decrease with increasing intertidal elevation (Le Hir et al., 2000), which may lead to a fining of sediment along this hydrodynamic energy gradient (Bartholoma and Flemming, 2007).

Environmental gradients are also present in the long-shore direction. For example, the tidal amplitude may increase or decrease with distance to the mouth, depending on the specific morphology of the estuary (Moreira et al., 1993). Furthermore, the salinity varies spatially depending on the position along the estuarine gradient, and temporally depending on the amount of freshwater runoff (Herman et al., 2001). Waves are present in estuaries due to the propagation of offshore waves or can be locally wind-induced. Waves may contribute to resuspension of sediments, whereby the contribution of offshore waves generally decreases with distance to the mouth (Le Hir et al., 2000). These abiotic conditions all regulate the spatial distribution of biota (Ysebaert et al., 2003; Van der Wal et al., 2017).

1.3 *The function of microphytobenthos in intertidal ecosystems*

In mesotidal and macrotidal estuaries, where wide intertidal flats are present, benthic microalgae or microphytobenthos (hereafter referred to as MPB) are the main primary producers (McLusky, 1989; Underwood and Kromkamp, 1999). MPB are at the base of the intertidal food web that consists of microbial life forms, microbenthos, meiobenthos and benthic macrofauna (Heip et al., 1995). MPB provides food to an important part of the macrofaunal community, which is consumed by epibenthic crustaceans, birds and fish (Heip et al., 1995; Herman et al., 1999). Therefore, MPB are an essential part of the estuarine and coastal food web (Graf, 1992; Herman et al., 1999; Levinton and Bianchi, 1981; Thrush et al., 2012) and form an important link in carbon cycling in intertidal areas (Gattuso et al., 2006).



Figure 2. Intertidal sediments containing MPB in the Oosterschelde (left) and Westerschelde (right), The Netherlands. Photos taken by Tisja Daggars.

Benthic microalgal communities mainly consist of benthic diatoms (Meleder et al., 2007; Pomeroy, 1959; Underwood and Kromkamp, 1999). Green algae (chlorophytes), dinoflagellates and blue-green algae (cyanobacteria) are also common, but usually occur in small quantities in temperate climates (Pinckney and Zingmark, 1993; Whitney and Darley, 1983). Benthic diatoms produce extracellular polymeric substances (EPS) that glue sediment particles together and form a 'biofilm' (Figure 2), that may reduce sediment erosion and increase sediment deposition (Yallop et al., 1994). In this way, MPB function as ecosystem engineer by physically altering their environment (Van De Koppel et al., 2001). The biofilm facilitates settlement of other biota, such as larvae of the Baltic tellin (Van Colen et al., 2009). Muddy sediments are mainly dominated by epipelagic taxa, which are able to migrate within the sediment, whereas intertidal sands mainly contain epipsammic, immotile diatom species (Palmer and Round, 1967; Underwood and Kromkamp, 1999). The epipelagic diatoms migrate to the sediment surface at low tide (Paterson et al., 1998) and migrate downwards before immersion (Perkins et al., 2011). In this way, the diatoms actively ensure that light availability is optimal for photosynthesis and that overexposure to light is avoided (Admiraal et al., 1984; Cartaxana et al., 2016; Blommaert et al., 2018). Benthic diatom migration is only observed during daytime low tides (Serodio et al., 1997). Several studies demonstrated that MPB growth is likely limited by CO₂ availability (Admiraal et al., 1984; Cook and Roy, 2006; Oakes and Eyre, 2014). Due to the position of MPB in the sediment, transport of CO₂ to the algal cells is limited by diffusion across the sediment pore water (Jorgensen, 2001). Nutrient availability is generally not considered a limiting factor to growth rates of natural MPB communities in estuaries (Admiraal et al., 1984; Barranguet et al., 1998; Kromkamp et al., 1998; Blackford, 2002). Seasonal variability in MPB biomass has been associated with environmental factors, including light availability, temperature and wind velocity (Figure 3) (Ubertini et al., 2012) and references therein). As macrofauna constitute a major food source for e.g. migratory birds, considerable efforts have been focused on the prediction of macrofaunal

distributions (Ysebaert et al., 2002; Ellis et al., 2006; van der Wal et al., 2008) in order to sustainably manage these ecosystems. The availability of the food sources for benthic macrofauna, such as MPB, is typically not taken into account to predict the distribution of benthic macrofauna (van der Wal et al., 2008). Little is known about the quantity of the consumption of MPB. Laboratory experiments have been performed to quantify grazing by a single species on MPB, but to what extent these results can be transferred to macrofaunal communities is largely unknown (Savelli et al., 2018). Most existing models that predict macrofaunal species occurrence, abundance or biomass use habitat characteristics, such as sediment grain-size and elevation as explanatory variables (Thrush et al., 2003; Thrush et al., 2005; Ellis et al., 2006; van der Wal et al., 2008; Cozzoli et al., 2013). There is a need for consistent data on food availability for macrofauna (Van der Wal et al., 2008; Olsen et al., 2011; Kanaya et al., 2013; Christianen et al., 2017). In particular, large-scale spatiotemporal information on MPB biomass or primary production would be required as an important explaining variable (Herman et al., 2000; Van der Wal et al., 2008).

1.4 Characterization of spatial variability in MPB biomass

For numerous ecosystems, an effect of predator-prey interactions on spatial patterning of ecological communities has been demonstrated (Andrew, 1993; Edwards et al., 1996; Maron and Harrison, 1997). Furthermore, spatial variability of species can be regulated by various other mechanisms, including zonation in environmental factors (Levine et al., 1998; Silvertown, 2004), intra- and interspecific competition, dispersal (Seabloom et al., 2005) or spatial self-organization (Weerman et al., 2010). Spatial variability of MPB biomass can have important implications for the intertidal community structure and ecosystem functioning (Brito et al., 2013). Therefore, it is critical to elucidate the factors that cause this variability and the consequences for ecosystem structure and function. Spatial variability of MPB can be studied on the micro (up to ca 1 meter), meso (i.e. meters to kilometers) and macro scale (kilometers up to an entire estuary, and among estuaries). Many studies have demonstrated that spatial variation of MPB biomass is not governed by a single variable, but depends on a combination of factors.

Spatial variability of algae on the micro scale has been related to grazing by benthic fauna, although studies on the subject are scarce. For example, Hillebrand (2008) showed that the spatial distribution of grazed periphyton (organisms, including microalgae, attached to submerged surfaces) was more heterogeneous than ungrazed periphyton. Furthermore, macrofauna has been demonstrated to lower MPB biomass and patchiness in late spring and summer (Weerman et al., 2011). On the meso and macro scale, spatial variability in

MPB biomass has frequently been associated with sediment characteristics, bathymetry and emersion duration (Guarini et al., 1998; Orvain et al., 2012; van der Wal et al., 2010). MPB biomass is positively correlated with bathymetric level (van der Wal et al., 2010) and silt content (Orvain et al., 2012) and negatively correlated with median grain size (Orvain et al., 2012). Low lying intertidal areas are generally less stable (i.e. higher resuspension and export of material) due to the shorter emersion duration and high energy present from currents (Orvain et al., 2012). In addition, the shorter emersion duration results in a more limited light availability for photosynthesis (Barranguet et al., 1998). On the contrary, the reduced disturbance and increased light exposure are favourable for MPB growth in the higher intertidal (Orvain et al., 2012). High in the intertidal zone, wind has shown to negatively affect MPB biomass (Benyoucef et al., 2014). In addition, MPB growth may become limited at high elevation due to desiccation (Coelho et al., 2009). Lastly, there is evidence that grazing or physical disturbance by macrofauna may influence meso scale spatial patterning of MPB (e.g., Pratt et al., 2015). Pratt et al. (2015) found a positive correlation between chl *a* concentrations of the sediment (an indicator for MPB biomass) and the interaction between the density of a suspension feeder (*A. stutchburyi*) and silt content. The study, however, also demonstrates that on the meso and macro scale, factors often co-vary along environmental gradients. Field or laboratory experiments may help to elucidate the effect of individual factors on MPB biomass.

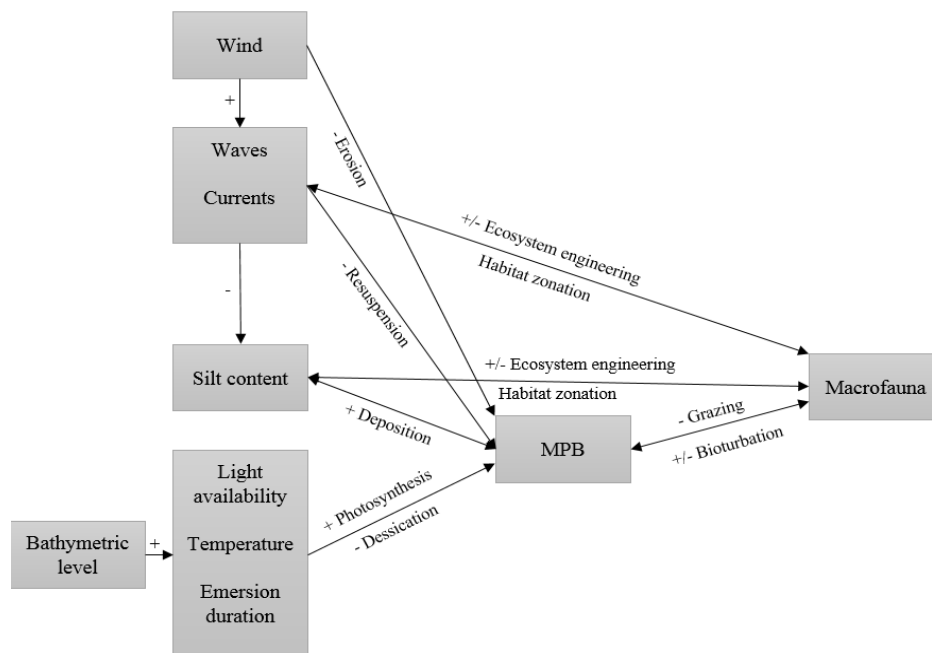


Figure 3. Various ecological interactions in the intertidal ecosystem associated with MPB

1.5 Remote sensing of intertidal areas

To better understand the functional role of MPB in the intertidal ecosystem, large scale monitoring of the spatial distribution of MPB is needed. Extensive field sampling campaigns are time consuming and therefore scarce. Consequently, satellite remote sensing is used increasingly. Satellite sensors can be separated into multispectral and hyperspectral sensors. Multispectral imagery contains 3 to 10 typically wide spectral bands. In contrast, hyperspectral imagery contains narrower bands (of 10-20 nm wavelength) and could contain hundreds to thousands of bands in total. The quantification of MPB biomass remains a challenge, as spectral characteristics on tidal flats may vary as function of physical (environmental and instrumental) and biological factors (Kazemipour et al., 2012). Environmental factors include variation in irradiation and surface roughness, while biological factors include biodiversity of MPB and associated pigment composition and ecophysiology, i.e. variation in pigment composition as response to light variation (Jesus et al., 2008; Pniewski et al., 2015).

When using multispectral sensors, total MPB biomass is usually expressed as the Normalized Differential Vegetation Index (NDVI) based on reflectance in the red bands (absorbed by photosynthesizing organisms, including MPB) and infrared bands (reflected by photosynthesizing organisms that have a complex cell structure, and neutral response in the case of MPB, see Van der Wal et al., 2010). Using hyperspectral imagery, characteristics of different MPB groups (including diatoms, euglenids and cyanobacteria) can be distinguished using group specific indices (Launeau et al., 2018). In addition, physical models have been developed to obtain a more accurate estimation of MPB biomass, taking possible effects of the background (e.g. mud and sand) on for example the NDVI into account (Kazemipour et al., 2012; Launeau et al., 2018), while controlled laboratory experiments have shown that such background effects are small (Barille et al., 2011).

1.6 Research objectives and thesis outline

The overall aim of this thesis is:

To study to what extent MPB 1) can be used as indicator for ecosystem functioning and 2) can structure higher trophic levels

Spatial variation in MPB biomass and production are quantified using Sentinel-2 and Landsat 8 satellite imagery, respectively. The role of MPB in structuring spatial variability of the benthic macrofauna that feed on MPB is studied, and, in reverse, the influence of macrofaunal presence on the observed MPB standing stock is studied. That is, does remotely sensed information on MPB

biomass and production provide a suitable indicator for food availability or is the MPB standing stock kept low by grazing?

Hence, the following research questions are addressed:

1. Can primary production rates of MPB be retrieved from multispectral remotely sensed information? Which factors are most important in determining spatial variability in MPB production rates?

In Chapter 2, a generic method is developed to model MPB production based on remotely sensed information (Landsat 8 OLI satellite imagery) on MPB biomass and sediment type, information on the tidal regime, ambient temperature and field measurements of photosynthetic parameters. Using a sensitivity analysis, we identify which parameters were most important in determining spatial variation in MPB primary production rates in the studied system. The model was calibrated and validated using field measurements of MPB biomass, photosynthetic parameters and sediment characteristics.

2. Does the importance of MPB in the diet of benthic macrofauna vary spatially? Is there an (indirect) relationship between MPB production in spring (when MPB has its bloom) and grazing pressure of benthic macrofauna in summer/autumn (when macrofauna has their maximum biomass)?

In Chapter 3, we quantify the importance of MPB as food source compared to other available food sources for macrofauna and tested whether the diet composition of macrofauna varies spatially, i.e. between tidal basins and as function of elevation. We hypothesize that the relative importance of MPB varies in the diet of suspension feeders and facultative suspension/deposit feeders, depending on spatial variability in the availability of MPB and phytoplankton. Furthermore, we hypothesize that the importance of MPB in the diet of macrofauna (determined using a natural stable isotope approach) increases with elevation. Furthermore, we study whether MPB production rates measured in spring, when macrofaunal grazing rates are low, are spatially linked to grazing rates by benthic macrofauna in summer. We hypothesize that MPB production in spring may be used as proxy for macrofaunal grazing pressure on MPB in summer/ autumn, as during spring the influence of grazing by macrofauna on spatial variability in MPB production is still limited.

3. To what extent does grazing of benthic macrofauna affect the standing stock of MPB biomass under varying hydrodynamic conditions? How does the presence of macrofauna influence spatial heterogeneity in MPB biomass

at the small scale (centimeter to meter) under varying hydrodynamic conditions?

In Chapter 4, we study the effect of top down control by benthic macrofauna on MPB biomass standing stock and spatial heterogeneity (centimeter to meter scale) of MPB under varying hydrodynamic conditions. We experimentally excluded macrofauna in low, intermediate and high elevation zones in two tidal basins and evaluated MPB heterogeneity using a variogram analysis on UAV images. We hypothesize that the effect of macrofaunal presence on MPB biomass depends on hydrodynamic activity, and that the effect is strongest when grazing pressure of macrofauna on MPB is high, and hydrodynamic forces are weak. At locations with high hydrodynamic activity, the influence of waves and currents on spatial variability in MPB biomass may overrule the influence of macrofaunal presence.

4. Does patch size and degree of patchiness of MPB vary among seasons and depend on sediment characteristics and hydrodynamic conditions at the mesoscale (meters to kilometers)?

In Chapter 5, we study spatial variability in MPB biomass on the meso and macro scale. We test whether MPB patch size and degree of patchiness vary among seasons, salinity zones, tidal flat type (muddy fringing versus sandy mid-channel tidal flats) or ecotopes (defined by hydrodynamics, silt content and elevation). Sentinel-2 imagery is used to derive semi-variogram parameters from the NDVI, which is used as indicator for MPB biomass. We hypothesize that hydrodynamic energy homogenizes spatial variability in MPB biomass and, therefore, the degree of patchiness (represented by the sill of a semi-variogram) is lower and the patch size (represented by the range of a semi-variogram) of MPB is higher on the relatively sandy mid-channel tidal flats than on the relatively muddy fringing tidal flats. We hypothesize that patch size and degree of patchiness of MPB increases in early spring when usually a spring bloom occurs, and decreases again in summer and winter. We expect that in spring, patch size and degree of patchiness are mainly coupled to abiotic factors, while in summer macrofauna may influence these parameters by increased grazing activity and bioturbation.

The role of MPB in the intertidal ecosystem is studied in two temperate tidal basins located in the Netherlands: the relatively clear, mesotrophic tide-dominated Oosterschelde and the relatively turbid, eutrophic, tide-dominated Westerschelde (van der Wal et al. 2010) (see Figure 1). In Chapter 6 (Synthesis), the main findings of the research presented in this thesis are discussed and put into a wider perspective, and implications for the

management of tidal flats are presented. Furthermore, an outlook and recommendations on future research on the use of satellite remote sensing for monitoring of properties of MPB and higher trophic levels are provided.

Chapter 2 A model to assess microphytobenthic primary production in tidal systems using satellite remote sensing

Tisja D. Daggars, Jacco C. Kromkamp, Peter M. J. Herman, Daphne van der Wal

STATUS: Adapted from the published version in Remote Sensing of Environment 211, 129-145 (2018), with Corrigendum published in Remote Sensing of Environment 230: 11206 (2019)

2.1 Abstract

Quantifying spatial variability in intertidal benthic productivity is necessary to guide management of estuaries and to understand estuarine ecological processes, including the amount of benthic organic carbon available for grazing, burial and transport to the pelagic zone.

We developed a model to assess microphytobenthic (MPB) primary production using (1) remotely sensed information on MPB biomass and remotely sensed information on sediment mud content, (2) surface irradiance and ambient temperature (both from local meteorological observations), (3) directly-measured photosynthetic parameters and (4) a tidal model. MPB biomass was estimated using the normalised-difference vegetation index (NDVI) and mud content was predicted using surface reflectance in the blue and near-infrared, both from Landsat 8 satellite imagery. The photosynthetic capacity (maximum photosynthesis rate normalised to MPB chl-*a*) was estimated from ambient temperature, while photosynthetic efficiency and the light saturation parameter were derived from *in situ* fluorometry-based production measurements (PAM). The influence of tides (submergence by turbid water) on MPB production was accounted for in the model. The method was validated on several locations in two temperate tidal basins in the Netherlands (Oosterschelde and Westerschelde). Model based production rates ($\text{mg C m}^{-2} \text{ h}^{-1}$) matched well with an independent set of *in situ* (PAM) measurement based production rates (Oosterschelde: RMSE = 66.8, mean error = 41.3, $\chi = 3.3$; Westerschelde: RMSE = 89.8, mean error = -45.2, $\chi = 1.1$). The relationship between photosynthetic capacity and temperature shows considerable variation and may be improved by using sediment surface temperature instead of ambient temperature. A sensitivity analysis revealed that emersion duration and mud content determine most of the variability in MPB production. Our results demonstrate that it is possible to derive a satellite remote sensing-based overview of average hourly and daily MPB primary production rates at the macro scale. As the proposed model is generic, the model can be applied to other tidal systems to assess spatial variability in MPB primary production at the macro scale after calibration at the site of interest. Model calibration, results and possible applications for regular monitoring of MPB production are discussed below.

Key words: Microphytobenthos; Primary production; Tidal flats; Photosynthesis; Remote Sensing; Multiple linear regression; Mapping

2.2 Introduction

Estuarine intertidal zones rank among the most productive and potentially economically valuable ecosystems in the world (Costanza et al., 1997; Heip et al., 1995; Schelske and Odum, 1962). Microphytobenthos (MPB), consisting of microalgae and photosynthesizing bacteria, are the main primary producers in intertidal ecosystems depending on the total surface area of intertidal flats present (McLusky, 1989; Underwood and Kromkamp, 1999). MPB primary production rates on intertidal flats are typically in the range of $100 \text{ g C m}^{-2} \text{ y}^{-1}$ (Underwood and Kromkamp, 1999) but can exceed $300 \text{ g C m}^{-2} \text{ y}^{-1}$ (MacIntyre et al., 1996).

Production in terms of carbon assimilation can be several orders of magnitude higher in benthic sediments than in the water column (Guarini et al., 2008) and benthic primary productivity provides a main food source for the majority of macrofaunal species in intertidal ecosystems (Christianen et al., 2017). The global annual productivity of MPB is estimated to be in the order of 500 million tons of carbon (Cahoon, 1999). MPB are therefore expected to play an important role in the global carbon cycle.

Due to the high ecological and economic importance of intertidal ecosystems and their current deterioration as a result of human activities (Barbier et al., 2011; Lotze et al., 2006), extensive *in situ* sampling campaigns and monitoring programs are being conducted in these regions. For example, Rijkswaterstaat (Dutch Ministry of Infrastructure and Water Management) has monitored MPB biomass in the Westerschelde (The Netherlands) from 1987 until 2013 and extensive project-based sampling campaigns have been conducted worldwide (e.g. Colijn and De Jonge, 1984; Lomas et al., 2002; Santos et al., 1997; Yamaguchi et al., 2007). However, *in situ* sampling is costly and only provides limited spatial information on large scale ecosystem dynamics. Satellite remote sensing provides the opportunity to upscale *in situ* measurements to the entire estuary and provide further insight into large scale intertidal ecosystem structure and dynamics.

MPB primary production rates on intertidal flats are strongly influenced by the tidal cycle (Pratt et al., 2013; Serôdio and Catarino, 1999). In ecosystems with high water turbidity (which limits light penetration through the water column), benthic primary production mainly occurs during daytime low tides (Colijn, 1982; Serôdio and Catarino, 2000). In muddy sediments, MPB biomass is mostly concentrated at the sediment surface and decreases exponentially with depth (De Brouwer and Stal, 2001; Kelly et al., 2001). Light attenuation is strong in these sediments (Forster and Kromkamp, 2004) and resuspension rates are low (Herman et al., 1999). MPB biomass in sandy sediments shows a more homogeneous distribution with depth, a result of sediment mixing by tidal currents and bioturbation, and light penetrates deeper (Kuhl and

Jorgensen, 1994). Generally, resuspension rates are higher in sandy sediments (Jesus et al., 2006; Yallop et al., 1994).

Several 1D models have been developed to calculate MPB primary production in intertidal areas (Barranguet et al., 1998; Blackford, 2002; Brotas et al., 1995; Forster et al., 2006; Forster and Kromkamp, 2006; Forster and Kromkamp, 2004; Serôdio and Catarino, 2000). Some of these models aim to describe the vertical movement of MPB within the sediment as a function of tidal phase and/or irradiance (Pinckney and Zingmark, 1993; Serôdio and Catarino, 2000), while others use a sediment-optical model to calculate areal primary production rates (Barranguet and Kromkamp, 2000; Barranguet et al., 1998; Forster and Kromkamp, 2006). However, few studies have focused on mapping and monitoring of large scale spatial variability in MPB production. Guarini et al. (2002) made a spatial primary production model by combining measurements of photosynthesis-irradiance curves with a deterministic model of tidal elevation and ambient irradiance to calculate daily aerial production rates for intertidal mud flats. However, spatial variation in mud content and chlorophyll-*a* (chl-*a*) concentrations and their effect on primary production rates were not taken into account in this study. Remote sensing studies have mainly focussed on quantifying the MPB biomass standing stock (Kazemipour et al., 2012; Meleder et al., 2003; Van der Wal et al., 2010) and not on production. Remote sensing has also been used to assess the grain-size characteristics of the sediment, such as mud content (Rainey et al., 2003; Van der Wal and Herman, 2007), which can support spatial estimates of primary production. Several methods have been developed to retrieve sediment properties from hyperspectral *in situ* remote sensing (Adam et al., 2011; Hakvoort, 1997), hyperspectral airborne remote sensing (Adam et al., 2006; Rainey et al., 2003) and multispectral satellite remote sensing (Ryu et al., 2004; Van der Wal & Herman, 2007).

The aim of this study is to develop a generic method to assess MPB primary production rates at the estuary scale using optical remote sensing. The model is applied to two intertidal ecosystems in the Netherlands (the Oosterschelde and Westerschelde) and is validated with *in situ* measurements on muddy and sandy sediments on intertidal flats in these systems. We performed a sensitivity analysis that provides insight in the model response to variation in chl-*a* concentration, mud content, ambient irradiance, emersion duration and photosynthetic parameters (photosynthetic efficiency (α) and capacity (P_s)).

2.3 Methodology

2.3.1 Study area

The proposed model was tested in two shallow tidal basins located in the southwestern part of the Netherlands: the relatively clear, mesotrophic tide-dominated Oosterschelde (E 4°00', N 51°35', Van der Wal et al., 2010) and the eutrophic turbid, tide-dominated Westerschelde estuary (E 3°50', N 51°20', Van der Wal et al., 2010). Both basins are part of the Dutch delta system where the Scheldt, Meuse and Rhine rivers flow into the North Sea. In the Oosterschelde, the construction of dams and a storm surge barrier resulted in a tidal basin with a reduced tidal range and little freshwater input (Nienhuis and Smaal, 1994). The tidal basin is polyhaline and consists of relatively clear water (Secchi depth: 3.3 ± 0.9 m; k_d : 1.3 ± 1.2 m⁻¹, spring 2011-2016, NIOO/NIOZ monitoring data, unpublished results). The spring tidal range is around 3 m (Van der Wal et al., 2010). The surface area of the intertidal zone in Oosterschelde is approximately 50 km² (Van der Wal et al., 2010). The Westerschelde estuary is about 60 km long and 5 km wide at the mouth. The estuary is well-mixed and has a clear salinity gradient, varying from mesohaline at the Dutch-Belgium border to polyhaline at the mouth. The estuary is macrotidal and has a spring tidal range varying from 4.5 m on springs at the mouth, and 5.5 m on springs at the transition of the polyhaline and mesohaline zone (water height data from 2012; Rijkswaterstaat 2017). The intertidal zone of the Westerschelde has a surface area of approximately 70 km² (Van der Wal et al., 2010). The sediments in the Westerschelde consist of coarse to fine sands and mud. The Westerschelde is relatively clear at the mouth (Secchi depth: 0.86 ± 0.38 ; k_d : 2.8 ± 0.9 , spring 2011-2016, NIOO/NIOZ monitoring data, unpublished results) and more turbid in the mesohaline zone (Secchi depth: 0.34 ± 0.08 ; k_d : 4.9 ± 1.9 , unpublished results).

2.3.2 Model overview

The goal of the proposed model is to retrieve average daily estimates of MPB primary production for intertidal coastal areas. The model describes spatial variability in MPB primary production using remotely sensed information on MPB biomass and sediment type (mud content, % < 63 µm) as input. The model was subdivided into a primary production module and a tide module (Figure 1). In the primary production module, MPB primary production is calculated for the photic zone within the sediment. Sediment-optical relationships and the vertical distribution of MPB biomass within the sediment are accounted for and depend on mud content and MPB biomass, which were derived from *in situ* sediment characteristics and surface reflectance in specific wavelengths using multiple linear regression (described in detail in section

2.3.4.2). Earlier studies have shown that the photosynthetic capacity (maximum photosynthesis rate) depends on temperature (Blanchard et al., 1997; Blanchard et al., 1996; Morris and Kromkamp, 2003). We have used the formulation of Blanchard et al. (1996) to calculate variations in the photosynthetic capacity as function of ambient temperature over time, which is described in detail in section 2.3.4.4.2. Other photosynthetic parameters (photosynthetic efficiency α and optimal light intensity E_{opt}) necessary to calculate primary production rates were measured in the field. The primary production module was applied to a Landsat 8 OLI image taken at the same time period as a series of *in situ* fluorometry-based production measurements, to validate the calculation of instantaneous hourly MPB primary production rates from satellite remote sensing. Subsequently, the primary production module was combined with a tide module to account for variation in MPB production over time associated with emersion versus immersion of the tidal flats and vertical migration of MPB within the sediment. The combined modules were applied to the intertidal areas of the Oosterschelde and Westerschelde to identify potential spatial variability in daily MPB production rates.

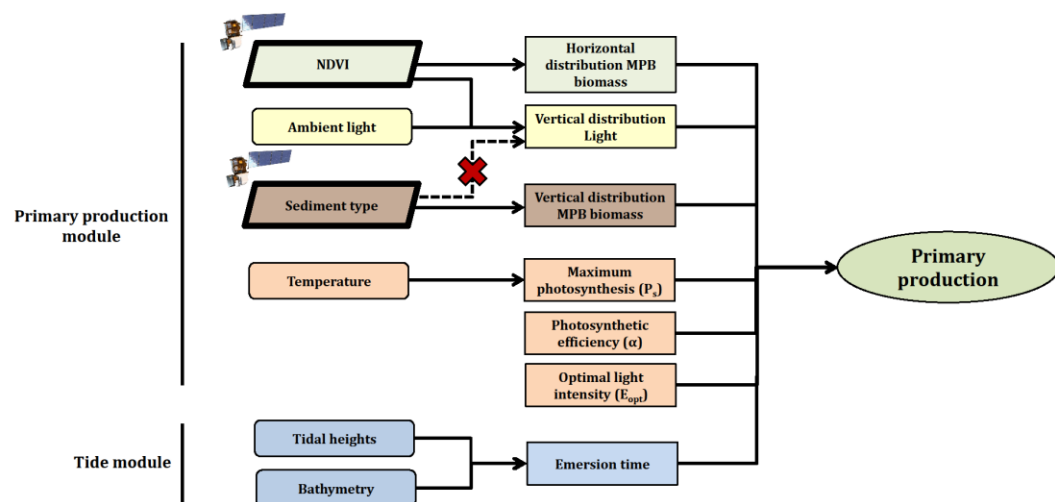


Figure 1. Model concept. Solid arrows indicate model dependencies as specified in section 2.3.4. The dotted arrow indicates that the vertical distribution of light does not depend on sediment type. A stepwise linear regression of light attenuation as a function of chl-*a* concentration, mud content, organic content and moisture content as input gave a best model (lowest AIC) with chlorophyll-*a* as single explanatory factor ($R^2 = 0.49$, Figure 4).

2.3.2.1 Primary production module

The proposed primary production module aims to provide a depth-integrated value for the MPB production rate. The module describes the upper 2 mm of the sediment, as earlier studies have shown that the euphotic depth of estuarine sediments does not exceed this value (range approximately 0.8 -

1.8 mm (Barranguet and Kromkamp, 2000; Kromkamp et al., 1995). Light attenuation within these 2 mm is known to be influenced by several factors, including sediment type, MPB biomass, organic content and water content (Blanchard et al., 2000; Forster and Kromkamp, 2004; Jesus et al., 2006; Kelly et al., 2001; Serôdio, 2004). As many of these factors are highly correlated, a stepwise regression-based approach was used to derive an estimate of the light attenuation coefficient based on a set of field measurements of light attenuation (k_d), chl-*a* concentrations, organic content, moisture content and mud content of the upper 2 mm of the sediment (section 2.3.4.3).

The relative distribution of MPB biomass within the sediment was described according to Jesus et al. (2006) and varies as function of mud content:

$$\text{Chl}a_{\text{accumulated},d} = \frac{d}{d_{\text{max}}} + \text{mud} \left(1 - \frac{d}{d_{\text{max}}} - e^{-2ed/d_{\text{max}}} \right)$$

$\text{Chl}a_{\text{accumulated}}$: amount of accumulated chl-*a* at depth d relative to total amount of chl-*a* in the upper 2 mm of the sediment

d : layer depth (mm)

d_{max} : maximum depth (mm)

mud: % particles < 63 μm

As a result, biomass decreases exponentially with depth in muddy sediments and has a more homogeneous vertical distribution in sandy sediments.

Several studies have confirmed the suitability of *in vivo* chlorophyll fluorometry (PAM) to estimate MPB primary production (carbon uptake) in the field (Lefebvre et al., 2007). Barranguet and Kromkamp (2000) estimated carbon fixation (primary production) rates as the product of the chl-*a* concentration, the photosynthetic activity (measured with a PAM fluorometer, see section 2.3.3.1.4), and an empirical factor (EE) for the conversion of photosynthetic electron transport rates into carbon (C) fixation units. This equation was modified by using the model of Eilers and Peeters (1988), rewritten by Herlory et al., (2007) to describe the photosynthetic activity. To convert photosystem II electron transport (ETR, measured with a PAM) values to C fixation rates, we used the following formula (Barranguet and Kromkamp, 2000):

$$\text{C fixation rate (mg C / mg chl-}a \text{ / h)} = \text{chl-}a * \text{EE} * \text{ETR}$$

The average value of the electron requirement (EE) in the data described in detail in section 2.3.3.1.4 is 0.04, which matches with the average found by Barranguet and Kromkamp (2000) who found values of EE between 0.03 and 0.05. Therefore, the PAM data was used to obtain the photosynthetic

parameters that were used as model input and $EE = 0.04$ was used to convert ETR rates to carbon fixation rates.

The upper 2 mm of the sediment was divided into sub layers with a thickness of 10 μm . Subsequently, gross hourly C-fixation rates were calculated for each sub layer:

$$P = EE * \frac{E_{PAR}}{\frac{1}{\alpha * E_{opt}^2} * E_{PAR}^2 + \left(\frac{1}{p_s} - \frac{2}{\alpha * E_{opt}}\right) * E_{PAR} + \frac{1}{\alpha}} * chl - a \quad (1)$$

α = photosynthetic efficiency ($\text{mg C mg}^{-1} \text{ chl-}a \text{ h}^{-1} [\mu\text{mol photon m}^{-2} \text{ s}^{-1}]^{-1}$)

$chl-a$ = chlorophyll- a concentration (mg m^{-2})

EE = ETR efficiency for C fixation, here taken as 0.04

E_{PAR} = photosynthetically active irradiance ($\mu\text{mol photon m}^{-2} \text{ s}^{-1}$)

E_{opt} = optimal light intensity ($\mu\text{mol photon m}^{-2} \text{ s}^{-1}$)

P = gross hourly carbon fixation rate ($\text{mg C m}^{-2} \text{ h}^{-1}$)

p_s = photosynthetic capacity ($\text{mg C mg}^{-1} \text{ chl-}a \text{ h}^{-1}$)

The carbon fixation rates calculated for each sub layer are added up to provide a depth-integrated MPB production rate per hour.

2.3.2.2 Primary production and tide module

Muddy sediments are mainly dominated by epipellic diatom taxa, which are able to migrate within the sediment. This is generally assumed to be regulated by light availability and tidal phase. The epipellic diatoms migrate to the sediment surface at low tide, reaching a steady state about an hour after emergence of the sediment (Paterson et al., 1998). This migration pattern is only observed during daytime low tides (Kromkamp, Personal communication; Serôdio et al., 1997). Because of upward migration during the first periods of low tide, most of the biomass will be below the photic depth or in very dim light, hence production of MPB will be negligible. Therefore, it is assumed in the model that no production occurs within the first hour after emersion of the sediment. Furthermore, it is assumed that benthic production occurring during immersion is negligible due to light limitation.

The tide model was used to calculate for each hour whether grid points were emersed or immersed. The tide model uses bathymetry from laser altimetry of the intertidal areas of the Oosterschelde (2013) and Westerschelde (2015) acquired from Rijkswaterstaat (Dutch Ministry of Infrastructure and Water Management).

Time series measurements of water heights were retrieved from four stations in the Oosterschelde and six stations in the Westerschelde (Rijkswaterstaat, 2017) and spatially interpolated using inverse distance weighting to obtain

water heights with a 10-minute resolution for the entire surface area of each intertidal system. Subsequently, it was calculated for each pixel (30 x 30 m) whether a pixel was emerged or immersed for each hour within the study period. For each time step a pixel is emerged, an hourly primary production rate is calculated using the primary production module. Subsequently, average daily primary production rates averaged over a month were calculated.

2.3.3 Data collection

To test the validity of the model, two independent datasets were used for model calibration and validation, respectively. In spring 2014, a series of surface reflectance measurements in the VIS-NIR domain (314 – 948 nm) using a RAMSES-ARC-VIS radiometer, Trios GmbH) and sediment samples was collected. This dataset was used for calibration of the relationship between surface reflectance (measured *in situ* and retrieved from Landsat 8, 10-04-2014) and chl-*a* (a proxy for MPB biomass) and mud content, respectively. A set of chl-*a*, mud content and fluorometry-based production measurements was collected in spring 2015 simultaneously with the collection of a Landsat 8 image (12-03-2015). A random selection of the production measurements (41% of PAM fluorescence measurements) was used to obtain photosynthetic parameters to be used as model input and to calibrate the dependency of the photosynthetic capacity on ambient temperature. The chl-*a* and mud content measurements and the production measurements not utilized for model calibration were used for model validation.

2.3.3.1 *In situ* measurements

2.3.3.1.1 Surface reflectance and sediment samples

In April 2014, a set of 9 surface reflectance measurements was performed at 50 random locations in the Oosterschelde and Westerschelde using the RAMSES-ARC-VIS radiometer. At each location, three points were measured in triplicate in a triangular set-up with approximately 5 m distance between points. This set-up allows linkage of the three points to a 30 by 30 m Landsat 8 satellite pixel. The measurements were taken 30 cm above the sediment, measuring a surface area of 31.5 cm² per set of three points. Following Kromkamp et al. (2006), each measurement consisted of a measurement of radiance, using a piece of white styrofoam (Lu_r), and a measurement of radiance of the sediment (Lu_s); surface reflectance was calculated from this set as Lu_s/Lu_r . All radiometer measurements were done at least one hour after emergence of the sediment, in order to minimize bias due to vertical migration of the MPB. Within the measured surface area, ten sediment cores were taken up to a depth of 2 mm that were pooled into one sample using a 1.5 cm diameter syringe, of which we removed the top. The dry bulk density of the samples was determined gravimetrically after freeze drying the sediment for

48h. The samples were transported in ice and stored in -80°C within eight hours. The ten cores were pooled and homogenized, of which 700 mg was used for pigment analysis. Photosynthetic pigments were extracted using a cell homogenizer (Braun, Type 8530220) for 20 seconds after addition of 10 ml acetone (90%) and glass beads. The samples were cooled with carbon dioxide during extraction. The extract was centrifuged (2000 rpm, 3 min) and absorption was measured with a Specord 210 spectrophotometer. Chl-*a* content ($\mu\text{g/g}$) was calculated using the equation from Ritchie (2006). These were then converted to chlorophyll-*a* concentrations (mg/m^2) using the dry bulk density of the sampled volume. For obtaining the relationship between NDVI (radiometer-based) and chlorophyll-*a* concentration, measurement points with standing water were removed ($n=12$). Likewise, Landsat 8 pixels containing water ($\text{NDWI} > 0$, section 2.3.3.2) or an $\text{NDVI} > 0.3$ (possibly containing macroalgae, see section 2.3.3.2), were excluded from the Landsat-8 based calibration of the NDVI and chlorophyll-*a* concentration ($n=8$). The sediment grain size distribution was determined using a Malvern laser particle sizer (Malvern Mastersizer 2000, serial number S/N: 34403/139) coupled to an autosampler (ASA 2000) after sieving samples with a $1000\ \mu\text{m}$ sieve. Sediments were classified based on the nomenclature proposed by Folk (1954). In March 2015, a dataset for the validation of modelled mud content and chl-*a* concentration was collected at 9 sites in the Oosterschelde (Dortsman, Rattekaai and Viane) and Westerschelde (Hellegat, Middelpmaat, Molenplaat, Paulinapolder, Rilland and Waardepolder). In each of the 9 locations, three plots, $16\ \text{m}^2$ each, were randomly selected in the high intertidal ($0 - 1\ \text{m}$ NAP, where NAP is Dutch Ordnance level, which is about mean sea level) and in the low intertidal ($-1 - 1\ \text{m}$ NAP), respectively. At each plot, 9 surface reflectance measurements were performed using the RAMSES-ARC-VIS radiometer. Sediment cores were taken up to a depth of 1 cm using a syringe with a diameter of 3 cm below each surface reflectance measurement, which were pooled into three samples and analyzed for grain size distribution and chl-*a* content. Subsequently, chlorophyll-*a* concentrations were calculated using the dry bulk density and sampled volume.

2.3.3.1.2 Photosynthetic activity

The photosynthetic activity was repeatedly measured in each plot in March and May 2015 in triplicate by constructing a rapid light curve (RLC) using a Pulse Amplitude Modulation (PAM) fluorimeter (Mini PAM; Heinz Walz GmbH). The fibre optic probe was placed in a dark chamber perpendicular to the sediment surface at a distance of 4 mm above the sediment. Rapid light curves were constructed without prior dark acclimation using eight actinic increasing light levels ($160, 228, 347, 485, 742, 1079, 1589$ and $2630\ \mu\text{mol photons m}^{-2}\ \text{s}^{-1}$). The duration of each light step was 30s. Saturation pulses were applied prior to starting the rapid light curve and at the end of each actinic light increase to determine the F_m' . The relative electron transport rate ($rETR$) was calculated

as the product of the light utilization efficiency, the photon flux density and a light absorption constant of 0.84 and a factor of 0.5 to account for absorption by photosystem-II only (default values in the PAM-Control software), as it was assumed that in diatoms both photosystems receive an equal amount of light energy (Suggett et al., 2004). The PAM provides depth integrated values for the photosynthetic activity, as its measuring depth on intertidal flats is 100-200 μm (Barranguet and Kromkamp, 2000).

2.3.3.1.3 Ambient irradiance and temperature

Average hourly measurements of ambient irradiance were retrieved from a LiCOR LI191 SA PAR quantum sensor connected to a LI-1000 data logger located at the roof of the nearby NIOZ institute, Yerseke, The Netherlands. Ambient irradiance was assumed to be homogeneous within the study area. The irradiance recordings were used to obtain (1) *in situ* production rates from PAM fluorescence measurements and (2) satellite-based production rates. The maximum distance between *in situ* PAM fluorescence measurements and the LiCOR sensor was 45 km.

Ambient temperature was used to model the photosynthetic capacity (P_s) and was retrieved from a nearby weather station of the Royal Netherlands Meteorological Institute (KNMI) located at the mouth of the Westerschelde (Vlissingen, The Netherlands). The maximum distance between *in situ* PAM fluorescence measurements and the weather station was 57 km. It was assumed that ambient temperature was homogeneous within the study area.

2.3.3.1.4 ^{14}C -uptake

In the Westerschelde estuary, we performed 30 surface reflectance, 24 RLC's (PAM) and 27 potential primary production (^{14}C -uptake) measurements to test for possible variability in photosynthetic parameters during daytime emersion and compare production estimates from PAM fluorescence with C fixation rates. Measurements were performed in two randomly selected 1 m^2 plots at approximately 15 m distance from each other in September 2014. The minimum water level at the measurement location occurred around 2 PM. The plots had a similar mud content of $27 \pm 11\%$ and $29 \pm 2\%$, respectively. Three replicate surface reflectance, RLC and ^{14}C uptake measurements were performed at five time steps during a single low tide, with one and a half hour intervals. The first measurements were done one hour after emergence of the sediment, while the last measurements were performed 15 minutes before immersion. Fluorescence measurements could not be performed at the last time step (18:00) due to a low battery of the PAM. At every time step, three points were randomly selected within each plot and the surface reflectance was measured using the same methodology as described in section 2.3.3.1.1. Subsequently, an RLC was performed at the exact same spot with a PAM

fluorimeter (Mini PAM), following the same methodology as described in section 2.3.3.1.2. A sediment sample was then scraped from the same surface area as where the RLC was performed ($\pm 26 \text{ cm}^2$), for analysis of potential primary production rates using ^{14}C -uptake (slurries) in a photosynthetron (see Barranguet and Kromkamp, 2008). ^{14}C -uptake measurements (slurries) provide potential production estimates as vertical gradients in e.g. nutrient availability, CO_2 , and light present in intertidal sediments are destroyed. ^{14}C -uptake measurements were done *ex situ* as there was no permission for the use of ^{14}C *in situ* (for health and safety reasons). Furthermore, *in situ* ^{14}C -uptake measurements using the bell-jar technique may underestimate production rates, as the specific activity of the DIC pool cannot easily be measured (detailed discussion in Underwood and Kromkamp, 1999). Barranguet et al. (1998) found a reasonable agreement between primary production rates measured with ^{14}C -uptake (slurries) in a photosthetron and *in situ* production measurements with O_2 -microelectrodes.

The samples were stored in a cooling box, ensuring the samples did not get in immediate contact with ice. The samples were transported to the laboratory right after sampling and measured on the same day. The samples were homogenized and 6 ml was pipetted out of the sample (while stirring). 75 ml of filtered water was added which was collected upon arrival at the field site. From the resulting suspension, 2 ml was incubated in 20 ml glass scintillation vials in the photosynthetron and 100 μl $\text{NaH}^{14}\text{CO}_3$ was added (925 kBq ml^{-1} , Amersham) to each vial. The vials were exposed for 30 minutes to ten different irradiances varying from 0 to 630 $\mu\text{mol photons m}^{-2} \text{ s}^{-1}$. The samples were incubated at *in situ* temperatures, which were measured in the upper $\pm 0.5 \text{ cm}$ of the sediment at each plot, at each one-and-a-half-hour time interval. After incubation, 100 μl of concentrated HCl was added to each vial to stop the reaction and drive off the unbound CO_2 . The vials were kept for at least 12h in a fumehood before adding 18 ml of scintillation fluid (Instagel-Plus, Perkin-Elmer), after which the radioactivity was counted using a Perkin Elmer Tri-Carb2910 TR scintillation counter.

The chl-*a* concentration of the slurry was determined by centrifuging 10 ml of the slurry in triplicate (3500 rpm, 10 min). The overlying supernatant was discarded and 5 ml of acetone (90%) was added for chl-*a* extraction. The extracts were vortexed and stored in the dark at 4 °C till the next day. Subsequently, the extracts were centrifuged and measured with a UV-VIS Varian spectrophotometer (750-400 nm) after which the chl-*a* concentrations were calculated according to Ritchie (2006). Carbon fixation rates were normalized to the chl-*a* concentration present in the suspension.

2.3.3.2 Satellite imagery

Two satellite scenes acquired by the Landsat-8 Operational Land Imager (OLI) were used for calibration and validation of the model, respectively: one image that was collected at 01-04-2014 and one that was collected at 12-03-2015 (Table 1). Both images are taken at approximately 10:30 UTC at low tide (01-04-2014) and about one and a half hours after low tide (12-03-2015), respectively. The images were converted from top of atmosphere radiance to surface reflectance (NASA). Land was masked in a Geographical Information System. The intertidal areas of the Oosterschelde and Westerschelde were selected by excluding water pixels using the Normalized Difference Water Index (NDWI) (Li et al., 2013):

$$NDWI = \frac{R_{Green} - R_{NIR}}{R_{Green} + R_{NIR}}$$

where R_{Green} and R_{NIR} are surface reflectance in the green and near-infrared, respectively. Pixels with an $NDWI < 0$ were defined as intertidal area. Earlier studies have shown that MPB is the dominant benthic primary producer in the intertidal systems of interest, as benthic macroalgae contribute less than 10% to benthic primary production in the Oosterschelde and less than 5% in the Westerschelde (Nienhuis, 1992). Saltmarsh vegetation and areas with dominance of macroalgae were excluded by using $NDVI > 0.3$. Here, $NDVI$ is the normalized difference vegetation index:

$$NDVI = \frac{R_{NIR} - R_R}{R_{NIR} + R_R}$$

where R_{NIR} and R_R are surface reflectance in the near-infrared and red, respectively (Rouse, 1973). Furthermore, a vegetation map (2012, Rijkswaterstaat, Dutch Ministry of Infrastructure and Water Management) based on surveys and false colour aerial photos was used to exclude pixels which partly contain (saltmarsh) vegetation (mixels).

Table 1. Designations of the Landsat-8 OLI bands used in this study.

Band number	Spectral range (nm)
2	R_{blue} : 450 - 510
3	R_{green} : 530 - 590
4	R_{red} : 640 - 670
5	R_{NIR} : 850 - 880
6	R_{SWIR1} : 1570 - 1650
7	R_{SWIR2} : 2110 - 2290

2.3.4 Model input

2.3.4.1 Microphytobenthic biomass

Several indices have been developed to obtain quantitative image-derived information on MPB biomass in intertidal sediments, including the Normalized Difference Vegetation Index (NDVI) (Rouse, 1973) as defined in the previous section, the MPB Index (MPBI) (Mélédér, 2010), two indices specifically for diatoms (I_{Diatom}) and euglenids (I_{Euglenid}) (Kazemipour et al., 2012) and derivative-based approaches (Murphy et al., 2005b). However, hyperspectral information is required for all indices, except the NDVI. Since this is not available for Landsat-8 OLI, we used the NDVI only.

The NDVI is a widely used optical measure for the biomass of photo-autotrophs and has been applied in earlier studies to obtain image-derived information on MPB biomass (Kazemipour et al., 2012; Van der Wal et al., 2010). We tested the usability of the NDVI for mapping of quantitative information on MPB biomass in intertidal areas using Landsat 8.

Two NDVI – chl-*a* calibration curves were constructed: (1) by matching chl-*a* concentrations of sediment samples to surface reflectance measurements performed above the sediment with a RAMSES-ARC-VIS radiometer (Trios GmbH) and (2) by matching chl-*a* concentrations to spectral reflectance derived from the Landsat 8 OLI satellite image acquired on 01-04-2014. In this way, the presence of possible scaling effects on the parameters of the resulting regression can be tested. For both calibration curves the dataset collected in 2014, described in section 2.3.3.1.1 was used. The NDVI derived from surface reflectance measurements was calculated from the wavelength spectra obtained with the radiometer using the same bandwidths of R_{red} and R_{NIR} of Landsat 8, taking into account the spectral sensitivity of the Landsat 8 OLI sensor. Subsequently, both regression formulas were applied to the second Landsat 8 OLI image (12-03-2015) and the obtained estimations of MPB biomass were validated using an independent set of *in situ* chl-*a* measurements collected during Landsat 8 image acquisition.

2.3.4.2 Mud content

Several techniques have been developed to retrieve sediment characteristics from hyperspectral and multispectral remote sensing, including unsupervised classification techniques such as Principal Component Analysis (PCA) or ISODATA (Adam et al., 2006; Ryu et al., 2004), supervised classification using for example a Spectral Angle Mapper (Adam et al., 2006), spectral unmixing (Rainey et al., 2003) and regression methods (Van der Wal and Herman, 2007). See Van der Wal and Herman (2007) for a detailed discussion of different techniques.

In this study, regression modelling was used to derive an estimate of the mud content (% particles < 63 μm) from surface reflectance, as this sediment property provides information on light attenuation within the sediment and the vertical distribution of MPB biomass (Jesus et al., 2006). The advantage of regression modelling compared to other available techniques, such as unsupervised or supervised classifications, is that a measure of the mud content can be obtained on a ratio scale. Furthermore, Van der Wal and Herman (2007) have shown that regression methods have the potential to allow for time series analysis of maps. A two-way approach was used: (1) field measurements of mud content were regressed against *in situ* surface reflectance measured with a RAMSES-ARC-VIS radiometer (Trios GmbH) (section 2.3.3.1.1) and (2) the same field measurements of mud content were regressed against surface reflectance of Landsat 8 OLI bands of the image acquired on 01-04-2014 (Table 1). Landsat 8 OLI bands were simulated from *in situ* reflectance measurements by multiplying the measured wavelength spectrum with the spectral radiance response of the Operational Land Imager (OLI). In both approaches, a stepwise linear regression (both forward and backward) was applied to the average surface reflectance of the bands. $R_{\text{ultrablue}}$ and R_{red} were excluded from the analysis as $R_{\text{ultrablue}}$ is highly sensitive to fine atmospheric particles, and R_{red} is sensitive to photosynthetic organisms, such as MPB, whose presence varies over time. Subsequently, the resulting regression equation is applied to an independent image (Landsat 8 OLI, 12-03-2015) and validated against an independent set of field measurements (spring 2015).

2.3.4.3 Vertical light distribution

Light attenuation within the sediment is known to be influenced by several factors, including grain size, MPB biomass, organic content and water content (Blanchard et al., 2000; Forster and Kromkamp, 2004; Jesus et al., 2006; Kelly et al., 2001; Serôdio, 2004). As measuring light attenuation in undisturbed sediments poses a challenge, light attenuation was in previous studies modelled as function of chl-*a* concentration (Serôdio, 2004), mud content (Jesus et al., 2006) or using a separate component for biological (MPB) and non-biological components (sediment grains and dead organic material) (Forster and Kromkamp, 2004). Forster and Kromkamp (2004) assumed attenuation due to non-biological components to be proportional to the amount of sediment dry weight, whereas attenuation due to biological components was assumed to be proportional to chl-*a* content.

As mud content and chl-*a* concentrations can be highly correlated, a stepwise regression-based approach was used on a set of field measurements from the Eden estuary, United Kingdom (Kromkamp, unpublished results) to estimate the light attenuation coefficient as a function of chl-*a* concentrations, mud

content, organic content and water content of the sediment. Chlorophyll-*a* concentration instead of chlorophyll-*a* content was used, as chlorophyll-*a* concentration is a parameter that can best be retrieved from satellite remote sensing (Murphy et al., 2005a). Measurements were performed on a relatively sandy site with mud contents varying from 0 to 21 % (mud contents may increase up to > 80% on tidal flats) and chl-*a* concentrations varying from 20 to 960 mg/m². Light attenuation (k_d) was measured on sediment cores using custom made scalar microfiber sensor probes with a small ($\sim 70 \mu\text{m}$ diameter) highly diffusing sphere made of titanium dioxide (TiO₂) and methacrylate primers (Kühl and Jorgensen, 1992) attached to a tapered multimode graded F-MLD index silica fiber (Newport Corporation). The resulting regression model (described in section 2.4.1.3) gives a depth-integrated measure of light attenuation. Light availability (E_{PAR}) in each vertical sediment layer (z) is calculated as function of light availability in the overlying sediment layer (E_{z-1}) and the depth-integrated light attenuation coefficient $k_{d(\text{sum})}$ following the formula of Forster and Kromkamp (2004):

$$E_{z,\text{PAR}} = E_{(z-1),\text{PAR}} \times e^{-k_{d(\text{sum})} \times z}$$

2.3.4.4 Photosynthetic parameters

2.3.4.4.1 Photosynthetic parameters over a tidal cycle

A random selection of the PAM fluorometer (Mini PAM; Heinz Walz GmbH) measurements of photosynthetic activity (rETR) described in section 2.3.3.1.2 were used to obtain average values of the photosynthetic parameters α (photosynthetic efficiency) and E_{opt} (optimal light intensity) to be used as model input ($\alpha=0.171 \text{ r.u.}$, $\text{sd}=0.06 \text{ r.u.}$, $\alpha_{\text{min}}=0.06 \text{ r.u.}$, $\alpha_{\text{max}}=0.26 \text{ r.u.}$; $E_{\text{opt},\mu}=779 \mu\text{mol photons m}^{-1} \text{ s}^{-1}$, $\text{sd}=283 \mu\text{mol photons m}^{-1} \text{ s}^{-1}$, $E_{\text{opt},\text{min}}=321 \mu\text{mol photons m}^{-1} \text{ s}^{-1}$, $E_{\text{opt},\text{max}}=1416 \mu\text{mol photons m}^{-1} \text{ s}^{-1}$, $n=17$). The remaining measurements of photosynthetic activity were used for model validation as described in section 2.3.5.1. Rapid light curves were fit using the model of Eilers and Peeters (1988) rewritten by Herlory et al. (2007), as the majority of measured rapid light curves showed photoinhibition at higher light intensities and this model showed a better fit than the model of Platt et al. (1980). The α parameter gives information on the initial slope of the photosynthesis light curve and is known to vary with season and is highest in spring (Pniewski et al., 2015). α is generally higher in low light acclimated algae and lower in low light acclimated algae (Falkowski and Raven, 2007). Moreover, the α parameter may decline under high light (when measured in suspension) (Serôdio et al., 2006). Here, it is assumed that the obtained parameter values of α and E_{opt} are representative for MPB photosynthesis rates during the spring season. Furthermore, we assume that α and E_{opt} do not vary during a tidal cycle, which is supported by the PAM data described in detail in section

2.3.3.1.4 (Wilcoxon test, $p > 0.05$, Figure S1). As can be observed in section 2.4.4, the sensitivity of the model for α and E_{opt} is limited.

2.3.4.4.2 Photosynthetic capacity (P_s)

The photosynthetic capacity (P_s), i.e. the photosynthesis rate at E_{opt} , is modelled as a function of ambient temperature, according to the non-linear model described by (Blanchard et al., 1996):

$$P_s(T) = P_{MAX} \left(\frac{T_{max} - T}{T_{max} - T_{opt}} \right)^\beta \times \exp \left\{ -\beta \left(\frac{T_{max} - T}{T_{max} - T_{opt}} - 1 \right) \right\}$$

with $T \leq T_{max}$ and $T_{opt} < T_{max}$

P_s = photosynthetic capacity ($\mu\text{g C } \mu\text{g}^{-1} \text{ chl-}a \text{ h}^{-1}$)

P_{MAX} = maximum photosynthetic capacity ($\mu\text{g C } \mu\text{g}^{-1} \text{ chl-}a \text{ h}^{-1}$) at T_{opt}

T = temperature ($^{\circ}\text{C}$)

T_{opt} = optimal temperature ($^{\circ}\text{C}$), set to 25

T_{max} = maximum temperature ($^{\circ}\text{C}$), set to 38

β = dimensionless

With this formulation, the maximum photosynthetic capacity P_{MAX} is inhibited at temperatures exceeding the optimal temperature (T_{opt}), which is the temperature at which measured values of the photosynthetic capacity are highest. For model calibration the plots from the dataset described in section 2.3.3.1.2 from May 2015 were used. The measured values of P_s (photosynthetic capacity, Eilers and Peeters, 1988) were multiplied by a conversion factor (EE) in order to approximate carbon fixation rates measured with ^{14}C -labelling as used by Blanchard et al. (1996) to quantify the temperature effect on photosynthetic capacity.

According to Blanchard et al. (1998) T_{opt} is close to 25°C throughout the year. T_{max} is the threshold beyond which no photosynthesis occurs and is estimated by Blanchard et al. (1998) and Morris and Kromkamp (2003) to be ca. $38\text{--}40^{\circ}\text{C}$. P_{MAX} , the value of P_s at the optimal temperature may vary highly throughout the year (Blanchard et al., 1997). β is a dimensionless coefficient that influences the sensitivity of P_s to temperature changes and doesn't vary significantly throughout the year (Blanchard et al., 1997). However, due to the high sensitivity of the model to β and considerable variation in β observed by Blanchard et al. (1997), we used both P_{MAX} and β as calibration parameter, while T_{opt} and T_{max} were set to 25 and 38, respectively. The resulting model ($\beta = 2.75$, $P_{MAX} = 4.98$) explained 40% of the observed variation in field measurements of P_s (Figure S2).

2.3.5 Model validation

2.3.5.1 Validation primary production module

Aerial primary production rates ($\text{mg C m}^{-2} \text{ h}^{-1}$) at the moment of sampling were calculated for nine sites in the Oosterschelde and Westerschelde using the validation dataset described in section 2.3.3.1.1 and 2.3.3.1.2 and using the primary production module described in section 2.3.2.1. Primary production rates were only calculated for points where both PAM fluorescence and satellite data (Landsat 8, 12-03-15) were available to allow comparison of primary production rates calculated with *in situ* versus satellite-based data.

Two combinations of data were used to calculate production:

- (1) Chl-*a* concentrations and mud content derived from Landsat and P_s modelled based on ambient temperature (section 2.3.4.4.2) at the time of sampling ("satellite-based point model").
- (2) Chl-*a* concentrations and mud content based on field samples and photosynthetic parameters were derived from PAM measurements ("*in situ* based point model").

In both the *in situ* based point model and the satellite-based point model, the vertical distribution of chlorophyll-*a* was estimated using the (observed versus modelled) mud content and the vertical distribution of light (k_d) was estimated using the (observed versus modelled) chlorophyll-*a* concentration. Primary production rates were averaged per site and the satellite-based point model (1) was compared to *in situ* based point model (2). An analysis of variance (Kruskal-Wallis) was performed on the *in situ* based point model to test whether *in situ* production rates differed per estuary, site, elevation (low: -1 – 0 NAP, high: 0 – 1 NAP) or weather type (sunny/cloudy, field observations).

Model fit was calculated per estuary using the RMS error, mean error (model minus observation) and a cost function to compare accuracy of model variables in a systematic way (Holt et al., 2005):

$$\chi^2 = \frac{1}{n\sigma_o^2} + \sum (A_m - A_o)^2$$

where A_m and A_o are the modelled and observed variables, n is the number of observations and σ is the standard deviation of observed values. A model is considered to have predictive skill when the χ value is smaller than 1 (Holt et al., 2005).

2.3.5.2 Validation primary production and tide module

Average daily primary production rates were calculated per pixel for the entire study area using the the combined primary production and tide module described in section 2.3.2.2, therefore taking spatial and temporal variability

in emersion duration into account. The validation dataset described in section 2.3.3.1.1 and 2.3.3.1.2 was used to calculate daily production rates averaged over approximately one month (12-03-15 - 10-04-15), which is the time period in which *in situ* measurements of chl-*a*, mud content and RLC's (PAM) were performed. Average daily production rates were calculated per site for points where both *in situ* data and satellite data were available and compared. The ability of the model to capture within site variability was inspected visually by plotting PAM fluorescence based production rates on the map of modelled production rates.

2.3.6 Sensitivity analysis

A sensitivity analysis was performed on the combined primary production and tide module to study the influence of varying one of the model parameters on average daily production rates while keeping other parameters at their nominal values. The sensitivity analysis was performed per tidal system, hence for the Oosterschelde and Westerschelde separately. The following parameters were considered: temperature (which determines P_s), photosynthetic efficiency (α), mud content, chl-*a* concentration, emersion duration and ambient irradiance. The aforementioned parameters were varied from their minimal to maximum value occurring in model input data and were kept constant spatially and over time during a model run, while other parameters are kept equal to the nominal parameter settings. For example, the chosen range to test model sensitivity to ambient irradiance was determined by the days with on average the highest versus the lowest irradiance during the study period (12-03-15 - 10-04-15). During a model run the other parameters vary naturally in space (mud content, chl-*a* concentration, emersion) or vary naturally over time (light intensity, temperature, emersion duration). Model sensitivity was calculated using the difference between the minimum and maximum primary production rate of an estuary (D_{\min} and D_{\max}) caused by varying a parameter over its entire range of possible values as they occur in the model input dataset.

2.4 Results

2.4.1 Model calibration

2.4.1.1 Microphytobenthic biomass

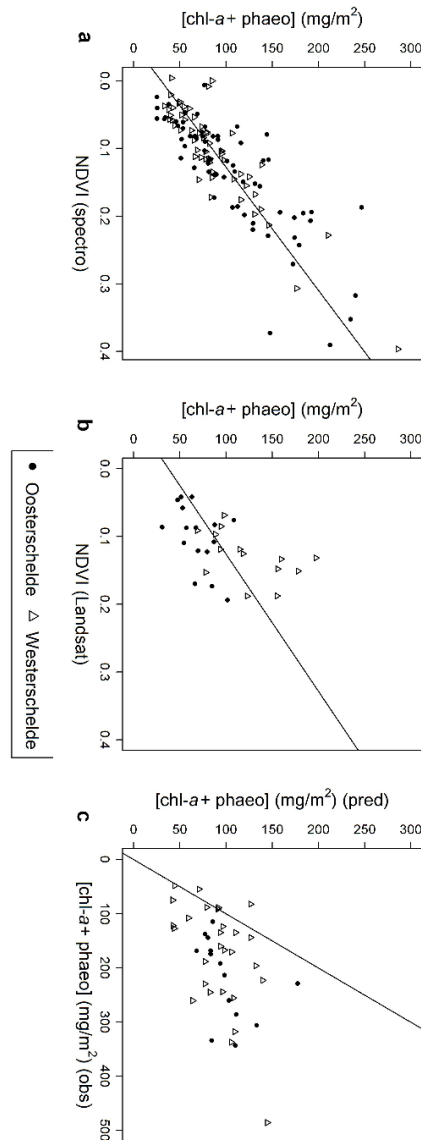


Figure 2. (a) Calibration curve of measured NDVI (Ramses) and sampled chl-a in the upper 2 mm of the sediment ($R^2 = 0.75$, $p < 0.0001$, $n=138$). (b) Calibration curve of NDVI retrieved from satellite remote sensing and sampled chl-a ($R^2 = 0.27$, p -value = 0.002, $n=138$). (c) Sampled chl-a concentrations in the upper 1 cm of the sediment and predicted chl-a concentrations from the NDVI derived from a validation image (Landsat 8, 12-03-2015) using the radiometer-derived regression formula (Pearson's $r = 0.49$, $p < 0.001$, $n=42$). The lines in figure 2a and 2b indicate regression lines, whereas in figure 2c a 1:1 line is

The NDVI retrieved from radiometer measurements was a good predictor of chl-a concentrations sampled below the radiometer ($\text{chl-a} = a \times \text{NDVI} + b$, $a = 556 \pm 36.4$ (95% confidence intervals), $b = 30 \pm 4$, $R^2 = 0.75$, $p < 0.0001$,

n=138, Figure 2a). The model that predicts chl-*a* from satellite-derived NDVI retrieved from pixels located above the same chl-*a* samples gives similar coefficients ($a = 493.8 \pm 160$ $b = 38.5 \pm 18.2$ (95% confidence intervals), $R^2 = 0.27$, p-value = 0.002, n=138, Figure 2b). Both the radiometer-derived and satellite-derived regression models were applied to a validation image (Figure 2c) and gave a similar RMS error ($RMSE_{ramses} = 82.7$, $RMSE_{sat} = 81.3$). Chl-*a* concentrations were somewhat underestimated by both the radiometer-derived model (Figure 2c). As the radiometer-derived regression model is more robust ($R^2 = 0.75$) than the satellite derived model ($R^2 = 0.27$) and covers a wider range of NDVI values, this formula was subsequently applied in the primary production model.

2.4.1.2 Mud content of the sediment

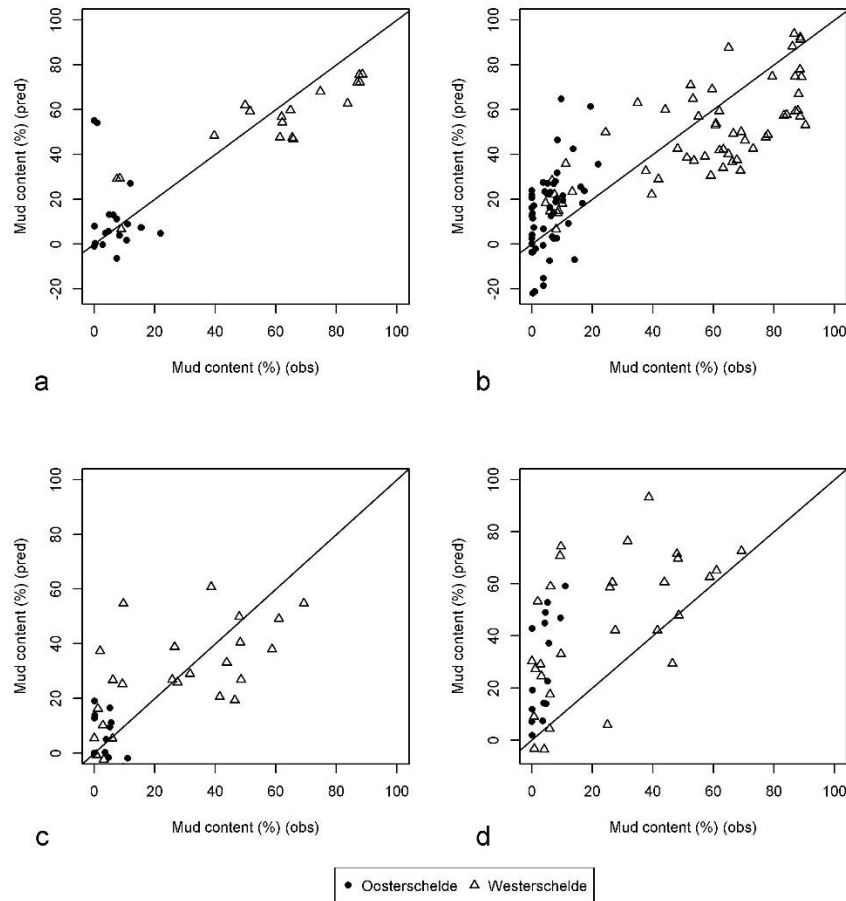


Figure 3. (a) Calibration curve using field measurements of the mud content from random locations in intertidal areas of the Oosterschelde and Westerschelde and predicted mud content from a linear regression using OLI bands R_{blue} and R_{NIR} ($mud = a$

$\times R_{blue} + b \times R_{NIR} + c$. $a = -488 \pm 311$ $b = 1488 \pm 171$ $c = -116 \pm 21$ (95% confidence intervals), $R^2 = 0.72$, $p < 0.001$, Landsat-8, 10-04-2014). (b) Calibration curve using field measurements of the mud content and predicted mud content from a linear regression using *in situ* surface reflectance measured with a radiometer. OLI bands were simulated by multiplying the measured reflectance spectrum with the spectral radiance response of the OLI ($mud = a \times R_{blue} + b \times R_{green} + c \times R_{NIR} + d$. $a = 1978 \pm 628$ $b = -3922 \pm 760$ $c = 2407 \pm 244$ $d = -15 \pm 9.8$ (95% confidence intervals), $R^2 = 0.65$, $p < 0.0001$). (c) Field measurements of the mud content and predicted mud content from a validation image (Landsat 8, 12-03-2015) based on the satellite derived linear regression (Pearson's $r = 0.65$, $p < 0.0001$, Figure 3a). (d) Field measurements of the mud content (obs) and predicted mud content (pred) based on the *in situ* surface reflectance derived linear regression (Pearson's $r = 0.45$, $p < 0.002$, Figure 3b). The lines in figure 3a and 3b indicate regression lines, whereas in figure 3c and 3d a 1:1 line is displayed.

The performed stepwise linear regression with OLI bands R_{blue} , R_{green} , R_{NIR} , R_{SWIR1} and R_{SWIR2} (Landsat 8, 10-04-2014) resulted in a best model (lowest AIC) that included the bands R_{blue} and R_{NIR} ($R^2 = 0.72$, $p < 0.001$, Figure 3a). A stepwise linear regression using simulated bands measured *in situ* with a radiometer gave a best model that included band R_{blue} , R_{green} and R_{NIR} ($R^2 = 0.65$, $p < 0.0001$, Figure 3b). Mud content was overestimated by the *in situ* derived formula when applied to a validation image (Landsat 8, 12-03-2015) (Figure 3d). The OLI-derived formula gave an acceptable fit when applied to the validation image (Pearson's $r = 0.65$, $p < 0.0001$, Figure 3c) and was therefore used in the primary production model.

2.4.1.3 Vertical light distribution

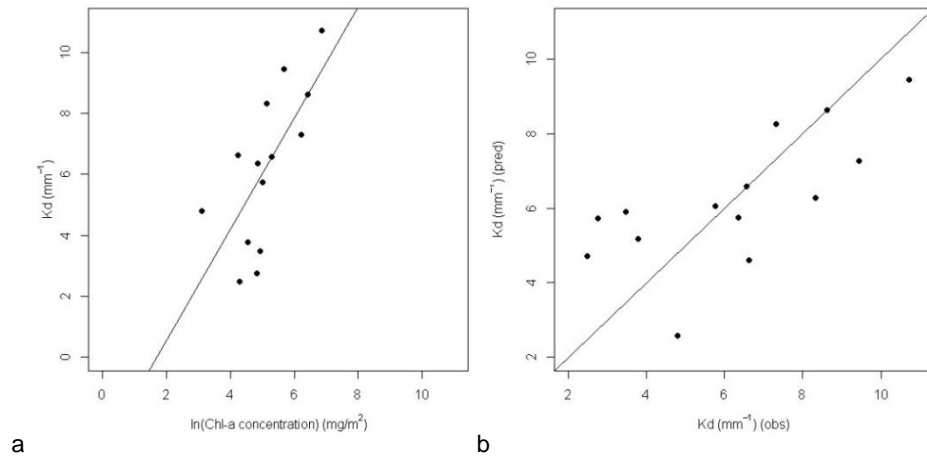


Figure 4. (a) Calibration curve of measured light attenuation as function of chl-a ($k_d = -3.1 \pm 2.8 + 1.8 \pm 0.53 \times \log(chl-a)$ (95% confidence intervals), $p = 0.005$, $n=14$, $R^2 = 0.49$). (b) Measured and predicted light attenuation coefficients (Pearson's $r = 0.7$, $p = 0.005$). The line in figure 4a indicates the regression line, whereas in figure 4b a 1:1 line is displayed.

A stepwise linear regression of light attenuation as a function of chl-*a* concentration, mud content, organic content and moisture content as input gave a best model (lowest AIC) with chlorophyll-*a* as single explanatory factor ($R^2 = 0.49$, Figure 4). Chlorophyll-*a* concentrations were log-transformed to obtain a linear relationship with light attenuation.

2.4.2 Primary production module

2.4.2.1 Satellite-based versus in situ based primary production

The primary production module to calculate hourly primary production rates at sampling time was applied to 7 sites, of which 2 were located in the Oosterschelde and 5 in the Westerschelde (Table 2). The sites Rattekaai (Oosterschelde) and Middelplaat (Westerschelde) were excluded from analysis as none or only a limited number of PAM measurements above the used biomass detection limit ($Ft > 200$ at highest sensitivity settings) were available (Rattekaai: $Ft\ 54 \pm 7$; Middelplaat: $Ft\ 98 \pm 71$). Note that when PAM measurements were below the detection limit, production was likely very low. Stations with a low (< 200) Ft were not associated with a low chl-*a* concentration or mud content. The sites located in the Oosterschelde had low average mud contents ($< 5\%$), but MPB biomass was clearly present (mean chl-*a* concentration: 125 mg m^{-2}). Mean emersion is comparable among sites, but there was a large spread in emersion within sites (9 -20%). In the Westerschelde, average mud contents were low on the mid-channel tidal flats locations ($< 5\%$, Middelplaat and Molenplaat) and higher on the tidal flats located alongside the main channels (17 – 55%).

*Table 2. Site characteristics (mud content, chl-*a* concentration and mean emersion) of validation plots measured in spring 2015. Mean emersion is here defined as the average percentage of time the sites were emersed during the study period (12-03-2015 – 10-04-2015).*

Estuary	Site	Mud content (% < 63 μm)	Chl- <i>a</i> (mg m^{-2})	Mean emersion (%)
Oosterschelde	Dortsman	2.4 ± 2.7	175.4 ± 56.3	62 ± 20
	Rattekaai	4.9 ± 4.3	244.3 ± 64.6	53 ± 16
	Viane	2.9 ± 2.4	208.2 ± 89.1	47 ± 16
Westerschelde	Hellegat	29.3 ± 12.5	294.8 ± 113.5	36 ± 10
	Middelplaat	2.5 ± 2.9	83.6 ± 29.6	37 ± 9
	Molenplaat	4.2 ± 2.2	156.3 ± 75.5	36 ± 10
	Paulina	54.6 ± 11.2	157.3 ± 64.4	35 ± 12
	Rilland	16.9 ± 16.3	113.5 ± 50.8	43 ± 15
	Waarde	34.5 ± 14.7	215.7 ± 95.1	31 ± 18

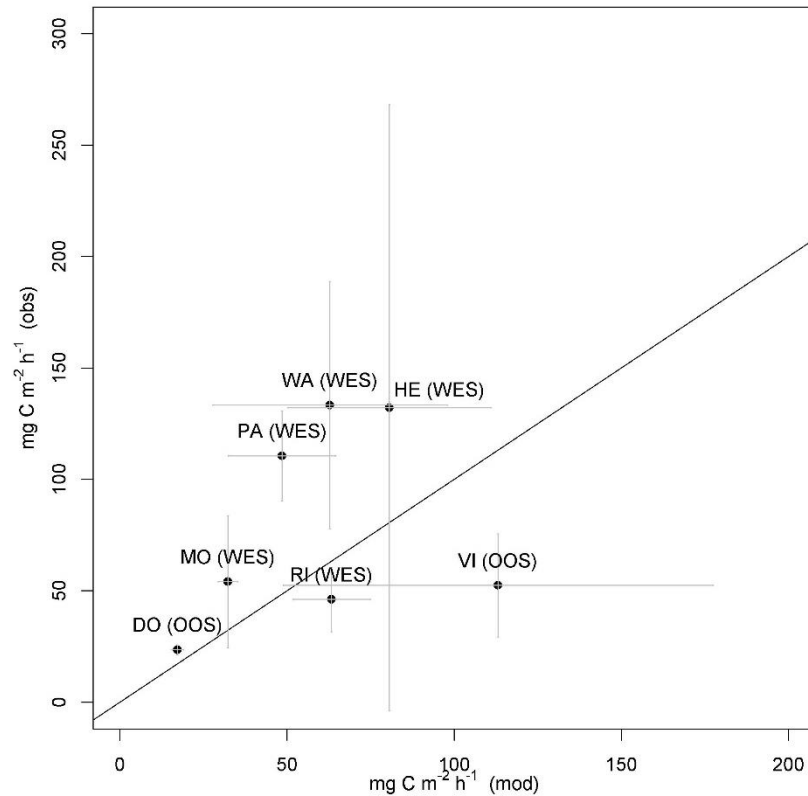


Figure 5. Hourly primary production rates ($\text{mg C m}^{-2} \text{h}^{-1}$) per site at the moment of sampling calculated with the primary production module described in section 2.3.2.1 in the Oosterschelde (OOS) and Westerschelde (WES). Production rates were calculated from (1) chl-*a* concentrations and mud content derived from Landsat and the photosynthetic capacity from ambient temperature (mod) and (2) chl-*a* concentrations and mud content from sediment samples and photosynthetic parameters derived from PAM measurements (obs). Only plots for which PAM measurements were available ($F_t > 200$) were included in both modelled and observed primary production rates; sites Middelplaat (MI) and Rattekaai (RA) were therefore omitted. Sites in the Oosterschelde: Dortsman (DO, $n=2$) and Viane (VI, $n=4$). Sites in the Westerschelde: Hellegat (HE, $n=4$), Molenplaat (MO, $n=4$), Paulinapolder (PA, $n=4$), Rilland (RI, $n=3$) and Waardepolder (WA, $n=5$).

At all sites except Paulinapolder, primary production rates calculated using satellite-based input data were not statistically different from primary production rates calculated using *in situ* based input data (Wilcoxon signed rank test, $p > 0.05$). There was a relatively large spread in primary production rates calculated with *in situ* measurements at Hellegat (HE), which can be attributed to two high values of measured P_s in one of the six plots ($> 4 \mu\text{g C } \mu\text{g}^{-1} \text{chl-}a \text{ h}^{-1}$).

2.4.2.2 Fit of model variables per tidal basin

Model fit expressed as the RMS error, the mean error and a cost function for various model variables are summarized in Table 3. The mud content was predicted better for the Westerschelde ($\chi = 0.8$) than the Oosterschelde ($\chi = 2.6$). The mean error in predicted mud content in both tidal basins was 2.1 and -0.16 in the Oosterschelde and Westerschelde, respectively. Chl-*a* concentrations were somewhat underestimated by the model in both tidal basins with a mean error of -109.1 in the Oosterschelde and -77.2 in the Westerschelde. Primary production rates were predicted better in the Oosterschelde ($\chi = 3.3$) than in the Westerschelde ($\chi = 1.1$).

Table 3. RMSE, mean error and a cost function of modelled mud content, chl-*a* concentration, photosynthetic capacity (P_s) and primary production rates at the moment of sampling per estuary (W: Westerschelde; O: Oosterschelde) in validation plots measured in spring 2015.

Estuary		Mud content (% < 63 μm)	Chl- <i>a</i> (mg m^{-2})	P_s ($\mu\text{mol m}^{-2} \text{s}^{-1}$)	Production ($\text{mg C m}^{-2} \text{h}^{-1}$)
Modelled ($\mu \pm \sigma, n$)	O	5.9 \pm 6.9 n=15	113 \pm 39.4 n=15	36.5 \pm 9.4 n=10	79.3 \pm 66 n=8
	W	24.0 \pm 19.2 n=29	95.4 \pm 30.8 n=29	42.5 \pm 17.5 n=24	59.9 \pm 31.4 n=22
Observed ($\mu \pm \sigma, n$)	O	3.8 \pm 3.4 n=15	222.0 \pm 73.2 n=15	35.5 \pm 14.3 n=10	38.0 \pm 19.9 n=8
	W	24.2 \pm 22.1 n=29	172.2 \pm 97.7 n=29	52.9 \pm 23.6 n=24	105.2 \pm 79.7 n=19
RMSE	O	8.9	69.7	12.2	66.8
	W	17.5	85.4	30.1	89.8
Mean error	O	2.1	-109.1	0.98	41.3
	W	-0.16	-77.2	-15.9	-45.2
Cost function (χ)	O	2.6	1.74	0.85	3.3
	W	0.8	1.17	1.27	1.1

2.4.2.3 Variability in *in situ* data based primary production rates

Spatial variability in *in situ*-based primary production rates at the moment of sampling could be explained by prevailing weather conditions (sunny versus cloudy) (Table 4). In addition, *in situ* production differed significantly between tidal basins and sites. Elevation had no significant effect on primary production rates.

Table 4. Kruskal-Wallis test for in situ production ($\text{mg C m}^{-2} \text{ h}^{-1}$).

	Tidal basin	Site	Elevation low: -1 – 0 NAP high: 0 – 1 NAP	Weather sunny/cloudy
Production	< 0.001	< 0.001	0.416	< 0.001
Chi-squared	27.933	48.794	0.66165	15.829
df	1	6	1	1

2.4.3 Primary production and tide module

The primary production module and tide module combined as described in section 2.3.2.2 were applied to the study area (Figure 6) and validated at nine sites in the Oosterschelde and Westerschelde. The spatial model generally captures variability between sites well (Figure 7), although production rates are somewhat underestimated by the model at sites with high observed primary production rates Paulinapolder, Waarde and Hellegat, Fig. 7).

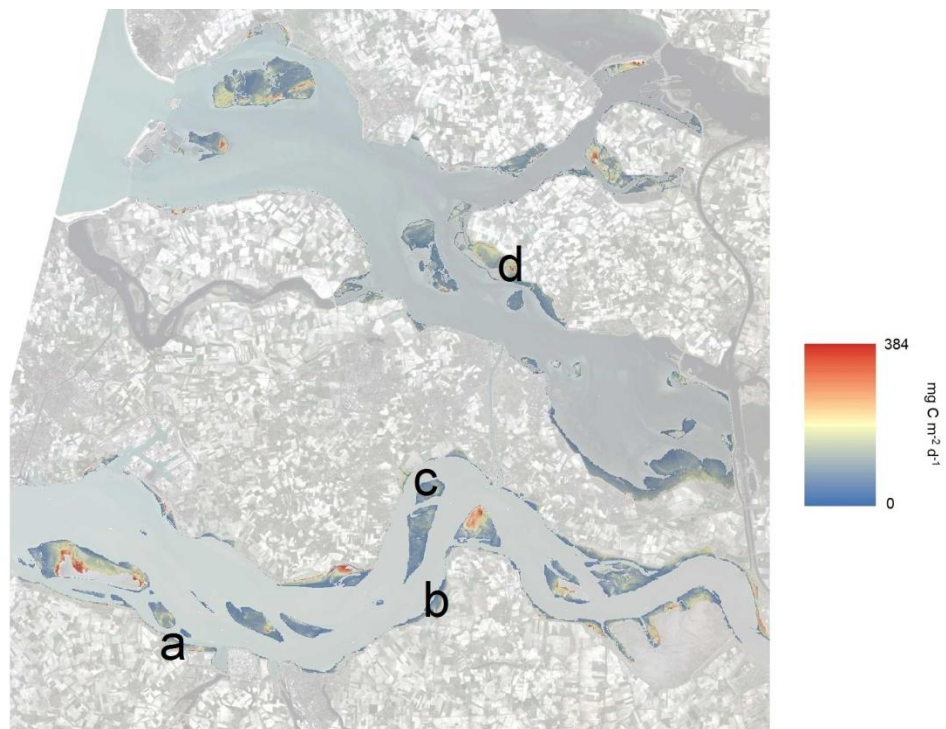


Figure 6. Modelled average daily production in the Oosterschelde and Westerschelde, spring 2015. Daily production values were calculated by running the model for one month (12-03 - 10-04-2015). The letters indicate sites that are shown in detail in Figure 8.

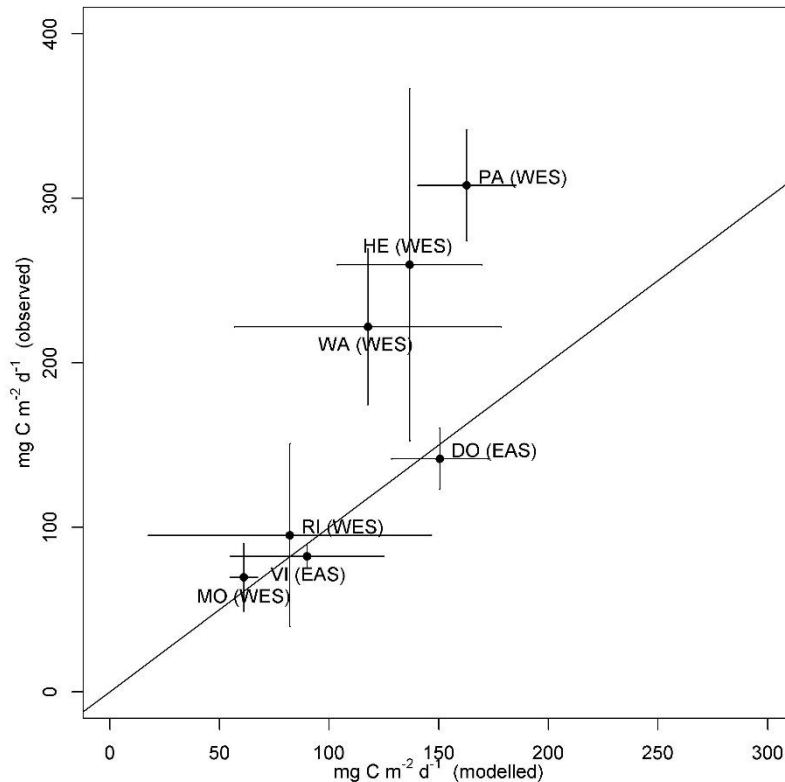


Figure 7. Modelled and observed average daily production (\pm SE) per site. Daily production values were calculated by running the model for one month (12-03-15 - 10-04-2015). Primary production rates were modelled with chl-a concentrations and mud content derived from Landsat 8 (12-03-2015) and the photosynthetic capacity from ambient temperature (mod). Observed primary production rates were calculated using chl-a concentrations and mud content based on field samples and photosynthetic parameters derived from PAM measurements (obs). Only plots for which PAM measurements were available ($F_t > 200$) were included in both modelled and observed primary production rates. Sites in the Oosterschelde: Dortsman (DO, $n=2$) and Viane (VI, $n=4$). Sites in the Westerschelde: Hellegat (HE, $n=4$), Molenplaat (MO, $n=4$), Paulinapolder (PA, $n=4$), Rilland (RI, $n=3$) and Waardepolder (WA, $n=5$).

Within site variability in primary production rates is generally captured (Figure 8). For example, at Paulinapolder a clear gradient is present with decreasing production rates towards the water line, which is reflected by modelled and observed primary production rates.

There is a clear effect of tidal phasing on hourly primary production rates, whereby the tide generates periods of production alternated with periods without production (Figure 9). The exact duration of periods during which production occurs varies with elevation and the tidal range (e.g., spring and neap tides), or can be governed by wind-induced variations in water heights

(Figure 9b). Highest production rates occur during peaks of PAR coinciding with emersion of the tidal flat.

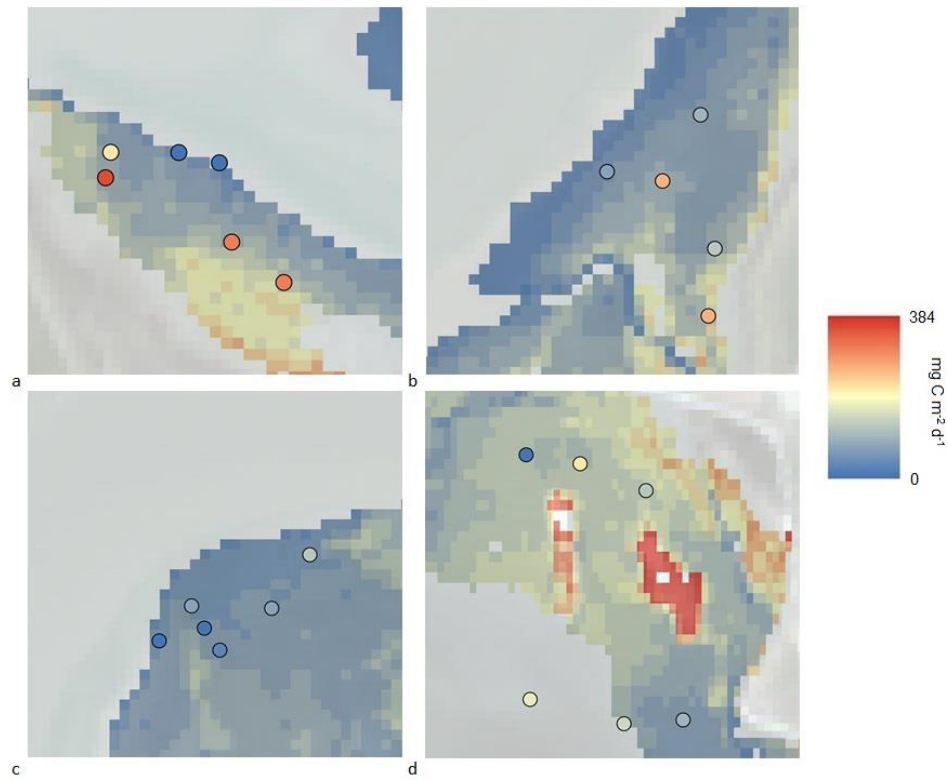


Figure 8. Modelled and observed average daily production at four different sites. a. Paulinapolder, Westerschelde, b. Hellegat, Westerschelde, c. Molenplaat, Westerschelde, d. Dortsman, Oosterschelde. Daily production values based on Landsat 8 (map) and field measurements (dots) were calculated by running the model for one month.

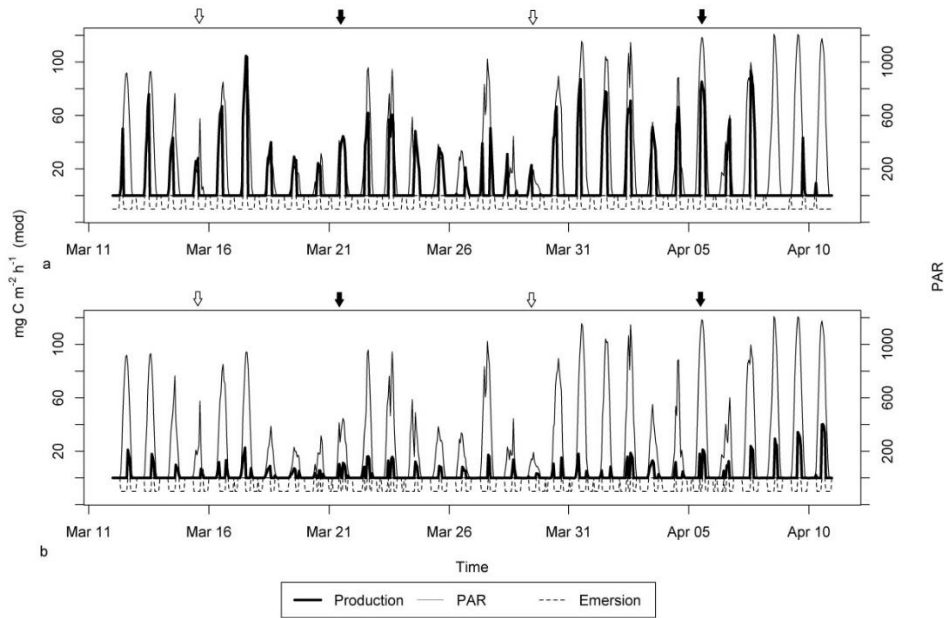


Figure 9. Modelled hourly MPB production rates at a station at Dortsman (chl-*a* concentration: 215 mg/m², mud content: 5.6%, Oosterschelde; Figure 9a) and a station at Molenplaat (chl-*a* concentration: 44 mg/m², mud content: 0.78%, Westerschelde; Figure 9b). The stations are both located at an elevation of -35 to -40 cm NAP. The dashed line displays the hours during which MPB production is assumed to occur (one hour after emersion till immersion). Spring and neap tides are indicated with black and white arrows, respectively. PAR is the photosynthetically active irradiance ($\mu\text{mol photon m}^{-2} \text{s}^{-1}$).

2.4.4 Sensitivity analysis

Model sensitivity of the spatial model for each parameter is approximately linear, except for the photosynthetic efficiency and light intensity which follow a slightly saturating curve (Figure 10). The model is most sensitive to emersion ($S_{\text{oos}} = 7.9$, $S_{\text{wes}} = 6.8$, Table 5) and mud content ($S_{\text{oos}} = 4.8$, $S_{\text{wes}} = 6$, Table 5) and least sensitive to the photosynthetic efficiency ($S_{\text{oos}} = 1.4$, $S_{\text{wes}} = 1.7$, Table 5). Model sensitivity to ambient temperature, chl-*a* concentration and light intensity varies between 1.4 and 3.3.

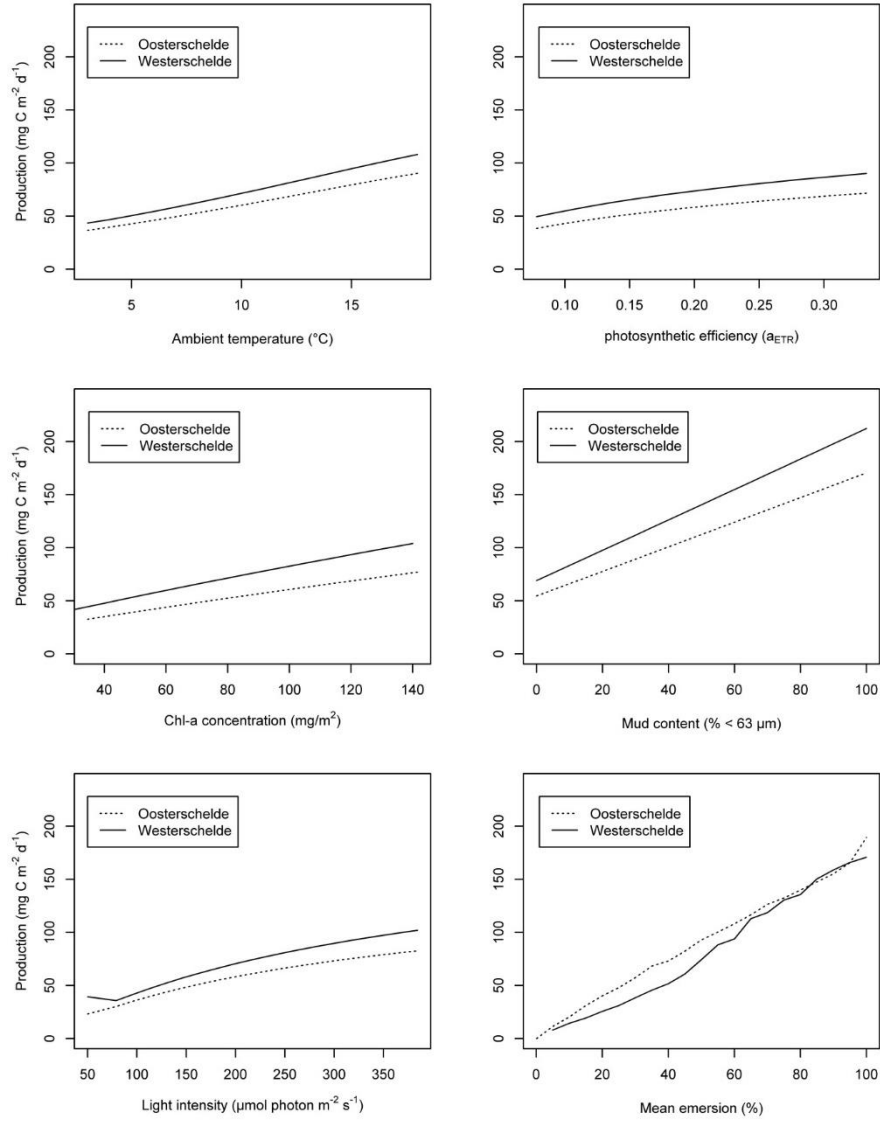


Figure 10. Sensitivity analysis of calculated microphytobenthic primary production rates (mg C m⁻² d⁻¹). Input parameters a and ambient temperature were varied from their minimum to maximum value that occurred in the calibration dataset. The mud content and chl-a concentrations were varied from the minimum to maximum value calculated from the 12-03-2015 Landsat 8 image occurring in the Oosterschelde and Westerschelde and were kept constant spatially and over time. Other parameters were kept equal to the nominal parameter settings.

Table 5. Sensitivity (S , maximum production rate – minimum production rate) for each model parameter.

Estuary	Ambient temperature	Photosynthetic efficiency	Chl- <i>a</i>	Mud content	Light intensity	Emersion
Ooster-schelde	52.8	33.6	33.6	115.2	60	189.6
Wester-schelde	64.8	40.8	79.2	144	62.4	163.2

2.5 Discussion

MPB is known to have a very patchy distribution (Saburova et al., 1995; Spilmont et al., 2011), and this patchiness makes it challenging to upscale production measurements made at the cm scale to the macro (basin) scale. To gain insight in the spatial variability in MPB primary production on the macro scale, a model was developed to calculate MPB primary production rates from satellite remote sensing, ambient temperature and a tide model. Model calibration, results and possible applications for regular monitoring of MPB production are discussed below.

2.5.1 Model calibration

MPB biomass (expressed as chl-*a* concentration) was predicted from the satellite retrieved NDVI using a regression model where chl-*a* concentration was regressed against a radiometer-derived NDVI. Similar regression coefficients were obtained from radiometer-based and satellite-based regression models of chl-*a* as a function of NDVI, which supports the applicability of *in situ* derived relationships between the NDVI and chl-*a* to satellite imagery. Furthermore, the radiometer-derived regression coefficients are very similar to those found by Kromkamp et al. (2006), who sampled chlorophyll-*a* to the same depth (2 mm). Kromkamp et al. (2006) showed that the relationship between NDVI and chl-*a* does not differ among sites or tidal basins (except at one site), which confirms the potential for the use of NDVI as a proxy for MPB biomass.

The satellite-based regression model was less robust than the radiometer-based model. This may partly be associated with a limited representativeness of the sampled surface area (18 cm²) for the spatial resolution of the used Landsat pixels (30 m). The average chl-*a* concentrations of sediment samples frequently have large standard deviations due to the high patchiness of MPB biomass at the centimetre to metre scale. Furthermore, at the subpixel level the NDVI may have been lowered by the presence of surface water pools or raised by the presence of low densities of macroalgae. Application of the radiometer-based regression model to a validation image shows that MPB biomass was predicted well, although chl-*a* concentrations higher than ± 125 mg/m² tend to be underestimated by the model. This may be associated with

a nonlinear relationship between NDVI and chl-*a*. However, no nonlinearity was observed in our calibration dataset. Meleder et al. (2003) found a nonlinear relationship between NDVI and chl-*a* concentrated on microfiber paper, where the NDVI starts to saturate at values higher than 0.4. Serôdio et al. (2009) found the same nonlinear relationship and attributed this to the influence of chlorophyll fluorescence emission at 683 nm (near the red absorption peak) by MPB, which is most pronounced at high MPB biomass levels. However, chl fluorescence is not likely to play a role in our datasets, as the used OLI bands for NDVI (4: 640-670, 5: 850-880) will hardly capture the red light emitted due to chl-*a* fluorescence. Most likely, high small scale spatial variability and possibly unconscious 'selection' of points with a higher MPB biomass leads to incidentally high chl-*a* concentrations in sediment samples used for validation. In the chlorophyll-*a* calibration dataset, a pencil was thrown and sampling was performed at the point the pencil pointed at. However, during collection of the chlorophyll-*a* validation dataset this was not practical, as samples needed to be collected from the edge of a plot.

Lastly, it should be kept in mind that chlorophyll-*a* concentrations were sampled to a depth of 1 cm in the validation dataset, while calibration data was sampled to 2 mm. Although the majority of chlorophyll-*a* is present in the upper 2-3 mm of the sediment (Jesus et al., 2006), significant amounts of chlorophyll-*a* can be present at depths below 2 mm (Pinckney et al., 1993). Therefore, predicted chlorophyll-*a* concentrations are expected to be slightly lower than chlorophyll-*a* concentrations in our validation dataset.

A stepwise linear regression that included all Landsat-8 bands listed in Table 1 resulted in a regression model to predict mud content of the sediment that included R_{blue} and R_{NIR} . The radiometer-based regression model included the same bands (R_{blue} and R_{NIR}) plus R_{green} , but gave different regression coefficients and had less predictive skill than the satellite-based regression model when applied to a validation image (Figure 3d). Van der Wal and Herman (2007) estimated mud content based on a combination of R_{green} and short-wave infrared (SWIR) wavelengths. In our study, the added value of SWIR reflectance for the prediction of mud content (Rainey et al., 2003; Van der Wal and Herman, 2007) did not become apparent.

Depth-integrated light attenuation within the sediment is predicted using empirical data for the first time in this study. A stepwise linear regression using mud content, MPB biomass (chlorophyll-*a* concentration, organic content and water content as possible explanatory variables identified bulk MPB biomass in the upper 2 mm of the sediment as most important predictor. MPB biomass highly correlates with mud content in the used empirical data (Pearson's $r = 0.64$, $p=0.02$). Light attenuation is approximately 2 mm^{-1} in the near absence of algae ($\sim 20 \text{ mg chl-}a \text{ m}^{-2}$) in the calibration dataset, which is in accordance

with earlier measurements in intertidal sediments (Forster and Kromkamp, 2004; Kuhl and Jorgensen, 1994), and increases up to 10 mm^{-1} at chl-*a* concentrations of 617 mg/m^2 . Measured light attenuation coefficients do not correlate with the rate of decline of MPB biomass within the sediment as predicted by Jesus et al. (2006). In highly scattering sands subsurface irradiance peaks may occur (Forster and Kromkamp, 2004; Kuhl and Jorgensen, 1994; Kuhl et al., 1994) which cannot be described with the depth-integrated approach used here.

A conversion factor (EE) of 0.04 was used to convert ETR to carbon fixation rates (an approximation of gross photosynthesis), as suggested by Barranguet and Kromkamp (2000) and confirmed by our own PAM and ^{14}C -uptake measurements. However, the relationship between photosystem II electron transport and carbon fixation can be nonlinear at irradiances exceeding E_{opt} , which may be due to the photo acclimation state of the algae (Lefebvre et al., 2007; Morris and Kromkamp, 2003) or downward migration of epipelagic diatoms during the PAM measurement (Barranguet and Kromkamp, 2000). This may lead to an overestimation of production rates in the presented model at high incident irradiances. However, PAR exceeds E_{opt} only for 10% of the time during the study period. As demonstrated by Barranguet and Kromkamp (2000), limiting ETR values to the maximum value observed at E_k (or E_{opt} , in the present study) can improve the relationship in some (mainly muddy) stations, but this needs further investigation. Furthermore, it has to be kept in mind that carbon fixation rates obtained with ^{14}C -labelling in slurries are potential primary production rates and can overestimate true production rates as the algae are brought into suspension, which optimizes light availability compared to the steep light gradient present on tidal flats (Cadée and Hegeman, 1974) and destroys the chemical gradients in the sediment. For example, sediments may be CO_2 limited due to diffusion (Cook and Roy, 2006; Kromkamp et al., 1995; Oakes and Eyre, 2014), while slurries are not likely to be DIC limited. However, as shown by Barranguet et al. (1998), based on a comparison of primary production measured with ^{14}C -uptake (slurries) and O_2 -microelectrode in intact sediments, this effect seems to be limited.

In the presented model, it was assumed that the photosynthetic efficiency (α) does not vary in space or over a tidal cycle, which was supported by our PAM measurements. Likewise, Uthicke (2006) showed that photosynthetic efficiency of MPB does not vary spatially along a water quality gradient. The photosynthetic efficiency derived from our ^{14}C -uptake measurements appears to be inversely related to ambient irradiance. Earlier studies on variation of α as function of environmental factors give mixed results. The photosynthetic efficiency was shown to occasionally vary during low tide (Kromkamp et al., 1998) and has been linked to light availability (Serôdio et al., 2005; Spilmont et al., 2007). The light response may show a time lag (hysteresis) during

daytime low tides associated with the activation of photoprotective mechanisms, of which the magnitude depends on morning light history (Serôdio et al., 2008).

Sediment desiccation or vertical migration of epipellic diatoms likely complicate the characterisation of variability in the photosynthetic efficiency measured *in situ* leading to a lack of identification of clear ecophysiological patterns thus far (Brotas et al., 2003; Kromkamp et al., 1998; Serôdio, 2004).

For the first time, *in situ* PAM measurements of the photosynthetic capacity (P_s) were linked to ambient temperature. The observed relationship could be fitted using the non-linear model of Blanchard et al. (1996), who have used the formulation to describe short-term (daily) physiological acclimation of microphytobenthos to temperature changes and quantified model parameterisations for different seasons (Blanchard et al., 1997). The retrieved value for β (2.75, dimensionless) after model calibration using PAM measurements performed in May is similar to the values found by Blanchard et al. (1997) in April ($\beta = 3.9 \pm 2.54$) and June (2.07 ± 1.21). The value for P_{MAX} ($4.98 \mu\text{g C } \mu\text{g}^{-1} \text{ chl-}a \text{ h}^{-1}$) is comparable to the value found by Blanchard et al. (1997) in June ($7.56 \pm 0.34 \mu\text{g C } \mu\text{g}^{-1} \text{ chl-}a \text{ h}^{-1}$), and is somewhat lower than the value found by Blanchard et al. (1997) in April ($11.18 \pm 0.42 \mu\text{g C } \mu\text{g}^{-1} \text{ chl-}a \text{ h}^{-1}$), but within the low end of the range observed by Barranguet and Kromkamp (2000). Considerable variation was observed in the relationship between ambient temperature and photosynthetic capacity in the present study, which may be attributed to a discrepancy between ambient temperature and sediment surface temperature. A model to describe sediment surface temperature fluctuations was developed by Guarini et al. (1997), which may improve predictions of the photosynthetic capacity. Necessary parameters include: average daily water temperature, air temperature, wind speed measured at 10 m, air humidity, mud porosity and mineralogy. The model was not applied in the present study, as not all necessary model parameters were measured (i.e., mud surface temperature, porosity and mineralogy). Guarini et al. (1997) point out that mud surface temperature could also be predicted using an empirical relationship between meteorological data and soil surface characteristics, however, this would require a new parameterisation or model formulation at each point and would not be suitable for spatial studies.

2.5.2 Primary production module

Calculation of hourly primary production rates at the moment of sampling per site with the primary production module described in section 2.3.2.1 showed that in most cases (4 out of 7 sites) primary production rates can be predicted quite accurately. At some sites a small (Paulina, Westerschelde) or larger (Viane, Oosterschelde, and Waarde, Westerschelde) discrepancy is observed

between satellite-based versus *in situ*-based production rates, which can be attributed to accumulated errors in the estimation of the chl-*a* concentration or mud content from satellite remote sensing and errors in estimation of the P_s from temperature. For example, at Hellegat (Westerschelde) the P_s was underestimated by the model. As the number of pixels available per site was low (max. 6), performance of the primary production module for separate model variables was evaluated per tidal basin. Mud content was predicted well in the Westerschelde and somewhat overestimated in the Oosterschelde, but the error was small in absolute terms (mean error = 2.1) as the total range of the mud content is 0-100%. Our sensitivity analysis performed with the primary production module combined with the tide module showed that an error in the mud content of 2% would lead to a small change in predicted production rates (approximately $0.1 \text{ mg C m}^{-2} \text{ h}^{-1}$). Chl-*a* concentrations were slightly more underestimated in the Oosterschelde than in the Westerschelde (Table 3), which might be associated with the lowering of NDVI due to the presence of surface water pools that are more abundant on the relatively gently sloping tidal flats than the steeper, better drained tidal flats in the Westerschelde.

An analysis of variance (Kruskal-Wallis test) of the *in situ* production rates showed that production varies with tidal basin, site and weather conditions (sunny/cloudy). The effect of spatial variation in PAR due to clouds on production rates cannot be analyzed using a satellite remote sensing based approach, as a clear sky is needed for image analysis.

2.5.3 Primary production and tide module

In the model it is assumed that no production occurs during immersion. The water turbidity in the Westerschelde is quite high (see section 2.3.1), leading to strong light limitation. However, the water in the Oosterschelde is more clear (see section 2.3.1) and production may continue during immersion. Therefore, production rates modelled with the combined primary production and tide module are likely significantly underestimated in the Oosterschelde, and to a smaller extent in the Westerschelde. Billerbeck et al. (2007) have shown that in the Wadden Sea (The Netherlands) photosynthesis continues during immersion and suggested that benthic photosynthesis may even be enhanced due to increased availability of carbon dioxide and nutrients via pore water flows and a more active metabolic state of MPB in permeable sands. However, as mentioned by Barranguet et al. (1998) this is unlikely to play a role in the MPB communities of the Westerschelde. As mentioned in the model description, the first hour after emersion the diatoms migrate towards the sediment surface, hence a large fraction of the population is below the photic zone or in dim light during immersion. The model assumption that no MPB production occurs during the 1st h after emersion of the sediment likely leads

to an underestimation of true production rates, as migrating algae may start entering the photic zone during this hour. When total production was calculated with:

$$\text{production rate}_{\text{first hour after emersion}} = 0.5 * \text{production rate}_{\text{second hour after emersion}}$$

production rates were 16% and 24% higher in the Oosterschelde and Westerschelde, respectively. The high sensitivity of the model to the inclusion of either none or low primary production rates during the first hour after emersion shows the importance of accurate prediction of vertical migration patterns of MPB within the sediment for the estimation of MPB primary production rates.

Vertical migration mostly occurs in the upper 3 mm of the sediment, whereby about one third of the biomass present in the upper 1 mm migrates (Pinckney et al., 1994). The motility of microalgae is predominantly controlled by the tidal cycle and irradiance (Coelho et al., 2011; Spilmont et al., 2007; Pinckney et al., 1991), but is also known to respond to environmental factors such as temperature (Cohn et al., 2011), nutrient availability in the sub-surface of the sediment (Kingston, 2002) or dessication (Coelho et al., 2009) among other factors (Consalvey et al., 2004). Vertical migration of microalgae is generally modelled as (1) an upward movement shortly after emersion of the sediment, after which the quantity of biomass in the photic zone remains stable (e.g. Guarini et al., 2000), or (2) as function of tides and sun angle (Pinckney and Zingmark, 1991; Serôdio and Catarino, 2000). Pinckney and Zingmark (1991) formulated a curvilinear regression equation to predict biomass-specific MPB productivity from sun angle and tidal stage, assuming that productivity was proportional to the amount of biomass present in the photic zone. Pinckney et al. (2004) showed that migration patterns are indeed highly correlated with predicted production rates following the model of Pinckney and Zingmark (1991). The model was expanded by Serôdio and Catarino (2000) to account for (1) the elevation of the tidal flat with respect to the tides and (2) the amplitude of the migrational movement during each migratory cycle depending on the phase difference between the diurnal and tidal cycle, predicting the largest amplitude of migrational movement during daytime low tides. However, care should be taken in the interpretation of these results, as productivity as well as the extent of vertical migration are associated with light availability. Further research into the mechanisms that determine migration patterns is required; especially the effect of light intensity on vertical movement may be better quantified. Furthermore, spatial models could be optimized by taking into account that in muddy sediments a large fraction of the microalgal community present in the sediment consists of epipellic diatom taxa, whereas in sandy sediments more non-migrating taxa are present (Palmer and Round, 1967; Underwood and Kromkamp, 1999). The present study has shown that

emersion and mud content are important variables in determining intertidal MPB production rates. We demonstrated the effect of tidal phasing on production as low tide at midday brings the longest periods of production, where the production peak height is closely associated with peak values of light intensities. Likewise, Guarini et al. (2002) has emphasized the importance of emersion on the quantification of intertidal MPB production.

It has to be noted that this inference is associated with the assumption that no production occurs during immersion. In the present model, the mud content determines the vertical distribution of the MPB biomass. A higher mud content leads to a stronger exponential decrease of the biomass with depth and therefore a relatively higher concentration of biomass near the surface, where more light is available for production.

2.5.4 Conclusion

Our results clearly show that MPB primary production estimates at high spatial resolution at the estuary scale are possible. Satellite based estimates of MPB biomass compare well with those measured from high resolution spectral measurements. Primary production was estimated by modelling fluorescence-based P_s from temperature data and converting ETR to C-fixation rates.

This approach works well and circumvents the need for many in-situ photosynthesis measurements. Improvements in the estimation of P_s can be made if not ambient temperature, but sediment surface temperature can be estimated from remote sensing data or using the model of Guarini et al. (1997). Further research is required to derive a good estimate of the photosynthetic efficiency (α) from remote sensing techniques or environmental variables. However, our analysis shows that the sensitivity of monthly average production of MPB to photosynthetic efficiency is low which justifies the use of an average value. Our data also corroborate the algorithm to estimate C-based primary productivity from PAM measurements, as the average coefficient EE obtained by Barranguet and Kromkamp (2000) are nearly identical to the ones obtained in this study.

Many factors are potentially important in determining spatial variability in MPB primary production rates, including sediment surface temperature (Guarini et al., 1997), nutrient concentrations (Barranguet et al., 1998) and the position of cells in the upper layer of the sediment (Consalvey et al., 2004). However, due to the high costs associated with monitoring programs it is often not possible to routinely measure all these factors. Our relatively simple model formulation that accounts for spatial variability in vertical distributions of MPB biomass may provide a useful tool to routinely map large scale spatial variability of benthic primary productivity in intertidal areas – which is an

important step towards better understanding of estuarine ecological processes. In addition, the approach offers opportunities to predict the effect of human activities or environmental changes, for example as a result of morphological change, on MPB primary production rates. However, a good calibration and validation of the model is required.

The presented model is suitable to be applied in other estuaries and implemented as operational system. In the present study, further evidence was given that the relationship between NDVI and MPB biomass measured *in situ* may be generic and therefore does not need to be calibrated per image. However, no distinction can be made between microphytobenthos and other photosynthetic organisms that may occur on tidal flats such as macroalgae. Use of the new Sentinel-2 MSI data might allow for this distinction, as more spectral bands are available to discriminate between benthic diatoms and macroalgae (see Kromkamp et al. (2006) for a possible approach), combined with a higher spatial resolution (10 m). For example, a spectral unmixing approach may provide a more generic method for quantification of MPB biomass. This would require a set of radiometric measurements of different photosynthetic organisms and bare sediment present in the estuary of interest. In addition, a higher accuracy in the prediction of mud content is expected with the higher number of spectral bands available from Sentinel-2 MSI. Bathymetries of tidal flats and time series of tidal heights are also required to obtain the timing of emersion versus immersion over approximately one month of time. With this information, hourly production rates can be calculated over this time period and average daily production rates can be obtained for the month of interest. Furthermore, sediment samples from the upper 2 mm of the sediment will need to be collected in the estuary of interest during approximately the same time as image acquisition for calibration and validation of the mud content. Relationships between optical measures and mud content may be estuary specific, due to differences in, for example, drainage which influences total absorption of electromagnetic radiation. The photosynthetic capacity (P_s) can be estimated from ambient temperature or mud surface temperature using e.g. the thermodynamic model of Guarini et al. (1997). For the photosynthetic efficiency (α) an average value of a series of *in situ* PAM fluorescence values may be used, as model sensitivity for the parameter is low, or the parameter may be linked to irradiance.

Acknowledgements

This research was supported by the 'User Support Programme Space Research' of the Netherlands Organisation for Scientific Research (NWO). We gratefully acknowledge Annette Wielemaker for processing of Landsat imagery, Lennart van IJzerloo, Jeroen van Dalen and many others for field assistance, Joeri Minderhoud and Jan Sinke for chlorophyll-*a* analyses, Jetta Vlaming for

performance of the ^{14}C incubations and Sven Ihnken for assistance with processing of PAM fluorescence measurements. The field data and model script used in this study are available via [doi:10.4121/uuid:50e164ef-aaf3-4f77-8adf-c1e10663ce39](https://doi.org/10.4121/uuid:50e164ef-aaf3-4f77-8adf-c1e10663ce39)

Chapter 3 Spatial variability in macrofaunal diet composition and grazing pressure on microphytobenthos in intertidal areas

Tisja D. Dagers, Dick van Oevelen, Peter M. J. Herman, Henricus T. S. Boschker, Daphne van der Wal

STATUS: Published in Limnology and Oceanography (2020) 65, 2819-2834.

3.1 Abstract

Microphytobenthos forms an important part of the diet of macrofauna (macrozoobenthos) in many intertidal ecosystems. It is unclear, however, whether the dependence of macrofauna on microphytobenthos varies spatially within and among tidal systems. We aim 1) to assess the spatial variability in the importance of microphytobenthos in the diet of macrofauna (i.e., between and within two tidal basins and as function of elevation), 2) to quantify grazing pressure of the macrofaunal community on different potential food sources (microphytobenthos, phytoplankton and terrestrial organic material) for several sites in two tidal basins and 3) to compare microphytobenthos production and summer/autumn grazing of the total macrofaunal community and grazing pressure per feeding type, with potential microphytobenthos production estimated from rates in early spring, when grazing was low. Using a natural stable isotope approach, we identified microphytobenthos as a more important food source for macrofauna than phytoplankton and terrestrial organic material. Microphytobenthos dependency differed between tidal basins for the genera *Bathyporeia* (sand digger shrimp), *Macoma* (Baltic tellin) and *Peringia* (mudsnail) and for sampled individuals of all genera combined, and did not vary as function of elevation. We showed that macrofaunal grazing on microphytobenthos is quantitatively important and, in some cases, approached microphytobenthos production rates in early spring. No positive relation between microphytobenthos production in early spring and macrofaunal grazing in summer/autumn was observed. This suggests that the studied consumer-resource interactions are coupled on a larger spatial scale (i.e. mesoscale, ≈ 10 to 100 kilometers), rather than the fine (mm to m) scale.

Key words: Tidal flats; macrobenthos; stable isotopes; intertidal food web; estuary, microphytobenthos; phytoplankton; diet composition; spatial variability; primary production

3.2 Introduction

Understanding food webs is highly relevant for assessments of the impact of environmental changes (e.g. eutrophication, erosion or sea level rise) on aquatic ecosystems (Middelburg, 2014). Benthic primary producers or microphytobenthos (microphytobenthos), consisting of unicellular eukaryotic algae and cyanobacteria, can form a significant part of total estuarine primary production (Underwood and Kromkamp, 1999). Microphytobenthos provides an important source of organic material for benthic micro-, meio- and macrofauna on intertidal flats (Middelburg et al., 2000; Christianen et al., 2017). Benthic macrofauna, in particular, form an important link to higher trophic levels, such as birds and carnivorous fish in estuaries (Heip et al., 1995).

Microphytobenthos can also form an important part of the diet of suspension feeders, as the activity of waves and tidal currents may induce resuspension of surface sediments and associated microphytobenthos (Christianen et al., 2017). Other possible food sources available for macrofaunal species include saltmarsh vegetation (Galván et al., 2008), macroalgae, phytoplankton and terrestrial organic material (Kang et al., 2006). Furthermore, carbon originating from DOC may be transferred to macrofauna via microbenthos (Van Oevelen et al., 2006).

The diet composition and trophic level of macrofauna can be studied using carbon and nitrogen stable isotopes (Peterson and Fry, 1987). A limited number of studies have reported on the spatial variation in the relative importance of microphytobenthos in the diet of macrofaunal species. The relative importance of phytoplankton in the diet of the semelid bivalve *Theora Lubrica*, which inhabits estuarine subtidal sediments, increases seaward in Gokasho Bay, Japan (Yokoyama, 2003). Furthermore, the proportion of macroalgae in the diet of herbivores was found to increase with the availability of these macroalgae among three sub-estuaries (Olsen et al., 2011). Christianen et al. (2017) demonstrated large spatial heterogeneity on the scale of tens of kilometers in the contribution of microphytobenthos in the diet of macrofaunal species in the Wadden Sea (the Netherlands), which could, however, not be attributed to a specific factor. In estuaries, major abiotic gradients are presently associated with distance from the estuarine mouth (salinity, temperature, hydrodynamics and sediment composition) and gradients from tidal flats to subtidal channels (elevation and hydrodynamics, and resulting depth of overlying water and sediment composition of the bed) (Van der Wal et al., 2017). Some papers have used the spatial distribution and temporal dynamics of microphytobenthos biomass to correlatively explain patterns in macrofaunal species composition (e.g., Van Colen et al., 2008) and macrofaunal biomass (Van der Wal et al., 2008). However, it is not yet clear if

and how the dependence of macrofaunal species on microphytobenthos differs between tidal basins, or varies with the aforementioned abiotic gradients.

Field experiments where macrofauna were removed showed that macrofauna can exert significant top-down control on microphytobenthos and thereby constrain microphytobenthos biomass (e.g. Weerman et al., 2011). Pratt et al. (2015) found a negative relationship between recent deposit feeding activity of the bivalve *Macomona liliana* and microphytobenthos biomass at a scale of 10s of meters in a subtropical Manukau Harbour, New Zealand. Grazing pressure can be quantified using ^{13}C -labelling (Herman et al., 2000). Middelburg et al. (2000) showed at a relatively sandy tidal flat in the Westerschelde estuary (southwest Netherlands) that during a period of 2.4 days half the amount of labelled microphytobenthos was removed, of which 40% was respired and 60% was resuspended. However, Middelburg et al. (2000) emphasized that the resuspended fraction may depend on weather conditions and bioturbation by macrobenthos, while the respired fraction may depend on the benthic community composition. Moerdijk-Poortvliet et al. (2018) found large (temporal) variation in the net loss of carbon fixed recently by microphytobenthos in the Oosterschelde (southwest Netherlands).

Microphytobenthos biomass shows a strong temporal variability in temperate regions, which is often seasonal (Sundbäck et al., 2000), although exceptions are found (Thornton et al., 2002). In the Westerschelde, a microphytobenthos bloom generally occurs in March/April and disappears in May/June likely due to top-down control (Weerman et al., 2011). Recruitment of larvae (using microphytobenthos) starts approximately in May (Van Colen et al., 2008). After larval recruitment, macrofauna is relatively sessile (Herman et al., 1999). Estuary scale averages of microphytobenthos production measured in June have been linked to averages of the proportion of macrofaunal biomass that depends on microphytobenthos (macrofauna sampled in June one year after microphytobenthos production was measured) (Herman et al., 2000). It is unclear, however, to what extent microphytobenthos production and macrofaunal grazing pressure are linked on smaller spatial scales (within tidal basins).

In this research, we aim 1) to assess the spatial variability in the importance of microphytobenthos in the diet of macrofauna using a natural stable isotope approach, 2) to quantify grazing pressure of the macrofaunal community on microphytobenthos, phytoplankton and terrestrial organic material for several sites in two tidal basins and 3) to quantify the (indirect) relationship between microphytobenthos production in early spring (when grazing pressure is still low) and grazing pressure of the total macrofaunal community and of separate macrofauna feeding types in summer/autumn. The study is conducted in two contrasting tidal basins in terms of species assemblages and salinity (Ysebaert et al., 2003), at contrasting elevations in the tidal zone (high and low). For the

first aim, we hypothesize that the relative importance of microphytobenthos in the diet of macrofauna only varies for suspension feeders and facultative suspension/deposit feeders, depending on spatial variability in the availability of microphytobenthos and phytoplankton. Furthermore, it is hypothesized that the relative importance of microphytobenthos in the diet of macrofauna increases with elevation, as the availability of microphytobenthos biomass is typically positively linked to elevation (Van der Wal et al., 2010). For the third aim, we hypothesize that grazing pressure of the total macrofaunal community sampled in summer/autumn depends on initial microphytobenthos production in early spring. Microphytobenthos production in early spring may be a proxy for potential food availability for macrofauna in summer/autumn, as during early spring the influence of grazing by macrofauna on spatial variability in microphytobenthos production is limited (Weerman et al., 2011).

3.3 Methodology

3.3.1 Study sites

The study was performed in the Westerschelde estuary and Oosterschelde tidal basin in the Netherlands, two mesotrophic, tide-dominated systems (Fig. 1). The Westerschelde estuary has a salinity gradient varying from mesohaline at the Dutch-Belgium border to polyhaline at the mouth. It has an intertidal surface area of approximately 70 km² (Van der Wal et al., 2010) and a total surface area of about 312 km² (22% intertidal area). In the Westerschelde, phytoplankton productivity varies from approximately 100-300 g C m⁻² y⁻¹ along the estuarine gradient (10 – 30‰) (Kromkamp et al., 1995). Deposit feeders form an important part of the total biomass of macrofauna in the (eastern part of) the Westerschelde (Ysebaert and Herman, 2002) and the biomass of suspension feeders is relatively low (41%, Herman et al., 1999).

The Oosterschelde is a polyhaline, semi-enclosed sea-arm, only closed at the mouth during storms, and with only very limited river input (Nienhuis and Smaal, 1994). The Oosterschelde has an intertidal surface area of approximately 50 km² (Van der Wal et al., 2010) and a total surface area of around 350 km² (14% intertidal area). It has a phytoplankton productivity of approximately 155 g C m⁻² year⁻¹ (Smaal et al., 2013). Suspension feeders compose a relatively large part (82%) of the total macrofaunal biomass; the remaining biomass mainly consists of deposit feeders (Herman et al., 1999).

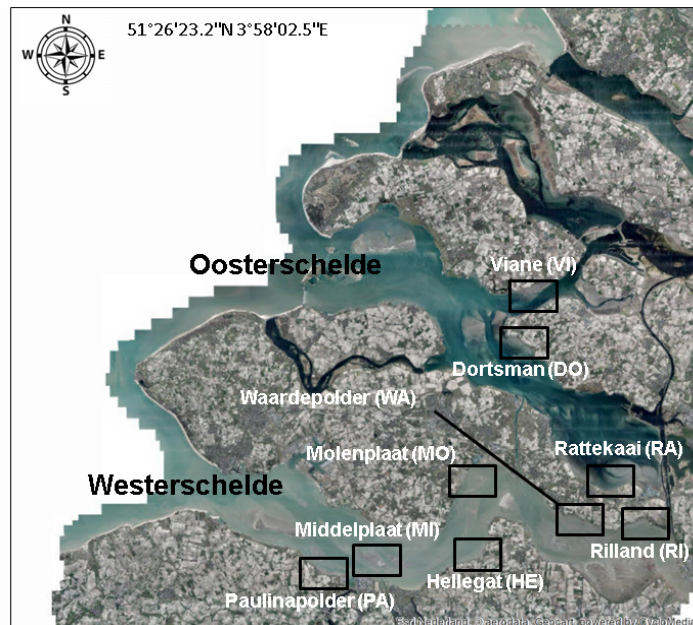


Figure 1. Selected study sites in the Oosterschelde and Westerschelde, southwest Netherlands, with center coordinates.

3.3.2 Field methods

Sampling stations were selected from a set of existing stations, from which historical macrofauna data were available. The density and biomass of the historical macrofauna data was used to calculate macrofaunal grazing pressure, along with macrofauna samples collected in this study to determine the macrofaunal diet composition using natural stable isotopes. A stratified random selection was applied within the zone -1 to 0 m NAP ('low' elevation; where NAP is Dutch Ordnance level, approximately mean sea level) and within the zone 0 to 1 m NAP ('high' elevation). Six study sites were selected in the Westerschelde and three sites in the Oosterschelde (Fig. 1). A historical macrofauna community composition dataset was collected by the Royal Netherlands Institute for Sea Research (NIOZ) for Rijkswaterstaat yearly in summer/autumn (August – October, 2003-2012) in the BIOMON programme using a 15 cm diameter cylinder corer, up to a depth of 30 cm, and sieved on a 1 mm mesh size sieve. In this data set, in the Oosterschelde, samples were collected at the same stations each year while in the Westerschelde a fixed number of samples was collected randomly from each ecotope each year (Bouma et al., 2006). For our field campaigns (see below), 26% of our selected stations were not sampled at the exact same location as NIOZ/Rijkswaterstaat sampling stations due to limited data availability, but within a distance of 300m. Macrofaunal species distributions are strongly related to sediment grain size distributions (Van der Wal et al., 2008) and are relatively homogeneous

in fine sands at scales from 50 cm to 500 m, but more heterogeneous at distances of >50m in muddy sediments (Kendall and Widdicombe, 1999; Ysebaert and Herman, 2002). The density and biomass of the macrofauna community sampled by NIOZ/Rijkswaterstaat from August – October were used to calculate the grazing pressure of the macrofauna community on selected food sources.

Field work was carried out in 2015 in the early spring (Hellegat: 12 Mar; Waarde: 13 Mar; Paulina: 23 Mar; Dortsman: 24 Mar; Rilland: 27 Mar; Rattekaai: 3 Apr; Molenplaat: 7 Apr; Viane: 8 Apr; Middelpaat: 10 Apr) and late spring (Hellegat: 4 May; Paulina: 7 May; Dortsman: 18 May; Rilland: 21 May; Waarde: 22 May; Rattekaai: 26 May; Viane: 1 Jun; Molenplaat: 3 Jun; Middelpaat: 8 Jun). At each station, one high and one low elevation plot of 16 m² each was marked. Within a plot, three sediment cores (ø 15 cm) were taken during both sampling periods up to a depth of 1 cm using a 3 cm diameter syringe for the analysis of grain size distribution and chlorophyll-*a* content, which was used to calculate microphytobenthos production. Sediment samples up to a depth of approximately 1 cm were collected with a spoon for phospholipid derived fatty acids PLFA extractions for analysis of the $\delta^{13}\text{C}$ of PLFAs characteristic for diatoms. In addition, sediment samples up to a depth of approximately 1 cm were collected with a spoon for stable isotope analysis ($\delta^{13}\text{C}$ and $\delta^{15}\text{N}$) of bulk sediment. Water (3-L jars) was collected at each site during low tide at the edge of the tidal flat for the analysis of the stable isotope composition of Suspended Particulate Organic Matter (SPOM) as indicator for phytoplankton. It has been demonstrated that the $\delta^{13}\text{C}$ of POC in the water column ($\pm -26\text{‰}$) deviates little from the isotopic signature of phytoplankton (-30‰) in the middle part of the Westerschelde considered in this study (Hansweert and Zandvliet; Van den Meersche et al., 2009). Also Currin et al. (1995) report similar values of the $\delta^{13}\text{C}$ of suspended particulate organic matter and phytoplankton. In the Oosterschelde, no riverine input of organic material is present and, consequently, terrestrial organic material is scarce. Therefore, the isotopic signal of SPOM was assumed to be representative for the isotopic signal of phytoplankton in the Oosterschelde. Suspended particulate organic matter (SPOM) is a frequently used indicator for phytoplankton (Galván et al., 2008).

Photosynthetic activity was measured in each plot in triplicate by constructing a rapid light curve (RLC) using a Pulse Amplitude Modulation (PAM) fluorometer (Mini PAM; Heinz Walz GmbH). In late spring, species of macrofauna that were most commonly observed in the NIOZ/Rijkswaterstaat dataset were collected using three sediment cores (ø 15 cm) per plot for analysis of the diet composition using natural stable isotopes. Cores were sieved on a 1 mm mesh size sieve and stored in open jars containing water collected on site, to keep benthic species alive (to preserve the isotope signal without transporting ice

into the field). The ragworm *Hediste diversicolor* was kept in separate jars to prevent the species from predating on other specimens. After returning to the lab, the water was removed and macrofauna samples were stored frozen (-20°C).

3.3.3 Laboratory methods

Sediment samples were transported in ice and stored in -80°C within eight hours after sampling. Sediment samples were freeze dried for minimally 48h and the dry bulk density of sediment samples was determined gravimetrically. Of each sediment sample, 700 mg was used for pigment analysis. 10 ml acetone (90%) and glass beads were added to extract photosynthetic pigments using a cell homogenizer (Braun, Type 8530220) for 20 seconds. Subsequently, the extract was centrifuged (2000 rpm, 3 min) at 20°C immediately after homogenization and light absorption was measured with a Specord 210 spectrophotometer. Chlorophyll-*a* content ($\mu\text{g/g}$) was calculated according to the equation described in Ritchie (2006) and also includes phaeopigments. These were converted to chlorophyll-*a* concentrations (mg/m^2) using the dry bulk density. The sediment grain size distribution was determined using a Malvern (laser) particle sizer.

PLFAs were extracted from approximately 6 g of wet sediment using a modified Bligh and Dyer extraction (Boschker et al., 1999). The followed procedure is described in detail in Middelburg et al. (2000). Fatty acid methyl esters (FAME) were identified based on the comparison of the retention time of sampled FAME with internal FAME standards (12:0, 16:0 and 19:0). The isotopic composition of FAME was measured with a Varian 3400 gas chromatograph containing a Varian SPI injector, which was coupled to a Finnigan Delta S isotope ratio mass spectrometer via a type II combustion interface. Carbon isotope ratios of the PLFAs were corrected for the addition of one carbon atom in the methyl group during derivatization. The carbon isotope ratios of the 16:2 ω 4, 20:5 ω 3 and 22:6 ω 3 fatty acids were used as proxy for the carbon isotope composition of benthic diatoms. The fatty acids are characteristic for diatoms, dinophytes and haptophytes (Dijkman and Kromkamp, 2006) and are a suitable indicator for microphytobenthos at our study site, as microphytobenthos assemblages are generally dominated by diatoms in the Scheldt estuary (Sabbe and Vyverman, 1991). Fractionation within the diatom cell was accounted for by adding 5.4 per mil to the $\delta^{13}\text{C}$ of 16:2 ω 4, according to Schouten et al. (1998). Fractionation factors within the diatom cell of 20:5 ω 3 and 22:6 ω 3 were calculated using the ratio between $\delta^{13}\text{C}$ values of 16:2 ω 4 and 20:5 ω 3 (1.07 ± 2.21), and 16:2 ω 4 and 22:6 ω 3 (2.1 ± 2.81) in the dataset used in this study. The $\delta^{13}\text{C}$ of diatom cells was calculated as the weighted average of measured $\delta^{13}\text{C}$ values of the three fatty acids using the relative concentrations as weights.

Water samples for determination of the isotopic composition of SPOM were filtered onto a glass fiber filter (Ø47 mm, Whatman ref no 421026). The $\delta^{13}\text{C}$ and $\delta^{15}\text{N}$ of bulk suspended particulate matter and bulk sediment material was measured using a Fisons elemental analyzer coupled to a Finnigan delta S isotope ratio mass spectrometer after samples were acidified using an *in situ* acidification method to remove inorganic carbonates (Nieuwenhuize et al., 1994).

To test whether spatial variability exists in the diet of macrofauna, ten common species were selected as target species (see Table S2) and retrieved from macrofauna samples collected at 'high' and 'low' sampling stations in late spring. Hereby, we ranked the species according to their occurrence in the highest number of locations, based on abundance data in the historical macrofauna dataset (2003 – 2012) collected by the Royal Netherlands Institute for Sea Research (NIOZ) and Rijkswaterstaat from the Westerschelde and Oosterschelde combined. It was ensured that all feeding types were represented in the species selection. Feeding types were retrieved from the historical macrofauna dataset and updated using recent literature. *Macoma* was considered a facultative suspension/ deposit feeder (Rossi et al., 2004). From each plot, three individuals of each target species present in the sample were retrieved, identified to genus level, pooled, and freeze dried for minimally 48h. *Macoma balthica* was divided into three size classes: 5-10, 10-15 and > 15 mm shell length, and pooled per size class for stable isotope analysis. *Macoma balthica* may show a gradual shift in diet with small juveniles feeding entirely on microphytobenthos and larger individuals depending more on phytoplankton (Rossi et al., 2004). Soft parts of the bivalves were removed from the shells and the mudsnail *Peringia ulvae* was treated with 2 N HCL to remove inorganic carbonates. Gut contents were not removed. Herman et al. (2000) demonstrated that gut contents had a minimal influence on the bulk $\delta^{13}\text{C}$ of macrofauna; even after tracer addition with high $\delta^{13}\text{C}$ of the food, the influence of the gut content on the $\delta^{13}\text{C}$ of the bulk organism was 1-5% after 4 days in their study. Therefore, the influence of natural gut contents can be considered negligible (Rossi et al., 2004).

3.3.4 Modelling

3.3.4.1 Calculation of microphytobenthos primary production

The rapid light curves measured with the PAM in early spring 2015 were fit using the model of Eilers and Peeters (1988) rewritten by Herlory et al. (2007) for all measurements above the detection limit: $F_t > 200$. This yielded the photosynthetic activity (α) and photosynthetic capacity (P_s). Microphytobenthos production rates were then calculated based on these two parameters, as well as incident irradiance, chlorophyll-*a* concentrations and

mud content (% particles < 63 μm) as described in Daggers et al. (2018) and Daggers et al. (2019). Monthly averages of daily microphytobenthos production rates were calculated using a sediment-optical model, taking into account temporal variability in irradiance and emersion duration (as a function of tides and bathymetry); production during immersion was modelled using light attenuation values within the water column measured at the nearest monitoring stations averaged over the period 2011-2016 (Daggers et al., 2018; Daggers et al., 2019). Daily production rates were calculated over one month corresponding to the sampling period.

3.3.4.2 Estimation of macrofaunal diet composition

The fraction of microphytobenthos in the diet of macrofauna sampled in late spring was estimated assuming that the isotopic signature of macrofauna is a weighted average of its food sources, plus a fractionation factor. A Bayesian mixing model (MixSIAR; Stock and Semmens, 2013) was used to estimate the proportional contribution of food sources to the diet of macrofauna from the $\delta^{13}\text{C}$ and $\delta^{15}\text{N}$ in the Oosterschelde and Westerschelde. The diet composition was estimated for each selected (most common) species per site per elevation category. $\delta^{13}\text{C}$ values of microphytobenthos were determined from PLFAs extracted from sediment sampled in each plot. To obtain $\delta^{15}\text{N}$ values of benthic algae, $\delta^{15}\text{N}$ values of bulk sediment were used +2‰ for the Oosterschelde and +10‰ for the Westerschelde, using the difference between SOM (Sedimented Organic Matter) and benthic algae in the Oosterschelde and Westerschelde reported by Riera et al. (2000). The average values of the $\delta^{15}\text{N}$ of the sampled bulk sediment in the Oosterschelde ($6.7 \pm 0.9\text{‰}$, $n=18$) and Westerschelde ($9.1 \pm 1.3\text{‰}$, $n=36$), respectively, closely resembled the average $\delta^{15}\text{N}$ of the SOM in the Oosterschelde ($7.3 \pm 0.1\text{‰}$, $n=3$) and Westerschelde ($8.6 \pm 0.2\text{‰}$, $n=8$) reported in Riera et al (2000). As proxy for phytoplankton, $\delta^{13}\text{C}$ and $\delta^{15}\text{N}$ values of bulk suspended particulate matter from the site of interest and the two nearest sites were used. $\delta^{13}\text{C}$ and $\delta^{15}\text{N}$ values of the macroalgal genus *Ulva* which dominates macroalgal spring blooms in the Oosterschelde (Rossi, 2006) derived from Riera et al. (2002) were added as potential food source in the Oosterschelde. Diet compositions were calculated with and without inclusion of macroalgae in the Oosterschelde. In the Westerschelde, macroalgae predominantly occur on hard substrates and hardly contribute to the diet of macrofauna present on these structures (Riera et al., 2004). Therefore, their contribution to the diet of macrofauna on tidal flats is expected to be even lower. $\delta^{13}\text{C}$ and $\delta^{15}\text{N}$ values of terrestrial organic matter in the water column near Antwerp in April, May and June were added as potential food source in the Westerschelde, as the estuary received large amounts of terrestrial organic material throughout the year (Van den Meersche et al., 2009). In the Oosterschelde, the input of terrestrial organic material is low (Nienhuis and Smaal, 1994). It has been demonstrated that the contribution

of saltmarsh plants to the diet of macrofauna on mudflats in front of a saltmarsh is low (Galván et al., 2008). Therefore, saltmarsh plants were not included as possible food source in the dual stable isotope analysis. We examined visually whether $\delta^{13}\text{C}$ and $\delta^{15}\text{N}$ values of macrofauna were in between values of $\delta^{13}\text{C}$ and $\delta^{15}\text{N}$ values, to check whether all possible food sources were taken into account.

The Bayesian mixing model accounts for uncertainty associated with multiple resources, fractionation values and isotope signatures (Parnell et al., 2013). The analysis was performed in the R package MixSIAR (v3.1.7; Stock and Semmens, 2013). In the isotope mixing model, we assumed an isotopic shift between diet and consumer of C of $0.3 \pm 0.14\text{‰}$ and of N of $2.2 \pm 0.3\text{‰}$ following McCutchan et al. (2003). Isotopic shift of N is known to vary among species, but an average isotopic shift of N of +2.2 is supported by a number of studies measuring isotopic shift of N in marine organisms (Dittel et al., 1997; Macko et al., 1982). As we were interested in the total grazing pressure on microphytobenthos, we assumed that only one trophic level was present in the calculation of diet coefficients. The method uses Markov Chain Monte Carlo (MCMC) algorithms to calculate a posterior probability distribution of the proportion of each resource in the diet of a macrofaunal species. The default parameters for MCMC were used ("very long" option, with three parallel chains, 300,000 iterations for each chain). We used the Gelman-Rubin and Geweke diagnostics to test whether the MCMC converged on the posterior distributions for all calculated diet contributions.

3.3.4.3 Estimation of macrofaunal grazing pressure

Grazing pressure of the macrofaunal community (Grazing_{com}) on microphytobenthos, phytoplankton and terrestrial organic material was calculated for each station using a simple energy budget model for each species that was based on an allometric relation for respiration (Soetaert and Van Oevelen, 2009). Mahaut et al. (1995) found the following allometric relation for biomass-specific respiration (d^{-1}): $0.0174 \times \text{biomass}_{\text{spec}}^{-0.156}$, in which $\text{biomass}_{\text{spec}}$ is the individual mass. The total C demand for a species is calculated by multiplying the biomass-specific respiration by the areal biomass (mg C m^{-2} , derived from macrofauna samples of NIOZ/Rijkswaterstaat) and subsequently dividing by the assimilation efficiency (AsE), to include the non-assimilated matter in the C demand, and by $(1-\text{NGE})$, in which NGE is net growth efficiency, to include biomass production in the C demand (Soetaert and Van Oevelen, 2009). The microphytobenthos grazing for each species is subsequently calculated by multiplying the total C demand by the microphytobenthos diet fraction (i.e. the results from the isotope data). In summary,

$$Grazing_{com} = \sum_{spec=1}^n \frac{1.74 \times 10^{-2} \times biomass_{spec}^{-0.156} \times biomass_{com} \times Food_{coef,spec}}{(1 - NGE) \times AsE}$$

Assimilation efficiencies were derived from the review of AsE and NGE values for macrofauna in shallow marine ecosystems provided in Stratmann (2018), which matched for 35% on genus level, 39% on family level and for 48% on order level. For remaining species, the median value of 0.55 was used. The NGE was taken from the same review, which matched for 48% of the biomass on genus level, 48% on family level and 49% on order level. For remaining species, the median of 0.54 was used. Grazing pressure of the total macrofaunal community and of each feeding type was calculated for each station. When a species was not sampled at a particular station for stable isotope analysis, values reported by Herman et al. (2000) (24% of the biomass) or the median microphytobenthos dependency for bivalves versus non-bivalves were used (4% of the biomass). A median value was calculated per estuary, if the food dependency differed significantly between estuaries (Table S1).

3.3.5 Statistical data analysis

Analysis of variance (ANOVA and HSD posthoc Tukey test, significance level $P = 0.05$) was conducted on chlorophyll-a concentrations and microphytobenthos production using 'estuary' (with levels Oosterschelde/Westerschelde), 'elevation' (high/ low) and 'season' (early spring/late spring) as fixed factors and 'site' as random factor. In addition, a possible interaction effect of 'estuary' and 'elevation' on chlorophyll-a concentrations was taken into account. We tested whether a linear correlation was present between elevation and chlorophyll-a concentrations using the Pearson product-moment correlation coefficient. Analysis of variance (ANOVA) was conducted on macrofaunal biomass to test for differences between estuaries, where each 'site' within each estuary was considered a random factor. Species having a high contribution to the total grazing pressure were listed per site (Table S3).

Differences in the proportion of microphytobenthos in the diet of individual species and the total of sampled individuals due to the categorical predictors 'estuary' (with levels Oosterschelde and Westerschelde), 'elevation' (with levels high and low), possible interaction effects between 'estuary' and 'elevation' and the random factor 'site' were tested with an ANOVA followed by a HSD posthoc Tukey test (significance level $P = 0.05$) when significant.

Variance in grazing pressure of the macrofaunal community on food sources was tested using an ANOVA for the factors 'estuary', 'food source' (with levels microphytobenthos, phytoplankton, macroalgae and terrestrial organic matter) and the random factor 'site', followed by a Tukey's test when significant. Linear regression tested the ability of microphytobenthos production in early spring

to predict grazing pressure of 1) the total macrofaunal community on microphytobenthos and 2) grazing by macrofauna of separate feeding types on microphytobenthos.

3.4 Results

3.4.1 Site characteristics

3.4.1.1 Mud content and microphytobenthic biomass

The Oosterschelde contains relatively sandy tidal flats, while sediments of tidal flats in the Westerschelde have a highly varying mud content (Fig. S1). The microphytobenthos biomass, measured as chlorophyll-a, was higher in high than in low elevation plots (ANOVA, $P=0.0003$, $F_{1,474}=13.14$, $n=486$; HSD Tukey, $p < 0.01$; Fig. 2). Furthermore, microphytobenthos biomass differed significantly between early spring and late spring (ANOVA, $F_{1,474}=6.06$, $P=0.014$, $n=486$), although the HSD Tukey test revealed no significantly different means (HSD Tukey, $p = 0.06$). A significant interaction effect of elevation and estuary on chlorophyll-a concentrations was observed ($F_{1,474}=5.75$, $P = 0.017$, $n=486$); chlorophyll-a concentrations were lower in the low lying intertidal areas of the Westerschelde than in the other areas (HSD Tukey, $p < 0.01$).

Microphytobenthos biomass did not correlate with elevation in the early spring (Pearson's $r = 0.006$, $p = 0.93$, $n = 162$) and was weakly positively correlated with elevation in the late spring (Pearson's $r = 0.16$, $p = 0.005$, $n = 324$).

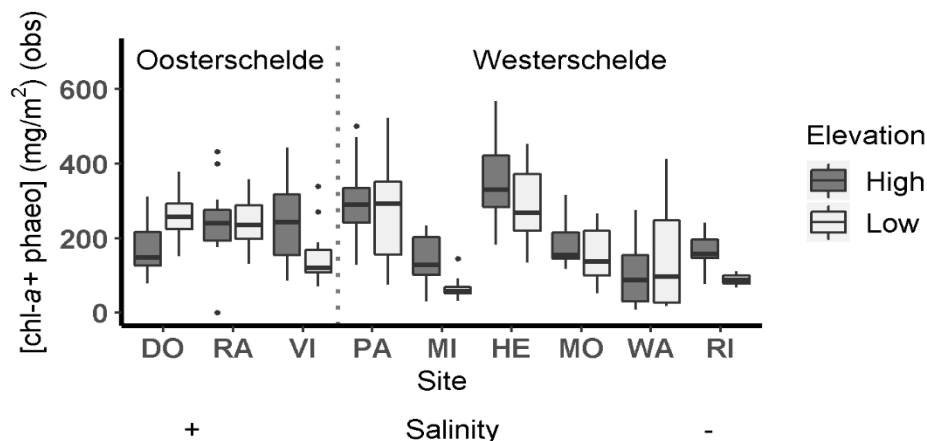


Fig. 2. Chlorophyll-a + phaeopigment concentrations (mg/m^2) in the upper 1 cm of the sediment at sites in the Oosterschelde sampled during the period of 12 March to 10 April and 4 May to 8 June 2015. See caption Fig. 1 for site names. Boxes represent the first quantile, median and third quantile. Whiskers extend to the largest versus lowest value no further than 1.5 times the interquartile range.

3.4.1.2 Microphytobenthic production

Microphytobenthos production did not differ significantly between high and low plots (ANOVA, $F_{1,4}=0.13$, $P = 0.74$, $n=95$), between early spring and late spring (ANOVA, $F_{1,4}=0.87$, $P = 0.41$, $n=95$) or between tidal basins (ANOVA, $F_{1,4}=1.03$, $P = 0.37$, $n=95$; Fig. 3). In the early spring, at Rattekaai, no photosynthetic activity could be measured with the PAM, as the fluorescence signal was below detection limit. In late spring, no fluorescence signal above detection limit was measured at all sites in the Oosterschelde and at two sites in the Westerschelde (Molenplaat, MO, and Rilland, RI; Fig. 3).

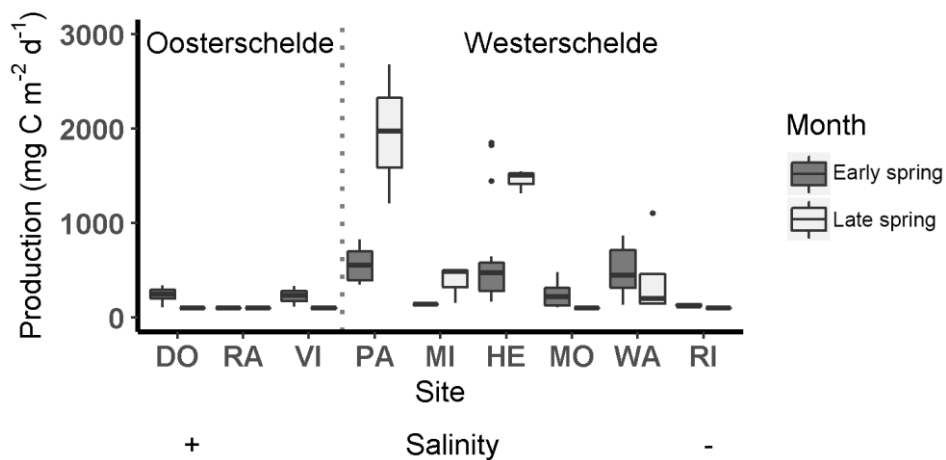


Fig. 3. Average daily microphytobenthos production (\pm SE) per site. Daily production rates were calculated over one month corresponding to the sampling period. See caption Fig. 1 for site names. Boxes represent the first quantile, median and third quantile. Whiskers extend to the largest versus lowest value no further than 1.5 times the interquartile range.

3.4.1.3 Macrofaunal biomass and community composition

Macrofaunal biomass sampled by NIOZ/Rijkswaterstaat was on average 18373 mg AFDW m^{-2} ($\sigma = 33570$) and did not differ significantly between tidal basins (ANOVA, $F_{1,6}=0.02$, $P = 0.88$, $n=73$; Fig. 4). *Cerastoderma edule* formed an important part of the total biomass comprising 8-43% at 5 out of 9 sites (Table S3). The lugworm *Arenicola marina* formed a significant part of the total macrofaunal biomass in the Oosterschelde and constituted 31-38% of the total macrofaunal biomass at these sites. At 4 sites in the Westerschelde, the capitellid worm *Heteromastus filiformis* was among the three species with the highest total biomass relative to other species present, comprising 27-51% of the total biomass. An overview of the actual biomass of the species is presented in Fig. 5.

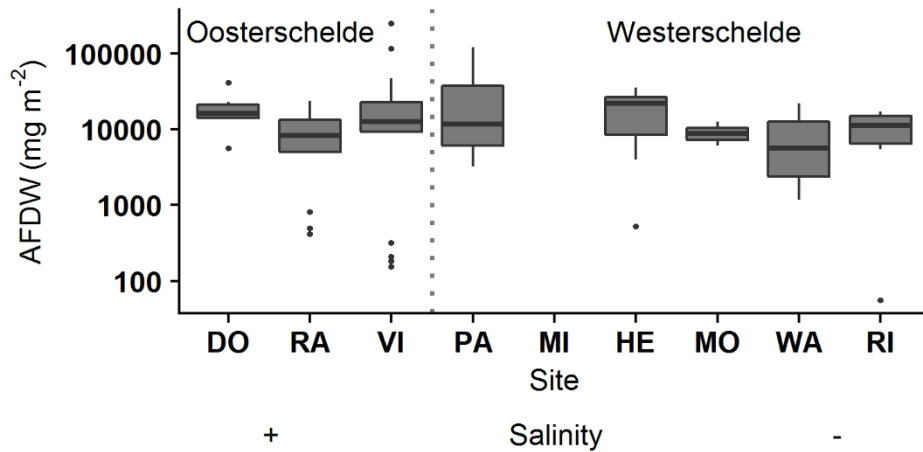


Fig. 4. Total biomass of the macrofaunal community (mg AFDW m^{-2}) sampled by NIOZ/Rijkswaterstaat during the period 2003 – 2012 from August – October. See caption Fig. 1 for site names. Boxes represent the first quantile, median and third quantile. Whiskers extend to the largest versus lowest value no further than 1.5 times the interquartile range.

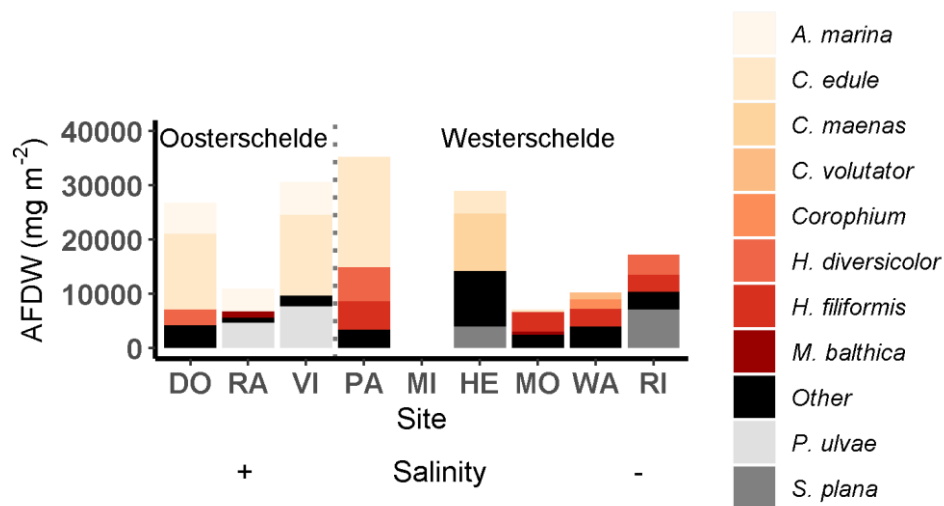


Fig. 5. Average biomass (mg AFDW m^{-2}) for the three species with the highest average biomass (mg AFDW m^{-2}) and the average biomass of the sum of remaining species (Other) at each site. For site MI no (nearby) data (from the period 2003-2012) was available. See caption Fig. 1 for site names.

3.4.2 Dietary proportions of macrofauna

3.4.2.1 $\delta^{13}\text{C}$ and $\delta^{15}\text{N}$ values of food sources and macrofauna

At most sites (Rattekaai, Paulina, Middelplaat, Hellegat, Molenplaat, Waarde and Rilland) the majority of macrofauna samples collected in late spring had an isotopic signature in between those of possible food sources (Fig. 6). At

Viane, Waarde and Rilland, the $\delta^{15}\text{N}$ of some macrofaunal species was slightly heavier than available food sources. At sites in the Westerschelde, the signatures of the majority of macrofaunal species were in between those of microphytobenthos and phytoplankton and not similar to terrestrial organic matter.

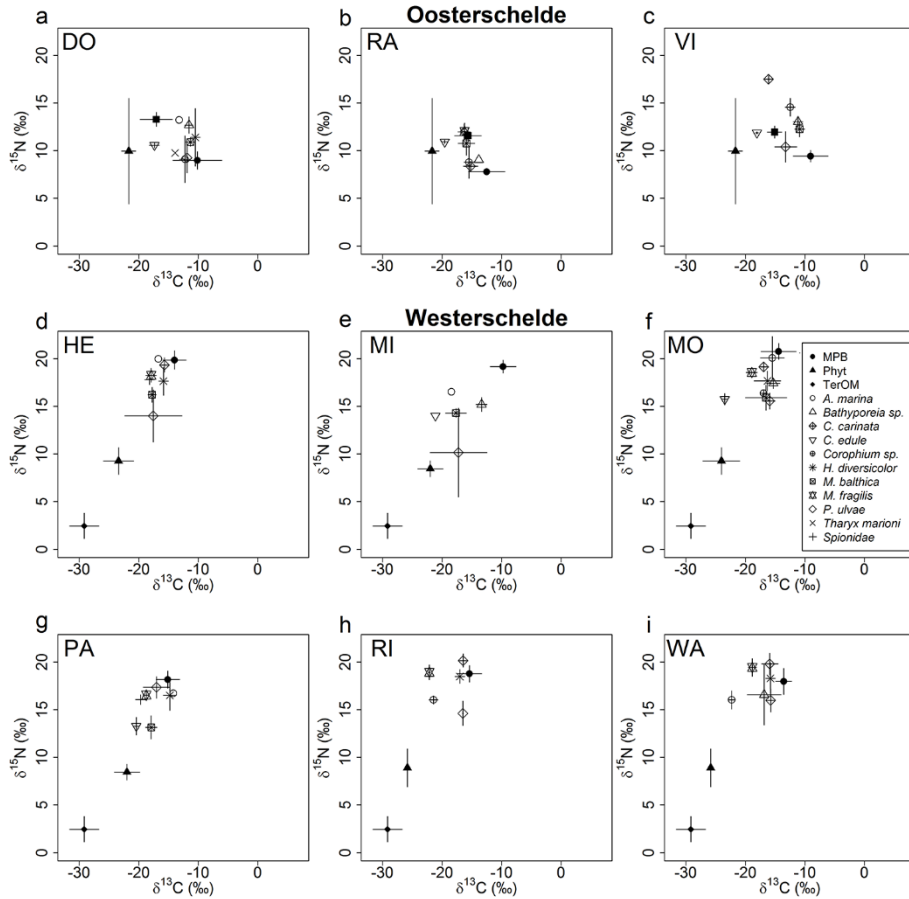


Fig. 6. The average and standard deviation of carbon ($\delta^{13}\text{C}$ ‰) and nitrogen ($\delta^{15}\text{N}$ ‰) isotopic composition for main food sources (closed symbols; microphytobenthos, microphytobenthos; Phyt, phytoplankton; TerOM, terrestrial organic matter) and sampled macrofaunal species (open symbols) at nine sites. See caption of Fig. 1 for site names. Closed squares in figure 6a, b and c indicate haphazardly collected macroalgae samples of various species, which have not been used the analyses of the current study because of the low observed macroalgal cover (0-4%).

3.4.2.2 Stable isotope mixing model

Including macroalgae as possible contribution to the diet of macrofauna resulted in unrealistically high proportions of macroalgae in the diet of macrofauna for the Oosterschelde (Fig. S2). Observed macroalgae cover (%)

was only < 1% at Dortsman and Viane and \pm 4% at Rattekaai (Table S4). Therefore, macroalgae were excluded and the diet composition of macrofauna in the Oosterschelde was recalculated using microphytobenthos and phytoplankton as only possible food sources.

The Gelman-Rubin diagnostic gave acceptable (< 1.05) values for the Bayesian mixing model fit in all cases (Table S5), indicating that each Markov chain converged to stable means and the same dietary proportions were obtained from each replicate Markov chain. The Geweke diagnostic exceeded acceptable values more frequently (in 56% of cases the diagnostic is equal to or $> 5\%$), indicating that target distributions were not yet reached within the first 10% of the chain. However, plots of the running means as function of iteration showed that in model runs where the Geweke diagnostic was exceeded, stable means were always reached.

3.4.2.2 Spatial variability in microphytobenthos dependence of macrofauna

Microphytobenthos were an important food source for the majority of macrofaunal genera (fraction in the Oosterschelde: 0.70 ± 0.20 ; Westerschelde: 0.61 ± 0.16 , Fig. 7 and Table S6), including for the facultative suspension feeder/ grazer *Macoma* (Oosterschelde: 0.83 ± 0.09 ; Westerschelde: 0.44 ± 0.08). Phytoplankton composed a minor part of the diet of the majority of macrofaunal species (Westerschelde: 0.28 ± 0.12 ; Oosterschelde 0.30 ± 0.20) as well as terrestrial organic material (Westerschelde: 0.11 ± 0.05).

The contribution of microphytobenthos to the diet of macrofaunal genera did not differ between estuaries for the total of sampled individuals (ANOVA, 'Estuary': $F_{1,5}=5.7$, $P = 0.06$, $n=102$; Table S1). However, the contribution of microphytobenthos was higher in the Oosterschelde than in the Westerschelde for the sand digger shrimp *Bathyporeia* (HSD Tukey, $p < 0.005$), the balthic tellin *Macoma* (HSD Tukey, $p < 0.0005$) and the mudsnail *Peringia* (HSD Tukey, $p < 0.05$). No difference in the contribution of microphytobenthos to the diet of all sampled individuals or individual macrofaunal species was observed between high and low stations (Table S1).

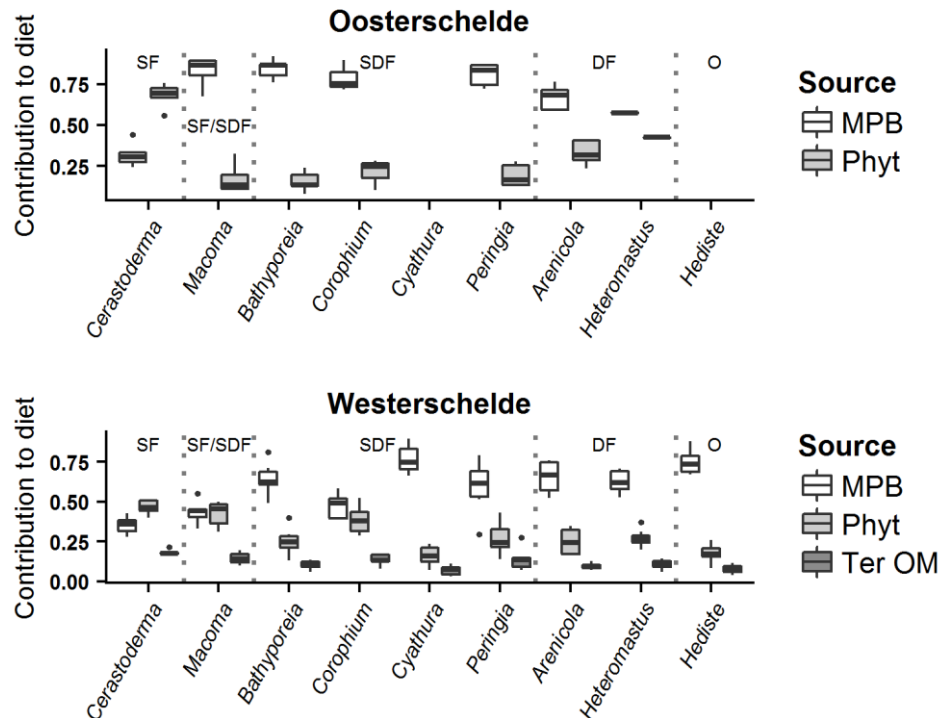


Fig. 7. Diet contribution (fraction) of microphytobenthos, phytoplankton and terrestrial organic material to sampled macrofaunal genera in the Oosterschelde and Westerschelde. The known feeding group of each genus is indicated as SF= suspension feeders, DF=deposit feeders, SDF= surface deposit feeders, O=omnivores. Hediste and the isopod Cyathura are not displayed for the Oosterschelde and the bristleworm Tharyx and the polychaete Spionidae are not displayed, as only a small number of individuals of those genera was collected there. Boxes represent the first quantile, median and third quantile. Whiskers extend to the largest versus lowest value no further than 1.5 times the interquartile range.

3.4.3 Grazing on different food sources

Grazing pressure was not significantly different among food sources and did not vary significantly between estuaries (ANOVA, 'source': $F=5.48$, $P = 0.07$, 'estuary': $F_{1,78}$, $P = 0.25$; microphytobenthos: $341 \pm 384 \text{ mg C m}^{-2} \text{ d}^{-1}$; phytoplankton: $220 \pm 532 \text{ mg C m}^{-2} \text{ d}^{-1}$; terrestrial OM: $74 \pm 120 \text{ mg C m}^{-2} \text{ d}^{-1}$; Fig. 8).

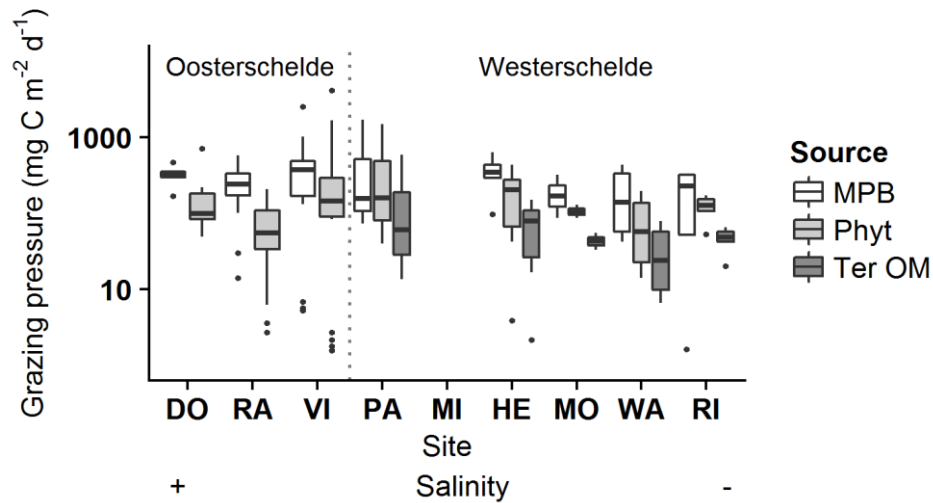


Fig. 8. Grazing pressure (mg C m⁻² d⁻¹) of macrofauna on main available food sources per site. Boxes represent the first quantile, median and third quantile. Whiskers extend to the largest versus lowest value no further than 1.5 times the interquartile range.

3.4.4 Comparison of faunal grazing on microphytobenthos with microphytobenthos production

Total grazing pressure on microphytobenthos was of the same order of magnitude as microphytobenthos production in early spring (Fig. 9a; Oosterschelde: microphytobenthos_{production,μ} = 235 mg C m⁻² d⁻¹, microphytobenthos_{grazing,median} = 312 mg C m⁻² d⁻¹; Westerschelde = microphytobenthos_{production,μ}: 435 mg C m⁻² d⁻¹, microphytobenthos_{grazing,median} = 290 mg C m⁻² d⁻¹). At a number of stations, grazing pressure on microphytobenthos exceeded local microphytobenthos production in early spring (Fig. 9a and Fig. 9b, points above the 1:1 line). In most cases, grazing pressure was a factor 1.3 to 10 higher than local microphytobenthos production. There are, however, two stations where grazing pressure is several orders of magnitude higher than local production: Viane (Oosterschelde) and Paulinapolder (Westerschelde) (Fig. 9b). The high grazing pressure at these stations can be explained by a high biomass of suspension feeders present (Fig. 9c), that partially fed on microphytobenthos. Microphytobenthos production was exceptionally high (> 1600 mg C m⁻² d⁻¹) at one station, which was associated with a high average chlorophyll-*a* concentration (486 mg m⁻²) and high average photosynthetic capacity (82 μmol photon m⁻² s⁻¹). Total grazing pressure of macrofauna on microphytobenthos could not be predicted from microphytobenthos production using a linear regression in the Oosterschelde (R² = 0.01, p = 0.81) or Westerschelde (R² = 0.10, p = 0.24).

Microphytobenthos production could not be used as significant predictor for grazing of separate macrofauna feeding types, using macrofauna and microphytobenthos production data of both tidal basins merged (Carnivores: $R^2 = 0.02$, $p = 0.70$; Deposit feeders: $R^2 = 0.004$, $p = 0.71$; Omnivores: $R^2 = 0.14$, $p = 0.17$; Surface deposit feeders: $R^2 = 0.01$, $p = 0.62$; Suspension feeders: $R^2 = 0.0005$, $p = 0.93$). The predictive power of microphytobenthos production for macrofaunal grazing pressure did not improve when tidal basins were analysed separately.

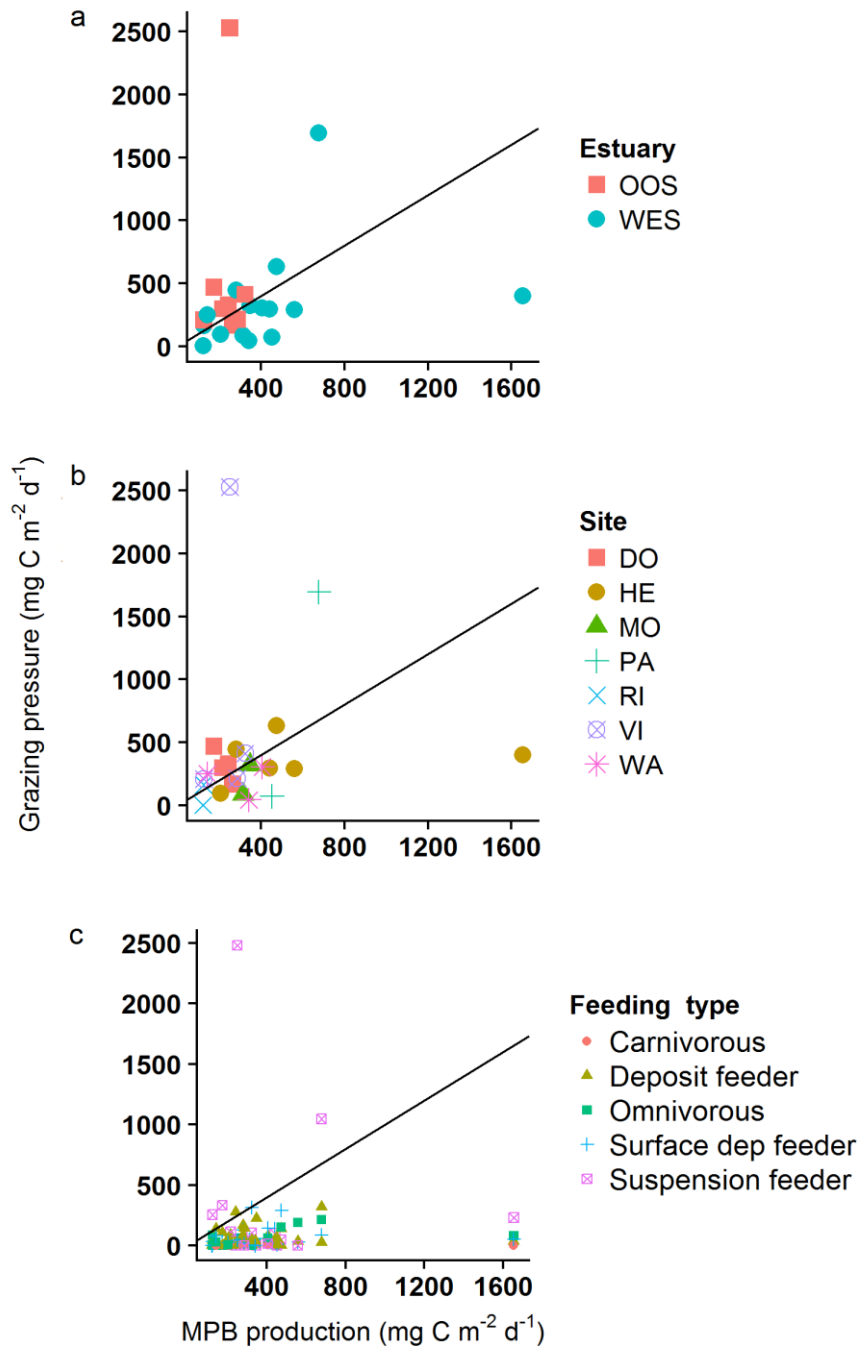


Fig. 9. Average daily production rates of microphytobenthos (mg C m⁻² d⁻¹) and grazing pressure of macrofauna on microphytobenthos (mg C m⁻² d⁻¹) in (a) different estuaries, (b) at different sites and (c) for macrofaunal species of different feeding types in the Oosterschelde and Westerschelde combined. The solid black line indicates a 1:1 line.

3.5 Discussion

In this study, the diet composition of macrofauna was calculated using a dual stable isotope model in contrasting tidal basins and elevations. Microphytobenthos production in early spring was linked to macrofaunal grazing pressure in summer/autumn. Microphytobenthos was the main ultimate food source for macrofauna species in the two studied tidal systems. External material imported through rivers and streams contributed only marginally to the diet of the studied macrofaunal genera. This finding is in line with earlier stable isotope studies conducted in temperate, subtropical and tropical tidal basins (see below). The contribution of microphytobenthos in the diet of macrofauna varied between tidal systems for a number of species, but did not vary as function of elevation. Very few studies have been conducted on spatial variability in the contribution of microphytobenthos in the diet of macrofauna (Christianen et al., 2017). To our knowledge, this is the first study where the diet contribution of microphytobenthos was compared among tidal systems or linked to tidal elevation. We demonstrated that grazing pressure on microphytobenthos is of the same order of magnitude as microphytobenthos production, which likely explains the frequently observed drop in microphytobenthos biomass in early summer in temperate systems. Spatial variability in microphytobenthos production in early spring did not explain spatial variation in macrofaunal grazing pressure in summer/autumn, which may be associated with the time difference between sampling of macrofauna and measurement of microphytobenthos production. Assuming that macrofauna communities are relatively stable over time, our results suggest that consumer-resource interactions are coupled on a larger spatial scale (i.e. mesoscale, ≈ 10 to 100 kilometers) rather than the fine (millimeter to meter) scale.

3.5.1 Isotope composition of food sources and macrofauna

The relative contribution of sources to the diet of organisms can be studied using bulk isotope signatures (e.g. Yokoyama, 2003) or compound-specific stable isotope analysis (e.g. Oxtoby et al., 2016). Bulk isotopic signatures are suitable to obtain a quantitative estimate of dietary proportions, although limitations include isotopic routing and fractionation after consumption (Federer et al., 2010). Compound-specific analyses allow the use of biomarkers with little structural modification, such as polyunsaturated fatty acids, but require detailed knowledge on tissue composition to estimate proportions of sources in consumers (Wolf et al., 2009).

The $\delta^{13}\text{C}$ of sampled macroalgae was in the same range as the $\delta^{13}\text{C}$ of microphytobenthos and phytoplankton (Table S7 and S8) and could contribute

to the diet of macrofaunal genera when macroalgae cover is high. Several studies have quantified isotopic signatures of food sources for benthos on tidal flats in the Oosterschelde and Westerschelde (Herman et al., 2000; Moens et al., 2005; Riera et al., 2000; Van den Meersche et al., 2009) and in other intertidal areas worldwide (Kang et al., 2003). Moens et al. (2005) demonstrated that carbon isotopic signatures of the food sources SPOM and microphytobenthos are generally narrowly constrained ($\delta^{13}\text{C}_{\mu, \text{microphytobenthos}}$: -15.7 to -14.3; $\delta^{13}\text{C}_{\mu, \text{SPOM}}$: -24 to -20) in the Westerschelde. The range of the $\delta^{13}\text{C}$ of microphytobenthos is somewhat larger in the current study. ($\delta^{13}\text{C}_{\mu, \text{microphytobenthos}}$: -18.2 to -12.2; $\delta^{13}\text{C}_{\mu, \text{SPOM}}$: -21.7 to -25.8). The $\delta^{13}\text{C}$ of microphytobenthos in our study was negatively correlated with mud content (Pearson's $r = 0.53$). This could be related to a general lowering of the $\delta^{13}\text{C}$ of DIC in the upstream direction in estuaries as function of salinity (Chanton and Lewis 1999) and a concomitant increase in mud content. Generally, the $\delta^{13}\text{C}$ of DIC is lighter in riverine waters than in marine waters (e.g. Chanton and Lewis, 1999). In our study, we also observed relatively low $\delta^{13}\text{C}$ values of microphytobenthos at a relatively silty location close to the polyhaline estuary mouth (Paulinapolder: $\delta^{13}\text{C}_{\mu, \text{microphytobenthos}}$: -18.2 to -17.7). It is likely that more estuarine phytoplankton deposits at such sheltered sites. Part of the PLFAs used in this study as microphytobenthos markers could therefore be derived from this more ^{13}C depleted phytoplankton ($\delta^{13}\text{C}$ of 20:5 ω 3 characteristic for diatoms, sampled from surface water: ~ 20 -25‰; Boschker et al., 2005), explaining the lighter signatures. However, the species composition of algae in the Westerschelde intertidal flats is dominated by microphytobenthos (Sabbe and Vyverman, 1991), rather than plankton species. This suggests that the relatively low microphytobenthos $\delta^{13}\text{C}$ ratios at relatively muddy sites are more likely due to site dependent differences in growth conditions on isotopically depleted DIC.

The range of nitrogen isotopic signatures of microphytobenthos reported in the current study ($\delta^{15}\text{N}_{\mu, \text{microphytobenthos}}$: 7.7 to 21.2) are similar to the values reported by Moens et al. (2005) ($\delta^{15}\text{N}_{\mu, \text{microphytobenthos}}$: 7.4 to 17.7; $\delta^{15}\text{N}_{\mu, \text{SPOM}}$: 7 to 15) for the Westerschelde, whereas a smaller range of $\delta^{15}\text{N}$ values of SPOM was found ($\delta^{15}\text{N}_{\mu, \text{SPOM}}$: 8.4 to 9.9). The generally high range of nitrogen isotopic signatures of microphytobenthos and SPOM found in estuaries is associated with assimilation of the relatively heavy NH_4^+ by bacteria and microalgae, likely resulting from isotopic fractionation by nitrifiers and/or fractionation by phytoplankton uptake (Mariotti et al., 1984; Moens et al., 2005; Riera et al., 2000). However, the relative importance of nitrification and, therefore, availability of heavy NH_4^+ for microalgae may vary among sites (Moens et al., 2005) and seasons (Rysgaard et al., 1995).

Furthermore, nitrogen in suspended matter of marine origin is known to have a higher nitrogen isotopic signature than suspended matter of terrestrial origin ($\delta^{15}\text{N}_{\mu, \text{marine OM}}$: 8 ± 1.8 ; $\delta^{15}\text{N}_{\mu, \text{terrestrial OM}}$: 1.5 ± 0.2 ; Mariotti et al., 1984).

Especially in winter, when autochthonous primary production is low, terrestrial organic material may form a significant part of SPOM of estuarine systems. In summer, SPOM in the Westerschelde is dominated (>50%) by autochthonous phytoplankton (Mariotti et al., 1984). The observed spatial variability in nitrogen isotopic signatures of SPOM in the Oosterschelde and Westerschelde emphasize the importance of sampling and determining isotopic signatures of SPOM locally.

The carbon and nitrogen isotopic signatures of macrobenthic genera used to determine the diet composition are determined by 1) the $\delta^{13}\text{C}$ and $\delta^{15}\text{N}$ of consumed food sources, 2) changes in the $\delta^{13}\text{C}$ and $\delta^{15}\text{N}$ due to differential digestion or fractionation during metabolic and assimilation processes (isotopic shift or trophic fractionation) and 3) the position of the consumer in the food chain (trophic level). Here we have adopted an average isotopic shift of $0.3 \pm 0.14\text{‰}$ for carbon and of $2.2 \pm 0.3\text{‰}$ for nitrogen per trophic level, as proposed by McCutchan et al. (2003). However, isotopic shift varies among individual consumers (McCutchan et al., 2003) and have, to our knowledge, not been quantified for the specific intertidal macrobenthic genera considered in this study. Furthermore, we assumed that the macrobenthic genera considered in this study are separated from the considered food sources by one trophic level, which is the generally accepted position of macro-invertebrates in the food chain of intertidal ecosystems (Kuwaie et al., 2012). By correcting for shifts in $\delta^{15}\text{N}$ after food ingestion, the calculated diet composition values represent an 'ultimate food source' diet composition. Likewise, the calculated grazing pressure represents the grazing pressure that is ultimately present on the considered food sources. It has been demonstrated that primary food sources may be transferred to macro-invertebrates via bacteria or meiofauna (Middelburg et al., 2000). As a consequence, the number of trophic levels may be underestimated and the grazing pressure on microphytobenthos and the contribution of the considered food sources to the diet of macrofauna may be slightly overestimated. Lastly, it should be noted that diet composition or even trophic level may vary over time, due to seasonal changes in food availability.

3.5.2 Microphytobenthos as food source for macrofauna

We showed that microphytobenthos is the dominant food source for the majority of abundant macrofaunal species in two contrasting tidal systems, including predators, suspension feeders and facultative suspension feeder/grazers. This is in accordance with earlier findings on tidal flats in the Westerschelde (Herman et al., 2000), in other regions with a temperate climate such as the Wadden Sea, The Netherlands (Christianen et al., 2017), the Plum Island estuary, Massachusetts, USA (Galván et al., 2008), but also in

regions with a subtropical (e.g. Kang et al., 2003) or tropical climate (e.g. Kon et al., 2015). The contribution of microphytobenthos in the diet of suspension feeders (24 – 44% for *Cerastoderma*) was somewhat higher in this study than previously reported values (17%, Herman et al., 2000; < 5%, Christianen et al., 2017). Our study suggests that it is not correct to assume a priori that suspension feeders (almost) exclusively depend on phytoplankton. Instead, resuspended microphytobenthos may contribute significantly to the diet of suspension feeders (cf. Fig. 6).

3.5.3 Spatial variability in the diet of macrofauna

In our study, the contribution of microphytobenthos to the diet of macrofauna did not differ between estuaries for all sampled individuals combined. However, the contribution of microphytobenthos in the diet of the genera *Bathyporeia* sp., *Macoma balthica* and *Peringia ulvae* was higher in the Oosterschelde than in the Westerschelde. Our macrofaunal community dataset shows that in the Westerschelde, *Bathyporeia pilosa* is the most dominant species of the *Bathyporeia* genus, whereas in the Oosterschelde *Bathyporeia pelagica* and *Bathyporeia elegans* occur. All three species are surface deposit feeders, indicating that the composition of organic material differs between the tidal systems. This may also explain the larger contribution of microphytobenthos in the diet of *Peringia ulvae* (a surface grazer) in the Oosterschelde than in the Westerschelde. *Macoma* is well known to be a facultative surface deposit feeder and suspension feeder (Rossi et al., 2004). As phytoplankton production in spring is generally lower in the Oosterschelde than in the Westerschelde (Kromkamp and Peene, 2005), this may explain the higher proportion of microphytobenthos in the diet of *Macoma* in the Oosterschelde. We did not observe size dependent (ontogenetic) differences in microphytobenthos dependence of *Macoma* as described by Rossi et al. (2004) and Herman et al. (2000). However, the possibility that a systematic error in the estuary-specific offset used to obtain $\delta^{15}\text{N}$ values of microphytobenthos from the $\delta^{15}\text{N}$ of the bulk sediment resulted in significant differences in the diet of macrofauna between estuaries cannot be ruled out. The contribution of microphytobenthos in the diet of macrofauna did not vary as function of elevation in the tidal zone. This finding may be counter intuitive, as microphytobenthos biomass is generally positively correlated with emersion duration (Van der Wal et al., 2010) and the studied species generally occurred at high and low elevations (Table S6). However, the lack of a significant difference in the contribution of microphytobenthos in the diet of macrofauna is in line with the finding that microphytobenthos production did not differ between high and low plots, indicating that there is no difference in the amount of microphytobenthos available for macrofaunal species between high and low tidal flats. Although sample size did not allow analysis for the factor 'site', some variation in the microphytobenthos diet coefficient appeared to be site-

dependent (Table S8). This may be associated with local differences in the availability of different food sources. For example, a sheltered tidal flat may contain a relatively large amount of deposited terrestrial organic material.

3.5.4 Relation between microphytobenthos production and macrofaunal grazing

We showed that grazing pressure of macrofauna on microphytobenthos in summer/autumn (i.e. calculated using the density and biomass of the macrofauna community sampled by NIOZ/Rijkswaterstaat from August – October) is in the same order of magnitude as microphytobenthos production in early spring. This suggests that microphytobenthos is strongly subject to top down control by macrofauna, as microphytobenthos production is generally highest in spring. This finding is consistent with the results of defaunation experiments in intertidal areas (e.g. Weerman et al., 2011), which showed a rapid increase in microphytobenthos biomass after removal of macrofauna. Furthermore, Savelli et al. (2018) modelled grazing of *Peringia ulvae* on microphytobenthos on a mudflat in Northwest France, where grazing was regulated by microphytobenthos availability and mud surface temperature, and found that grazing rates exceeded microphytobenthos production rates in spring. Labelling experiments indicated a low transfer of carbon from microphytobenthos to macrofauna (Herman et al., 2000; Middelburg et al., 2000). However, such experiments only provide information on carbon transfer on a time scale of a few days. As carbon originating from microphytobenthos may initially be taken up by bacteria or meiofauna (e.g. Middelburg et al., 2000), carbon transfer from microphytobenthos to macrofauna may occur on longer time scales.

Microphytobenthos production in early spring did not explain local spatial variability in total macrofaunal grazing pressure in summer/autumn (August – October). This may partly be associated with the presence of large suspension feeders, which feed on non-locally produced microphytobenthos from the water column. As suspension feeders form a significant part of the total macrofaunal biomass per unit area, the link between microphytobenthos production and total macrofaunal grazing per unit area is weak. In addition, microphytobenthos production was not linked to grazing pressure by macrofauna of separate feeding types. The macrofauna community composition is highly variable among stations, leading to large variation in the total biomass of different feeding types among stations. Microphytobenthos production was not always measured at the exact same location as where samples for the determination of the macrofaunal community composition were taken (within 300m), and there was a time difference between measurement of microphytobenthos production (2015) and sampling for the macrofauna community composition (2003–2012). This may have caused non-

linearity in the link between available microphytobenthos production and the grazing pressure of a macrofaunal feeding type on microphytobenthos. Earlier studies have demonstrated that the large-scale spatial distribution of macrofaunal species is relatively stable in the Westerschelde (Ysebaert et al., 2003), albeit with variation (Ysebaert and Herman, 2002). Likewise, the spatial patterns in microphytobenthos biomass are relatively consistent over time, superimposed on seasonal, and year-to-year variability (Van der Wal et al., 2010).

It should be noted that the presented microphytobenthos primary production rates are gross primary production rates, while the actual carbon availability for the food web is represented by net primary production rates. Therefore, the presented microphytobenthos production rates are not 1:1 comparable to the presented macrofaunal grazing rates, i.e. not all of the carbon fixed by the microphytobenthos is available for consumption. In a review, Langdon (1993) showed that the biomass-specific dark respiration of diatoms is a fixed fraction of gross primary production of on average $0.06 \pm 0.01\%$, depending on algal growth rates. Net primary production rates approach gross primary production rates under low specific growth rates (Halsey et al., 2010).

Our results confirm the key role of microphytobenthos on intertidal flats in the diet of macrofauna, which are in turn eaten by secondary consumers such as (wading) birds and fish. This highlights the pressing need to preserve these intertidal flats, as decreasing availability of microphytobenthos may have cascading effects up the estuarine food web. Furthermore, we demonstrated that the diet composition of macrofauna likely differs among estuaries, which suggests that estuary-specific food web modelling can support management of these ecosystems.

Acknowledgements

This research was supported by the 'User Support Programme Space Research' of the Netherlands Organisation for Scientific Research (NWO grant no. ALW-GO 13/14 to DvdW) and by the Netherlands Organisation for Scientific Research (VIDI grant no. 864.13.007 to DvO). We gratefully acknowledge Jacco Kromkamp for discussions on primary production, Lennart van IJzerloo, Jeroen van Dalen and Joost Hamoen for field assistance, Jan Sinke and Joeri Minderhoud for chlorophyll-a analyses, Angela Dekker, Daniel Blok and Anke Engelberts for assistance with macrofauna species identification and Anke Engelberts for assistance with identification of macroalgae species. The authors declare no conflict of interest.

Chapter 4 The influence of macrofauna on biomass and spatial heterogeneity of intertidal microphytobenthos under varying hydrodynamic conditions: an experimental approach

Tisja D. Dagers, Laura M. Soissons, P. L. M. (Lodewijk) de Vet, Tjeerd J. Bouma, Peter M. J. Herman, Daphne van der Wal

STATUS: to be submitted

4.1 Abstract

In marine intertidal environments, abiotic gradients at the landscape scale, e.g. in mud content and elevation, are generally considered the most important source of variation in the abundance and composition of microphytobenthos (MPB). However, earlier studies have demonstrated that at a more local scale, macrofauna may exhibit strong top down control on MPB, resulting in a low MPB biomass standing stock. Here, we investigate under (large scale) contrasting hydrodynamic conditions the effect of (local scale) top down control on *i)* the overall MPB biomass and *ii)* the spatial heterogeneity in MPB biomass on the centimeter to meter scale. We experimentally excluded benthic macrofauna in plots at low, intermediate and high elevation zones on two tidal flats with contrasting hydrodynamic exposure, in two separate tidal basins in the Netherlands. We followed macrofauna grazing pressure and chlorophyll, and evaluated microphytobenthos patterns using a geostatistical approach on drone (UAV) images of control and defaunated plots. Macrofauna grazing pressure did not influence the MPB biomass standing stock under all hydrodynamic conditions. However, grazing pressure of macrofauna decreased the distance (range) up to which MPB biomass is spatially autocorrelated. Areas with a similar MPB biomass ('patches') occupy smaller surfaces in the presence of macrofauna than they would without macrofauna. The magnitude of this effect shows an increasing trend with mud content. The present finding implies that macrofauna not only enhances sediment erodibility by bioturbation, but also prevents MPB from forming continuous biofilms that shield the sediment from erosion.

Key words: Macrofauna, microphytobenthos, benthic diatoms, top-down control, UAV images

4.2 Introduction

A reappearing challenge in ecology is to understand and predict the factors that determine the spatial structure of ecological communities (Cozzoli et al., 2013; Harte et al., 2005; Peres-Neto and Legendre, 2010). The relative influence of biotic and abiotic factors on the community structure can differ across spatial scales (Cottenie, 2005; Leibold et al., 2004). In marine intertidal environments, abiotic factors such as inundation time (Santos et al., 1997), sediment type (Zou et al., 2018) and hydrodynamic exposure (Warwick and Uncles, 1980) are generally regarded as the most important sources of community variation. However, biotic factors have also been shown to increase sediment resuspension (de Deckere et al., 2001; Orvain et al., 2004) or stabilize the sediment (Weerman et al., 2010). It is interesting to note that abiotic and biotic controls may be expected to work at a different spatial scales, with abiotic gradients being driven at the landscape-scale while biotic controls can act at a smaller, much more local scale (Zajac et al., 1998). This may mean that biotic and abiotic effects on a community may be visible as scale effects. We aim to unravel these scale effects using microphytobenthos (hereafter MPB) as model system.

Photoautotrophic microorganisms, referred to as benthic microalgae or MPB, are at the base of the food web in these intertidal communities (Christianen et al. 2017). The main groups of MPB in estuarine and saltmarsh sediments are diatoms, cyanobacteria and chlorophytes (Pinckney and Zingmark, 1993). Diatoms often dominate the MPB of intertidal sediments and contribute significantly to estuarine primary production (Underwood and Kromkamp, 1999). Benthic diatoms produce extracellular polymeric substances (EPS) that reduce sediment erosion (Yallop et al., 1994) and were found to be a major food source for part of the macrofauna living in intertidal areas (Christianen et al., 2017; Daggers et al., 2020; Page, 1997).

Several studies have focused on the analysis of spatial variability in MPB biomass (Kazemipour et al., 2012; Meleder et al., 2003; Seuront and Spilmont, 2002) or primary productivity (Guarini et al., 2002; Daggers et al., 2018) on the macro (tidal basin) scale. Spatial variability in MPB biomass at the scale of a tidal basin has been attributed to emersion duration or bathymetry (Meleder et al., 2003; van der Wal et al., 2010), mud content (van der Wal et al., 2010) and nutrient inputs (Meleder et al., 2003). The distribution of the mud content within a tidal basin is typically correlated with hydrodynamic exposure, and hence often used as proxy for hydrodynamic exposure (Molinarioli et al., 2009).

On smaller scales (centimetres to metres), macrofauna may play an important role in explaining spatial variability of MPB biomass (Pratt et al., 2015), as for numerous ecosystems it has been demonstrated that predator-prey

interactions influence spatial patterning of ecological communities (Andrew, 1993; Edwards et al., 1996; Maron and Harrison, 1997). Furthermore, local environmental conditions may constrain predator-prey interactions (Abrahams and Kattenfeld, 1997; Menge et al., 1997). Both growth of MPB (Connor et al., 1982; Van Colen et al., 2008) and spatial pattern formation on the meter scale (Weerman et al., 2011b) can be inhibited by the activity of benthic macrofauna on intertidal mudflats sheltered from waves and high current speeds. Van Colen et al. (2008) observed an inhibitory effect of benthic macrofauna on the amount of MPB biomass present in the Westerschelde, where MPB biomass peaked one month after opening of defaunated plots (in late April), while MPB biomass in control plots (non-defaunated) remained low. Weerman et al. (2011b) empirically showed an inhibitory effect of macrofauna on the amount of MPB biomass in May. Furthermore, it has been shown that the presence of sediment-reworking organisms, such as the lug worm *Arenicola*, lowers MPB biomass in intertidal areas (Volkenborn et al., 2007).

To the best of our knowledge, interactive effects between macrofaunal presence and hydrodynamic exposure on MPB biomass have been studied sparingly (Savelli et al., 2018; Ubertini et al., 2012). Interactive effects can be expected, as the community composition of macrofauna also strongly depends on abiotic conditions such as sediment characteristics, bathymetry and hydrodynamics (Cozzoli et al., 2013; Thrush et al., 2003; van der Wal et al., 2017; Ysebaert et al., 2003). Furthermore, resuspension rates of MPB may strongly differ between sandy and muddy sediments, depending on current speeds (Lucas et al., 2000). In this study, we examined (1) to what extent MPB is subject to local-scale top down control by macrofauna versus large-scale gradients like varying hydrodynamic conditions and (2) how local-scale grazing pressure by macrofauna on MPB influences spatial heterogeneity in MPB biomass at the small scale (centimetres to metres). It is hypothesized that the effect of top down control on MPB biomass depends on interactive effects between grazing pressure by macrofauna and hydrodynamic activity (current speeds and/or waves). That is, we expect that (H1) the top down control on MPB is strongest when grazing pressure of macrofauna on MPB is high, and hydrodynamic forces are weak, while (H2) at locations with high hydrodynamic activity, the influence of waves and currents on spatial variability in MPB biomass is expected to overrule the influence of macrofaunal presence.

4.3 Materials and methods

4.3.1 Study site

A defaunation experiment was performed *in situ* at a tidal flat in the Westerschelde (Paulinapolder, 51° 21' N; 3°43' E) and in the Oosterschelde (Viane, 51° 37' N; 4° 1' E), Scheldt delta, The Netherlands (Fig. 1). The

Westerschelde is a nutrient-rich and turbid ecosystem (Kromkamp and Peene, 2005). The Oosterschelde is a relatively clear semi-enclosed sea arm with little freshwater input (Nienhuis and Smaal, 1994). Paulinapolder is located close to the estuarine mouth (salinity 18-30‰; tidal range 4.1 m; Fig. 1). Viane has a characteristic salinity of > 30 psu (Nienhuis and Smaal, 1994) and an average tidal range of 2.9 m. MPB biofilms usually appear in March-April (Asmus and Bauerfeind, 1994) and disappear in late May-June, which is likely due to increased grazing pressure by benthic meio- and macrofauna (de Brouwer et al., 2000; Savelli et al., 2018; Underwood, 1994; Weerman et al., 2011b).

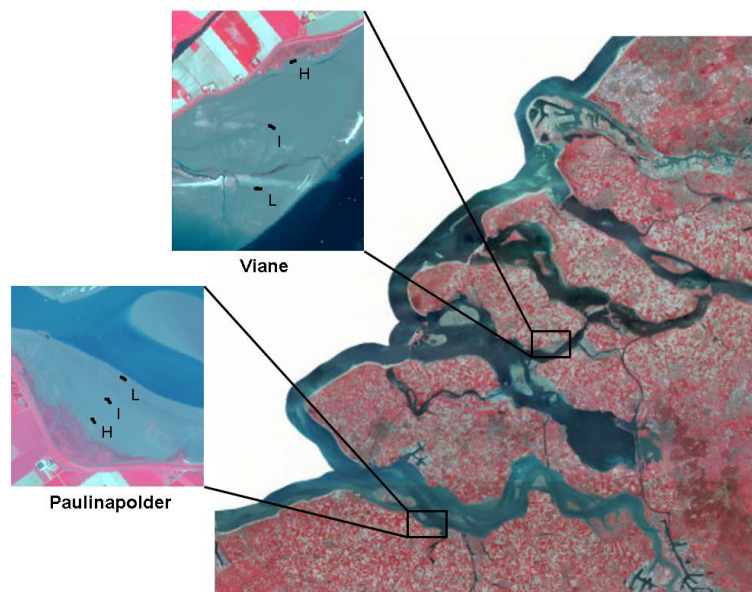


Fig. 1. Study sites located at Paulinapolder (Westerschelde) and Viane (Oosterschelde), southwest Netherlands. At each elevation category (L: low, I: intermediate and H: high) two control and two defaunated plots were placed (indicated with black dots). Source image: Aerial photograph of the Netherlands CIR – 25 cm resolution, 2017 (beeldmateriaal.nl)

4.3.2 Experimental design, sampling and laboratory analyses

4.3.2.1 Defaunation experiment

The defaunation experiment was conducted from end of April – September 2016. Two replicate defaunated and two replicate control plots were positioned within the study site using a stratified random design at low elevation (± -1 m NAP, where NAP is Dutch Ordnance level, approximately mean sea level), intermediate elevation (± 0.15 m NAP) and high elevation (Paulinapolder: 0.47 m NAP; Viane: 0.84 m NAP), with a minimum distance of 5m between plots

(Fig. 1). Earlier defaunation studies have demonstrated that this distance allows for frequent monitoring of the plots without disturbing the sediment in the experimental plots (Van Colen et al. 2008). The plots were defaunated by placing a polyethylene sheet with a thickness of 1.2 mm over the sediment, whereby the edges of the sheet were dug into the sediment up to approximately 30 cm depth (Beukema et al., 1999; Van Colen et al., 2008). The sheets were removed after three weeks, whereby the dug-in edges of the sheet were left in place. In this way, horizontal migration of macrofauna within the sediment was prevented. Earlier defaunation experiments demonstrated that the sediment was completely devoid of macrofauna after a period of three weeks (Thrush et al., 1996). We observed that the sediment surface was black after removal of the sediment, indicating that anoxic conditions were present. The sheets were installed and removed two weeks earlier at Viane than at Paulinapolder (see Table 1).

Table 1. Field visiting dates.

Weeks after opening	Paulina	Viane
T0	12-05-2016 / 13-05-2016	25-04-2016
T2	26-05-2016	11-05-2016
T4	09-06-2016	23-05-2016
T8	06-07-2016	23-06-2016
T12	04-08-2016	21-07-2016
T19/T18	22-09-2016	06-09-2016

4.3.2.2 Sediment sampling and analysis

Three replicate sediment samples (\emptyset 3 cm, depth 1 cm) for analysis of the mud content were collected in each plot at the start (T0, 0 weeks after opening of the sheets) and end of the experiment (T19/T18, 19 and 18 weeks after opening of the sheets, Table 1). The grain size distribution was determined using a Malvern laser particle sizer and classified following Folk (1954), with mud content defined as the fraction of particles $<63 \mu\text{m}$.

MPB biomass was sampled 6 times, namely at T0, T2, T4, T8, T12 and T18 at Viane or T19 at Paulinapolder (Table 1). Sediment cores (\emptyset 1 cm, depth 1 cm) were collected in each plot at three points that were randomly chosen beforehand, whereby the outer 30cm of the plot was avoided to prevent edge effects. Furthermore, the central square meter of each plot was left undisturbed to avoid disturbance of spatial patterns of MPB. The sediment samples were analyzed in the laboratory for chlorophyll-a content ($\mu\text{g/g}$) with a Specord 210 spectrophotometer (analysis of the supernatant extracted from lyophilized sediment by adding 10 ml 90% acetone) following Ritchie (2006) and subsequently converted to chlorophyll-a concentrations (mg/m^2) using the dry bulk density.

Images of the plots were taken with an RGB camera mounted on a DJI Inspire UAV (drone) from T2 (i.e., 2 weeks after sheet removal) to T18/T19 for the analysis of spatial variability in MPB biomass. The images were taken from a height of approximately 5m above the sediment. The spatial resolution of the drone images varied from ca 1 to 3 mm.

4.3.2.3 Macrofauna sampling and analysis

Samples for the determination of the macrofaunal community composition were collected at T0 in each control plot and at T8 and T18/T19 in control and defaunated plots at random points (chosen beforehand) from the outer 0.85 m margin of the plots. Macrofauna was sampled with three replicate cores (\varnothing 15 cm, depth 30 cm) in each plot and sieved. The sample material > 1 mm was fixed with a neutralised 8% formalin solution and 0.01% Rose Bengal within 6h after sampling. In the laboratory, all macrofauna was identified to genus level and counted. Subsequently, the dry weight and ash-free dry weight was determined for each genus. At T0 and T18/T19, the AFDW was determined by leaving the samples in a stove including the shells (4h, 560°C), whereas at T8 the flesh was removed from the shells before entering the stove. This may have led to higher AFDW of bivalves at T0 and T18/T19, as they could have contained additional organic materials such as algae. Therefore, correction factors were applied to convert the AFDW of flesh plus shells to the AFDW of flesh of the following bivalves present at T0 and T18/T19: *Abra alba* (1.74) (unpublished data, J. Craeymeersch), *Limecola balthica* (1.21) and *Ensis* (1.17) (unpublished data, J. Craeymeersch), *Scrobicularia plana* (1.1), *Mya arenaria* (1.1), *Peringia ulvae* (1.1) and *Retusa obtusa* (1.1) (Dekker, 1987) and *Cerastoderma edule* (1.5) (Mohammad et al., 2015).

At T18/T19, additional macrofauna samples were collected for analysis of the diet composition of macrofaunal genera using a natural stable isotope analysis. Three replicate cores (\varnothing 15 cm) were collected in each control plot, sieved and material > 1 mm was stored in open jars containing water collected on site. *Hediste* was kept in separate jars to prevent predation. Upon arrival at the laboratory, the water was removed and samples were stored frozen (-20°C). In the laboratory, macrofauna were identified to genus level, counted and freeze-dried. Soft parts of bivalve molluscs were removed from the shells before freeze-drying. Gut contents were not removed, as they have a minimal influence on the bulk $\delta^{13}\text{C}$ of macrofauna (Herman et al., 2000). The freeze-dried tissues were homogenized using a mortar. The freeze-dried *Peringia* was treated with 2 N HCL to dissolve inorganic carbonates, which could not be removed manually. Subsequently, the $\delta^{13}\text{C}$ and $\delta^{15}\text{N}$ of macrofauna samples was determined using a Fisons CN analyser coupled on-line via a Finnigan conflo 2 interface, to a Finnigan Delta S mass spectrometer. For the majority of genera, the $\delta^{13}\text{C}$ and $\delta^{15}\text{N}$ was analyzed in the CN analyser for each sampled

individual separately. Individuals of the genera *Mediomastus*, *Pygospio*, *Tharyx*, *Capitella* and *Heteromastus* were merged per three individuals of each genus and analyzed jointly, to obtain enough mass to perform the stable isotope analysis.

4.3.2.4 Sampling and stable isotope analyses of food sources

At T8 and T18/T19, sediment samples were collected with a spoon (~1 cm depth) for the extraction of PLFA's characteristic for diatoms. Using a modified Bligh and Dyer extraction (described in detail in (Middelburg et al., 2000), PLFA's were extracted from wet sediment (~6 g) (Boschker et al., 1999). The $\delta^{13}\text{C}$ of the 20:5w3 and 22:6w3 fatty acids were used as proxy for the carbon isotope ratios of benthic diatoms (Dijkman and Kromkamp, 2006) and are considered suitable as indicator of available benthic algae in the study area, as MPB mainly consist of diatoms in the Westerschelde (Sabbe and Vyverman, 1991). The $\delta^{13}\text{C}$ of the fatty acids was determined using a Varian 3400 gas chromatograph containing a Varian SPI injector, which was coupled to a Finnigan Delta S isotope ratio mass spectrometer (Middelburg et al., 2000). The $\delta^{13}\text{C}$ of the entire diatom cell was determined using fractionation factors of +6.5 (20:5w3) and +7.5 (22:6w3) as described in Daggars et al. (2020). The $\delta^{13}\text{C}$ of diatom cells was calculated as the weighted average of the measured $\delta^{13}\text{C}$ values of the two fatty acids using the relative concentrations as weights. Sediment samples (depth \pm 1 cm) for the determination of the natural stable isotope composition of the bulk sediment were collected with a spoon at T0, T8 and T18/T19. Sediment samples were freeze dried/ stored frozen and subsequently acidified to remove inorganic carbonates (Nieuwenhuize et al., 1994) and measured for the $\delta^{13}\text{C}$ and $\delta^{15}\text{N}$ using the mass spectrometer. The $\delta^{15}\text{N}$ values of diatoms were estimated using the $\delta^{15}\text{N}$ of the sampled bulk sediment +2 for the Oosterschelde and +10 for the Westerschelde, using the difference between the $\delta^{15}\text{N}$ of sedimented organic matter and benthic algae as reported by Riera et al. (2000) (Daggars et al., 2020). Water samples for the determination of the natural stable isotope composition of Suspended Particulate Organic Matter (SPOM) were collected at T8 and T18/T19 and used as indicator for phytoplankton (Galvan et al., 2008; Evrard et al., 2010; Daggars et al., 2020). Earlier studies have demonstrated that in summer, SPOM in the Westerschelde is dominated by autochthonous phytoplankton (Mariotti et al., 1984). The water samples were filtered onto a glass fiber filter (\varnothing 47 mm, Whatman ref no 421026) and the $\delta^{13}\text{C}$ and $\delta^{15}\text{N}$ of the filter residue was measured using the mass spectrometer.

4.3.3 Data analyses

4.3.3.1 Modelling of current velocities

Current velocities at the two tidal flats of interest were calculated using a one-month model run (August 2014) of the ScalOost model (Viane, Oosterschelde) (Pezij, 2015) and the NeVla model (Paulinapolder, Westerschelde) (Van der Werf, 2015; de Vet et al. 2017). From the modelled current velocities, the average maximum current velocity at a fixed point was calculated at each elevation category at each site. The average maximum current velocity at each elevation category was checked for correlation with the average mud content which was sampled at the start and end of the experiment at the plots. Subsequently, the mud content is used as indicator for hydrodynamic activity (Molinarioli et al., 2009).

4.3.3.2 Calculation of spatial heterogeneity of MPB

Drone images (RGB) are available for most plots, but a number of them did not cover all four corner points (50%) and were not used for further analyses. Images containing all four corner points of the plots were corrected for camera angle by resampling the image to its original plot size (which was measured in the field). The original pixel size was $\pm 1\text{-}3\text{ mm}$. Pixels were resampled to a pixel size of 5 mm using bicubic interpolation. A subplot at the center of the plot (301 x 301 pixels; $\pm 1.5 \times 1.5\text{ m}$), which was left undisturbed for the duration of the experiment, was selected for further analysis. The digital numbers (DN) of each band (R, G and B) were converted to a matrix of real numbers (RN) with a value between 0 and 1. To eliminate saturated pixels, the real numbers of each of the 3 bands were summed up and divided by 3, and subsequently only pixels with a resulting value of < 0.9 were included in further calculations. In addition, RGB images were inspected visually for presence of other photosynthetic organisms than MPB, shells (which may contain algae) and measurement equipment (presence is indicated in table S2). In 43% of the images (i.e. control plots) a wave recorder was present, which was removed in Photoshop by cutting out a rectangular shape from the image around the instrument. Macroalgae were present in 69% of the images and were removed by cutting out a rectangular shape around the algae (89% of images containing macroalgae) or using the 'Magic Wand' tool in Photoshop, when macroalgae had a diffuse distribution over the plot (18%). The tool automatically selects pixels with a similar tone and color. Tone and color tolerance was determined by trial and error for each image and selection of macroalgae fragments by the tool was inspected visually. Macroalgae cover was on average $\pm 3\%$, but remarkably high (30%) in a control plot (C2) at Viane (VI) at intermediate elevation (M) at time T2 (VIMC2-T2) and a control (10%) and defaunated plot (D, 40%) at low elevation (L) at time T12 and T18 (VILD2-T12 and VILC2-T18). In all other images macroalgae cover was $<5\%$.

Shells were present in 46% of the images and were removed by cutting out a rectangular shape around the shells (68%) or using the Magic Wand tool (46%). Shell cover was on average $\pm 5\%$ and notably high at VIMD1-T2 (40%) and VIMD2-T2 (25%). In all other images shell cover was $< 6\%$.

In order to calculate spatial variability in MPB biomass, it was necessary to convert the real numbers (RN) in each image to relative reflectance using a flat-field correction. For each image, the raw RN values over two grey cards (10% reflectivity) were extracted and averaged for each grey card for each band. The RN values of the complete image were converted to relative reflectance using the following formula (Murphy et al., 2004):

$$\rho_{\lambda} = \frac{R_{grey\ card} * RN_{image,\lambda}}{\overline{RN}_{grey\ card,\lambda}}$$

where,

ρ_{λ} = Reflectance at each band (λ , R,G, and B)

$RN_{image,\lambda}$ = Real numbers at each image pixel for each band (λ , R,G, and B)

$R_{grey\ card,\lambda}$ = Reflectance of the neutral Fotowand grey cards (10%)

$\overline{RN}_{grey\ card}$ = Average reflectance over the grey cards

To retrieve MPB biomass from multispectral remotely sensed information, the Normalized Difference Vegetation Index is a widely used index, which uses reflectance in the red and near-infrared (Rouse, 1973). For RGB pictures, the Visible-band Difference Vegetation Index (VDVI) is an alternative which proved to have an accuracy of over 90% in vegetated areas (Wang, 2015):

$$VDVI = \frac{2 * \rho_{green} - \rho_{red} - \rho_{blue}}{2 * \rho_{green} + \rho_{red} + \rho_{blue}}$$

The index has not frequently been applied to intertidal flats thus far (van de Vijssel et al., 2020). Visual inspection showed that VDVI maps closely reflected MPB biomass on the RGB images (see figure S1).

MPB biomass varies spatially along a continuous scale and varies from micro ($< 1\text{mm}$) to the estuary scale (Saburova et al., 1995). In this study, spatial heterogeneity of MPB biomass was studied from the 5mm to 0.7 m scale. We quantified spatial variance between the MPB biomass (expressed as VDVI) as function of their separation distance (lag) using a semi-variogram. The VDVI data was normalized to the mean for each picture separately. The variance of MPB biomass between any two pixels in all possible directions, $\gamma(h)$, at a lag of h was calculated as follows using the Gstat R-package (Pebesma, 2004):

$$\Gamma(h) = \frac{1}{2n} \sum_{i=1}^n [z(x_i) - z(x_i + h)]^2$$

where $z(x_i)$ is the MPB biomass at a pixel with coordinate vector x and n denotes the number of pairs of observations available in the RGB image. It is assumed that at this spatial scale ($< 0.7\text{m}$) there is no directionality in spatial variability of MPB biomass based on observation of available images (see Figure 1). From the resulting semi-variogram, where the lag is plotted against the semi-variance, a theoretical model can be fitted and three key parameters can be derived: the sill, range and nugget variance. A Matérn theoretical model was applied to all data, as it gave the best semi-variogram fit (smallest sum of squared errors of the fitted model) as opposed to a spherical or exponential model and the model could be fitted (i.e. converged) in all cases. The sill is the theoretical maximum variance and represents the inherent variance of the studied variable. The range is the lag at which the variogram reaches the sill, and up to which the data is spatially autocorrelated. The nugget is the positive intercept of the semi-variogram and can be caused by microscale (subpixel) variation or noise (Pebesma and Wesseling, 1998).

4.3.3.3 Calculation of macrofauna diet composition and grazing pressure

A Bayesian dual stable isotope mixing model (Parnell et al., 2013) was used to estimate the proportional contribution of MPB and phytoplankton to the diet of the sampled macrofauna at T18/T19 following the procedure described in (Daggers et al., 2020; see Chapter 3). The $\delta^{13}\text{C}$ and $\delta^{15}\text{N}$ of MPB and phytoplankton sampled were averaged over T8 and T18/T19, as the stable isotope values samples at both time steps were in close agreement. The isotope mixing model included in the R package MixSIAR was used (v3.1.7; Stock and Semmens, 2013), in which diet compositions were calculated for each macrofaunal genus per site per elevation category. It was assumed that the diet composition of macrofaunal genera did not differ within elevation zones. Phytoplankton and microphytobenthos were considered the main available food sources for macrofauna, whereas it was assumed that macroalgae and terrestrial organic material do not contribute significantly to the diet. Riera et al. (2000) concluded that terrestrial organic material is not likely to contribute to the diet of invertebrates in the Westerschelde, as their $\delta^{15}\text{N}$ is heavily enriched, while the $\delta^{15}\text{N}$ of terrestrial plants in forests and meadows of drainage areas are $>10\text{‰}$ lower. In the Oosterschelde, a semi-enclosed sea-arm, terrestrial organic material is scarcely present. Macroalgae biomass is negligible in the Westerschelde (Herman et al., 2000), but may be a missed food source in the Oosterschelde, mostly for the relatively mobile species such as *Hediste* (Kristensen et al., 1992) or surface grazers such as snails (Meziane and Tsuchiya, 2000). However, Daggers et al. (2020; Chapter 3) demonstrated that inclusion of macroalgae in a dual stable isotope mixing model results in unrealistically high values proportions of macroalgae in the diet of macrofauna, while macroalgae densities are generally low.

Total grazing pressure on MPB at T0, T8 and T18/T19 was calculated for each plot using 1) the collected macrofauna community composition data at T0, T8 and T18/T19 and 2) the proportions of MPB in the diet of macrofaunal genera calculated using the natural stable isotope values ($\delta^{15}\text{N}$ and $\delta^{13}\text{C}$) of available food sources and macrofaunal genera. Grazing pressure was calculated using the MPB diet fraction and total C demand derived from the macrofaunal biomass, following (Daggers et al., 2020; Chapter 3):

$$\text{Grazing}_{com} = \sum_{spec=1}^n \frac{1.74 \times 10^{-2} \times \text{biomass}_{spec}^{-0.156} \times \text{biomass}_{com} \times \text{food}_{coef, spec}}{(1 - \text{NGE}) \times \text{AsE}}$$

where,

AsE = Assimilation Efficiency (-)

biomass_{spec} = mean individual weight (mg C ind⁻¹)

biomass_{com} = total biomass of species per plot (mg C m⁻²)

density_{spec} = species density (N m⁻²)

$\text{food}_{coef, spec}$ = proportion of MPB in diet (-)

NGE_{spec} = Net Growth Efficiency (-)

Grazing_{com} = grazing macrofaunal community (mg C m⁻² d⁻¹)

The mean individual weight (biomass_{spec}) was converted to an individual respiration rate using the equation for shallow water organisms from Mahaut et al. (1995). The proportion of MPB in the diet of macrofauna ($\text{food}_{coef, spec}$) is the coefficient calculated with the dual stable isotope mixing model. Species specific assimilation efficiencies (AsE) and net growth efficiencies (NGE) were derived from Stratmann et al. (2018).

Assimilation efficiencies (AsE), net growth efficiencies (NGE) and food coefficients were matched to our community composition data on genus level. If no value was available from a particular genus, a value from the same family or ordo was assigned. Otherwise, a median value of the available dataset was assigned. Concerning the food coefficient, a separate median value for bivalves and non-bivalves was used.

For the grazing pressure of the macrofaunal community, the proportion of MPB in the diet of macrofauna was available for 77% at Viane and 94.4% (95.3% at ordo level) at Paulinapolder of the biomass of the total macrofauna community present in the studied plots. For the remaining species, a median value of all non-bivalve species (Paulinapolder: 0.74; Viane: 0.62) and bivalve species (Paulinapolder: 0.51; Viane: 0.56) was used, respectively. For 24.8% of the biomass from our macrofauna community composition data including exclusive suspension feeders we obtained the AsE from Stratmann et al. (2018) matched on genus level, 24.8% on family level and for 59.3% on ordo

level. For remaining species, the median value of all species in the dataset (0.61) was used. The NGE was available for 33.8% of the macrofaunal biomass on genus level, 33.8% on family level and 58.2% on ordo level. For remaining species, the median value of all species in the dataset (0.58) was used.

4.3.3.4 Statistical analyses

Variogram parameters were calculated with and without inclusion of shells. A paired t-test was used to test whether the range, sill and nugget were significantly influenced by inclusion or exclusion of shells.

The impact of the experimental removal of macrofauna (control versus defaunated treatment) on the MPB biomass (VDVI) and the range, sill and nugget derived from the semi-variograms of the MPB biomass was quantified using a repeated measures ANOVA test (factors: treatment, elevation, site).

The effect of the removal of macrofauna on the grazing pressure by macrofauna on MPB eight and eighteen weeks after opening of the defaunated plots was checked using an ANOVA for each time step (T8 and T18) separately (factors: treatment, elevation, site). Normality of the data was checked using a Shapiro-Wilk normality test and homogeneity of variances was checked using a Levene's test. The MPB biomass data (VDVI) of all time steps met the homogeneity of variance assumption ($F = 0.9$, $p = 0.34$), but the residuals of the MPB biomass data (VDVI) did not meet the normality assumption of ANOVA ($W = 0.95$, $p = 0.01$) and had a somewhat right-tailed distribution, which is characteristic for microphytobenthic biomass data (Guarini et al., 1998). No transformation resulted in compliance with both assumptions. Therefore, no data transformation was applied to the MPB biomass data. The residuals of the nugget and sill data of all time steps did not meet the normality assumption (nugget: $W = 0.68$, $p = 1.3 \times 10^{-10}$; sill: $W = 0.81$, $p = 9.0 \times 10^{-8}$; range: $W = 0.98$, $p = 0.65$), and the range did not meet the homogeneity of variance assumption (nugget: $F = 0.17$, $p = 0.68$; sill: $F = 3.12$, $p = 0.08$; range: $F = 6.63$, $p = 0.01$). The distribution of the three parameters was right-tailed.

The relation between mud content of sediment samples collected at the study sites and modelled current velocities was studied using a linear regression model and was used to characterize the hydrodynamic activity at each elevation category at both sites. To perform the linear regression mud contents were averaged per elevation category.

As the effect of macrofauna removal on MPB biomass (VDVI) and spatial heterogeneity is expected to be strongest 2 weeks after opening of the defaunated plots, an ANCOVA was performed on T2 data to gain insight in the effect of treatment and various environmental parameters (factors: treatment,

mud content, elevation, current speed, chl-a, grazing pressure, total macrofaunal biomass) on the range, sill and nugget of the MPB, followed by a HSD Tukey post-hoc test.

The effect of treatment, elevation and site on the macrofaunal grazing pressure was tested using an ANOVA for T8 and T18/T19 separately, to determine whether a difference in grazing pressure between control and defaunated plots was present at each time step, respectively. It was assumed that no macrofauna was present at T0 in defaunated plots.

4.4 Results

4.4.1 Characterisation of abiotic characteristics of the sites

Paulinapolder (Westerschelde) is characterized by a high mud content ($\pm 40\text{--}70\%$), whereas Viane (Oosterschelde) is relatively sandy (mud content $\pm 0\text{--}10\%$; Fig. 2). The average mud content at each elevation category, sampled at the start and end of the experiment, could be predicted at Paulinapolder by modelled current velocities using a site-dependent linear regression formula (Fig. 2; mud content = $-219 * \text{current velocity} + 107$ ($R^2 = 0.99$, $p=0.04$)). At Viane, no significant relationship was present between the mud content averaged per elevation category and the current speed (mud content = $-65 * \text{current velocity} + 16$ ($R^2 = 0.97$, $p = 0.1$)), although a clear trend is observed. Generally, mud content decreased as function of current velocity and with elevation (Fig. 2). For a given current velocity, mud contents were substantially higher in Paulinapolder than in Viane.

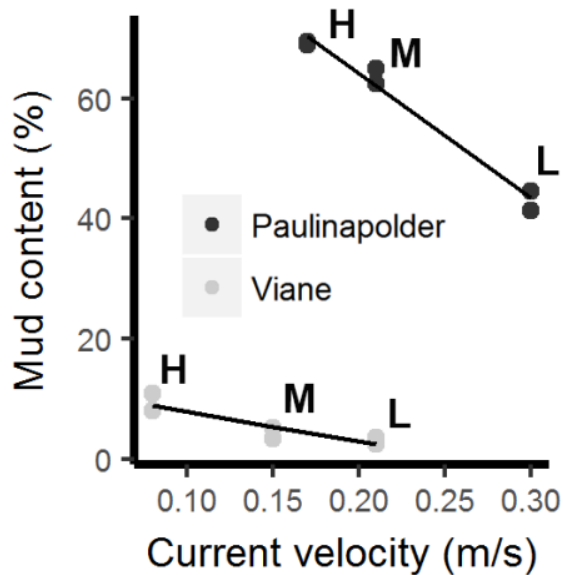


Fig. 2. Mud content (%) from sediment samples collected in control and defaunated plots at 'low' (L; ± 1 m NAP), 'intermediate' (M; ± 0.15 m NAP) and 'high' (H; ± 0.5 m NAP) at Paulinapolder and ± 0.85 m NAP at Viane) elevation. Sediment samples were collected at the start and end of the experiment. Average mud content values per elevation category are displayed for both dates. Modelled current velocities in each elevation zone are displayed.

4.4.2 Spatial characterization of MPB biomass

An ANOVA demonstrated that MPB biomass (VDVI) differed significantly between sites ($n=360$; Table 2) and was higher at Paulina than at Viane (Fig. 3). MPB biomass (VDVI) differed significantly between elevations and was highest at intermediate elevation and higher at high elevation than at low elevation (Fig. 3).

Table 2. ANOVA test for the sampled MPB biomass (VDVI) and variogram parameters (nugget, sill and range) calculated from the VDVI for T2 to T19. Significance level (P) is indicated by '****' = 0, '**' = 0.001, '*' = 0.05.

		Treatment (control / defaunated)	Elevation	Site
MPB biomass	F	1.78	8.36	5.25
	P	0.19	0.0006***	0.025*
	df	1,62	1,62	1,62
Nugget	F	1.22	0.11	0.35
	P	0.28	0.90	0.56
	df	1,62	2,62	1,62
Sill	F	0.21	0.42	3.33
	P	0.65	0.66	0.07
	df	1,62	2,62	1,62
Range	F	6.99	1.65	1.08
	P	0.01*	0.20	0.30
	df	1,62	2,62	1,62

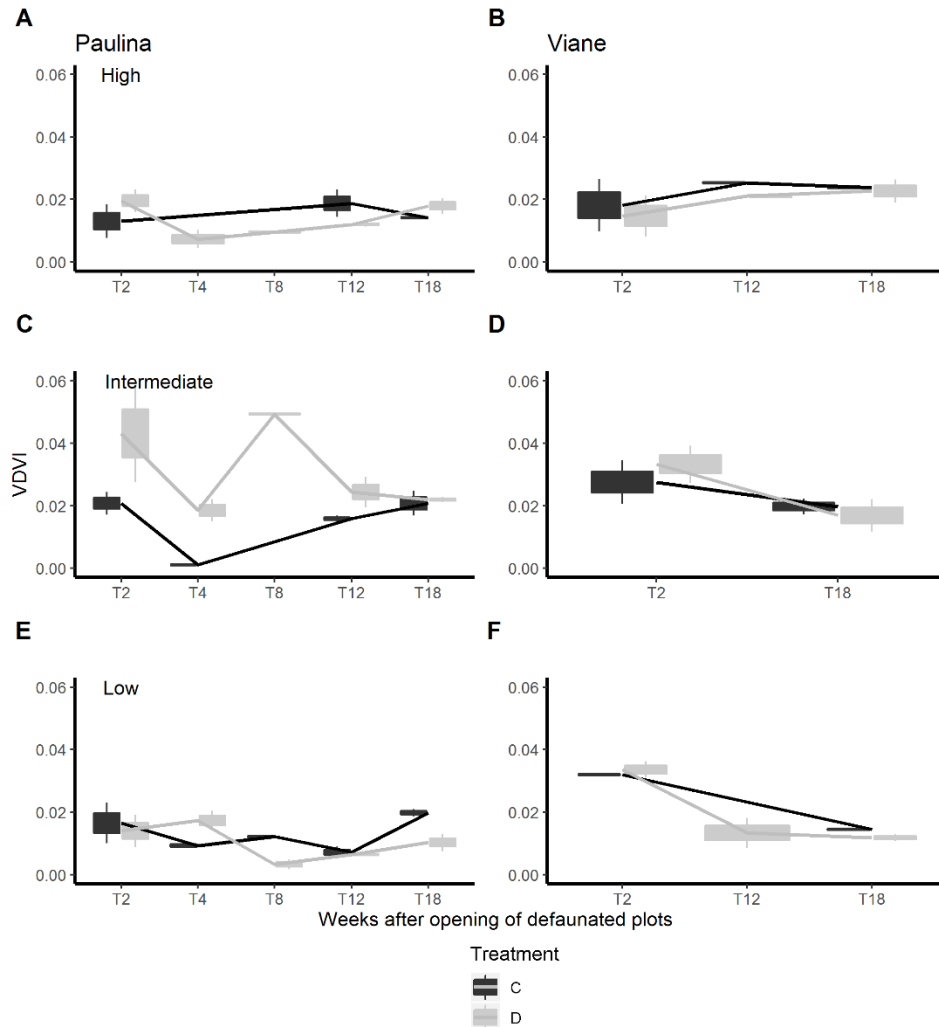


Figure 3. Microphytobenthic biomass (VDVI) in control (C) and defaunated (D) plots in the 'Low' ($\pm -1m$ NAP), 'Intermediate' ($\pm 0m$ NAP) and 'High' ($0.5-0.8m$ NAP) elevation zones. Chl-a was sampled 0, 2, 4, 8, 12 and 19 weeks after opening of the defaunated plots. The plot at Paulina were opened on April 25th 2016, while plots at Viane were opened two weeks later in May 12th and 13th 2016.

4.4.3 Top-down effects on biomass of MPB

No effect of the presence of macrofauna on MPB biomass (VDVI) was observed. The MPB biomass (VDVI) at T2 up to the end of the experiment did not differ significantly between control and defaunated plots ($n=71$; Table 2 and Fig. 3). The ANOVA test was performed separately for the MPB biomass data (VDVI) collected two weeks after opening of the plots (at T2), where the strongest effect of the defaunation would be expected. No significant effect of the

defaunation treatment on MPB biomass (VDVI) at T2 is present ($F_{1,17}=1.85$, $P=0.19$, $n=22$), although the VDVI derived from the RGB camera visually appears to be somewhat higher in defaunated plots than control plots at intermediate (Fig. 4; C2 and D2) and high elevation (Fig. 4; C1 and D1) at Paulinapolder.

4.4.4 Top-down effects of grazing on spatial heterogeneity of MPB

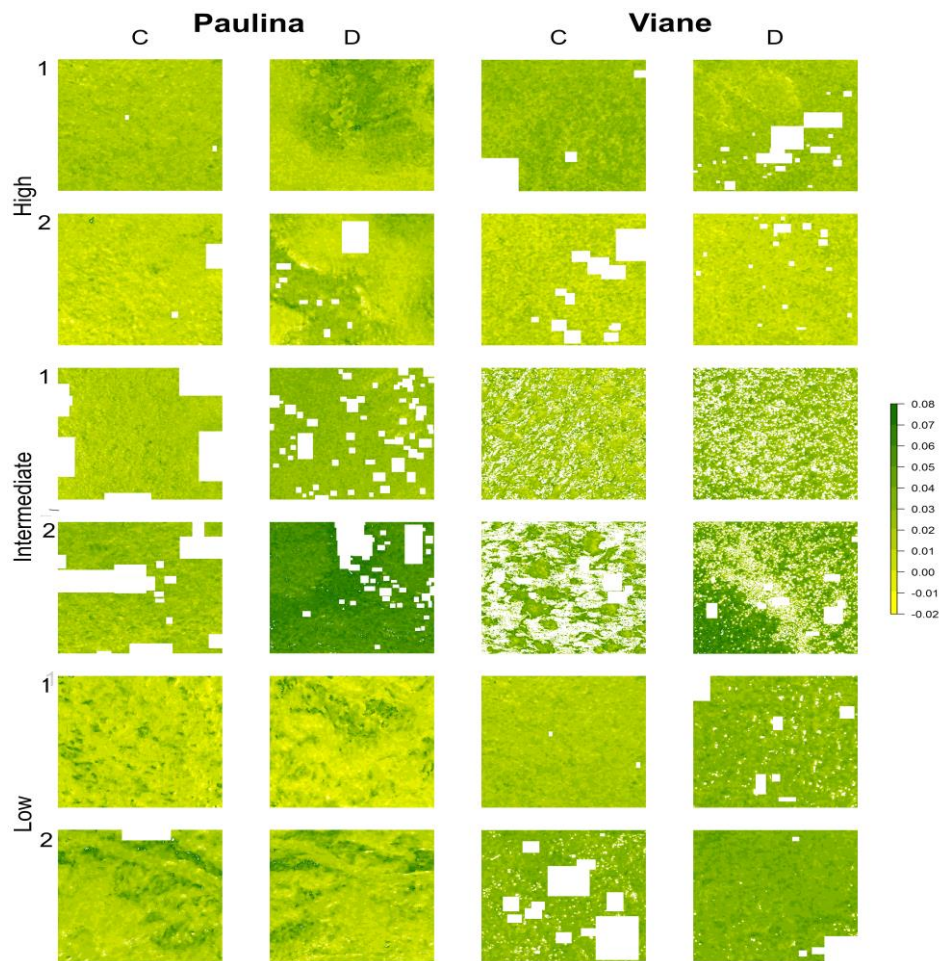


Figure 4. The VDVI two weeks (T2) after opening of the defaunated plots in control (C, with replicates C1 and C2) and defaunated (D, with replicates D1 and D2) plots at Paulinapolder (Westerschelde) at high, intermediate and low elevation and at Viane at high, intermediate and low elevation. Macroalgae and shells were removed from the images and excluded from the semi-variogram analysis. The original images can be found in Figure S1.

Shells were present in 46% of the images used for the analysis of spatial variability in MPB biomass, with shell cover only 5% on average. We checked whether shell presence influenced the calculation of variogram parameters, by calculating variogram parameters with and without exclusion of shells. A paired t-test demonstrated that the obtained major range, sill and nugget values were not significantly different with or without inclusion of shells in the VDMI matrix (major range: $P=0.5$; sill: $P=0.3$; nugget: $P=0.9$).

The major range of the variograms differed significantly between control and defaunated plots ($n=71$; Table 2 and Fig. 5). A HSD Tukey test revealed no statistically significant differences in the major range between the defaunated plots and control plots, ($D-C = 0.09$; $p = 0.3$), indicating that the presence of macrofauna decreases the distance up to which MPB biomass is spatially autocorrelated. The difference appears to be most apparent visually at Paulina at high and intermediate elevation and at Viane at intermediate elevation (Fig. 5). The difference in the range between control and defaunated plots shows an increasing trend with mud content (Fig. 8), except for Viane at intermediate elevation where the mud content is low and a large difference in the range between control and defaunated plots is observed. The observed trend is not statistically significant (Paulinapolder: $R^2 = 0.3$, $p=0.2$, $n=6$, Viane: $R^2 = 0.1$, $p=0.7$, $n=4$).

The nugget and sill did not differ over time or between sites, elevations or treatments. The sill differed significantly between sites and as function of MPB biomass (VDMI) at T2 ($n=23$; Table 4). The sill was higher at Paulina than at Viane, although not statistically significant (HSD Tukey, $p = 0.6$). No effect of the factors treatment, mud content, elevation, grazing pressure or total macrofaunal biomass on variogram parameters was present at T2 (Table 4).

*Table 4. ANCOVA test for the effect of abiotic and biotic variables on the variogram parameters (nugget, sill and range) at T2. Significance level (P) is indicated by '***' = 0, '**' = 0.001, '*' = 0.05.*

	Nugget		Sill				Range		
	F	P	df	F	P	df	F	P	df
Treatment (control / defaunated)	0.22	0.65	1,14	1.90	0.19	1,14	4.28	0.06	1,14
Mud content	2.67	0.13	1,14	0.04	0.85	1,14	1.78	0.20	1,14
Elevation	4.50	0.03*	2,14	0.42	0.66	2,14	0.80	0.47	2,14
Site	0.43	0.53	1,14	5.97	0.03*	1,14	0.33	0.57	1,14
Chl-a	1.95	0.19	1,14	5.97	0.03*	1,14	1.80	0.20	1,14
Grazing pressure	0.35	0.56	1,14	0.03	0.86	1,14	0.01	0.94	1,14
Total macrofaunal biomass	0.07	0.80	1,14	1.26	0.28	1,14	2.22	0.16	1,14

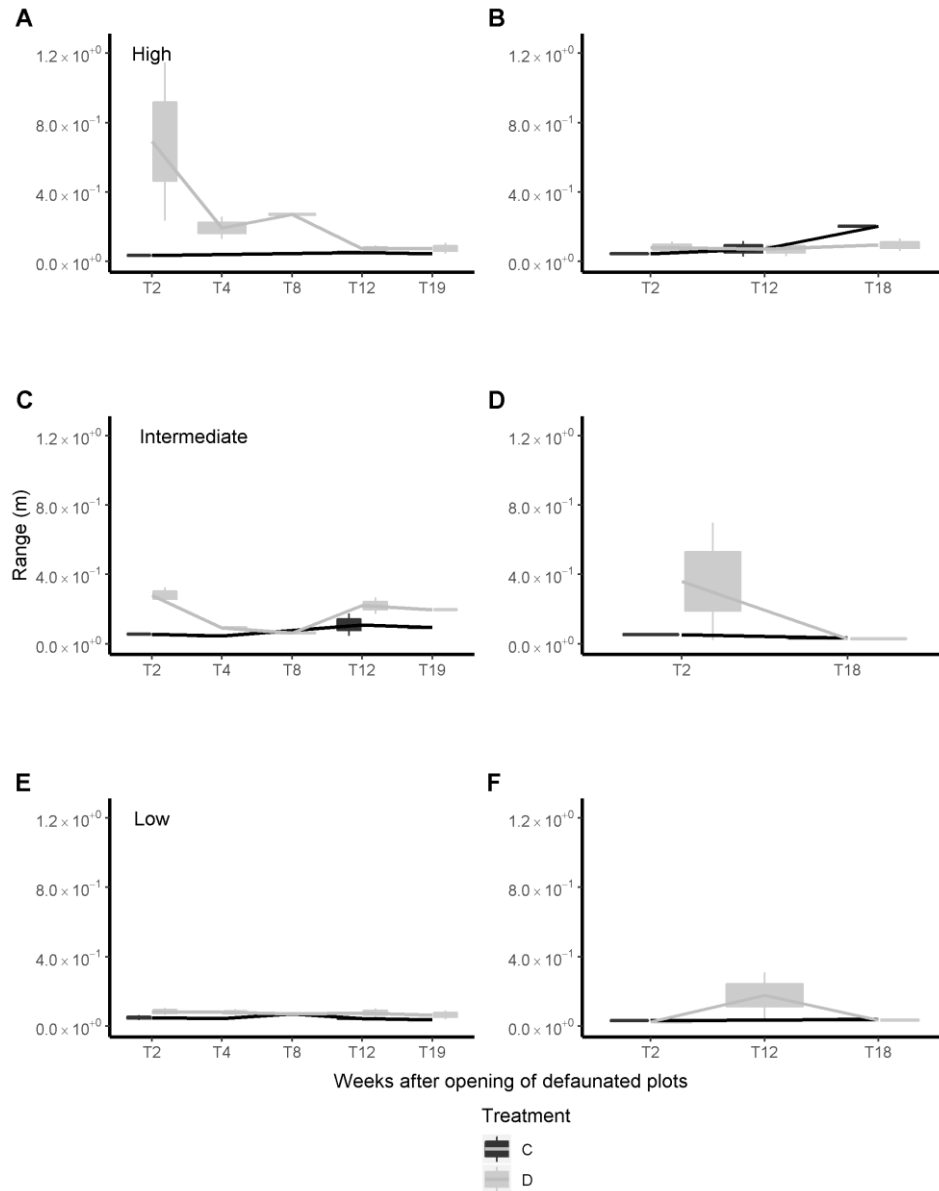


Figure 5. The major range calculated from a semi-variogram for control (C) and defaunated (D) plots at Paulinapolder (Westerschelde) at high (A), intermediate (C) and low elevation (E) and at Viane at high (B), intermediate (D) and low elevation (F).

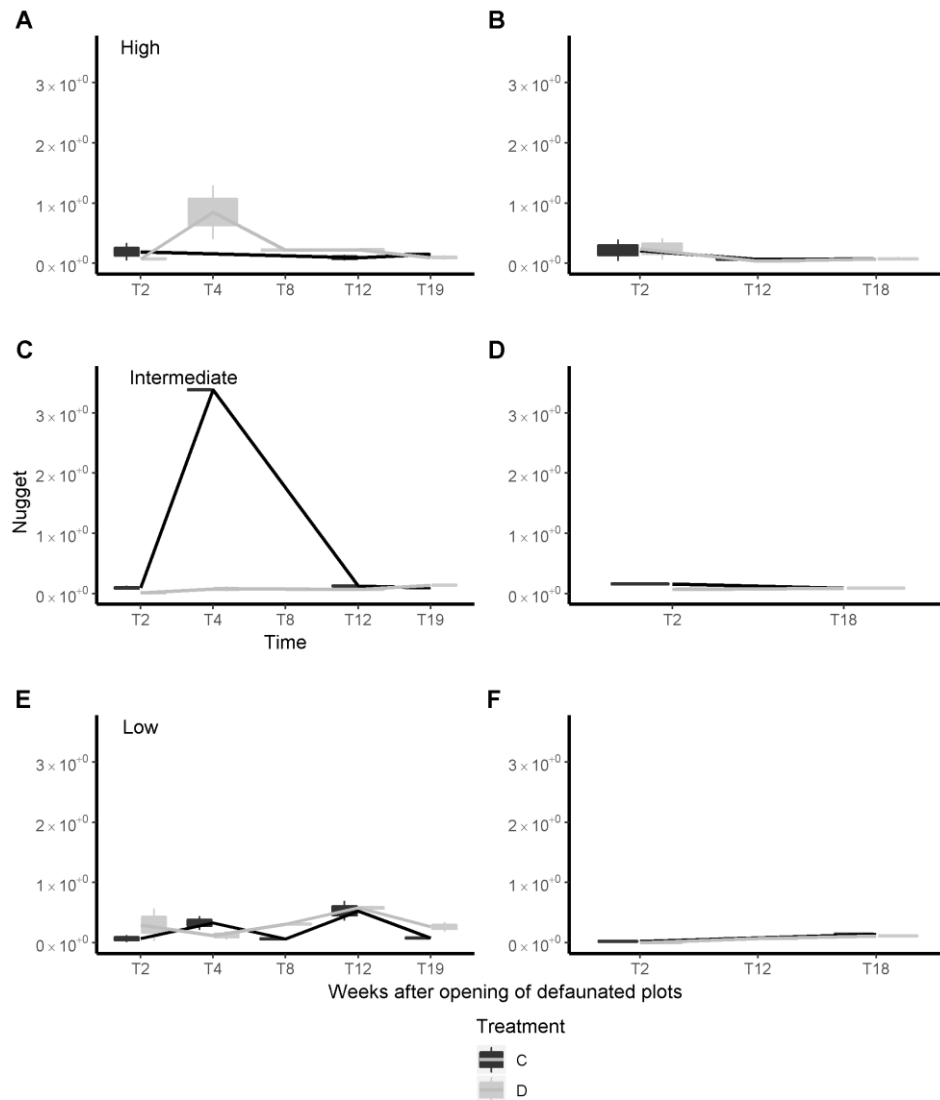


Figure 6. The nugget calculated from a semi-variogram for control (C) and defaunated (D) plots at Paulinapolder (Westerschelde) at high (A), intermediate (C) and low elevation (E) and Viane at high (B), intermediate (D) and low elevation (F).

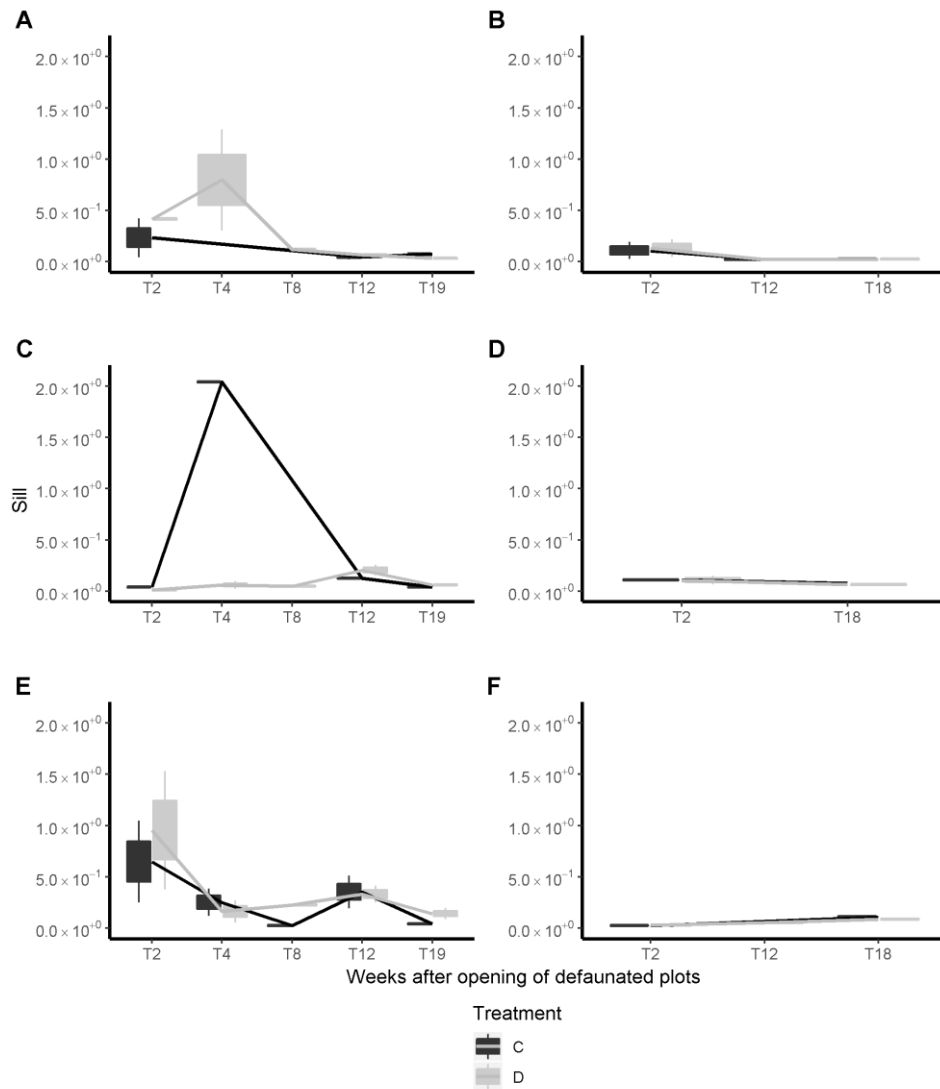


Figure 7. The sill calculated from a semi-variogram for control (C) and defaunated (D) plots at Paulinapolder (Westerschelde) at high (A), intermediate (C) and low elevation (E) and Viane at high (B), intermediate (D) and low elevation (F).

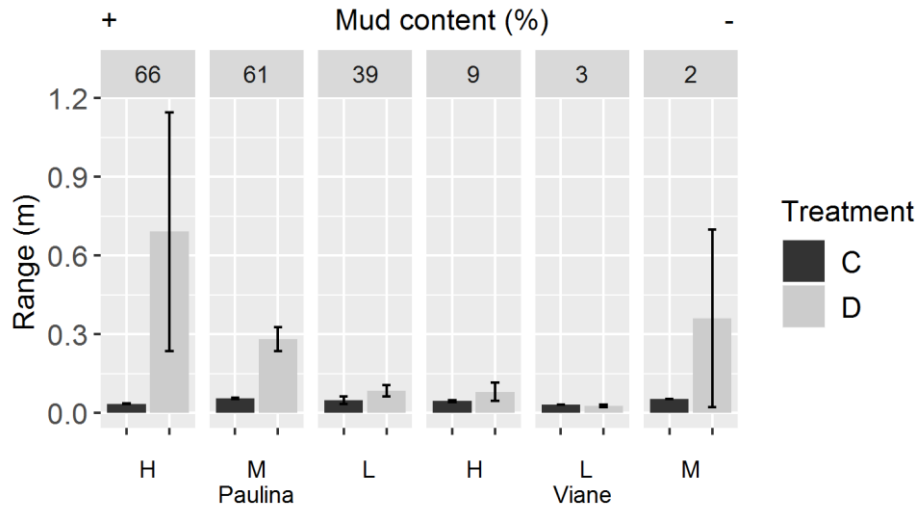


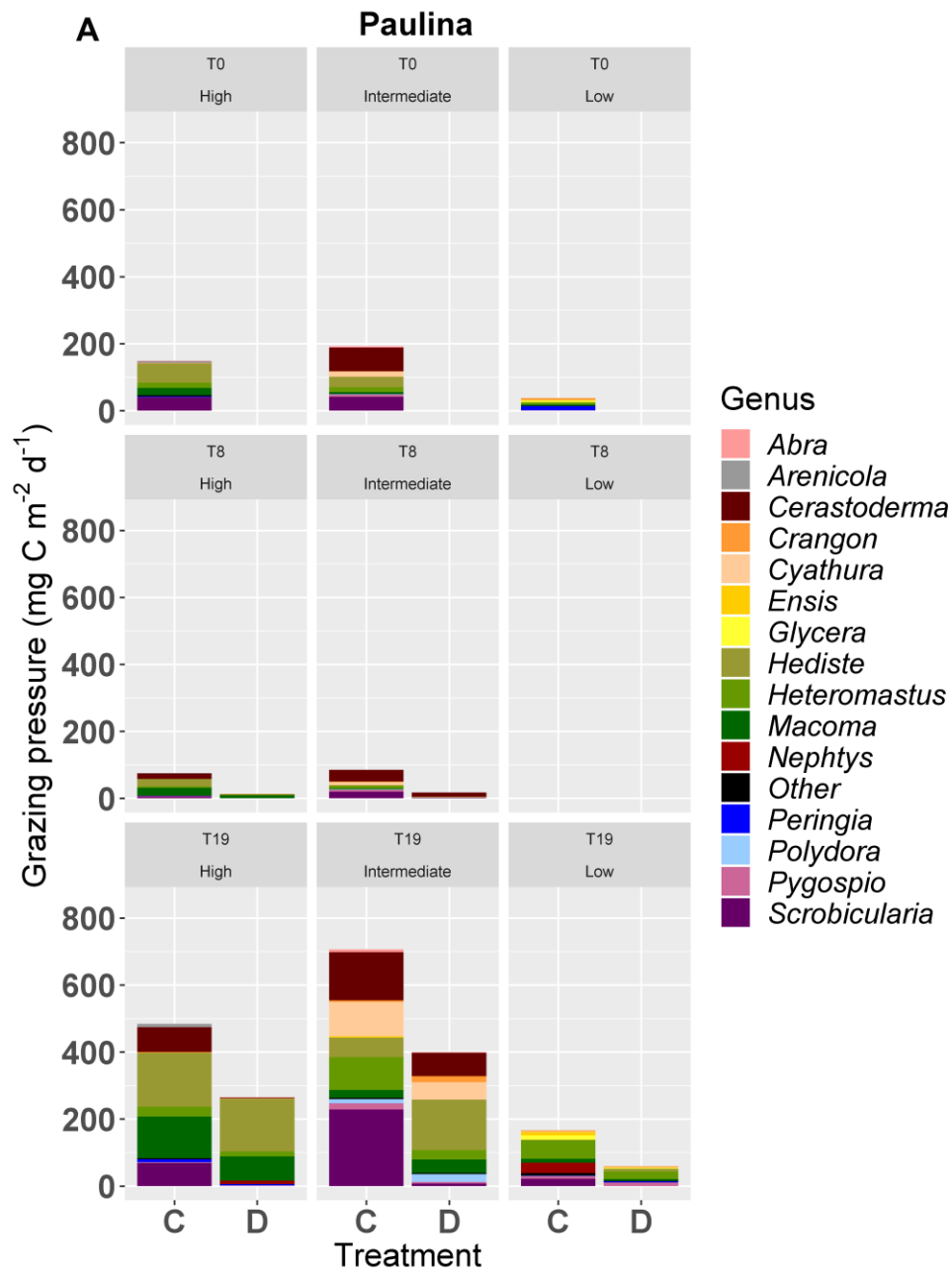
Figure 8. The range in MPB biomass calculated from a semi-variogram at control and defaunated plots (T2) along a gradient in mud content (mud content was sampled at the start of the experiment, i.e. 12/13-05-2016 at Paulinapolder and 25-04-2016 at Viane).

The macrozoobenthic taxa found at the sites are summarized in Table S1. At Paulinapolder, suspension feeders form the major part of the macrofaunal biomass (*Scrobicularia*, *Limecola* and *Cerastoderma*). At Viane, *Peringia* and *Cerastoderma* are the most dominant species in terms of biomass.

The grazing pressure of macrofauna on MPB increases over time in all control plots, except for Viane at high elevation (Fig. 9), in line with seasonal recruitment and growth. It was assumed that no macrofauna was present at T0 in defaunated plots. Eight weeks after opening of the sheets (T8), grazing pressure in defaunated plots is 1-35% of grazing pressure in control plots (Fig. 9B) and grazing pressure is lower in defaunated plots than control plots (ANOVA, factors: treatment, elevation, site, $F_{1,118}=4.51$, $P=0.035$, $n=123$). At the end of the experiment, there is no significant difference anymore between control and defaunated plots (ANOVA, factors: treatment, elevation, site, $F_{1,178}=1.03$, $P=0.31$, $n=183$). Grazing pressure is generally low at T8 and in most cases lower than at T0.

At Paulinapolder, at high and low elevation, the composition of species consuming MPB is mostly similar in control and defaunated plots at the end of the experiment. At high elevation, grazing on MPB mainly occurs by *Hediste*, *Cerastoderma*, *Limecola* and *Scrobicularia* in the control plots. In the defaunated plots at high elevation *Hediste* and *Limecola* are the most important grazers. At intermediate elevation, *Scrobicularia* is absent in defaunated plots, while *Cerastoderma*, *Cyathura*, *Hediste*, *Heteromastus*, *Limecola* and *Polydora* constitute the dominant grazers in both control and

defaunated plots. At low elevation grazing pressure is relatively low and dominated by *Nephtys* and *Heteromastus*. At Viane, grazing pressure is dominated by the surface grazer *Peringia* in control and defaunated plots. At intermediate elevation, the community composition of grazers differs between control and defaunated plots. While grazing is dominated by *Peringia* in control plots, the biomass of *Peringia* was reduced in defaunated plots and replaced by *Cerastoderma*, *Streblospio* and *Hediste*. At low elevation, grazing by *Cerastoderma* is somewhat reduced in defaunated plots compared to control plots. At the end of the defaunation experiment, the macrofaunal community has almost completely recovered (Fig. 9), i.e. the total grazing pressure is higher at the end of the experiment than at the start (Paulinapolder T0: 378, T8: 191, T19: 2078 mg C m⁻² d⁻¹; Viane: T0: 883, T8: 230, T18: 4032 mg C m⁻² d⁻¹). Macrofaunal grazing pressure is lower at T8 than at T0 at Paulinapolder (all elevation categories) and Viane (high and low elevation).



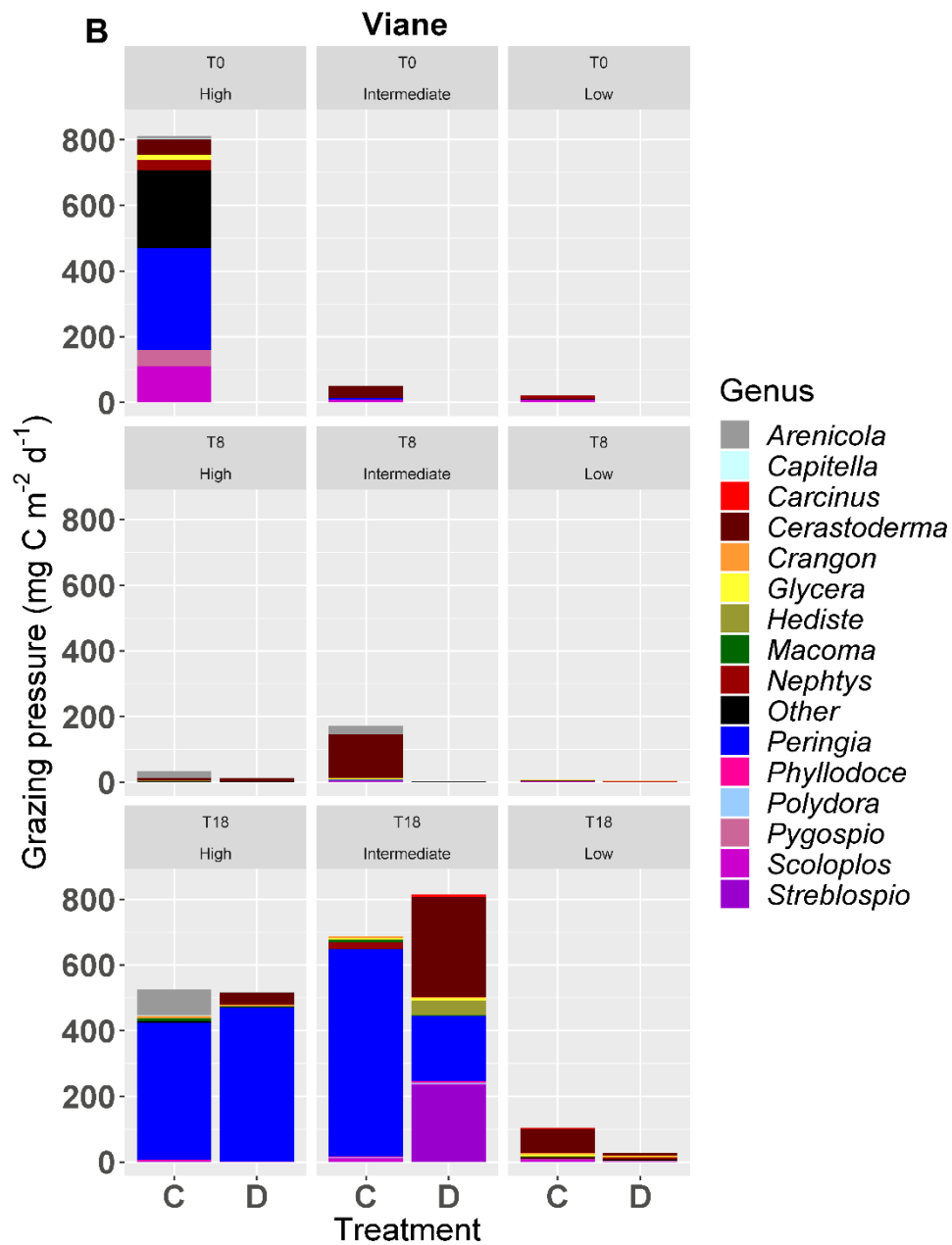


Figure 9. Macrofaunal biomass at control and defaunated plots at the start of the experiment (T0), eight weeks after opening of the plots (T8) and at the end of the experiment (T18) at Paulinapolder (A) and Viane (B). The 15 species with the highest total grazing pressure on MPB at each site are displayed.

4.5 Discussion

On the macro (tidal basin) scale, MPB biomass is known to vary spatially as a function of abiotic factors, such as mud content and elevation. To gain insight in the spatial heterogeneity of MPB biomass on smaller (centimetre to meter) scales and the effect of top down control on MPB biomass under varying hydrodynamic conditions, macrofauna was experimentally excluded at low, intermediate and high intertidal zones in two tidal basins in the Netherlands. We hypothesized that (H1) top down control on MPB is strongest when macrofaunal grazing pressure is high, and hydrodynamic exposure is low, while (H2) at locations with a high hydrodynamic exposure, the influence of waves and currents is expected to overrule influence of macrofaunal presence on spatial variability in MPB biomass. In our study, top down control by macrofauna on MPB did not influence the MPB biomass standing stock under all studied hydrodynamic conditions. However, the presence of macrofauna changed the small-scale spatial heterogeneity of MPB. That is, the major range resulting from a semi-variogram was higher at defaunated plots than control plots, demonstrating that macrofauna decreases the distance up to which MPB biomass is spatially autocorrelated. This means that areas with a similar MPB biomass occupy smaller surfaces in the presence of macrofauna than they would in the absence of macrofauna. The larger spatial heterogeneity of MPB due to macrofaunal grazing has important implications for the erodibility of tidal flats, as a homogeneous MPB cover typically smoothens the sediment surface and shields it from erosion.

4.5.1 The effect of macrofauna on biomass and spatial heterogeneity of microphytobenthos

Spatial patterning of MPB is known to be self-organized at the square meter scale under hydrodynamically sheltered (Weerman et al., 2010) and exposed (Seuront and Spilmont, 2002) conditions. However, few studies have addressed the role of macrofauna in MPB spatial pattern formation. Pratt et al. (2015) found a higher variation (standard deviation) in chl-a concentrations in areas with a higher cover of *Macomona Liliana* feeding traces, but specific spatial structures in the presence versus absence of macrofauna have rarely been studied. It has been demonstrated that under hydrodynamically sheltered conditions macrofauna can remove high density MPB patches within days, whereby a more homogeneous MPB distribution remains. Subsequently, macrofauna inhibits the formation of new high density patches (Weerman et al., 2011a). Our study, performed under hydrodynamically more exposed conditions, does not show homogenization of the MPB distribution, but demonstrates that large patches are replaced by smaller patches in the presence of macrofauna. This may increase the erodibility of the sediment, which is directly related to the sediment chlorophyll-a content (Andersen et al.,

2010). During low tide, water accumulates in the areas between MPB patches. The presence of overlaying water may inhibit the accumulation of extracellular polymeric substances (EPS) excreted by MPB, which 'glue' the MPB biofilm together, as the EPS dissolves in the overlaying water (Weerman et al., 2011b). In this way, reformation of a continuous biofilm is prevented.

Studies of spatial heterogeneity often focus on the description of patch sizes or the distance between patches. However, distinct patches can rarely be identified and observed patterns depend on the scale and spatial resolution considered (Azovsky et al., 2000). Also in the present study, MPB varies on a continuous scale and the range derived from the semi-variogram gives the size of areas with a similar MPB biomass ('patch'). Azovsky et al. (2000) analysed spatial heterogeneity of diatom species (rather than total diatom biomass) using a measure for spatial heterogeneity based on the Shannon diversity index. The heterogeneity of diatom biomass is described as highly variable and having a random-mosaic distribution, which means the evenness of the biomass increases linearly with the resolution of the data and (to a minor degree) the extent of the area of interest. Diatom biomass was equally heterogeneous on a scale of meters as on a scale of dozens of meters. Furthermore, a regular gradient was observed on the hundred meter to kilometre scale. Saburova et al. (1995) demonstrated that abundant diatom species show at least two orders of aggregation. The degree of aggregation (Cassie index) showed a peak at 60-70 cm² and is low at other considered distances < 1m². At spatial scales > 1m², aggregations occur at all scales of investigation considered (10-10000 m²), whereby the degree of aggregation increases logarithmically with distance. The spatial scale of 70 cm² coincides with a range of approximately 0.9m, assuming circle shaped patches. Our finding that the range of the MPB biomass is relatively low in control plots coincides with the finding of Saburova et al. (1995) that the degree of aggregation of MPB species is low < 1m², except at a range of 0.9m.

The difference in the geostatistical range of the MPB biomass between control and defaunated plots shows an increasing trend with mud content, although not statistically significant (Fig. 8). Further research, using a larger number of replicates per sediment type, could provide further insight in possible effects of mud content on the geostatistical range. The trend is in line with our second hypothesis (H2) that the influence of current speed dominates the effect on spatial heterogeneity over macrofaunal presence at the sandiest plots, and that this hydrodynamic dominance shifts to an effect of top-down control on spatial heterogeneity with decreasing hydrodynamic energy. However, it should be considered that the macrofaunal community composition, to some extent, co-varies with sediment grain-size characteristics (including mud content), elevation and MPB biomass (Cozzoli et al., 2013; Thrush et al., 2003; van der Wal et al., 2008). At Paulinapolder at low elevation and Viane at low and

intermediate elevation, macrofaunal grazing pressure was particularly low (Fig. 9). At Paulinapolder at high elevation, the most dominant species present are *Hediste* (omnivore), *Cerastoderma* (suspension feeder), *Limecola* (facultative surface deposit feeder and suspension feeder) and *Scrobicularia* (surface deposit feeder). At Viane at high elevation, *Peringia* (surface grazer), *Scoloplos* (deposit feeder) and *Gammarus* (omnivore) were the most dominant species present. As surface deposit feeders form an important part of the macrofaunal community, an effect of macrofauna on the range would be expected at both sites, not considering differences in hydrodynamic energy. As this is not the observed effect, the gradient in hydrodynamic energy is more likely to influence the difference in range between control and defaunated plots than the macrofaunal community composition.

4.5.2 The relative impact of top-down control on microphytobenthic biomass

An effect of top down control by macrofauna on the MPB biomass standing stock was demonstrated in various studies where MPB biomass was significantly higher in defaunated than control plots (de Deckere et al., 2001; Smith et al., 1996; Weerman et al., 2011b). However, some studies report no effect of predator exclusion on MPB biomass (Posey et al., 1995; Posey et al., 1999), including this study. The MPB biomass standing stock is regulated by bottom-up (Posey et al., 1999) and top-down factors along with disturbance events, where bottom-up effects may vary depending on the extent of top-down control (Hagerthey et al., 2002). The varying results of defaunation experiments may be attributed to i) local environmental conditions that may influence both the level of MPB biomass and the effect of the defaunation, ii) timing of the defaunation and iii) the macrofaunal community composition. Each relevant factor is discussed below.

4.5.2.1 Overruling local environmental conditions

In sandy versus muddy sediments, local abiotic conditions are different, which may affect MPB growth rates. Hydrodynamic energy (waves and currents) may move surficial MPB to deeper, light-limited, layers and deeper algal cells to the photic layer. As MPB can survive in dark conditions for years (Kamp et al., 2011) and even benefit from nutrients available at depth (Saburova and Polikarpov, 2003), the MPB community survives under conditions of frequent sediment mixing and the 'produced' MPB in the photic zone is divided over several sediment layers. In sandy sediments, sediment mixing occurs to a depth of approximately 3 to 6 cm, while in muddy sediments the effect is restricted to the upper 1 to 2 cm of the sediment (Billerbeck et al., 2007). The effect of sediment mixing on the surficial MPB stock can potentially overrule the effect of grazing in sandy sediments, where hydrodynamic energy is generally higher (Molinarioli et al., 2009). Furthermore, wave and current

energy induce resuspension of MPB into the water column. An annular flume experiment demonstrated that at sandy sites, resuspension rates increase gradually over a current velocity range of 0.1-0.4 m/s. At silty sites with well-developed diatom mats, large amounts of MPB resuspend at current velocities > 0.20-0.25 m/s (Lucas et al., 2000). Wind-induced waves cause resuspension of MPB as well (Dejonge and Vanbeusekom, 1995). In our study, the average current velocity exceeds the erosion threshold of 0.2 m/s at the muddy site Paulinapolder at intermediate and low elevation, suggesting that resuspension may have occurred.

Nutrient availability is generally not considered a limiting factor for MPB growth in intertidal sediments (Billerbeck et al., 2007), although nutrient limitation has been demonstrated in sandy sediments under experimental conditions (Nilsson and Sundback, 1991) which may have played a role in lowering the MPB biomass in the Oosterschelde (Viane) in both control and defaunated plots. In the Westerschelde, we expected nutrient limitation not to have played a role in controlling the MPB biomass standing stock (Barranguet et al., 1998; Kromkamp et al., 1998).

4.5.2.2 Timing of the defaunation

In an earlier defaunation experiment in the Westerschelde, at Paulinapolder, an increase in MPB biomass was observed four to twelve weeks after the defaunated plots were opened at the end of March (Van Colen et al., 2008). In the present study, such a steep increase in MPB biomass was not found. However, the defaunated plots were opened four to six weeks later in the season causing that defaunated plots may have been rapidly colonized by larval recruits, as recruitment generally peaks in May-June (Van Colen et al., 2008). Primary settlement of larvae mainly occurs on tidal flats located high in the intertidal zone (above mean tide level, ± 0 NAP) (van der Meer et al., 2003). Therefore, larvae would be expected at the intermediate and high elevation zones. A defaunation experiment that was performed by Weerman et al. (2011b) in the Westerschelde in May, resulted in significantly higher chl-*a* concentrations in defaunated plots than control plots. Weerman et al. (2011b) measured a rapid decline in MPB biomass in May during two consecutive years, after which macrofaunal biomass increased. The rapid decline in MPB biomass was attributed to settlement of macrofaunal species, including *Macoma* (*Limecola*) larvae, which consume MPB.

The observed decline in chl-*a* concentrations at Paulina at high elevation could be related to an increase in larvae biomass, although the decreasing trend is not observed at Paulina at intermediate elevation. However, as macrofauna was sampled using a 1 mm mesh sieve, the biomass of larvae was neither recorded nor included in the calculation of the total grazing pressure on MPB.

In the current study, macrofaunal grazing pressure was relatively low at T8, i.e. lower than at T0. The difference may be due to the fact that the AFDW was determined by removing the flesh from the shells before entering the stove, while at T0 and T18/T19 the AFDW was determined including the shells. Although we have applied correction factors available from literature (see section 2.2.3), it is possible that this may have influenced the result.

4.5.2.3 Varying macrofaunal community compositions

The effect of top down control by macrofauna on the MPB biomass standing stock should logically be related to the macrofaunal community composition and their diet. The most abundant species found in this study, namely *Peringia*, *Urothoe*, *Scoloplos*, *Heteromastus*, *Cyathura*, *Crangon*, *Limecola*, *Tellinoidea* and *Terebellidae*, feed mostly (>50%) on benthic diatoms. Based on the community composition alone and the total grazing pressure being relatively high compared to MPB production rates (Daggers et al., 2020), an effect on the MPB biomass would be expected. Hagerthey et al. (2002) found that chl-*a* concentrations were not reduced by high densities of *Peringia ulvae* or *Corophium volutator*, except by application of a high nutrient-high temperature treatment. This indicates that bottom-up processes such as nutrient availability can regulate the effect of top-down control on MPB standing stock.

Bioturbation of the sediment by high densities of macrofauna promotes mineralisation of organic matter, hereby stimulating MPB growth (Sandwell et al., 2009). However, bioturbation can indirectly cause a decline in MPB biomass as well as by disintegration of MPB biofilms and increasing the erodibility of the sediment (Orvain et al., 2004). At Paulinapolder, the dominant species *Hediste* has a high sediment reworking potential and *Limecola* has an intermediate reworking potential. At Viane, the dominant species *Scoloplos* has a high reworking potential. The sediment reworking potential of the dominant genera *Peringia* and *Gammarus* has not been classified, but is expected to be low. It should be taken into account that bioturbation plays a role in the MPB biomass standing stock visible at the sediment surface as well as spatial heterogeneity in MPB biomass.

Overall, we found a limited effect of benthic macrofaunal presence on the MPB biomass standing stock. Macrofaunal presence resulted in a shorter distance over which MPB showed spatial autocorrelation (range derived from a semi-variogram). This implies that macrofauna may prevent MPB from forming continuous biofilms, which stabilize the sediment and reduce sediment erodibility. The stabilizing effect of MPB biofilms may, therefore, be reduced at locations where macrofaunal bioturbation and/ or grazing occurs. Few studies have addressed interactive effects of macrofaunal and MPB presence on sediment erodibility (Le Hir et al., 2007; Orvain et al., 2004). Further research

under different conditions is required to test the generality of these findings. A controlled mesocosm experiment, where sediment surfaces with MPB are exposed to different macrofauna communities under varying hydrodynamic forcing, could shed further light on the role of macrofauna in MPB biomass and patterning.

Acknowledgements

We would like to thank Lennart van IJzerloo and Jeroen van Dalen for setting up the defaunation experiment and for carrying out field measurements and sampling. We would like to thank Tom Ysebaert and Brenda Walles for their help with setting up the experiment, Frank Brouwer for help with the determination of macrofauna samples and Jim van Belzen for help with image processing. This research was supported by the 'User Support Programme Space Research' of the Netherlands Organisation for Scientific Research (NWO), grant number ALW-GO 13/14, to DVDW.

Chapter 5 Seasonal and spatial variability in patchiness of microphytobenthos on intertidal flats from Sentinel-2 satellite imagery

Tisja D. Daggars, Peter M. J. Herman, Daphne van der Wal

STATUS: Published in Frontiers in Marine Science (2020) 7, 392.

5.1 Abstract

Understanding the spatial structure of microphytobenthos (MPB) on intertidal flats is necessary to gain insight in the benthic community structure and ecosystem processes. The increasing availability of high resolution satellite sensors provides the opportunity to better understand spatial patterns of MPB on various (meter to km) scales. We tested how MPB patch size (indicated by the range derived from a semi-variogram) and degree of patchiness (indicated by the sill) vary as function of seasons, salinity, tidal flat type (muddy fringing versus sandy mid-channel tidal flats) or ecotopes (defined by hydrodynamics, silt content and elevation), in the Westerschelde estuary, the Netherlands. We used Sentinel-2 imagery (2016-2019) with 10 m spatial resolution to derive (omnidirectional) semi-variogram parameters from the NDVI (used as indicator for MPB biomass) and evaluated (seasonality in) patchiness of MPB in the different categories. We demonstrated that MPB patch size (the range) remains constant from winter to summer, while the sill increased from winter to summer. The location of patches on tidal flats was variable throughout the year and shows a remarkable similarity with seasonality in the spatial heterogeneity of the silt content on tidal flats. The patch size and degree of patchiness is higher on relatively sandy mid-channel tidal flats than on relatively silt rich fringing tidal flats. This implies that spatial patterning of MPB biomass on the meso scale is likely closely linked to abiotic conditions and that spreading processes or grazing activity play a minor role.

We observed visually that some areas with a relatively high MPB biomass ('patches') remain visible throughout the year, while other patches were only present during a particular season.

Key words: microphytobenthos, patchiness, intertidal flats, silt, remote sensing

5.2 Introduction

Microphytobenthos (MPB) living on intertidal flats in estuaries, consisting of cyanobacteria and unicellular eukaryotic algae, can form a considerable part of the total primary production in estuaries (Underwood and Kromkamp, 1999). MPB on intertidal flats mainly consist of benthic diatoms (Meleder et al., 2007). Several studies have emphasized the key role of MPB in sustaining intertidal food webs (Christianen et al., 2017; Herman et al., 2000; Thrush et al., 2012) and stabilizing the sediment (Orvain et al., 2004; Ubertini et al., 2015). Strong environmental gradients are present in estuarine ecosystems associated with distance to the mouth (salinity, temperature and tidal amplitude) and elevation (current velocity and sediment composition) (Moreira et al., 1993). These environmental gradients, in turn, structure the spatial variability of biota, including the macrobenthic community and MPB.

Intertidal areas that are relatively homogeneous in terms of the environmental factors can be classified into ecotopes (Baptist et al., 2019; Bouma et al., 2006), and these may also structure the biota.

Meso-scale (i.e., meters to kilometers) and macro-scale (kilometers up to scale of an entire estuary) spatial variability in MPB biomass on intertidal sediments has often been associated with sediment characteristics, bathymetry and wave action (bottom-up control) (Benyoucef et al., 2014; Brito et al., 2013; Guarini et al., 1998; Orvain et al., 2012; van der Wal et al., 2010b), while micro scale (up to ca 1 meter) spatial variability has been associated with grazing by benthic fauna (top-down control) (Weerman et al., 2011). Orvain et al. (2012) identified median grain size of the sediment as the most important parameter explaining spatial variability of MPB, using a macro-scale *in situ* sampling campaign. Van der Wal et al. (2010b) identified positive correlations between MPB biomass and emersion duration, mud content and their interaction, using MODIS satellite imagery of various temperate tidal basins and estuaries. The species composition of benthic diatoms has been associated with sediment characteristics, with epipsammic (sand-fixed) species, mainly occurring in relatively sandy sediments and epipelagic (migrating) species, dominating relatively silty sediments (Paterson et al., 1998). Seasonal variability in MPB biomass has been associated with abiotic factors such as irradiance, temperature, nutrient concentrations and wind velocity (Ubertini et al., 2012 and references therein; Van der Wal et al., 2010b).

The macrofaunal community is known to vary as function of current velocity, sediment composition and salinity (Cozzoli et al., 2013; van der Wal et al., 2008). Macrobenthos may promote or inhibit MPB abundance through various mechanisms, including grazing and physical disturbances (bioturbation) (Solan et al., 2003). Bioturbation from motile infauna (e.g. bivalves, crustaceans, gastropods and polychaetes) may contribute to the decline of MPB biomass

through resuspension and burial below the photic zone (Andersen et al., 2002; de Deckere et al., 2001; Orvain et al., 2004). Small scale effects of macrofaunal grazing on spatial patterns of MPB have been observed, whereby fauna lowered MPB biomass and patchiness (Weerman et al., 2011). However, few studies have focused on meso-scale effects of macrofauna on spatial patterns of MPB biomass. In the Westerschelde, The Netherlands, species richness, biomass and abundance of macrofauna decreases with increasing grain size of the sediment, likely due to increasing hydrodynamic stress in sandy habitats (Cozzoli et al., 2013). The total biomass and number of species of macrofauna in the intertidal areas of the Westerschelde has been demonstrated to strongly decrease with decreasing salinity (Ysebaert et al., 2003). In the polyhaline zone, suspension feeders dominate in terms of biomass and decrease with decreasing salinity. Likewise, surface deposit feeders and sub-surface deposit feeders have a higher biomass in the polyhaline zone than in the mesohaline zone (Ysebaert et al., 2003).

Understanding of the spatial structure of microphytobenthos (MPB) on intertidal flats is necessary to understand community structure and ecosystem functioning (Brito et al., 2013; Murphy et al., 2008). The increasing availability of high resolution satellite sensors provides the opportunity to better understand spatial patterns of MPB on the scale at which ecosystem functioning can be analyzed (meso- and macro-scale). Furthermore, the increasing temporal resolution of satellite imagery may add to insight in changes in spatial patterns of MPB over time. As MPB usually forms small patches at a scale smaller than the resolution of most available satellite sensors, unmanned aerial vehicles (UAVs) may provide detailed information on spatial patterns of MPB on finer spatial scales (<1m) (Ryu et al., 2014).

Few studies have addressed specific sizes of MPB patches on the meso- or macro-scale. Guarini et al. (1998) performed a geostatistical semi-variogram analysis on MPB biomass data collected in winter and summer (1km grid resolution). The analysis revealed that patches of high MPB biomass were located at the same spots in summer and winter. A decrease in patch size was observed from summer to winter indicated by the semi-variogram range, which decreased from 6 to 2 km. The process leading to the observed pattern could not be identified. Morris (2005) performed *in situ* sampling campaigns on several tidal flats located in multiple estuaries and emphasized that, because of the dependency of chl-a distributions on topography and sediment properties, spatial patterns of chl-a can have a highly site specific nature.

In the Westerschelde, fringing tidal flats generally have a relatively high silt content, low hydrodynamic energy and high macrofaunal biomass compared to the relatively sandy tidal flats located in the mid-channel. We hypothesize that the degree of patchiness (represented by the sill of a semi-variogram) is

lower and the patch size (represented by the range of a semi-variogram) of MPB is higher on mid-channel tidal flats than on fringing tidal flats. We expect that the higher hydrodynamic activity on mid-channel tidal flats compared to fringing tidal flats homogenizes spatial variation in MPB biomass, due to the high resuspension rates of MPB associated with higher current velocities (Lucas et al., 2000). The degree of patchiness is expected to decrease with decreasing salinity due to lower grazing and bioturbation by macrofauna, while the patch size (range) may increase with decreasing salinity.

We hypothesize that patch size and degree of patchiness of MPB increases during the expected spring bloom (early spring) and decreases again in summer and winter. Hereby, it is assumed that MPB biomass follows a constant-density model (Guarini et al., 1998), whereby an increase in MPB biomass expands the patch sizes when an 'optimum' MPB biomass at the center of the patch is reached. We expect that in spring, patch size and degree of patchiness are mainly coupled to abiotic factors, while in summer macrofauna may influence these parameters by increased grazing activity and bioturbation

We analyze the seasonality in spatial patterns in MPB along a longitudinal gradient in the Westerschelde estuary, The Netherlands, using semi-variograms. Spatial patterns of MPB are studied on the meso scale at study sites located in varying abiotic and biotic environments along the estuarine gradient. Differences in MPB patch sizes (range of the semi-variogram), degree of patchiness (sill of the semi-variogram), micro-scale variability (nugget of the semi-variogram) and total MPB biomass are compared among seasons, salinity, tidal flat type (fringing, relatively silty or mid-channel, relatively sandy) and ecotopes whereby available Sentinel-2 imagery (10 m resolution) from 2016-2019 is used.

5.3 Methodology

5.3.1 Study sites

The study is performed in the Westerschelde, The Netherlands. The salinity decreases in upstream direction and varies from polyhaline to α -mesohaline. The selected study sites are located in a strongly polyhaline region (29.23 ± 1.36), weakly polyhaline region (23.96 ± 1.52) and α -mesohaline region (16.52 ± 2.04), respectively (Figure 1; (Ysebaert et al., 2003)). In each salinity zone, a tidal flat located in the mid-channel and a fringing tidal flat was selected. The sediment composition in the intertidal is similar along the estuarine gradient (Cozzoli et al., 2013).

MPB is the main benthic primary producer in the Westerschelde (Daggers et al., 2019). MPB biomass in the surface layer of intertidal sediments of the

Westerschelde (i.e. the upper 2 mm) varies from approximately 5 to 300 mg chl *a* m⁻² (Daggers et al., 2019; Sahan et al., 2007). In a study on the Molenplaat in the Westerschelde, MPB assemblages were dominated by benthic diatoms in spring and autumn, while in summer cyanobacteria and euglenoids became more abundant (Barranguet et al., 1997). In another study performed at the Molenplaat, benthic diatoms were found to be dominant in June (Kromkamp et al., 2006). Benthic diatoms consist of epipellic and epipsammic species. In a study on a brackish site in the Westerschelde, the epipsammic fraction was most abundant and dominated by *Achnantes delicatula*, *Opephora* cf. *perminuta* and *Catenula adhaerens* (Sabbe, 1993), but many other (episammic) species can be found in the Westerschelde, such as *Rhaphoneis amphioceros* and *R. munitissima* (Sabbe and Vyverman, 1991). The epipellic diatom community composition is related locally to the tidal regime and sediment composition (Sabbe and Vyverman, 1991) and on the estuary scale to the salinity gradient, whereby brackish sites e.g. contain *Navicula flautica*, *N. gregaria*, *N. phyllepta*, *Gyrosigma* sp., *Stauphora salina* and *Tryblionella hungarica* and marine sites e.g. contain the salt tolerant *Amphora* spp., *N. arenaria* var. *rostellata*, *N. microdsigitoradiata*, *N. cf. mollis* and *N. perminuta* (Sahan et al., 2007). The community composition of epipellic diatoms varies seasonally, notably at marine sites, containing a higher diversity and larger sized diatoms in late spring and summer than in early spring (Sahan et al., 2007).

Macroalgae densities are generally low and macroalgae are mainly located at the base of the dikes (Lucas and Holligan, 1999; Riera et al., 2000). Nevertheless, field surveys have revealed some patches with macroalgae (*Ulva* sp, *Vaucheria* sp.) in summer, particularly *Ulva* sp. at the southeastern side of the Molenplaat, and at the edge of a chenier on the southern side of Lage Springer.

The most common macrofauna species in the Westerschelde (observed in number of samples) are the capitellid worm *Heteromastus filiformis*, the saltwater clam *Macoma balthica*, the polychaete worm *Pygospio elegans*, the sand digger shrimp *Bathyporeia* spp., the ragworm *Hediste diversicolor* and the mudsnail *Peringia ulvae* (Ysebaert et al., 2003).

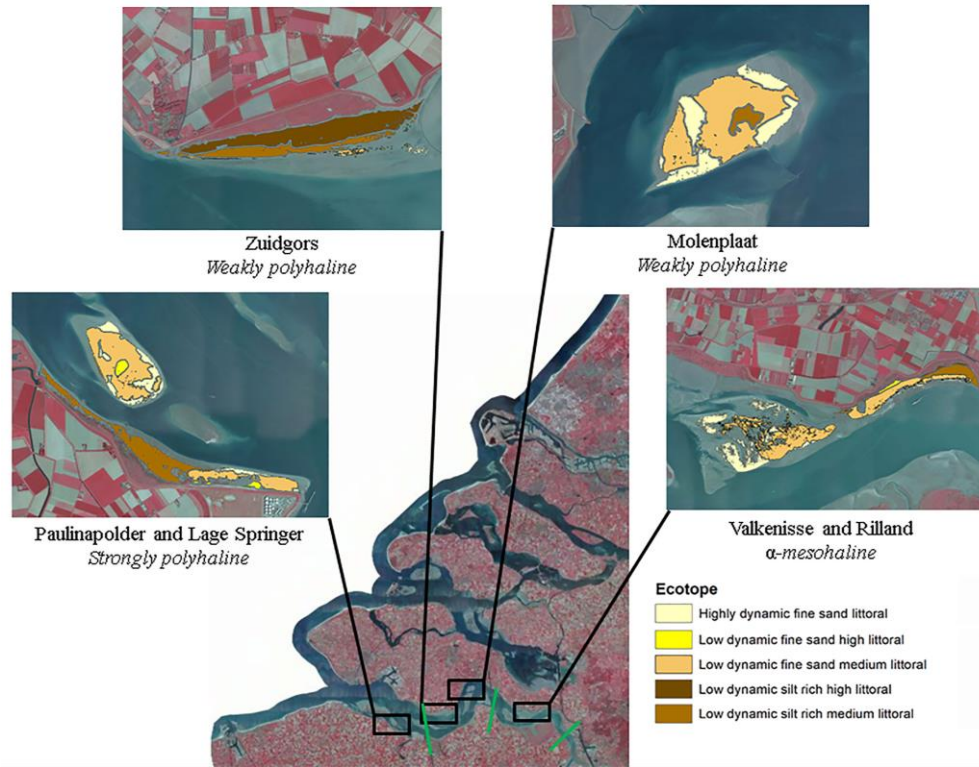


Figure 1. Study sites. The boundaries between different salinity zones (strongly polyhaline, weakly polyhaline and α -mesohaline) are indicated in green. The boundaries of the study areas are the outer boundaries of the displayed ecotopes and contain the part of the tidal flat that was emerged at all images (see 'Data analyses' for a detailed description of the followed procedure). Ecotope information was obtained from Rijkswaterstaat (2016). Source image: Esri, aerial photograph of the Netherlands CIR – 25 cm resolution, 2017

5.3.2 Sentinel-2 satellite data and pre-processing

Sentinel-2 MSI data for the tiles 31UES and 31UET from April 2016 to July 2019 were downloaded as level 1C data (before 2018) or level 2A (from 1 April 2017) from the Scientific hub at <https://scihub.copernicus.eu>. The level 1C data were atmospherically corrected using Sen2Cor v2.2; for level 2A the correction was already applied. For the atmospheric correction of the level 1C images, we assumed an aerosol type “maritime”, and used the default cirrus correction. Further default settings ensured that the temperature profile and ozone content were determined from the metadata of the image with a LUT to determine the best fit for the measured ozone concentration, and visibility was automatically calculated and averaged from the scene using a dark pixel approach (all images had a visibility of >20km, clear sky). The season was also taken from the image metadata. On all images, an empirical line calibration was applied to band 4 (surface reflectance in the red) and 8 (surface

reflectance in the near-infrared) of each image, using a set of reference points with semi-invariant surfaces (e.g. roofs, deep clear water) and regressed to surface reflectances in band 4 and 8 of an atmospherically corrected image with clear sky (March 12th 2016). This normalization was applied to best compare the images in time. In all cases, regressions had fits of $R^2 > 0.74$ and in most cases $R^2 \geq 0.90$. The equations for both bands in each image are provided in Table S1.

A Normalized Differential Vegetation Index (NDVI) was based on the resulting surface reflectance in band 4 (10 m resolution reflectance in the red RR) and band 8 (10m resolution reflectance in the near-infrared RNIR), following $(RNIR-RR)/(RR+RNIR)$ (Daggers et al., 2018; Kromkamp et al., 2006; Van der Wal et al., 2010b). Satellite images acquired during clear sky and low tide conditions were selected, considering groups of 3 images per season (Table 1). Pixels with clouds and cloud shadows were masked using manually defined polygons based on visual inspection of the image; such masks were applied for small areas in the sites of Rilland and Valkenisse on the image of July 5th 2019. The NDVI is used as proxy for MPB biomass on the emerged tidal flats, as elaborated below in section 2.4. on data analyses. This proxy is widely used (e.g., Kazemipour et al., 2012; Kromkamp et al., 2006; van der Wal et al., 2010b) and validated for this purpose with chlorophyll-a data collected at several sites along the estuarine gradient in the Dutch part of the Westerschelde (Daggers et al., 2018 and 2019).

Table 1. Overview of Copernicus Sentinel-2 MSI imagery used for data analyses. Water level and tidal stage at overpass were obtained from Rijkswaterstaat data at station Hansweert (data source: <https://waterinfo.rws.nl>).

Season	Satellite and sensor	Acquisition date (dd-mm-yyyy)	Acquisition time (UTC)	Water level (m NAP)	Tidal stage
Winter	Sentinel-2B MSI	05-02-2018	10:53	-2.40	Outgoing
(December	Sentinel-2B MSI	12-12-2018	10:54	-2.24	Outgoing
to February)	Sentinel-2B MSI	21-01-2019	10:55	-0.38	Incoming
Early spring	Sentinel-2A MSI	11-04-2016	10:50	-2.52	Outgoing
(March to	Sentinel-2A MSI	27-03-2017	10:50	-0.53	Incoming
April)	Sentinel-2B MSI	06-04-2018	10:50	-1.89	Outgoing
Late spring	Sentinel-2A MSI	26-05-2017	10:50	-0.95	Incoming
(May to	Sentinel-2B MSI	06-05-2018	10:50	-1.52	Outgoing
June)	Sentinel-2A MSI	30-06-2018	10:50	-1.31	Incoming
Summer	Sentinel-2A MSI	20-07-2016	10:55	-0.73	Incoming
(July)	Sentinel-2B MSI	15-07-2018	10:50	-1.56	Incoming
	Sentinel-2A MSI	05-07-2019	10:50	-1.55	Incoming

5.3.3 Ecotope and bathymetry maps

An ecotope map of the Westerschelde was obtained from Rijkswaterstaat (2016), and used to identify intertidal areas that are ecologically distinct (Bouma et al., 2006). The ecotope map of the Westerschelde considers the following abiotic factors for the ecotope classification of intertidal areas: hydrodynamics (high energy: maximum linear current velocity > 0.8 m/s, low energy: maximum linear current velocity < 0.8 m/s), depth (low littoral: 75% flood duration, medium high littoral: 75-25%, 25%) and sediment composition (silt rich: $\geq 25\%$ silt, < 63 μm ; fine sand: $> 25\%$ silt and median < 250 μm).

Airborne LiDAR data of the intertidal areas of the Westerschelde (2014-2018) were also obtained from Rijkswaterstaat (cm spatial resolution); these data were used to characterise the tidal flats of interest in terms of their mean elevation and standard deviation.

5.3.4 Data analyses

The pixels used for the semi-variogram analysis were selected using a mask. Pixels with NDVI < -0.05 were considered to be water, and were removed. The boundary NDVI value of -0.05 was determined empirically, as areas with NDVI values > -0.05 were visibly emerged. Pixels with an NDVI < 0 may contain some standing water. Pixels with NDVI > 0.3 were excluded to exclude areas containing macroalgae. A buffer of 10m along saltmarshes was applied, to exclude pioneer vegetation. Only pixels that were emerged and did not contain macroalgae or saltmarsh vegetation at all available imagery were used for further analyses, i.e. the same mask was applied to all images. Using the ecotope map, saltmarshes present at low to high densities, peat and hard substratum were excluded from the study area. A buffer of 20m was applied between ecotopes, to prevent edge effects in the semi-variogram analyses per ecotope. Semi-variograms of NDVI (as a proxy for microphytobenthos biomass MPB on emerged sediments), were used to quantify the degree (sill) and scale (range) of MPB patchiness (Rossi et al., 1992; Legendre and Legendre, 2012) for each tidal flat per image using the gstat package version 2.0-2 (Pebesma, 2004) in R version 3.6.0. Variograms were fit using the following default initial parameters: the maximum lag was taken as one third of the maximum sample variogram distance, the nugget parameter was taken as the mean of the first three sample variogram values and the partial sill was given the mean of the last five sample variogram values. To obtain the lag interval, the maximum lag was divided into fifteen equal lags. A fit was considered as 'converged' when the change in the weighted sum of squares of differences between the semi-variogram model and sample variogram became less than 10^6 times the last value of this sum of squares. The nugget represents random variation on the sub-pixel scale ($< 10\text{m}$). Omnidirectional semi-variograms were calculated for each tidal flat separately at each date (Table 1), where a tidal flat is defined as

a consecutive intertidal area with a minimum width of 100m. Furthermore, semi-variograms were calculated per ecotope on each tidal flat (see Figure 1 for an overview of ecotopes present). A spherical model gave the best semi-variogram fit (smallest sum of squared errors of the fitted model) at the majority of datasets as opposed to a Matern or exponential model and was therefore applied to all data. NDVI data per ecotope for which a semi-variogram could not be fitted, as autocorrelation was present in the entire study area, was excluded from further analyses (15% of ecotope data). The NDVI values were normally distributed (Shapiro-Wilk, $p > 0.05$). The NDVI data was 1) detrended using a 1st degree polynomial function to achieve stationary conditions, and 2) normalised by dividing by the standard deviation per tidal flat or ecotope.

Three images per season from winter to summer were considered (Table 1), whereby a distinction was made between early and late spring. The effect of season, salinity and tidal flat type (fringing or mid-channel) on MPB biomass, patch size (range), degree of patchiness (sill) and micro-scale variability (nugget) per tidal flat was quantified using an ANOVA test and HSD Tukey post-hoc test. The residuals did not meet the normality assumption (Shapiro-Wilk, $p < 0.01$) and showed a somewhat right-tailed distribution as commonly observed in biological datasets. Variation in semi-variogram parameters calculated per ecotope per site was tested using an ANOVA and HSD Tukey post-hoc test for the factors season, salinity and ecotope. We tested whether a linear correlation was present between the MPB biomass and sill using the Pearson product-moment correlation coefficient.

The locations on the tidal flats of interest where the NDVI was high or low, respectively, in particular seasons was similar over the years (2016-2019, inspected visually) and the NDVI was therefore averaged per season to produce maps with mean (non de-trended, non-normalized) NDVI per season. In addition, maps of the coefficient of variation in NDVI (calculated as σ/μ per pixel for the study period 2016-2019) were produced for each of the tidal flats and analysed visually.

5.4 Results

5.4.1 Site characteristics

The selected tidal flats, i.e. the surface area selected for semi-variogram analysis ($-0.05 < \text{NDVI} < 0.30$), had a similar surface area with the exception of Valkenisse (\pm a factor 2 larger) and similar average MPB biomass, i.e., NDVI (Table 2). The percentage of area covered with silt rich sediment derived from the ecotope map was profoundly larger on fringing tidal flats than on mid-channel tidal flats. The average elevation of the sites was similar, although Zuidgors was located somewhat higher in the intertidal (1.45 m NAP).

Table 2. General characteristics of the areas of interest of the selected tidal flats, i.e. $-0.05 < \text{NDVI} < 0.3$.

Site	Surface area (km ²)	NDVI (MPB) ($\mu \pm \sigma$)	% Silt rich area	Salinity	Tidal flat type	Height 2014-2018 $\mu \pm \sigma$ (m NAP*)
Paulinapolder	0.94	0.075 \pm 0.037	63	Strongly polyhaline	Fringing	0.61 \pm 0.05
Zuidgors	0.88	0.047 \pm 0.031	96	Weakly polyhaline	Fringing	1.45 \pm 0.18
Rilland	1.08	0.062 \pm 0.029	26	α -mesohaline	Fringing	0.87 \pm 0.08
Lage Springer	1.14	0.057 \pm 0.034	1	Strongly polyhaline	Mid-channel	0.71 \pm 0.06
Molenplaat	1.12	0.074 \pm 0.029	5	Weakly polyhaline	Mid-channel	0.36 \pm 0.10
Valkenisse	2.02	0.039 \pm 0.038	0	α -mesohaline	Mid-channel	0.58 \pm 0.54

*The elevation values are with regard to the Dutch ordnance system NAP (Normaal Amsterdams Peil), which is approximately similar to mean sea level

5.4.2 Seasonality in MPB biomass

The MPB biomass was higher in summer than in early spring (Table 3; ANOVA, $P=0.004$, $F_{3,55}=4.80$, $n=72$; HSD Tukey, $p < 0.05$). The MPB biomass did not differ significantly between fringing and mid-channel tidal flats (ANOVA, $P=0.9$, $F_{1,65}=0.02$, $n=72$) or among salinity zones (ANOVA, $P=0.45$, $F_{2,65}=0.81$, $n=72$). Particularly at Zuidgors, Molenplaat and Valkenisse an increasing trend in MPB biomass was observed from early spring to summer, while a large amount of variation in the biomass was present in winter among the years 2016-2019 at most sites (Figure 2).

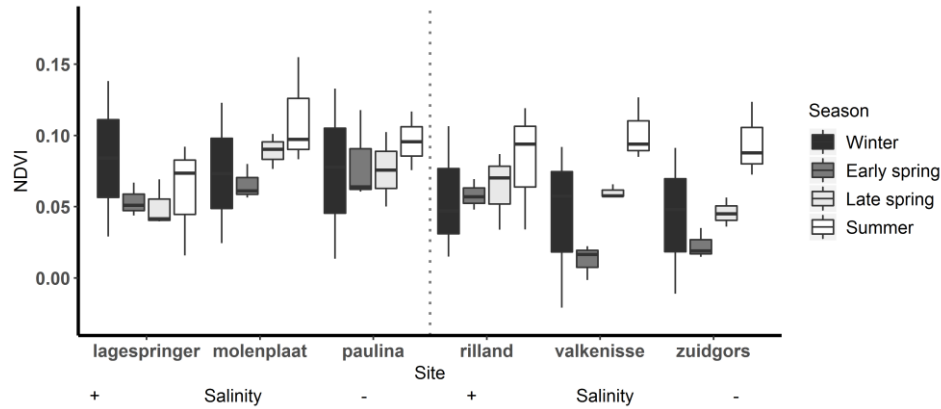


Figure 2. MPB biomass, expressed as the NDVI, on each tidal flat per season. Winter: December to February, early spring: March to April, late spring: May to June, summer: July.

5.4.3 Semi-variogram parameters per site

The range derived from the semi-variograms of the normalised NDVI showed a high degree of similarity among different dates at each site (Figure 3, Table S2). The range of the semi-variogram (patch size) did not vary among seasons (ANOVA, $P=0.17$, $F_{3,65}=1.72$, $n=72$) and appeared relatively constant throughout the year (Figure 4). Although the location of patches was in many cases constant throughout the year, the location of the patches may change over time (Figure 6 and Figure S1). The range was higher in the mesohaline zone (603 m) than in the weakly polyhaline (338 m) and strongly polyhaline zone (366 m) (ANOVA, $P=2.77 \times 10^{-6}$, $F_{2,65}=15.68$, $n=72$; HSD Tukey, $p < 0.0001$). Furthermore, the range was higher at tidal flats located in the mid-channel (510 m) than at fringing tidal flats (362 m) (ANOVA, $P<0.001$, $F_{1,65}=12.28$, $n=72$; HSD Tukey, $p < 0.001$). The angle of the major range was estimated visually from anisotropy maps and was highly consistent throughout the year (Lage springer: ± 135 , Molenplaat: ± 60 , Paulinapolder: ± 115 , Rilland: ± 70 , Valkenisse: ± 100 , Zuidgors: ± 80).

The sill showed an increasing trend throughout the year (Figure 4). The sill was higher in early spring, late spring and summer than in winter and the sill was higher in summer than in early spring (ANOVA, $P=1.7 \times 10^{-9}$, $F_{3,65}=20.6$, $n=72$; HSD Tukey, $p < 0.05$). The sill was higher on mid-channel tidal flats than on fringing tidal flats (ANOVA, $P=0.004$, $F_{3,65}=9.18$, $n=72$; HSD Tukey, $p < 0.01$). The sill was not significantly correlated with MPB biomass (Pearson's $r = 0.17$, $p=0.16$).

The nugget showed a decreasing trend throughout the year (Figure 4). The nugget did not vary significantly as function of salinity, but was lower in early spring, late spring and summer than in winter. Furthermore, the nugget was

lower in late spring and summer than in early spring (ANOVA, $P=2.54 \times 10^{-13}$, $F_{3,65}=33.95$, $n=72$; HSD Tukey, $p < 0.05$). The nugget was higher on fringing tidal flats than on mid-channel tidal flats (ANOVA, $P=0.01$, $F_{3,65}=6.85$, $n=72$; HSD Tukey, $p < 0.05$).

Table 3. Statistics of MPB biomass and semi-variogram parameters calculated per site. Significance level (P) is indicated by '****' = 0, '***' = 0.001, '**'=0.05.

		Season	Salinity	Type
MPB biomass	F	4.80	0.81	0.02
	P	0.004**	0.45	0.90
	df	3,65	2,65	1,65
Nugget	F	33.95	0.46	6.85
	P	2.54×10^{-13}	0.63	0.01*
	df	3,65	2,65	1,65
Sill	F	20.60	2.96	9.18
	P	1.7×10^{-9} ***	0.06	0.004**
	df	3,65	2,65	1,65
Range	F	1.72	15.68	12.28
	P	0.17	2.77×10^{-6} ***	0.0008***
	df	3,65	2,65	1,65

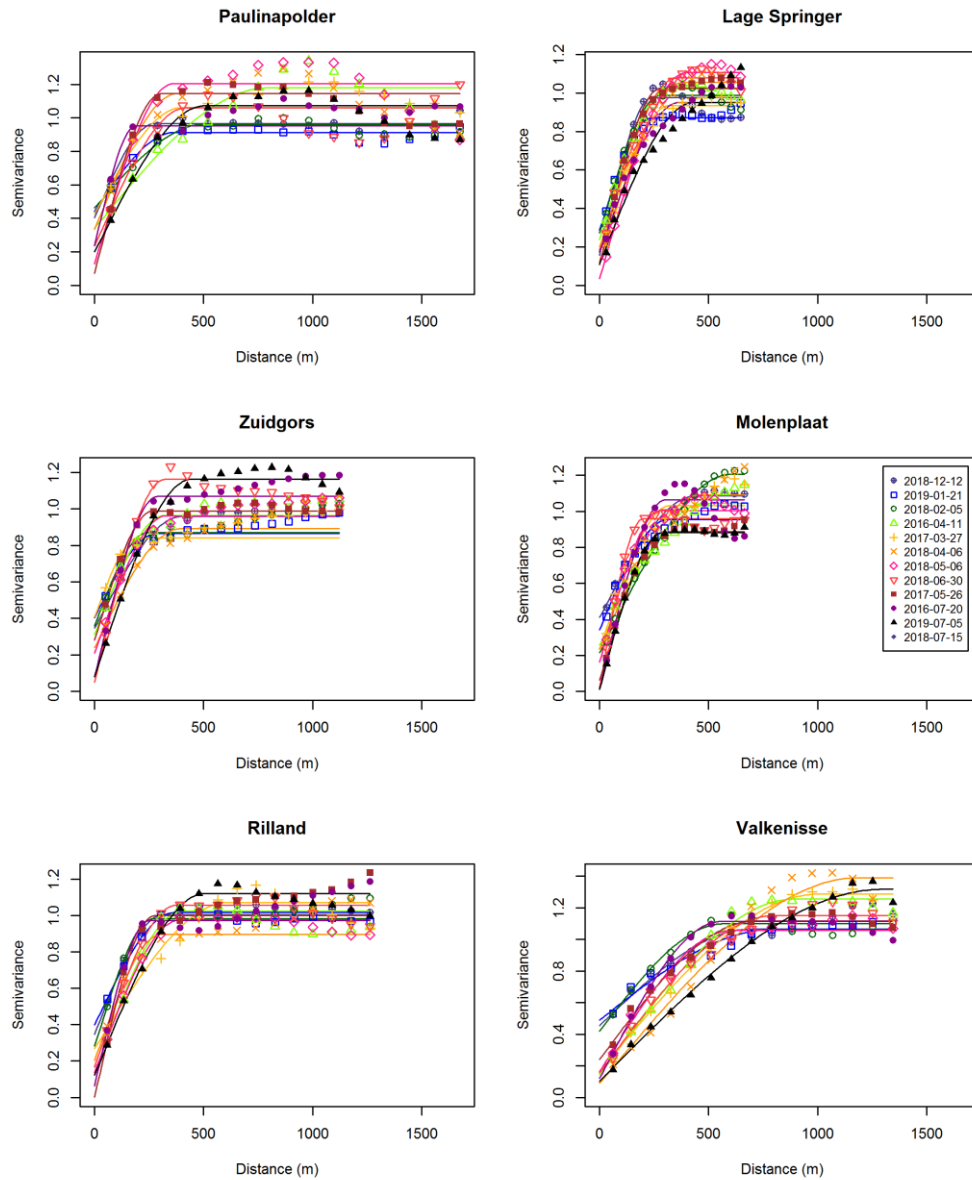


Figure 3. Semi-variograms per site.

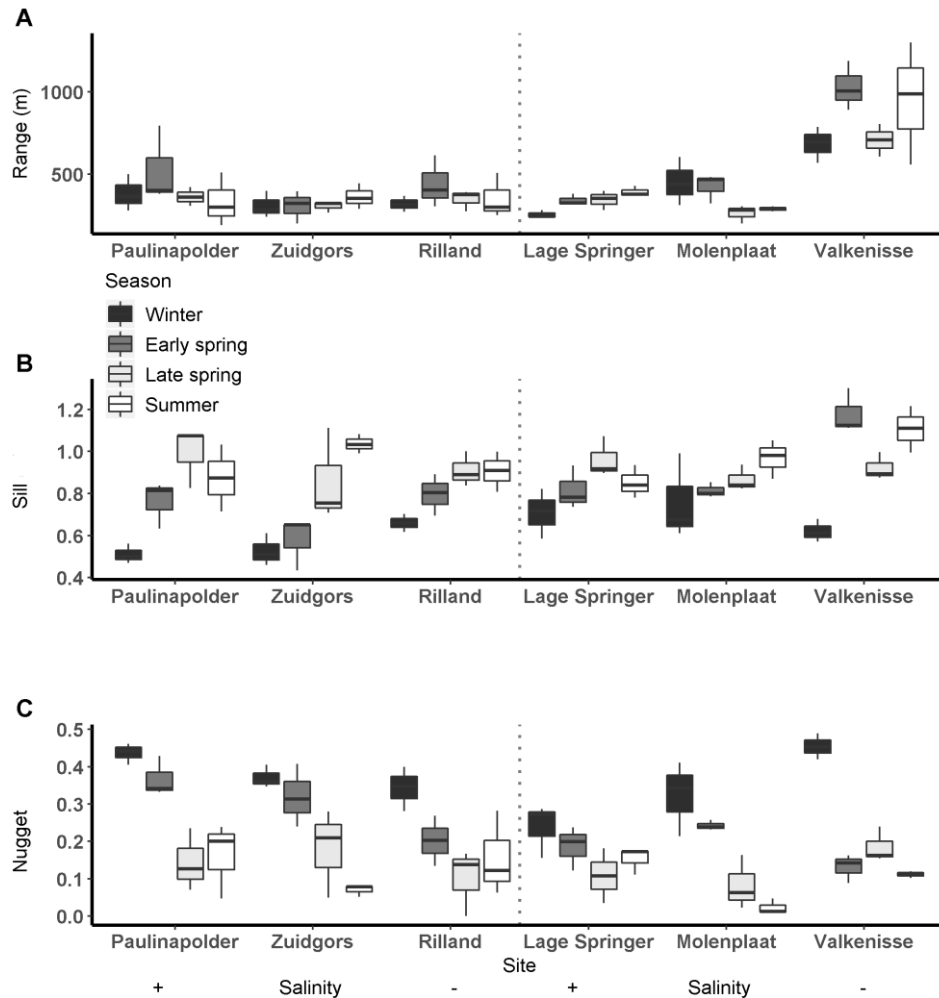


Figure 4. Semi-variogram parameters per season per site at fringing (left) and mid-channel (right) tidal flats (A: range (m), B: sill, C: nugget).

5.4.4 Semi-variogram parameters per ecotope

The range calculated per ecotope did not differ significantly among seasons or salinity zones (Figure 5, Table 4). The range was higher in the 'low dynamic silt rich medium high littoral' ecotope than the 'low dynamic fine sand high littoral' ecotope (ANOVA, $P=0.002$, $F_{3,111}=4.02$, $n=120$; HSD Tukey, $p=0.02$). Furthermore, the range was lower in the 'low dynamic fine sand high littoral' ecotope than in the 'highly dynamic fine sand littoral' ecotope (HSD Tukey, $p=0.001$). Lastly, the range was higher in the 'low dynamic fine sand medium high littoral' ecotope than in the 'low dynamic fine sand high littoral' ecotope (HSD Tukey, $p=0.01$).

The sill calculated per ecotope was higher in late spring and summer than in winter (ANOVA, $P=1.6 \times 10^{-5}$, $F_{3,111}=8.83$, $n=120$; HSD Tukey, $p < 0.001$). The sill did not differ significantly among ecotopes. The sill was higher in the weakly polyhaline zone than in the strongly polyhaline zone (ANOVA, $P=0.02$, $F_{3,111}=3.81$, $n=120$; HSD Tukey, $p < 0.05$). The ANOVA test revealed significant differences in the variance between ecotopes (ANOVA, $P=0.01$, $F_{3,111}=3.01$, $n=120$). However, an HSD Tukey test revealed no significant differences between individual ecotopes.

The nugget was higher in early spring, late spring and summer than in winter and higher in early spring than in summer (ANOVA, $P < 2 \times 10^{-16}$, $F_{3,111}=32.84$, $n=120$; HSD Tukey, $p < 0.05$). The nugget did not differ significantly among salinity zones. The nugget was higher in the 'low dynamic fine sand high littoral' ecotope than in the 'highly dynamic fine sand littoral' ecotope (ANOVA, $P < 0.002$, $F_{3,111}=3.93$, $n=120$; HSD Tukey, $p=0.01$). The nugget was higher in the 'highly dynamic fine sand high littoral' ecotope than in the 'low dynamic fine sand medium high littoral' ecotope (HSD Tukey, $p=0.02$).

Table 4. Statistics of MPB biomass and semi-variogram parameters calculated per ecotope.

		Season	Salinity	Ecotope
MPB biomass	F	7.05	0.39	1.98
	P	0.0002***	0.67	0.08
	df	3,192	2, 192	3, 192
Nugget	F	32.84	2.67	3.93
	P	$< 2 \times 10^{-16}$	0.07	0.002**
	df	3,192	2, 192	5, 192
Sill	F	8.83	3.81	3.02
	P	1.6×10^{-5} ***	0.02*	0.01*
	df	3, 111	2, 111	3, 111
Range	F	0.60	0.83	4.02
	P	0.62	0.44	0.002**
	df	3,192	2, 192	5, 192

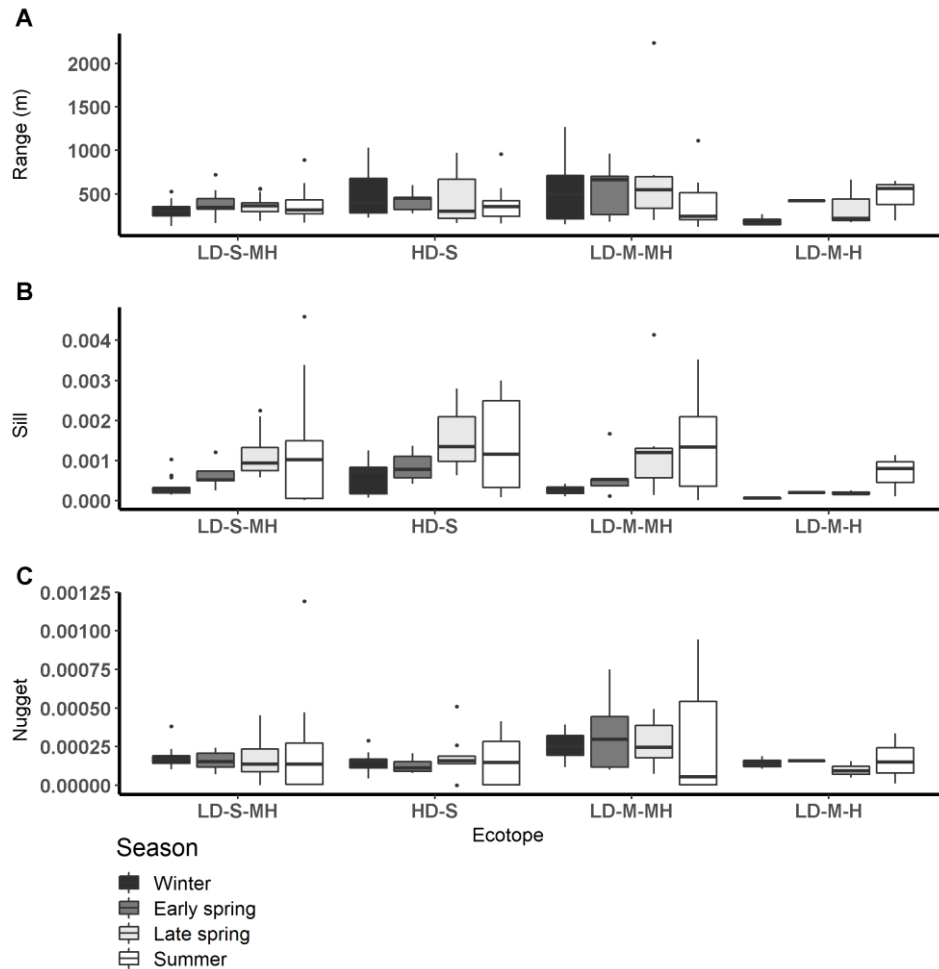


Figure 5. Semi-variogram parameters per season per ecotope (A: range (m), B: sill, C: nugget). HD-S = Highly dynamic fine sand littoral, LD-S-MH = low dynamic fine sand medium high littoral, LD-M-H = low dynamic silt rich high littoral and LD-M-MH = low dynamic silt rich medium high littoral.

5.4.5 Seasonality in the location of patches

Regular observation of the sites showed that that some areas with a relatively high MPB biomass ('patches') remain visible throughout the year, while other patches were only present during a particular season. For example, the patch located on the southeast side of the mid-channel tidal flat Lage Springer (Figure 6, a) can be clearly distinguished during all studied seasons. However, the patch located on the north side of Lage Springer was clearly visible in winter, but could hardly be detected in other seasons (Figure 6, b). At the fringing tidal flat Paulinapolder, an area of high MPB biomass was observed at the center of the tidal flat, which could not be distinguished clearly in winter or

spring (Figure 6, c). At the mid-channel tidal flat Valkenisse, the MPB biomass was consistently higher on the southeast side of the tidal flat throughout the year and the region with a relatively high biomass appeared to increase in surface area from spring to summer (Figure S1, a; Figure 2). The coefficient of variation confirmed that changes in MPB biomass were relatively low in this area (Figure 7, a). At the mid-channel tidal flat Molenplaat, the seasonal average of the MPB biomass was relatively high on the east side throughout the year (Figure S1, b). The MPB biomass was most variable over time on the west side (Figure 7, b), where a patch appeared in late spring (Figure S1, c). At the fringing tidal flats Zuidgors and Rilland, a cross-shore gradient from high to low in MPB biomass was present during all seasons. The MPB biomass was most variable throughout the year at low elevation at Zuidgors, Rilland and Valkenisse (Figure 7). In late spring, a band of high MPB biomass appeared at low elevation at Zuidgors (Figure S1, d).

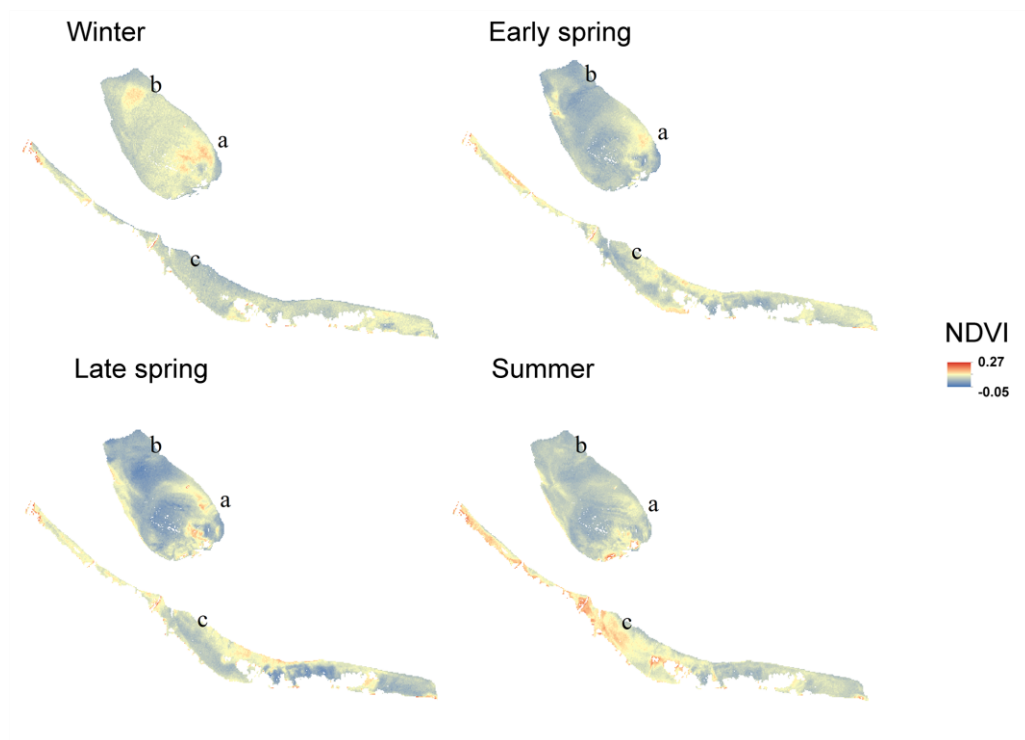


Figure 6. NDVI maps averaged per season for 'Lage Springer' (mid-channel tidal flat) and 'Paulinapolder' (fringing tidal flat).

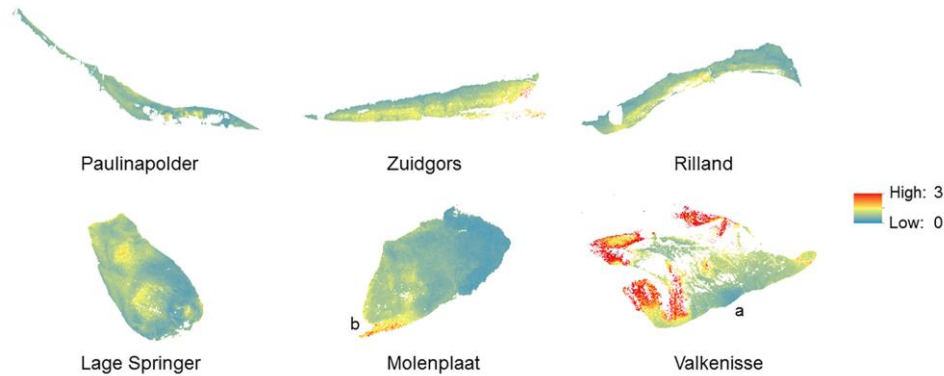


Figure 7. Coefficient of variation of the NDVI (2016-2019). The coefficient of variation ranged from -5176 to 13565.

5.5 Discussion

Spatial structure is a crucial component of ecological communities. Our results demonstrate that MPB show a remarkable seasonality in the degree of patchiness (sill) which increases from winter to summer, while the patch size (range) remains relatively constant. The location of the patches may change over time, which suggests that in these cases the increase in degree of patchiness is not associated with a general increase in MPB biomass but with locally changing abiotic conditions or grazing activity. Furthermore, the patch size and degree of patchiness is higher on relatively sandy mid-channel tidal flats than on relatively silt rich fringing tidal flats. This suggests that sediment composition plays an important role in pattern formation of MPB, as found in earlier studies (Morris, 2005; Méléder et al., 2007).

5.5.1 Seasonal dynamics of MPB biomass and patterning

Our results demonstrate that the MPB biomass averaged per tidal flat increased from early spring to summer, while in winter MPB biomass was highly variable among the years 2016-2019. We did not observe a clear spring bloom. Following a constant-density model, as hypothesized, the patch size (range) would be expected to increase from early spring to summer accordingly. However, the range of MPB did not change significantly over time and visual observation showed that the location of areas with a relatively high MPB biomass changed throughout the seasons (Figure S1). It should be noted that no boundary value for the NDVI was used to distinguish between 'MPB patches' versus 'bare sediment' in the current study. Variation in MPB biomass on tidal flats are gradual and the range derived from the semi-variogram quantifies the size of areas with a similar MPB biomass (referred to as 'patch'). A power law

analysis using a definition of patches with a fixed NDVI threshold may provide further insight in changes in the number and size of patches throughout seasons (Weerman et al., 2012). Visual observation showed that, at most sites, areas with a relatively low MPB biomass increased in biomass from early spring to summer, while the biomass was highly variable in winter in 2016-2019. In some areas, MPB biomass remained low throughout the seasons (Figure 8). Furthermore, it was visually observed that the number of areas with a relatively high MPB biomass increases from early spring to summer. At a few tidal flats, the spatial configuration of patches remained relatively constant from winter to summer (Valkenisse, Molenplaat and Rilland; Figure S1). Visual observation showed that at Valkenisse and the eastern side of Molenplaat, areas with a relatively high MPB biomass expand over time (Figure 8). Valkenisse and Rilland are located in the mesohaline zone, where macrofaunal biomass is relatively low (Ysebaert et al., 2003) and, therefore, a minor influence of grazing activity or bioturbation on spatial patterns of MPB is expected. The consistent patch size throughout the year is not in line with the finding of (Guarini et al., 1998), who studied spatial variability on a larger scale (1 km grid resolution) and found an increase in patch size from winter to summer along with an increasing MPB biomass. However, we did visually observe this phenomenon at Valkenisse and Molenplaat, where MPB biomass increased from early spring to summer and patches appeared to spread over the tidal flat (Figure S1). This suggests that, depending on local environmental conditions, pattern formation may indeed follow a constant-density model.

The sill was significantly higher in late spring and summer than in winter at mid-channel and fringing tidal flats. This is in line with our hypothesis and may be associated with increased grazing activity and bioturbation by macrofauna or with changed abiotic conditions. The higher sill in late spring and summer than in winter was observed in all ecotopes ('low dynamic fine sand medium high littoral', 'low dynamic silt rich medium high littoral' and 'highly dynamic fine sand littoral') except the ecotope 'low dynamic silt rich high littoral'. This ecotope was only present at Zuidgors, where the MPB biomass visually appeared relatively homogeneous in winter, early spring and late spring. In summer, a patch emerged on the east side of the tidal flat (Figure S1).

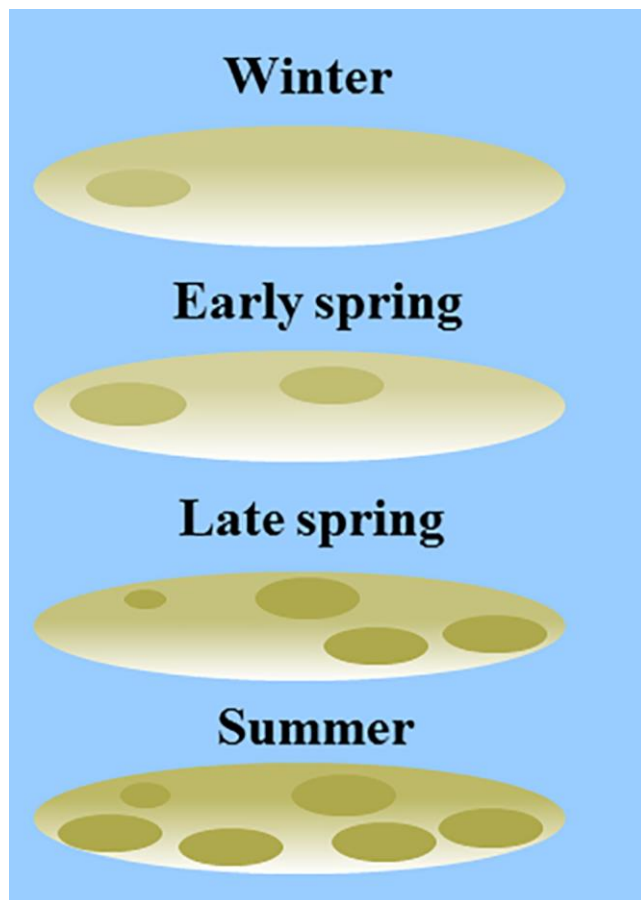


Figure 8. Conceptual model of seasonality in patch size (based on the range derived from a semi-variogram) and degree of patchiness (sill derived from a semi-variogram) in MPB biomass, complemented by visual observations of the sites. No boundary values for areas of 'MPB patches' versus 'bare sediment' were used in the current study.

5.5.2 Spatial patterning on fringing versus mid-channel tidal flats

As hypothesized, the patch size (range) was higher on mid-channel tidal flats than on fringing tidal flats. This suggests that the relatively high hydrodynamic activity on mid-channel tidal flats as opposed to fringing tidal flats homogenizes spatial variability in MPB biomass, possibly due to high resuspension rates associated with higher current velocities (Lucas et al., 2000). However, the observed difference was mainly due to the range being approximately a factor two higher at the site Valkenisse than all other study sites. Likewise, the range was significantly higher in the mesohaline zone than in the strongly and weakly polyhaline zone, mainly due to the range being higher at Valkenisse than at all other sites. At Valkenisse, there appears to be one prevalent patch on the

southeastern side of the tidal flat which is present throughout the year. In summer, more heterogeneity in MPB biomass appears within the patch which may be associated with increased grazing activity by macrofauna or changed abiotic conditions. The higher range at this site compared to other tidal flats is expected to be associated with the higher hydrodynamic activity and lower macrofaunal biomass at this location compared to other sites, as this site is located in the α -mesohaline zone and is characterised by mega-ripples (cf. Van der Wal et al., 2017). However, the larger surface area of Valkenisse may also play a role (Table 2), as no correction for the size of the study areas was applied in the semi-variogram analysis. Expansion of the current study to other estuaries and coastal embayments may increase insight on the possible effect of tidal flat size on the range of MPB patches.

The sill was higher on mid-channel tidal flats than on fringing tidal flats. This is not in line with our hypothesis, which stated that higher hydrodynamic energy and low macrofaunal biomass on mid-channel tidal flats is expected to homogenize MPB biomass. Instead, based on our findings, we suggest that the presence of an embankment at the top of the shore reduces the directionality in which heterogeneity in MPB biomass may emerge. At the fringing tidal flats, MPB patches mostly appeared in bands orientated alongshore (Figure S1), as was observed by Guarini et al. (1998), while at mid-channel tidal flats patches have an omnidirectional character.

5.5.3 Structuring processes

The proposition by Guarini et al. (1998) that seasonal dynamics of MPB biomass follow a constant density model is not supported by the current study, as the patch size remained constant throughout the year, but instead suggest a proportional-density model. Hereby, no relationship exists between the biomass of MPB and the occupied area, which is illustrated by the increase in MPB biomass over time while the patch size remained constant. From an ecological perspective, this implies that spatial patterning of MPB biomass is not governed by spreading processes.

Spatial variability of MPB biomass is caused by both physical and biological structuring processes. Morris (2005) found that the most important scales of variability in MPB biomass were around 200 to 300 m, ≤ 100 m and ≤ 2.5 m and that mean grain size and sediment sorting explain about 27% of the spatial variability in chl-a concentrations. A positive feedback exists between net silt accumulation and diatom growth, likely due to relatively high concentrations of nutrients in silt rich sediment compared to sandy sediments. Furthermore, diatoms secrete extracellular polymeric substances which lead to increased sediment cohesion, reducing the erodibility of sediment (Van De Koppel et al., 2001). This results in generally higher concentrations of MPB in silt rich

sediment than in sandy sediments (Van der Wal et al., 2010b). The silt content of intertidal sediments in the Westerschelde retrieved from surface roughness estimates from ERS-2 SAR revealed changes in spatial heterogeneity in the silt content throughout the year (van der Wal et al., 2010a). The seasonality in the spatial heterogeneity of the silt content observed in 2006 shows remarkable similarities with the seasonality in the spatial heterogeneity of MPB biomass surveyed in the current study. For example, the emerging MPB patch on the west side of the Molenplaat in late spring and summer (Figure S1) coincides with a strong increase in silt content in summer (van der Wal et al., 2010a). Furthermore, the high concentration of MPB biomass on the southeast side of Valkenisse corresponds with a high silt content at this location, which increases in surface area in summer like the surface area of MPB increases at this site. This provides a strong indication that seasonality in spatial patterns of MPB and silt content are linked on the meso-scale and that, on the meso-scale, grazing activity likely plays a minor role.

5.5.4 Spatial patterning in ecotopes

The patch size (range) was higher in the 'low dynamic silt rich medium high littoral' ecotope than the 'low dynamic fine sand high littoral', confirming our previous conclusion that sediment composition is likely closely linked to pattern formation of MPB. In addition, the range was significantly higher in the 'low dynamic fine sand medium high littoral' ecotope than in the 'low dynamic fine sand high littoral' ecotope. Therefore, the factor 'elevation' is additionally expected to influence the patch size, which may be associated with the presence of a gradient in hydrodynamic conditions or grazing activity. However, the relatively small surface area of the latter ecotope in the Westerschelde is likely to influence the observed difference in the range here.

5.5.5 Future requirements and perspectives

Regular in situ monitoring campaigns of MPB in intertidal areas are rare and provide limited information on ecosystem dynamics on the meso-scale. The use of satellite remote sensing seems a promising method to monitor spatial patterning of MPB at this scale. We demonstrated that Sentinel-2 MSI imagery provides a useful information source for mapping and analyses of spatial heterogeneity and seasonality in MPB biomass. Our results demonstrate that the location of MPB patches and, therefore, available food for higher trophic levels (including benthic macrofauna) varies from winter to summer. This information can be accounted for in spatially explicit food web models or sediment transport modelling.

The proposed method could be used in tidal systems worldwide to investigate to what extent patch characteristics and their seasonal dynamics vary among systems. This may provide further insight into the contribution of e.g. climate,

tidal regime and the specific morphology of tidal flats to seasonal dynamics of patch characteristics. Several studies where MPB biomass was quantified using the NDVI were performed in benthic diatom dominated estuaries (e.g. Benyoucef et al., 2014; Daggers et al., 2018; Kromkamp et al., 2006). However, further research is needed on possible effects of the microphytobenthic community composition (e.g. benthic diatoms versus euglenoids) on the relationship between the NDVI and MPB biomass. The relationship between the NDVI and MPB biomass should be calibrated for each site, as the relationship may vary per site and season.

5.6 Conclusion

Overall, we provided evidence that the degree of patchiness (sill derived from a semi-variogram) of MPB on the meso-scale varies from winter to spring, while the patch size (range derived from a semi-variogram) remains constant. The degree of patchiness and the patch size was higher on relatively sandy mid-channel tidal flats than on relatively silt rich fringing tidal flats. The location of patches may remain constant or vary throughout the year. The observed seasonality in MPB patchiness on the meso-scale appears to be closely linked to changes in the silt content.

Data availability statement

The datasets generated for this study are available on request to the corresponding author.

Author contributions

DW and TD designed the study. TD compiled the data, performed the analysis, and wrote the manuscript. PH and DW contributed to the study design, analyses, interpretation of the data, and editing of the manuscript.

Funding

This research was supported by the 'User Support Programme Space Research' of the Netherlands Organisation for Scientific Research (NWO grant no. ALW-GO 13/14 to DvdW).

Acknowledgements

We gratefully acknowledge Annette Wielemaker for her assistance in data collection, pre-processing of the imagery and valuable discussions on the used methodology. The authors declare no conflict of interest.

Supplementary material

The Supplementary Material for this article can be found online at: <https://www.frontiersin.org/articles/10.3389/fmars.2020.00392/full#supplementary-material>

Chapter 6 Synthesis

6.1 Introduction

Estuaries are heavily exploited ecosystems due to increasing agricultural and industrial activities over the last decades (Galbraith et al., 2002; Worm et al., 2006), which has led to the loss of >90% of species originally inhabiting estuaries (Lotze et al., 2006). Ecosystem services have been formulated to ensure that the services that nature provides to society are acknowledged and conserved (Alcamo, 2003; Pascual, 2010). To date, research on ecosystem services provided by marine systems has generally focused on charismatic organisms and habitats (e.g. coral reefs and mangroves) (Alongi, 2014; Barbier, 2017; Hope et al., 2019; Koch et al., 2009). However, also ecosystem services provided by the less charismatic soft-sediment habitats, including estuaries, have increasingly been recognized (Passarelli et al., 2018). Several studies have demonstrated that estuaries play an essential role in carbon sequestration, primary production, food production and contaminant processing, among other factors (Thrush et al., 2013). Many estuaries contain intertidal mud and sand flats, which have been recognized as 'secret garden', containing microphytobenthos (hereafter 'MPB') living in and on the sediment that contribute significantly to estuarine production, water quality, trophic dynamics and sediment stability (Cadée and Hegeman, 1974; Hope et al., 2019; MacIntyre et al., 1996; Passarelli et al., 2018; Varela and Penas, 1985). Since then, many studies have been dedicated to the ability of MPB to stabilize intertidal sediments, reduce erosion thresholds and influence sediment transport (Gerbersdorf and Wieprecht, 2015; Lubarsky et al., 2010; Orvain et al., 2004). Coastal protection and erosion control are important ecosystem services, as the costs of controlling coastal erosion are high (Landry, 2011). In addition, an increasing number of studies have been dedicated to the role on MPB in regulating oxygen, nutrient and CO₂ fluxes in estuaries (Hope et al., 2019; Larson and Sundback, 2008; Sundback et al., 2000) and its role in the estuarine food web (Christianen et al., 2017; Leguerrier et al., 2003). Carbon is fixed by MPB and transferred rapidly to heterotrophic bacteria and higher trophic levels (Herman et al., 2000; Middelburg et al., 2000). However, many of these studies have been performed on a small (local) scale. In this thesis, the functional role of MPB has been studied on a larger (local to ecosystem) scale. Hereby, the potential of satellite remote sensing to increase understanding of the role of MPB in intertidal ecosystems was investigated.

6.2 Summary of main findings

In this thesis, we aimed to study the extent to which MPB 1) can be used as indicator for ecosystem functioning and 2) can structure higher trophic levels. The use of satellite remote sensing is explored to retrieve indicators on the functional role of MPB in the intertidal ecosystem. A generic method is developed to retrieve MPB primary production rates from multispectral imagery (Landsat 8), which was calibrated and validated using an independent field

dataset. The method can be applied to temperate estuarine intertidal ecosystems worldwide after calibration at the estuary of interest (Chapter 2). A natural stable isotope analysis showed that MPB forms a major component in the diet of macrofauna and that the relative contribution of MPB in their diet may vary among tidal systems (Chapter 3). Furthermore, our field measurements of MPB primary production and sampling of macrofauna demonstrated that meso scale spatial variation in MPB primary production rates in spring is not directly linked to spatial variation in macrofaunal grazing pressure in summer/ autumn (Chapter 3). A defaunation experiment showed that removal of macrofauna did not result in higher MPB standing stocks, indicating that grazing by macrofauna does not lower MPB biomass under the studied environmental conditions (Chapter 4). UAV (drone) images of our experimental defaunation and control plots showed that on the micro scale (centimetre to meter scale), macrofauna altered the spatial heterogeneity of MPB in the top layer of the sediment. The presence of macrofauna decreased the 'patch size' of MPB and the magnitude of this effect showed an increasing trend with mud content (Chapter 4). Furthermore, a semi-variogram analysis on multispectral satellite imagery (Sentinel-2 MSI) revealed that the location of patches (on the meso scale) varied from winter to summer and that the degree of patchiness increased throughout the year. The location of patches showed a remarkable similarity with spatial variation of the silt content on tidal flats (Chapter 5).

In this Synthesis, the implications of these results are discussed, and scope for further research and applications is provided. We first discuss the application of remote sensing to spatially assess microphytobenthos biomass and production. Then we discuss the two main functional roles of MPB in the intertidal ecosystem (food source and sediment stabilisation) and the structuring role of MPB on the macrofauna community. Finally, the management implications of our findings are discussed.

6.3 Remote sensing of microphytobenthos biomass and production of intertidal sediments

To study the functional role of MPB at the ecosystem level and to quantify their productivity, large-scale information on MPB biomass and productivity is needed. MPB biomass can be retrieved non-destructively from remotely sensed information on various scales. On the small scale, MPB biomass present in the top layer of the sediment can be quantified using e.g. a hand-held hyperspectral spectroradiometer or camera which can be used in situ to collect information on the VIS-NIR domain (Chennu et al., 2013). This information may be used to quantify the total amount of MPB biomass using e.g. the NDVI (Van der Wal and Herman, 2007) or specific MPB groups (Kazemipour et al., 2012). Total MPB biomass can also be quantified in situ using pulse amplitude

modulated (PAM) fluorescence techniques (Serodio et al., 1997). On the meso scale, kite aerial photography (Bryson et al., 2013) or an unmanned aerial vehicle (UAV) with which an entire tidal flat can be mapped may be used (Brunier, 2020). On the large (estuary) scale, airborne imaging spectrometers (Combe et al., 2005) or multispectral (Benyoucef et al., 2014; Van der Wal et al., 2010b) and hyperspectral (Kazemipour et al., 2012) satellite remote sensing techniques are used.

The spatial resolution and accuracy in the detection of MPB using satellite remote sensing strongly depends on the type of sensor used. The use of the NDVI as index for the quantification of MPB biomass from multispectral imagery was validated (Chapter 2). Multispectral imagery currently provides advantages over the use of hyperspectral imagery, as they are generally freely available and cover a large part of the earth's surface. A boundary value $NDVI < 0.3$ has shown to be suitable to exclude the majority of macroalgae (Benyoucef et al., 2014), although mixed pixel effects cannot be ruled out (Van der Wal et al., 2010). However, using hyperspectral sensors such as HySpex (Kazemipour et al., 2012), a higher accuracy can be achieved in retrieving the total MPB biomass and distinguishing different MPB groups using an optical model (Launeau et al., 2018). In addition, hyperspectral imagery should allow distinction between MPB and other photosynthesizing organisms, such as macroalgae and pioneer vegetation (Kazemipour et al., 2012; Le Bris et al., 2016).

The increasing availability of high resolution satellite sensors allows the analysis of spatial variability in MPB biomass on the scale at which large scale ecosystem functioning can be studied (van der Wal et al., 2010b). In addition, the increasing availability of satellite imagery over time allows detailed analysis of seasonal (depending on local weather conditions) and interannual variability in MPB biomass (Brito et al., 2013). As MPB may form small patches, generally smaller than the resolution of most satellite sensors, UAV's are suitable to analyse spatial patterns of MPB on finer spatial scales (Chapter 4).

We show that MPB primary production can be estimated accurately at the estuary scale using multispectral imagery and requires information on MPB biomass and silt content retrieved from the imagery, ambient temperature measurements (indicator for the fluorescence-based photosynthetic capacity) and a tide model (Chapter 2). The silt content provides information on spatial variability in the vertical distribution of MPB biomass in the sediment (Jesus et al., 2006). In addition, both the MPB biomass and silt content provide information on the vertical light climate (Chapter 2). Using the presented method, calibration of the silt content would be needed for each image, although Van der Wal and Herman (2007) demonstrated that regression-based method using a combination of VNIR and SWIR was consistent over time, making it suitable for monitoring of intertidal sediments. However, the method

would need to be validated in other intertidal areas using e.g. Sentinel-2 imagery. Relationships between optical measures and the silt content may be area specific due to e.g. differences in topography and drainage, which influences the reflectance response (Van der Wal and Herman, 2007). The presented method to retrieve MPB production from multispectral imagery would be suitable to regularly monitor MPB production and to validate physical-biological coupled dynamic models (Savelli et al., 2018). Improvements to the model can be made by estimating the photosynthetic capacity from 1) remotely sensed sediment surface temperature instead of ambient temperature or 2) modelled sediment surface temperatures following a thermodynamic model (Guarini et al., 1997). In addition, further research is required to accurately estimate spatial and temporal variation in the photosynthetic efficiency (i.e. light use efficiency) of MPB. In the future, hyperspectral sensors may prove suitable to also quantify photosynthetic parameters such as light use efficiency and electron transport rates (Meleder et al., 2018), which could improve assumptions on how these parameters vary spatially. In addition, it should be taken into account that the photosynthetic parameters may vary during a tidal cycle as function of e.g. irradiation and temperature (Serodio et al., 2005).

6.4 *The functional role of microphytobenthos in the intertidal ecosystem*

The role of MPB in the intertidal ecosystem can be summarized by two major functions. First, MPB form a main food source for higher trophic levels in estuaries where wide intertidal flats are present. Second, MPB act as ecosystem engineer by stabilizing the sediment, which in turn facilitates settlement of juvenile macrofauna (Van Colen et al., 2008; Van Colen et al., 2009) and may reduce the erodibility of tidal flats (Le Hir et al., 2007; Orvain et al., 2004). Both major functions are discussed below in the light of the findings from this thesis. Biogeochemical functions were not taken into consideration in this thesis, such as mediation of nutrient cycling (Sundback et al., 2000), regulation of CO₂ (Hope et al., 2019) and O₂ fluxes (Larson and Sundback, 2008) and regulation of redox-sensitive metal concentrations in the water column (Kowalski et al., 2009).

6.4.1 Microphytobenthos as food source

MPB are the most important food source for higher trophic levels in intertidal ecosystems (Christianen et al., 2017), which is confirmed in this thesis (Chapter 3). Not only in temperate systems, but also in subtropical (Lee, 2000; Kang et al., 2003) and tropical climates (Kon et al., 2015) MPB was found to be a main food source. Our study was performed in the Oosterschelde and Westerschelde in the Netherlands, two contrasting tidal systems in terms of macrofaunal species composition and salinity (Meire et al., 1994; Ysebaert et

al., 2003). It was demonstrated in this thesis that the relative contribution of MPB in the diet of macrofauna may somewhat differ between tidal systems, which was the case for the mud snail *Peringia*, the sand digger shrimp *Bathyporeia* sp. and the Baltic tellin (*Limecola balthica*) (Chapter 3). The contribution of MPB in the diet of these species was higher in the Oosterschelde than in the Westerschelde, while the contribution of phytoplankton was lower in the Oosterschelde. Possibly, the difference can be explained by the relative availability of food sources, causing e.g. facultative suspension/ deposit feeders such as the Baltic tellin (*Macoma balthica*) to switch between grazing on MPB and water filtering, whereby phytoplankton is obtained. Generally, phytoplankton concentrations are lower in the Oosterschelde than in the Westerschelde in spring (Kromkamp and Peene, 2005; Wetsteyn and Kromkamp, 1994). Furthermore, the composition of deposited material may vary depending on the composition of organic material present in the water column, as phytoplankton may deposit under sheltered conditions (MacIntyre et al., 1996). Further research may elucidate the factors that cause differences in the diet composition of macrofaunal species between estuaries.

Grazing rates of the macrofaunal community on MPB were shown to be in the same order of magnitude as MPB production (Chapter 3), which may partly explain the high turnover rates of MPB found in earlier studies (Middelburg et al., 2000). Previous research in the Ems-Dollard and the Westerschelde estuaries showed high turnover rates of MPB due to resuspension of MPB into the water column during high tide (Dejonge and Vanbeusekom, 1995; Lucas et al., 2000). In the Bay of Marennes-Oléron, France, the portion of MPB to be resuspended has been estimated at 43% of the annually produced MPB using a physical-biological coupled model. Export of MPB to the water column was highest in spring (Savelli et al., 2019). As a consequence, MPB can also form an important part of the diet of suspension feeders (Choy et al., 2009; Herman et al., 1999), which is confirmed in this thesis (Chapter 3). In this thesis, no evidence was found that macrofaunal grazing lowers the MPB standing stock under the studied environmental conditions (Chapter 4). Likely, environmental factors such as hydrodynamic energy overruled possible effects of grazing on the MPB standing stock, as under more sheltered conditions top down control by macrofauna on MPB has been demonstrated to lower MPB biomass in summer (Weerman et al., 2011). A modelling study shows that a drop in MPB biomass is expected in summer due to macrofaunal grazing (Savelli et al., 2018). However, no clear summer depression in MPB biomass was measured in our study (Chapter 3). This suggests that remotely sensed information on MPB biomass or production may provide a good indicator for spatial variability in food availability for macrofauna.

In addition, other factors than grazing may control the MPB biomass standing stock, including desiccation, nutrient limitation and resuspension, and cause

interactive effects. For example, wave events may trigger sediment erosion, causing part of the MPB and macrofauna to resuspend into the water column (De Brouwer et al., 2000). A controlled mesocosm experiment in which MPB are exposed to varying nutrient concentrations, hydrodynamic conditions and macrofaunal communities may provide further insight in the role of different biotic and abiotic factors on the MPB standing stock.

6.4.2. Microphytobenthos as ecosystem engineer

MPB accumulate in the top layer of the sediment, where they may form a biofilm. MPB excrete extracellular polymeric substances (EPS, (Neumann et al., 1970), which 'glue' MPB and sediment particles together (Yallop et al., 1994). The biofilm strengthened by EPS increases sediment cohesion and decreases surface bottom roughness, which reduces the erodibility of the sediment (Paterson, 1989; Sutherland et al., 1998) caused by tidal currents and waves. The reduced erodibility of the sediment, in turn, creates favourable conditions for MPB growth as less MPB, silt and clay particles (which are favoured as substrate) are removed from the sediment resulting in a positive feedback loop (Van De Koppel et al., 2001). Therefore, MPB act as ecosystem engineers, moderating the physical environment and facilitating presence of other biota such as bacteria (Yallop et al., 2000). MPB biofilms also facilitate larval settlement of the Baltic tellin *Macoma balthica* (Van Colen et al., 2009) and macrofaunal juveniles (Van Colen et al., 2008). As a result, MPB biofilms promote the biodiversity on intertidal flats. The positive feedback mechanism results in the observation that silt-rich sediments generally contain higher MPB concentrations than sandy sediments (Orvain et al., 2012). In this thesis, we found that the location of MPB patches (meso scale) may vary among seasons (Chapter 5), which implies that the location of food availability for higher trophic levels also varies over time. The observed seasonal changes visually appeared closely related to seasonality in the spatial heterogeneity of the silt content (van der Wal et al., 2010a), Chapter 5), confirming that spatial heterogeneity of MPB is closely linked to the silt content. Expansion of the performed semi-variogram analysis in Chapter 5 to other estuaries may provide insight in the extent to which seasonality in patch characteristics may vary among systems. This may elucidate the role of e.g. climate, sediment type, tidal regime and the specific morphology and size of tidal flats in seasonal dynamics of MPB patch characteristics. Furthermore, meso scale patchiness of MPB may be studied using a power law analysis in which patches are defined using a fixed NDVI threshold. In this way, seasonal changes in the number and size of MPB patches containing a high biomass may be quantified (Weerman et al., 2012).

Chapter 4 revealed that areas with a similar MPB biomass ('patches') occupy smaller surfaces in the presence of macrofauna than in sediments where

macrofauna was experimentally removed in the field. Earlier studies indeed demonstrate that macrofaunal presence destabilizes sediment containing an MPB biofilm (Le Hir et al., 2007; Orvain et al., 2004). The destabilisation may be caused by macrofaunal grazing or bioturbation, i.e. reworking of sediment during burrow maintenance activities, foraging and feeding (Queiros et al., 2013). The decreased patchiness in the absence of macrofauna was observed under all studied environmental conditions. This conclusion signifies that macrofauna may not only increase sediment erodibility by bioturbation, but also prevents the formation of continuous MPB biofilms that increase sediment stability (De Brouwer et al., 2000). The effect of macrofaunal presence on the continuity of biofilms appeared to be most pronounced at a sheltered site with a relatively high silt content (although not statistically significant) (Chapter 4). Further research, using a larger number of replicates per sediment type category, could provide insight into possible effects of the silt content on the observed phenomenon. Furthermore, a controlled mesocosm experiment in which MPB are exposed to different macrofaunal communities under varying hydrodynamic conditions and sediment types, could provide further insight in the role of macrofauna in the erodibility of sediments containing MPB biofilms.

6.5 *The structuring role of microphytobenthos for the macrofaunal community*

As macrofauna form an essential food source for higher trophic levels (e.g. wading birds, large crustaceans and fish) and monitoring of macrofauna forms a labour intensive effort, studies have been performed on the prediction of macrofaunal community composition and biomass from abiotic variables (Cozzoli et al., 2013; Ellis et al., 2006; Ysebaert et al., 2002) including remotely sensed information (Van der Wal et al., 2008). In this way, observed changes on the macrofaunal community composition could be explained and insight could be gained on possible ecosystem responses to environmental change.

Important explanatory variables are median grain size, mud content, elevation and the NDVI retrieved from imagery in June (Van der Wal et al., 2008), demonstrating that MPB availability is important in determining spatial distributions of surface deposit feeders. However, as MPB biomass is the net result of MPB production and loss processes such as grazing and resuspension, MPB production may be a better proxy for food availability than MPB biomass. Building further on the previously mentioned work, we tested whether MPB production in spring, when macrofaunal biomass is still relatively low (Ysebaert et al., 2003) and spatial variability in MPB production (which is expected to be mainly determined by abiotic parameters), can be used as proxy for macrofaunal grazing pressure on MPB in summer/autumn. No relationship was found, also when grazing by surface deposit feeders was compared to MPB

production separately (Chapter 3). As spatial variation in MPB biomass varies from winter to summer (Chapter 5), MPB production in summer/ autumn in combination with abiotic variables may be a better explanatory factor of macrofaunal grazing in summer/ autumn or the macrofaunal community composition. Hereby, it should be taken into account that macrofaunal grazing is not directly related to macrofaunal biomass, as the contribution of MPB to the diet of macrofauna differs per species (Chapter 3). The finding that the MPB biomass standing stock is not lowered by macrofaunal presence (Chapter 4) supports the use of optical remote sensing techniques to quantify spatial variation in food availability for higher trophic levels.

6.6 Management implications

As MPB form a major food source for higher trophic levels, anthropogenic and naturally caused disturbances to intertidal areas and their associated MPB may affect the entire food web (Christianen et al., 2017). Human activities that may impact intertidal areas include dredging, changes in sediment supply due to e.g., dam building, sand nourishment, land reclamation, waste disposal, agriculture and aquaculture, oil and gas production, marine transportation and shipping (Kennish, 2002) and global warming (Cartaxana et al., 2015; Galbraith et al., 2002; Poulin and Mouritsen, 2006). For example, channel deepening may lead to higher residual current velocities (Van Maren et al., 2015), which may in turn increase resuspension rates of MPB (Lucas et al., 2000). Very few studies have addressed possible impacts of global warming on intertidal ecosystems. Galbraith et al. (2002) calculated that the projected sea level rise due to global warming, assuming a global warming scenario of 2°C in the next century, may lead to the loss of 20-70% of the current intertidal areas. Especially at locations where the coastline is unable to move inland, due to e.g. the presence of coastal defence structures, severe losses of intertidal habitat may occur. That is, in the scenario where tidal flats are not able to keep up with sea level rise due to a lack of sedimentation. Both direct anthropogenic stressors (e.g., dredging) and climate change (increased water depth and erosion) may cause a decrease in tidal flat area and emersion duration.

Our MPB primary production model can be used to evaluate effects of tidal flat area and emersion duration reduction on MPB production (Chapter 2). The modelling work in this thesis shows how light availability at the sediment surface decreases as a result of decreased emersion duration, leading to lower MPB production rates (Chapter 2). Our work also shows how MPB production responds to short-term (diurnal) fluctuations in ambient temperatures (Chapter 2). However, global warming may lead to complex feedbacks that affect MPB production and associated ecosystem services. In colder climates such as the polar regions, elevated temperatures may increase MPB production (Torstensson et al., 2012). In temperate climates, prolonged exposure to

elevated ambient temperatures may decrease MPB production rates and lead to a higher abundance of cyanobacteria (Cartaxana et al., 2015). Elevated CO₂ levels may promote MPB growth, although the combined effect of a temperature rise and increased CO₂ levels may lead to a lower MPB biomass (Cartaxana et al., 2015; Hicks et al., 2011). Very few studies have considered interactive effects of global warming on MPB communities (Hicks et al., 2011). For example, MPB species may adapt to long-term elevated temperatures, which could modulate the effects described above. The effects of elevated temperatures and CO₂ availability should be investigated further and could be incorporated in our model.

In addition, global warming may influence the reproduction, onset of spawning, embryonic and gonad development and mortality of macrofaunal species (Birchenough et al., 2015). For example, cold winters are known to cause a higher mortality of temperature sensitive species and higher recruitment of some macrofaunal species in the intertidal (Armonies et al., 2001). This implies that effects of global warming on macrofaunal community compositions can be expected (Schuckel and Kroncke, 2013), which may in turn change trophic and non-trophic interactions between MPB and macrofauna. Further research is required to elucidate these interactions in order to sustainably manage estuarine ecosystems.

Our work confirms the essential role of MPB in the diet of macrofauna, which are in turn an essential food source for secondary consumers such as fish and (wading) birds. Therefore, MPB are a crucial component of the estuarine food web. This highlights the urgent need to preserve these intertidal flats, as a decreasing availability of MPB may affect the entire estuarine ecosystem. Furthermore, our work suggests that the studied consumer-resource interactions between MPB and macrofauna are not coupled on the local (mm to m) scale, but on a larger spatial scale (i.e. mesoscale, \approx 10 to 100 kilometers). This implies that holistic conservation and management approaches are needed, such as the establishment of marine protected areas at appropriate spatial scales. Satellite remote sensing provides the opportunity to monitor MPB and its function in intertidal ecosystems on the estuary scale and detect long term trends as a consequence of global warming and other anthropogenic stressors. Furthermore, the inclusion of spatio-temporal information on MPB production in food web models and the prediction of macrofaunal distributions may support management of intertidal ecosystems.

Supplementary information

Supplementary material for: A model to assess microphytobenthic primary production in tidal systems using satellite remote sensing

STATUS: Published in Remote Sensing of Environment

Photosynthetic parameters were measured over a tidal cycle, following the methodology described in detail in section 2.3.1.4. In the primary production module, it is assumed that α and E_{opt} do not vary during a daytime low tide, which is supported by the PAM data (Wilcoxon test, $p > 0.05$, Figure S1). The E_{opt} and E_k values derived from the RLC (PAM) were higher than those obtained from the C-fixation experiments (Figure S1). This behaviour has been observed before (e.g. Barranguet et al., 2000), and results from the fact that C-fixation reaches its maximum values at lower irradiances than the maximum ETR rates. Values of E_{opt} were set to a maximum value of 1500 at point B, as light saturation was not always reached in the RLC's and ETR values could otherwise not be fitted. At point B, I_{opt} shows a diel cycle. In most cases, E_k co-varied with P_s and P_s derived from PAM clearly varies with temperature, as explained in section 2.4.4.2.

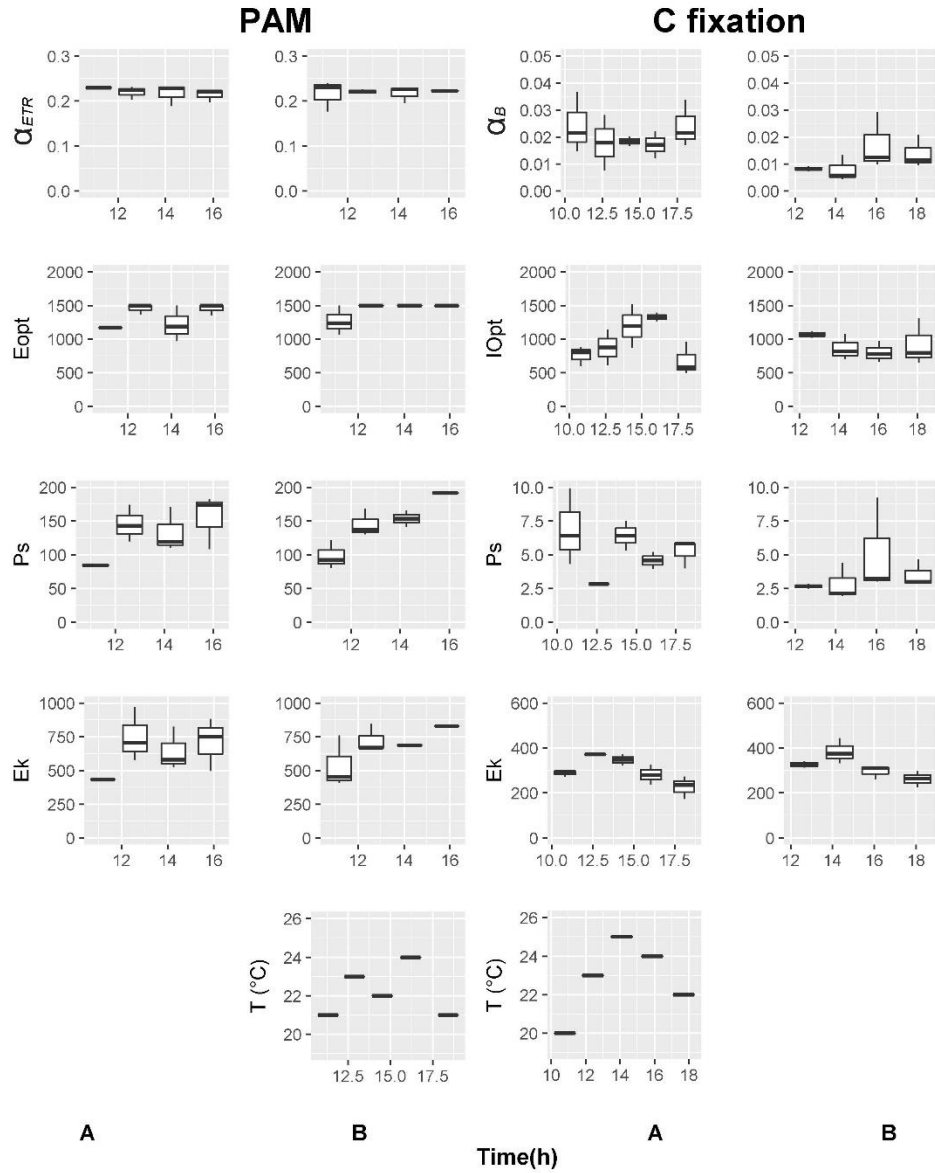


Figure S1. Box plot showing the maximum light utilisation efficiency α_{ETR} (r.u.) and α_B (mg C mg^{-1} chl-a h^{-1} [$\mu\text{mol photon m}^{-2} \text{s}^{-1}$] $^{-1}$), light saturation parameter E_{opt} and I_{opt} ($\mu\text{mol photon m}^{-2} \text{s}^{-1}$), photosynthetic capacity P_s (PAM: $\mu\text{mol photon m}^{-2} \text{s}^{-1}$; C fixation: mg C mg^{-1} chl-a h^{-1}) and the light saturation parameter E_k (fitted with the Jassby-Platt model (Jassby and Platt 1976), $\mu\text{mol photon m}^{-2} \text{s}^{-1}$) measured with a PAM fluorometer (left) and ^{14}C -uptake (right) and the sediment temperature ($^{\circ}\text{C}$) at two plots (A and B), at Biezelingse-Ham, Westerschelde. Fluorescence measurements were not performed at the last time step (18:00) due to a low battery of the PAM.

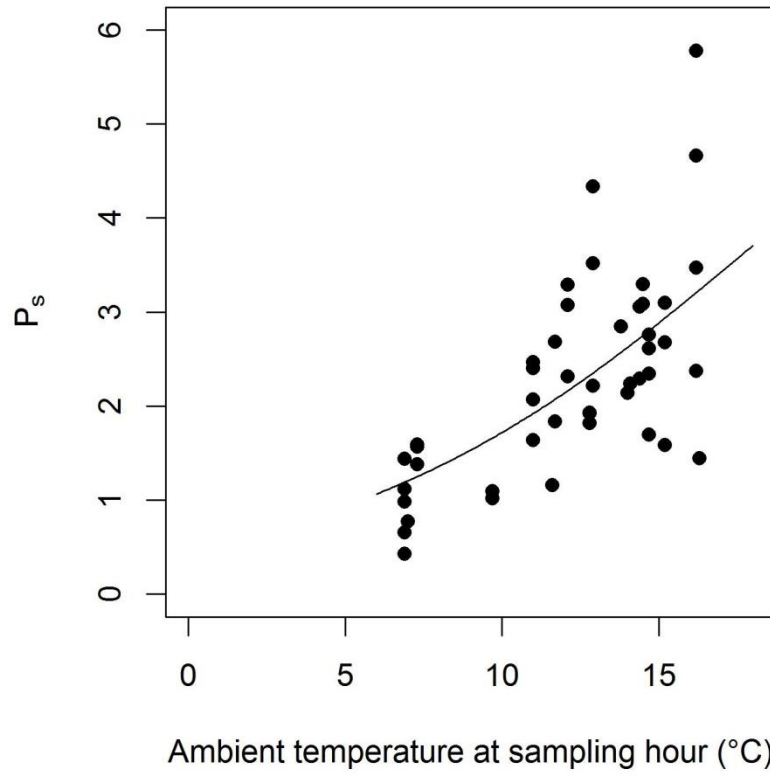


Figure S2. In situ fluorometric measurements performed at random locations in the Oosterschelde and Westerschelde in May 2015 of the 'photosynthetic capacity \times EE' modelled as function of ambient temperature following the non-linear model of Blanchard et al. (1996) ($\beta = 2.75$, $P_{MAX} = 4.98$, $T_{opt} = 25$, $T_{max} = 38$; $R^2 = 0.4$, $p < 0.0001$, $n=47$).

Supplementary information for: Spatial variability in macrofaunal diet composition and grazing pressure on microphytobenthos in intertidal areas

STATUS: Published in *Limnology and Oceanography*

Table S1. ANOVA test for dietary contribution of MPB to macrofaunal genera of macrofauna sampled in 2015 calculated with a Bayesian stable isotope mixing model¹.

Taxa	n	Estuary			Elevation			Estuary:Elevation		
		F	P	df	F	P	df	F	P	df
Total (ind)	102	5.7	0.06	1.5	3.9	0.1	1.5	5.1	0.07	1.5
<i>Arenicola</i>	10	0.005	0.9	1.3	0.04	0.9	1.3	2.1	0.4	1.3
		*								
<i>Bathyporeia</i>	11	99.2	0.002	1.3	0.6	0.5	1.3	0.3	0.6	1.3
			**							
<i>Cyathura</i>	9	-	-	-	0.1	0.8	1.3	0.1	0.8	1.3
<i>Corophium</i>	8	14.9	0.2	1.1	1.2	0.5	1.1	0.2	0.7	1.1
<i>Hediste</i>	11	-	-	-	4.9	0.1	1.4	1.2	0.3	1.4
<i>Macoma</i>	12	23.1	0.008	1.4	0.1	0.8	1.4	0.02*	0.9	1.4
			**							
<i>Heteromastus</i>	11	0.7	0.5	1.3	0.1	0.7	1.3	0.003	1.0	1.3
								*		
<i>Peringia</i>	14	7.9	0.04*	1.5	0.6	0.5	1.5	1.1	0.3	1.5
<i>Spionidae</i>	2	-	-	-	-	-	-	-	-	-
<i>Tharyx</i>	1	-	-	-	-	-	-	-	-	-
<i>Cerastoderma</i>	10	0.4	0.6	1.2	0.006	0.9	1.2	0.5	0.6	1.2
					*					

¹To test for the factor "estuary" (Westerschelde and Oosterschelde) and "elevation" (high and low) and their interaction effects, dietary coefficients were calculated per site per elevation category. The effect of the factors "elevation" and "estuary" on the dietary contribution of MPB to the total macrobenthic community (all samples merged, 1 sample contains 3 individuals) and individual genera was tested. Total relates to total individuals sampled (n=102). Missing values indicate a too low number of observations to perform the ANOVA. Significance level (P) is indicated by '***' = 0, '**' = 0.001, '*'=0.05.

Supplementary information

Table S2. Common taxa in the Oosterschelde and Westerschelde, ranked by number of sampling locations in which the taxa occurred (based on abundance data in the NIOZ/Rijkswaterstaat BIOMON data set 2003-2012, two basins combined).

Taxa	Feeding type	Nr of locations	Occurrence
<i>Spionidae</i>	Surface deposit feeder	1208	Oosterschelde (lower) and Westerschelde
<i>Corophium</i> sp.	Surface deposit feeder (facultative suspension feeder)	540	Oosterschelde and Westerschelde
<i>Bathyporeia</i> sp.	Surface deposit feeder	642	Oosterschelde (lower) and Westerschelde
<i>Peringia Ulvae</i>	Surface deposit feeder	878	Oosterschelde and Westerschelde
<i>Arenicola marina</i>	Deposit feeder	393	Oosterschelde and Westerschelde
<i>Tharyx marioni</i>	Deposit feeder	592	Oosterschelde and Westerschelde
<i>Hediste diversicolor</i>	Omnivorous	725	Oosterschelde and Westerschelde
<i>Cerastoderma edule</i>	Suspension feeder	477	Oosterschelde and Westerschelde
<i>Macoma balthica</i>	Surface deposit feeder & suspension feeder	1140	Oosterschelde and Westerschelde
<i>Heteromastus</i> sp.	Omnivorous	725	Westerschelde

Table S3. The three species with the highest average biomass at each site (total biomass and % biomass of the total macrofaunal community) and feeding guild (last updated following recent literature in 2015) as reported in macrofauna dataset collected by the Royal Netherlands Institute for Sea Research (NIOZ) and Rijkswaterstaat. SF = suspension feeder, DDF = deep deposit feeder, O = omnivore, SDF = surface deposit feeder. OOS = Oosterschelde, WES = Westerschelde.

Species per site	Phylum	Class	Feeding guild	Average biomass (AFDW mg m ⁻²)	Proportion of total biomass %
Dortsman (OOS)					
<i>Cerastoderma edule</i>	Mollusca	Bivalvia	SF	13908 ± 5268	43 ± 4
<i>Arenicola marina</i>	Annelida	Polychaeta	DDF	5707 ± 6809	31 ± 29
<i>Hediste diversicolor</i>	Annelida	Polychaeta	O	3019 ± 1500	26 ± 3
Rattekaai (OOS)					
<i>Peringia ulvae</i>	Mollusca	Gastropoda	SDF	4639 ± 3959	59 ± 33
<i>Arenicola marina</i>	Annelida	Polychaeta	DDF	4290 ± 5993	31 ± 35
<i>Macoma balthica</i>	Mollusca	Bivalvia	SDF	1107 ± 820	9 ± 7
Viane (OOS)					

<i>Cerastoderma edule</i>	Mollusca	Bivalvia	SF	14889 ± 20841	15 ± 19
<i>Peringia ulvae</i>	Mollusca	Gastropoda	SDF	7609 ± 5928	49 ± 37
<i>Arenicola marina</i> Hellegat (WES)	Annelida	Polychaeta	DDF	6052 ± 5312	38 ± 27
<i>Carcinus maenas</i>	Arthro- poda	Malacostra- ca	O	10560 ± -	59 ± -
<i>Cerastoderma edule</i>	Mollusca	Bivalvia	SF	4242 ± 4002	16 ± 16
<i>Scrobicularia plana</i> Middelplaat (WES)	Mollusca	Bivalvia	SDF	3874 ± 2033	16 ± 9
No data available					
Molenplaat (WES)					
<i>Heteromastus filiformis</i>	Annelida	Polychaeta	DF	3619 ± 4938	29 ± 39
<i>Macoma balthica</i>	Mollusca	Bivalvia	SDF	539 ± 659	6 ± 7
<i>Cerastoderma edule</i> Paulina (WES)	Mollusca	Bivalvia	SF	497 ± 932	8 ± 15
<i>Cerastoderma edule</i>	Mollusca	Bivalvia	SF	20428 ± 11494	30 ± 25
<i>Hediste diversicolor</i>	Annelida	Poly-chaeta	O	6275 ± -	53 ± -
<i>Heteromastus filiformis</i> Rilland (WES)	Annelida	Poly-chaeta	DF	5175 ± 4011	39 ± 39
<i>Scrobicularia plana</i>	Mollusca	Bivalvia	SDF	7012 ± -	40 ± -
<i>Hediste diversicolor</i>	Annelida	Polychaeta	O	3763 ± 2412	33 ± 15
<i>Heteromastus filiformis</i> Waarde (WES)	Annelida	Polychaeta	DF	3139 ± 1017	27 ± 9
<i>Heteromastus filiformis</i>	Annelida	Polychaeta	DF	3245 ± 3440	51 ± 34
<i>Corophium</i>	Arthro- poda	Malacostra- ca	SDF/ DF	1756 ± 2448	10 ± 10
<i>Corophium volutator</i>	Arthro- poda	Malacostra- ca	SDF	1233 ± 1202	11 ± 12

Table S4. Macroalgae cover estimates at sites in the Oosterschelde. Percentage cover of macroalgae was estimated using quadrants of 9 m².

Site	Macroalgae cover (%)	n
Dortsman	0.0003 ± 0.0005	6
Rattekaai	3.60 ± 8.04	6
Viane	0.17 ± 0.41	6

Supplementary information

Table S5. DIC (deviance information criterion), Gelman-Rubin and Geweke test statistics of the Bayesian mixing model runs used to calculate dietary proportions.

Estuary	Site	Elevation category	DIC	Gelman-Rubin (< 1.05)	Geweke (% of variables outside ± 1.96 in each chain) (< 5%)		
Oosterschelde	Dortsman	High	74	< 1.01	12	12	35
		Low	78	< 1.01	0	0	24
	Rattekaai	High	84	< 1.01	0	0	0
		Low	93	< 1.01	0	0	8
	Viane	High	85	< 1.01	31	0	46
		Low	69	< 1.01	0	0	54
Westerschelde	Hellegat	High	92	< 1.01	8	8	8
		Low	60	< 1.01	6	19	6
	Middelplaat	High	33	< 1.01	0	20	0
		Low	55	< 1.01	16	0	0
	Molenplaat	High	116	< 1.01	16	0	24
		Low	140	< 1.01	11	0	11
	Paulina	High	104	< 1.01	0	0	0
		Low	112	< 1.01	5	5	0
	Rilland	High	67	< 1.01	5	11	16
		Low	53	< 1.01	0	6	25
	Waarde	High	107	< 1.01	0	32	0
		Low	128	< 1.01	9	0	5

Table S6. Contribution of MPB phytoplankton and terrestrial organic matter (mean and standard deviation) to the diet of sampled macrofauna species calculated per site per elevation with a Bayesian mixing model, where terrestrial organic matter was included as possible source at sites in the Westerschelde only.

Species	Tidal system	Site	Elevation	Contribution MPB to diet ($\mu \pm \sigma$)	Contribution phytoplankton to diet ($\mu \pm \sigma$)	Contribution Terrestrial OM to diet ($\mu \pm \sigma$)
<i>Arenicola marina</i>	Oosterschelde	Dortsman	Low	0.765	0.235	
				± 0.079	± 0.079	
	Westerschelde	Hellegat	High	0.758	0.168	0.074
				± 0.072	± 0.091	± 0.05
	Westerschelde	Middelplaat	Low	0.524	0.349	0.127
				± 0.081	± 0.15	± 0.088
	Westerschelde	Molenplaat	High	0.743	0.171	0.086
				± 0.051	± 0.082	± 0.05
			Low	0.758	0.169	0.073
				± 0.076	± 0.091	± 0.048
	Westerschelde	Paulina	High	0.587	0.317	0.096
				± 0.1	± 0.138	± 0.071

<i>Bathyporeia</i> sp.	Oosterschelde	Rattekaai	High	0.592 ± 0.122	0.408 ± 0.122	
			Low	0.587 ± 0.13	0.413 ± 0.13	
	Oosterschelde	Viane	High	0.714 ± 0.104	0.286 ± 0.104	
			Low	0.683 ± 0.078	0.317 ± 0.078	
	Oosterschelde	Dortsman	High	0.759 ± 0.08	0.08 ±	
			Low	0.918 ± 0.059	0.082 ± 0.059	
	Westerschelde	Middelplaat	High	0.621 ± 0.073	0.242 ± 0.137	0.137 ± 0.086
			Low	0.602 ± 0.08	0.296 ± 0.143	0.103 ± 0.084
	Westerschelde	Molenplaat	High	0.624 ± 0.075	0.25 ± 0.145	0.126 ± 0.094
			Low	0.71 ± 0.107	0.201 ± 0.134	0.089 ± 0.072
	Oosterschelde	Rattekaai	High	0.866 ± 0.092	0.134 ± 0.092	
	Oosterschelde	Viane	High	0.869 ± 0.088	0.131 ± 0.088	
			Low	0.803 ± 0.08	0.197 ± 0.08	
	Westerschelde	Waarde	High	0.491 ± 0.079	0.398 ± 0.149	0.111 ± 0.091
			Low	0.812 ± 0.047	0.13 ± 0.064	0.058 ± 0.041
<i>Cerastoderma</i> <i>edule</i>	Oosterschelde	Dortsman	High	0.443 ± 0.072	0.557 ± 0.072	
			Low	0.333 ± 0.057	0.667 ± 0.057	
	Westerschelde	Middelplaat	Low	0.317 ± 0.117	0.506 ± 0.257	0.177 ± 0.156
	Westerschelde	Molenplaat	High	0.281 ± 0.107	0.506 ± 0.281	0.214 ± 0.187

Supplementary information

<i>Corophium</i> sp.	Westerschelde	Paulina	Low	0.426 ± 0.123	0.399 ± 0.237	0.175 ± 0.144
			High	0.385 ± 0.096	0.442 ± 0.223	0.173 ± 0.141
			Low	0.359 ± 0.136	0.461 ± 0.262	0.18 ± 0.146
		Rattekaai	High	0.244 ± 0.118	0.756 ± 0.118	
			Low	0.307 ± 0.118	0.693 ± 0.118	
			High	0.276 ± 0.069	0.724 ± 0.069	
	Oosterschelde	Viane	High	0.718 ± 0.091	0.282 ± 0.091	
			Low	0.896 ± 0.069	0.104 ± 0.069	
			Low	0.583 ± 0.11	0.289 ± 0.176	0.128 ± 0.104
		Rattekaai	High	0.751 ± 0.108	0.249 ± 0.108	
			High	0.49 ± 0.082	0.38 ± 0.191	0.131 ± 0.126
			Low	0.519 ± 0.082	0.314 ± 0.173	0.166 ± 0.11
<i>Cyathura</i> <i>carinata</i>	Westerschelde	Waarde	High	0.395 ± 0.082	0.524 ± 0.157	0.081 ± 0.09
			Low	0.393 ± 0.093	0.436 ± 0.237	0.171 ± 0.162
			High	0.835 ± 0.065	0.114 ± 0.077	0.051 ± 0.041
		Molenplaat	Low	0.746 ± 0.094	0.161 ± 0.106	0.093 ± 0.064
			High	0.663 ± 0.071	0.224 ± 0.129	0.113 ± 0.082
			High	0.723 ± 0.061	0.202 ± 0.1	0.075 ± 0.059
	Westerschelde	Paulina	Low	0.686 ± 0.092	0.234 ± 0.115	0.08 ± 0.055
			Low			
			Low			
		Hellegat	High			
			High			
			High			

<i>Hediste diversicolor</i>	Westerschelde	Rilland	High	0.844 ± 0.053	0.112 ± 0.061	0.043 ± 0.032
	Oosterschelde	Viane	Low	0.316 ± 0.104	0.684 ± 0.104	
	Westerschelde	Waarde	High	0.819 ± 0.05	0.137 ± 0.066	0.044 ± 0.036
			Low	0.894 ± 0.047	0.073 ± 0.05	0.033 ± 0.029
	Oosterschelde	Dortsman	High	0.921 ± 0.065	0.079 ± 0.065	
			Low	0.914 ± 0.072	0.086 ± 0.072	
	Westerschelde	Hellegat	High	0.722 ± 0.084	0.193 ± 0.125	0.086 ± 0.067
			Low	0.735 ± 0.089	0.17 ± 0.119	0.095 ± 0.074
	Westerschelde	Molenplaat	High	0.676 ± 0.065	0.207 ± 0.125	0.116 ± 0.081
			Low	0.687 ± 0.103	0.217 ± 0.138	0.095 ± 0.078
	Westerschelde	Paulina	High	0.671 ± 0.084	0.259 ± 0.122	0.07 ± 0.063
			Low	0.786 ± 0.123	0.166 ± 0.129	0.048 ± 0.044
	Westerschelde	Rilland	High	0.78 ± 0.059	0.154 ± 0.09	0.066 ± 0.055
			Low	0.834 ± 0.058	0.107 ± 0.072	0.059 ± 0.043
	Westerschelde	Waarde	High	0.729 ± 0.054	0.191 ± 0.095	0.08 ± 0.061
			Low	0.878 ± 0.047	0.082 ± 0.054	0.04 ± 0.034
	Westerschelde	Hellegat	High	0.653 ± 0.084	0.241 ± 0.143	0.107 ± 0.08
	Westerschelde	Molenplaat	High	0.59 ± 0.071	0.276 ± 0.155	0.134 ± 0.101
			Low	0.646 ± 0.091	0.247 ± 0.146	0.107 ± 0.085

*Heteromastus
sp.*

Supplementary information

<i>Macoma balthica</i>	Westerschelde	Paulina	High	0.706 ± 0.065	0.2 ± 0.111	0.093 ± 0.07
			Low	0.543 ± 0.118	0.313 ± 0.195	0.144 ± 0.111
	Oosterschelde	Rattekaai	High	0.577 ± 0.132	0.423 ± 0.132	
			Low	0.574 ± 0.171	0.426 ± 0.171	
	Westerschelde	Rilland	High	0.526 ± 0.137	0.372 ± 0.198	0.103 ± 0.111
			Low	0.594 ± 0.106	0.28 ± 0.169	0.125 ± 0.102
	Westerschelde	Waarde	High	0.69 ± 0.064	0.25 ± 0.101	0.06 ± 0.055
			Low	0.691 ± 0.061	0.23 ± 0.113	0.079 ± 0.073
	Oosterschelde	Dortsman	High	0.885 ± 0.073	0.115 ± 0.073	
			Low	0.897 ± 0.064	0.103 ± 0.064	
	Westerschelde	Hellegat	High	0.601 ± 0.091	0.278 ± 0.166	0.121 ± 0.093
			Low	0.443 ± 0.087	0.363 ± 0.222	0.194 ± 0.143
	Westerschelde	Middelplaat	High	0.33 ± 0.112	0.498 ± 0.252	0.172 ± 0.152
			Low	0.551 ± 0.1	0.31 ± 0.186	0.139 ± 0.109
	Westerschelde	Paulina	High	0.401 ± 0.091	0.481 ± 0.192	0.118 ± 0.114
			Low	0.449 ± 0.149	0.453 ± 0.221	0.098 ± 0.098
	Oosterschelde	Rattekaai	High	0.789 ± 0.113	0.211 ± 0.113	
			Low	0.673 ± 0.126	0.327 ± 0.126	
	Oosterschelde	Viane	High	0.846 ± 0.088	0.154 ± 0.088	

<i>Peringia</i> sp.	Oosterschelde	Dortsman	Low	0.892	0.108	
				±	±	
		High		0.072	0.072	
				0.807	0.193	
		Low		±	±	
				0.081	0.081	
	Westerschelde	Hellegat		0.869	0.131	
				±	±	
		High		0.071	0.071	
				0.698	0.211	0.091
		Low		±	±	±
				0.115	0.148	0.075
	Westerschelde	Middelplaat		0.294	0.43	0.275
				±	±	±
		Low		0.125	0.308	0.219
				0.513	0.36	0.127
		High		±	±	±
				0.109	0.187	0.11
	Westerschelde	Molenplaat		0.604	0.249	0.147
				±	±	±
		Low		0.073	0.158	0.104
				0.538	0.317	0.145
		High		±	±	±
				0.104	0.193	0.115
<i>Spionidae</i>	Oosterschelde	Rattekaai		0.862	0.138	
				±	±	
		Low		0.092	0.092	
				0.864	0.136	
		High		±	±	
				0.102	0.102	
	Westerschelde	Rilland		0.749	0.169	0.082
				±	±	±
		Low		0.088	0.113	0.073
				0.626	0.23	0.143
		High		±	±	±
				0.107	0.158	0.104
	Oosterschelde	Viane		0.726	0.274	
				±	±	
		Low		0.093	0.093	
				0.721	0.279	
		High		±	±	
				0.133	0.133	
	Westerschelde	Waarde		0.669	0.237	0.094
				±	±	±
		Low		0.078	0.124	0.078
				0.79	0.139	0.071
		High		±	±	±
				0.052	0.081	0.056
<i>Spionidae</i>	Westerschelde	Hellegat		0.642	0.249	0.109
				±	±	±
		Low		0.085	0.149	0.084
				0.736	0.167	0.097
		High		±	±	±
				0.111	0.128	0.079
	Westerschelde	Paulina		0.504	0.353	0.143
				±	±	±
		Low		0.149	0.219	0.12
		High				

Supplementary information

<i>Tharyx marioni</i>	Oosterschelde	Dortsman	High	0.633 ± 0.072	0.367 ± 0.072
-----------------------	---------------	----------	------	---------------------	---------------------

Table S7. Natural stable isotope values ($\delta^{13}\text{C}$ and $\delta^{15}\text{N}$) of macroalgae sampled at Dortsman, Viane and Rattekaai (Oosterschelde) in June 2017.

Stable isotope	Site	<i>Chaetomorpha linum</i> ($\mu \pm \sigma$)	<i>Fucus vesiculosus</i> ($\mu \pm \sigma$)	<i>Sargassum muticum</i> ($\mu \pm \sigma$)	<i>Ulva</i> sp. ($\mu \pm \sigma$)
$\delta^{13}\text{C}$	Dortsman			-19.5 ± 1.1	-14.7 ± 0.1
	Rattekaai	-14.4 ± 1.7	-17.3 ± 2.0	-17.2 ± 0.7	-13.6 ± 2.0
$\delta^{15}\text{N}$	Viane	-14.8 ± 0.3		-15.1 ± 1.1	-15.3 ± 2.0
	Dortsman			13.8 ± 0.5	12.8 ± 0.5
	Rattekaai	12.3 ± 0.7	11.4 ± 0.8	11.3 ± 0.5	11.2 ± 1.0
	Viane	11.3 ± 0.2		12.2 ± 0.2	12.0 ± 0.9

Table S8. Stable isotope values ($\delta^{13}\text{C}$ and $\delta^{15}\text{N}$) of sources per elevation category at each site.

$\delta^{13}\text{C}$					
Estuary	Site	Elevation	$\mu \pm \sigma$ $\delta^{13}\text{C}$ MPB	$\mu \pm \sigma$ $\delta^{13}\text{C}$ Phyto-plankton	$\mu \pm \sigma$ $\delta^{13}\text{C}$ Terrestrial OM
Oosterschelde	Rattekaai	High	-14.7 ± 0.6 (n=3)	-21.7 ± 1.2 (n=3)	-
		Low	-16.5 ± 3.2 (n=3)		
	Dortsman	High	-15.6 ± 0.2 (n=2)		
		Low	-15.5 ± 1.3 (n=3)		
	Viane	High	-12.2 ± 0.6 (n=3)		
		Low	-12.8 ± 2.5 (n=3)		
	Waarde	High	-12.9 ± 2.4 (n=3)	-25.8 ± 0.5 (n=3)	-29.2 ± 2.5 (n=3)
		Low	-14.9 ± 1.1 (n=3)		
Westerschelde	Rilland	High	-16.6 ± 2.3 (n=3)		
		Low	-15.9 ± 2.5 (n=3)		

	Molenplaat	High	-16.7 ± 2.3 (n=3)	-24.0 ± 3.1 (n=3)
		Low	-15.4 ± 0.1 (n=3)	
	Hellegat	High	-17.6 ± 0.8 (n=3)	-23.4 ± 2.6 (n=3)
		Low	-14.8 ± 1.9 (n=3)	
	Middelplaat	High	-8.9 ± 0.2 (n=3)	-22 ± 2.1 (n=3)
		Low	-10.8 ± 1.7 (n=3)	
	Paulinapolder	High	-18.2 ± 0.4 (n=3)	-22.0 ± 2.1 (n=3)
		Low	-17.7 ± 1.2 (n=3)	

δ¹⁵N

Estuary	Site	Elevation	$\mu \pm \sigma$ δ ¹⁵ N MPB	$\mu \pm \sigma$ δ ¹⁵ N Phyto- plankton	$\mu \pm \sigma$ δ ¹⁵ N Terres- trial OM
Oosterschelde	Rattekaai	High	7.8 ± 0.3 (n=3)	9.9 ± 5.6 (n=3)	
		Low	7.7 ± 0.3 (n=3)		
	Dortsman	High	8.2 ± 0.3 (n=3)		
		Low	9.7 ± 0.5 (n=3)		
	Viane	High	17.6 ± 0.9 (n=3)		
		Low	17.2 ± 0.3 (n=3)		
Westerschelde	Waarde	High	18.5 ± 0.8 (n=3)	8.9 ± 2 (n=3)	2.5 ± 1.3 (n=2)
		Low	17.4 ± 1.8 (n=3)		

Rilland	High	18.6 ± 0.5 (n=3)	
	Low	18.9 ± 1.2 (n=3)	
Molenplaat	High	21.2 ± 0.8 (n=3)	9.3 ± 1.4 (n=3)
	Low	20.4 ± 0.8 (n=3)	
Hellegat	High	19.5 ± 1.3 (n=3)	9.3 ± 1.4 (n=3)
	Low	20.2 ± 0.4 (n=3)	
Middelplaat	High	19.5 ± 0.8 (n=3)	8.4 ± 0.9 (n=3)
	Low	18.9 ± 0.5 (n=3)	
Paulinapolder	High	18.6 ± 0.6 (n=3)	8.4 ± 0.9 (n=3)
	Low	17.8 ± 1.1 (n=3)	

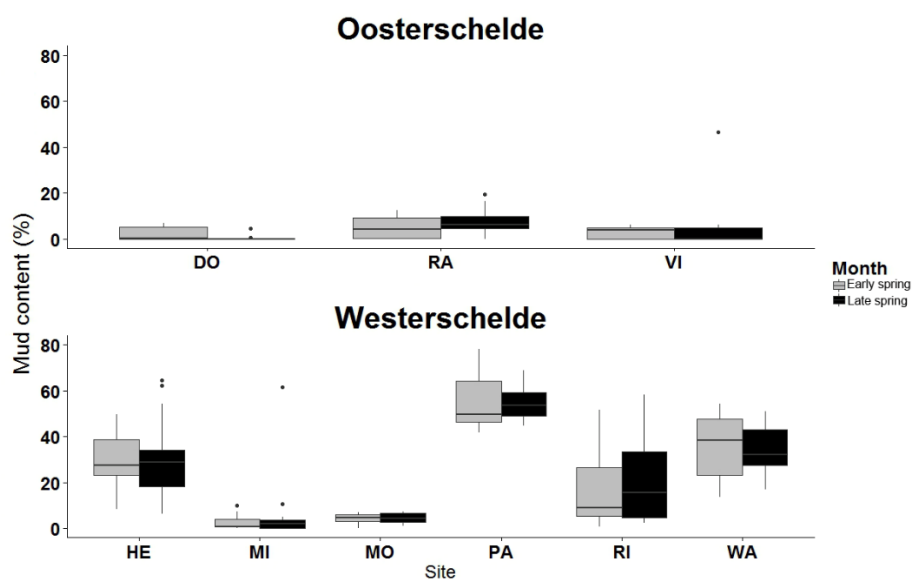


Fig. S1. Mud content (% particles < 63 μm) in early and late spring in sampled plots in the Oosterschelde and Westerschelde.

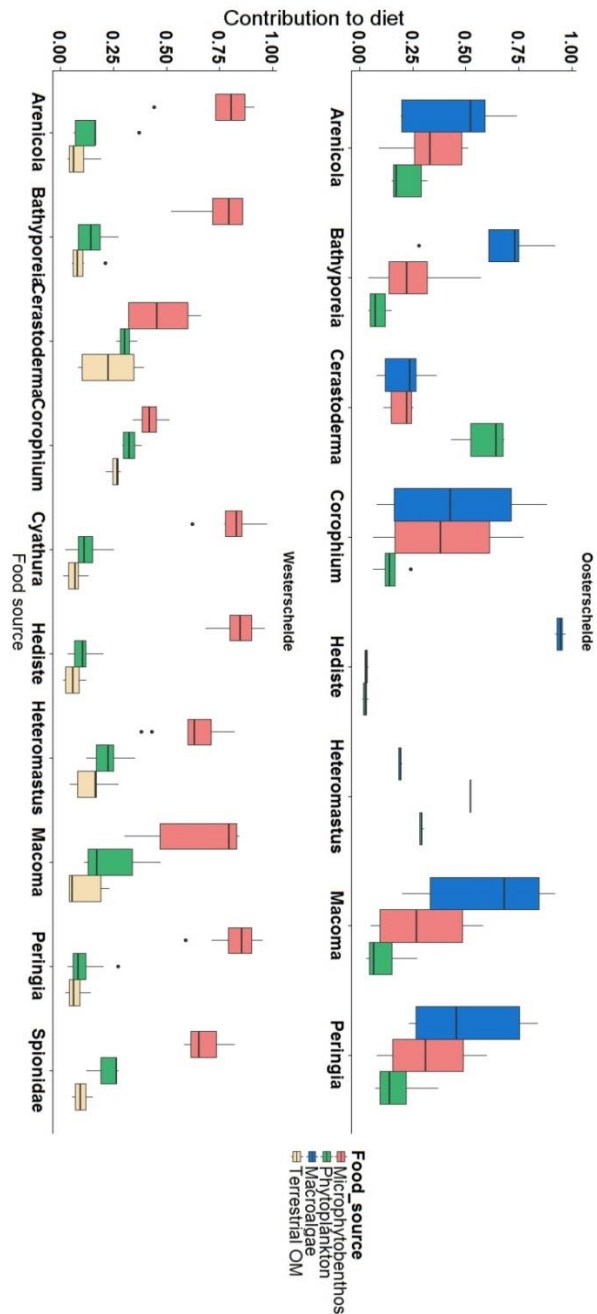


Fig. S2. Diet contribution of MPB, phytoplankton, macroalgae (only included in the Oosterschelde) and terrestrial organic material (only included in the Westerschelde) to sampled macrofaunal species in the Oosterschelde (upper panel) and Westerschelde (lower panel). Boxes represent the first quartile, median and third quartile. Whiskers extend to the largest versus lowest value no further than 1.5 times the interquartile range.

Supplementary material for: The influence of macrofauna on biomass and spatial heterogeneity of intertidal microphytobenthos under varying hydrodynamic conditions: an experimental approach

STATUS: to be submitted

Table S1. The 7 most abundant species in control and defaunated plots at the start of the experiment (T0). For each species, the feeding type is listed. SF=suspension feeder, SDF=surface deposit feeder, O=omnivorous, DF=deposit feeder, P=predator.

Viane

Species	Class	Feeding guild	Abundance (n m ⁻²)		Bio-mass (AFDW mg m ⁻²)		MPB in diet (sampled on site)
			Actual	%	Actual	%	%
High							
<i>Peringia ulvae</i>	Gastropoda	SDF	5199 ±	45 ±	0.4 ±	0.007 ±	0.8 ±
	Malacostraca	SDF	7333 ±	64 ±	0.5 ±	0.001 ±	0.1 Not
<i>Urothoe</i>	Polychaeta	DF	1443 ±	13 ±	1.8 ±	0.04 ±	sampled at this elevation
			2035 ±	18 ±	2.5 ±	0.06 ±	Not
<i>Scoloplos armiger</i>	Clitellata	DF	849 ±	7 ±	56 ±	1.2 ±	sampled at this elevation
			778 ±	7 ±	70 ±	1.6 ±	Not
<i>Oligochaeta</i>	Polychaeta	DF	488 ±	4 ±	87 ±	1.9 ±	sampled at this elevation
			509 ±	4 ±	123 ±	2.7 ±	Not
<i>Capitella</i>	Polychaeta	DF	467 ±	4 ±	0.6 ±	0.01 ±	sampled at this elevation
			658 ±	6 ±	0.8 ±	0.02 ±	0.8 ±
<i>Pygospio elegans</i>	Malacostraca	O	446 ±	4 ±	3.4 ±	0.08 ±	0.1 ±
			628 ±	5 ±	4.8 ±	0.1 ±	Not
<i>Gammarus</i>			127 ±	1 ±	0.5 ±	0.01 ±	sampled at this elevation
			178 ±	2 ±	0.8 ±	0.01 ±	
Inter-mediate							
<i>Oligochaeta</i>	Clitellata	O	721 ±	16 ±			Not sampled at this elevation
	Gastropoda	SDF	359 ±	9 ±	<0.0001 ±	0 ±	0.8 ±
<i>Peringia ulvae</i>	Polychaeta	DF	509 ±	11 ±	22 ±	0.9 ±	0.1 ±
			359 ±	8 ±	31 ±	1.3 ±	0.6 ±
<i>Scoloplos armiger</i>			424 ±	10 ±	8 ±	0.3 ±	0.1 ±
			419 ±	9 ±	7 ±	0.3 ±	

<i>Pygospio elegans</i>	Polychaeta	DF	382 ± 60	9 ± 1	0.2 ± 0.3	0.01 ± 0.01	0.6 ± 0.1
<i>Capitella</i>	Polychaeta	DF	212 ± 60	5 ± 1	0.5 ± 0.6	0.02 ± 0.02	Not sampled at this elevation
<i>Gammarus</i>	Malacostraca	O	106 ± 90	2 ± 2	<0.0001	0	Not sampled at this elevation
<i>Hediste</i> Low	Polychaeta	O	85 ± 60	2 ± 1	<0.0001	0	Not sampled at this elevation
	Malacostraca	SDF	700 ± 748	17 ± 18	1.3 ± 1.2	2.9 ± 2.9	Not sampled at this elevation
<i>Urothoe</i>	Polychaeta	DF	679 ± 60	17 ± 1	1.4 ± 1.4	3.1 ± 3.3	0.7 ± 0.1
<i>Pygospio elegans</i>	Polychaeta	DF	531 ± 30	13 ± 1	33 ± 39	77 ± 91	Not sampled at this elevation
<i>Scoloplos armiger</i>	Clitellata	DF	127 ± 120	3 ± 3	0	0	Not sampled at this elevation
<i>Oligochaeta</i>	Polychaeta	DF	85 ± 60	2 ± 1	0	0	Not sampled at this elevation
<i>Capitella</i>	Polychaeta	P	42 ± 60	1 ± 1	4.1 ± 5.8	9.6 ± 14	0.6 ± 0.1
<i>Nephtys hombergii</i>	Polychaeta	DDF	21 ± 30	1 ± 1	<0.0001	0	0.6 ± 0.1
<i>Arenicola</i>							

Paulina

Species	Class	Feeding guild	Abundance		Biomass		MPB in diet
			Actual	%	Actual	%	%
High	Bivalvia	DF	3247 ± 1586	31 ± 15	3.6 ± 1.5	0.3 ± 0.1	Not sampled at this elevation
<i>Tellinoidea</i>	Polychaeta	DF	1188 ± 0	11 ± 0	1.4 ± 0.4	0.1 ± 0.02	Not sampled at this elevation
<i>Pygospio elegans</i>	Polychaeta	DF	891 ± 419	8 ± 8	33 ± 17	2.3 ± 1.2	0.7 ± 0.1
<i>Heteromastus filiformis</i>	Polychaeta	SDF	828 ± 269	8 ± 3	5 ± 2	0.4 ± 0.1	0.6 ± 0.1
<i>Tharyx marioni</i>							

Supplementary information

	Polychaeta	DF	573	5	1.4	0.1	0.7
			±	±	±	±	±
<i>Capitella</i>			30	0.3	0.5	0.04	0.1
	Bivalvia	SDF	509	5	142	10	0.8
			±	±	±	±	±
<i>Limecola balthica</i>			60	0.6	20	1.4	0.1
	Bivalvia	SDF	318	3	856	60	0.7
			±	±	±	±	±
<i>Scrobicularia plana</i>			90	1	850	59.9	0.1
Inter-mediate							
	Bivalvia	DF	22111	54	19	0.3	Not sampled at this elevation
			±	±	±	±	
Tellinoidea			12152	30	1	0.02	
	Polychaeta	DF	9825	24	11	0.2	Not sampled at this elevation
			±	±	±	±	
<i>Pygospio elegans</i>			1347	3	3	0.05	
	Malacostraca	SDF	2801	7	9	0.16	0.9
			±	±	±	±	±
<i>Cyathura carinata</i>			180	0.4	3	0.05	0.1
	Polychaeta	DF	1294	3	27	0.49	0.6
			±	±	±	±	±
<i>Heteromastus filiformis</i>			389	1	4	0.07	0.0
	Polychaeta	DF	721	2	0.5	0.01	Not sampled at this elevation
			±	±	±	±	
<i>Polydora</i>			60	0.1	0.5	0.009	
	Polychaeta	SDF	573	1	1	0.02	Not sampled at this elevation
			±	±	±	±	
<i>Tharyx marioni</i>			509	1	1.4	0.025	
	Bivalvia	SF	233	1	0.2	0.004	Not sampled at this elevation
			±	±	±	±	
<i>Ensis</i>			329	1	0.3	0.006	
Low							
	Bivalvia	SDF	30451	84	5	13	0.8
			±	±	±	±	±
<i>Limecola balthica</i>			2544	7	7	18	0.0
	Malacostraca	P	1592	4	0.6	1.6	0.8
			±	±	±	±	±
<i>Crangon crangon</i>			1167	3	0.2	0.4	0.0
	Polychaeta	SDF	849	2	2.8	6.8	Not sampled at this elevation
			±	±	±	±	
<i>Terebellidae</i>			958	3	3.9	9.6	
	Polychaeta	DF	531	1	20	48	0.6
			±	±	±	±	±
<i>Heteromastus filiformis</i>			210	0.6	2	4.9	0.0
	Polychaeta	DF	509	1	0.6	1.5	0.7
			±	±	±	±	±
<i>Pygospio elegans</i>			180	0.5	0.4	0.9	0.0
	Polychaeta	SDF	340	1	1.7	4.2	0.5
			±	±	±	±	±
<i>Tharyx marioni</i>			180	0.5	0.4	0.9	0.0
	Malacostraca	O	106	0			Not sampled at this elevation
			±	±			
<i>Mysidae</i>			30	0.1	< 0.0001	0	

Table S2. Variogram parameters calculated using images excluding shells of each available image. For each image the presence of macroalgae or shells is indicated.

Paulina

Time	Elevation	Treatment (control / default)	Replicate	Plot length (m)	Macroalgae y/n	Instruments y/n	Shells (y/n)	Model	Nugget – without shells	Sill – without shells	Major range – without shells (m)
T2	High	C	1	2.9	n	n	y	Mat	0.046	0.044	0.034
T2	High	C	2	3	n	y	n	Mat	0.339	0.424	0.036
T2	High	D	1	2.4	n	n	n	Mat	0.064	0.435	1.146
T2	High	D	2	2.4	y	y	n	Mat	0.089	0.398	0.236
T2	Intermediate	C	1	3	y	n	n	Mat			
T2	Intermediate	C	2	2.95	y	y	n	Mat	0.130	0.036	0.058
T2	Intermediate	D	1	2.48	y	y	y	Mat	0.060	0.041	0.053
T2	Intermediate	D	2	2.69	y	y	y	Mat	0.023	0.016	0.235
T2	Low	C	1	3.07	n	n	n	Mat	0.008	0.009	0.326
T2	Low	C	2	3.01	n	y	n	Mat	0.129	1.046	0.034
T2	Low	D	1	2.41	n	n	n	Mat	0.006	0.250	0.063
T2	Low	D	2	2.45	n	n	n	Mat	0.570	1.531	0.105
T4	High	C	1	-	-	-	-	-	0.027	0.378	0.063
T4	High	C	2	-	-	-	-	-	-	-	-
T4	High	D	1	-	y	n	y	Mat	0.402	0.304	0.130
T4	High	D	2	-	y	y	n	Mat	1.296	1.291	0.258
T4	Intermediate	C	1	-	y	n	n	Mat			
T4	Intermediate	C	2	-	y	y	n	Mat	24.497	10.962	0.095
T4	Intermediate	D	1	-	y	n	y	Mat	3.382	2.039	0.046
T4	Intermediate	D	2	-	y	y	y	Mat	0.036	0.024	0.094
T4	Low	C	1	-	n	n	n	Mat	0.118	0.097	0.088
T4	Low	C	2	-	n	y	n	Mat	0.214	0.117	0.042
T4	Low	D	1	-	n	n	n	Mat	0.445	0.386	0.049
T4	Low	D	2	-	n	n	n	Mat	0.049	0.054	0.063
T8	High	C	1	-	-	-	-	-	0.188	0.272	0.097
T8	High	C	2	-	-	-	-	-	-	-	-
T8	High	D	1	-	-	-	-	-	-	-	-
T8	High	D	2	-	y	y	n	Mat	0.222	0.119	0.272
T8	Intermediate	C	1	-	-	-	-	-	-	-	-
T8	Intermediate	C	2	-	-	-	-	-	-	-	-
T8	Intermediate	D	1	-	n	n	n	Mat			
T8	Intermediate	D	1	-	n	n	n	Mat	0.079	0.047	0.062

Supplementary information

T8	Inter- medi- ate	D	2	-	-	-	-	-	-	-	-
T8	Low	C	1	-	n	n	n	Mat	-	-	-
T8	Low	C	2		n	y	n	Mat	0.065	0.026	0.070
T8	Low	D	1		y	n	y	Mat	-	-	-
T8	Low	D	2		n	n	n	Mat	0.312	0.225	0.071
T12	High	C	1		y	n	y	Mat	0.044	0.023	0.054
T12	High	C	2		y	y	y	Mat	0.147	0.067	0.049
T12	High	D	1		y	n	y	Mat	0.255	0.079	0.055
T12	High	D	2		y	y	n	Mat	0.198	0.058	0.093
T12	Inter- medi- ate	C	1		n	n	y	Mat			
									0.144	0.122	0.174
T12	Inter- medi- ate	C	2		y	y	y	Mat			
									0.109	0.127	0.046
T12	Inter- medi- ate	D	1		y	n	y	Mat			
									0.089	0.256	0.268
T12	Inter- medi- ate	D	2		n	y	y	Mat			
									0.049	0.155	0.172
T12	Low	C	1		n	n	n	Mat	0.692	0.513	0.044
T12	Low	C	2		n	y	n	Mat	0.365	0.193	0.042
T12	Low	D	1		n	n	y	Mat	0.620	0.413	0.102
T12	Low	D	2		n	n	n	Mat	0.539	0.252	0.049
T19	High	C	1	-	-	-	-	-	-	-	-
T19	High	C	2		y	y	n	Mat	0.149	0.075	0.044
T19	High	D	1		y	n	y	Mat	0.058	0.020	0.045
T19	High	D	2		y	y	y	Mat	0.138	0.047	0.108
T19	Inter- medi- ate	C	1		n	n	n	Mat			
									0.094	0.039	0.094
T19	Inter- medi- ate	C	2		n	y	n	Mat	-	-	-
T19	Inter- medi- ate	D	1		y	n	n	Mat			
									0.123	0.048	0.195
T19	Inter- medi- ate	D	2		y	n	n	Mat			
									0.150	0.074	0.196
T19	Low	C	1		y	n	n	Mat	0.078	0.035	0.039
T19	Low	C	2		y	n	n	Mat	0.081	0.049	0.033
T19	Low	D	1		n	n	n	Mat	0.186	0.085	0.090
T19	Low	D	2		y	n	n	Mat	0.342	0.198	0.039

Viane

Time	Eleva- tion	Treat ment (con- trol / defau- nated)	Re- pli- ca- te	Plot leng- th (m)	Ma- cro- al- gae y/n	In- stru- men- ts y/n	Shell s (y/n)	Mo- del	Nugg et – witho ut shells	Sill – witho ut shells	Major range – witho ut shells (m)
T2	High	C	1	3.9	y	n	y	Mat	0.037	0.027	0.049
T2	High	C	2	3.9	y	y	n	Mat	0.395	0.193	0.042
T2	High	D	1	3.8	y	n	y	Mat	0.062	0.047	0.115
T2	High	D	2	3.9	y	n	y	Mat	0.419	0.219	0.046
T2	Inter media te	C	1	3.6	y	n	y	Mat	-	-	-

T2	Inter media te	C	2	3.6	y	y	y	Mat			
									0.163	0.109	0.052
T2	Inter media te	D	1	3.6	n	n	y	Mat			
									0.042	0.063	0.021
T2	Inter media te	D	2	3.3	y	y	y	Mat			
									0.102	0.151	0.699
T2	Low	C	1	-	-	-		-	-	-	-
T2	Low	C	2	3.9	y	y	y	Mat	0.019	0.027	0.031
T2	Low	D	1	3.9	y	n	y	Mat	0.001	0.046	0.021
T2	Low	D	2	3.9	y	y	y	Mat	0.007	0.016	0.031
T4	High	C	1	-	-	-		-	-	-	-
T4	High	C	2	-	-	-		-	-	-	-
T4	High	D	1	-	-	-		-	-	-	-
T4	High	D	2	-	-	-		-	-	-	-
T4	Inter media te	C	1	-	-	-		-	-	-	-
T4	Inter media te	C	2	-	-	-		-	-	-	-
T4	Inter media te	D	1	-	-	-		-	-	-	-
T4	Inter media te	D	2	-	-	-		-	-	-	-
T4	Low	C	1	-	-	-		-	-	-	-
T4	Low	C	2	-	-	-		-	-	-	-
T4	Low	D	1	-	-	-		-	-	-	-
T4	Low	D	2	-	-	-		-	-	-	-
T8	High	C	1	3.9	y	n	y	-	-	-	-
T8	High	C	2	-	-	-		-	-	-	-
T8	High	D	1	-	-	-		-	-	-	-
T8	High	D	2	-	-	-		-	-	-	-
T8	Inter media te	C	1	-	-	-		-	-	-	-
T8	Inter media te	C	2	-	-	-		-	-	-	-
T8	Inter media te	D	1	-	-	-		-	-	-	-
T8	Inter media te	D	2	-	-	-		-	-	-	-
T8	Low	C	1	-	-	-		-	-	-	-
T8	Low	C	2	-	-	-		-	-	-	-
T8	Low	D	1	-	-	-		-	-	-	-
T8	Low	D	2	-	-	-		-	-	-	-
T12	High	C	1		y	n	y	Mat	0.049	0.019	0.027
T12	High	C	2		y	y	n	Mat	0.084	0.025	0.119
T12	High	D	1		y	n	y	Mat	0.028	0.024	0.031
T12	High	D	2		y	y	y	Mat	0.042	0.017	0.111
T12	Inter media te	C	1	-	-	-		-	-	-	-
T12	Inter media te	C	2	-	-	-		-	-	-	-

Supplementary information

T12	Inter media te	D	1	-	-	-		-	-	-	-
T12	Inter media te	D	2	-	-	-		-	-	-	-
T12	Low	C	1	-	-	-		-	-	-	-
T12	Low	C	2	-	-	-		-	-	-	-
T12	Low	D	1		y	n	y	Mat	0.072	0.044	0.045
T12	Low	D	2		y	y	n	Mat	0.072	0.065	0.310
T18	High	C	1		y	n	y	Mat	0.070	0.028	0.204
T18	High	C	2		-	-		-			
T18	High	D	1		y	n	y	Mat	0.042	0.017	0.059
T18	High	D	2		y	n	y	Mat	0.105	0.038	0.131
T18	Inter media te	C	1		y	n	y	Mat			
									0.092	0.077	0.034
T18	Inter media te	C	2		y	y	y	Mat	-	-	-
T18	Inter media te	D	1		y	n	y	Mat	-	-	-
T18	Inter media te	D	2		y	y	y	Mat			
									0.092	0.065	0.028
T18	Low	C	1		y	n	y	Mat	0.153	0.129	0.042
T18	Low	C	2		y	y	y	Mat	0.128	0.088	0.039
T18	Low	D	1		n	n	y	Mat	0.111	0.085	0.035
T18	Low	D	2		y	y	y	Mat	-	-	-

Table S3. Overview of measured mud content, current speed, MPB biomass, variogram parameters, and grazing pressure averaged over all time steps (except grazing pressure, see time steps in header).

Site	Elevation category	Treatment	Elevation	Chl-a (average all time steps)	Mud content	Current speed	Grazing pressure (T0)	Grazing pressure (T8)	Grazing pressure (T18/T19)	Nugget	Sill	Major range
Paulina	High	Control	0.48 ± 0.04	295 ± 110	69.4 ± 2.4	0.17	144 ± 26	75 ± 19	441 ± 118	0.14 ± 0.12	0.13 ± 0.17	0.04 ± 0.01
		Defaunated	0.49 ± 0.02	280 ± 162	68.9 ± 5.2	0.17	-	13 ± 2	257 ± 90	0.30 ± 0.39	0.31 ± 0.40	0.26 ± 0.34
	Intermediate	Control	0.19 ± 0.04	346 ± 152	62.4 ± 3.1	0.21	192 ± 85	84 ± 11	706 ± 138	0.65 ± 1.34	0.40 ± 0.80	0.08 ± 0.05
		Defaunated	0.15 ± 0.02	295 ± 132	64.9 ± 6.3	0.21	-	9 ± 8	384 ± 119	0.08 ± 0.05	0.08 ± 0.08	0.18 ± 0.09
	Low	Control	-0.95 ± 0.04	197 ± 89	41.3 ± 8.5	0.3	29 ± 2	-	136 ± 39	0.23 ± 0.22	0.29 ± 0.33	0.05 ± 0.01
		Defaunated	-1.03 ± 0.02	166 ± 61	44.6 ± 5.3	0.3	-	0.58 ± 0.06	50 ± 5	0.31 ± 0.22	0.38 ± 0.44	0.08 ± 0.02
	High	Control	0.85 ± 0.02	221 ± 55	10.9 ± 5.0	0.08	460 ± 456	32 ± 7	1511 ± 1245	0.13 ± 0.15	0.06 ± 0.08	0.09 ± 0.07
		Defaunated	0.84 ± 0.01	227 ± 121	8.0 ± 3.2	0.08	-	11 ± 2	513 ± 36	0.11 ± 0.15	0.06 ± 0.08	0.08 ± 0.04
	Intermediate	Control	0.17 ± 0.01	312 ± 55	5.2 ± 1.1	0.15	50 ± 35	155 ± 26	1044 ± 525	0.12 ± 0.05	0.09 ± 0.02	0.04 ± 0.01
		Defaunated	0.15 ± 0.02	261 ± 111	3.4 ± 3.1	0.15	-	2 ± 0	814 ± 536	0.08 ± 0.03	0.09 ± 0.05	0.25 ± 0.39
Viane	Low	Control	-0.92 ± 0.02	156 ± 67	2.5 ± 2.7	0.21	16 ± 14	4 ± 0	97 ± 100	0.10 ± 0.07	0.08 ± 0.05	0.04 ± 0.01
		Defaunated	-0.90 ± 0.02	127 ± 53	3.6 ± 3.7	0.21	-	4.86 ± 0.53	100	0.05 ± 0.04	0.05 ± 0.03	0.09 ± 0.12

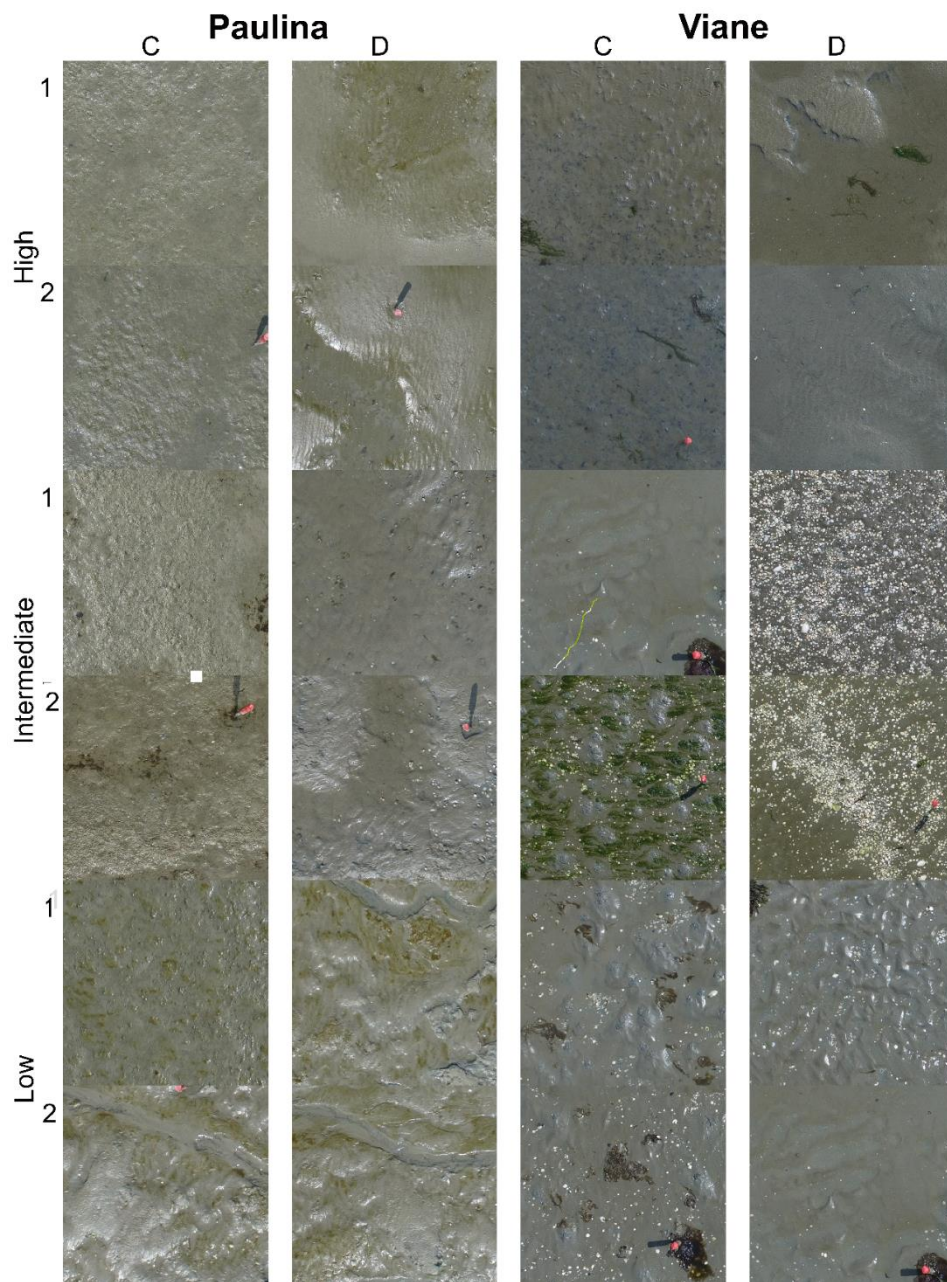


Figure S1. Original images two weeks (T2) after opening of the defaunated plots in control (C, with replicates C1 and C2) and defaunated (D, with replicates D1 and D2) plots at Paulinapolder (Westerschelde) at high, intermediate and low elevation and at Viane at high, intermediate and low elevation. Macroalgae and shells were removed from the images and excluded from the semi-variogram analysis.

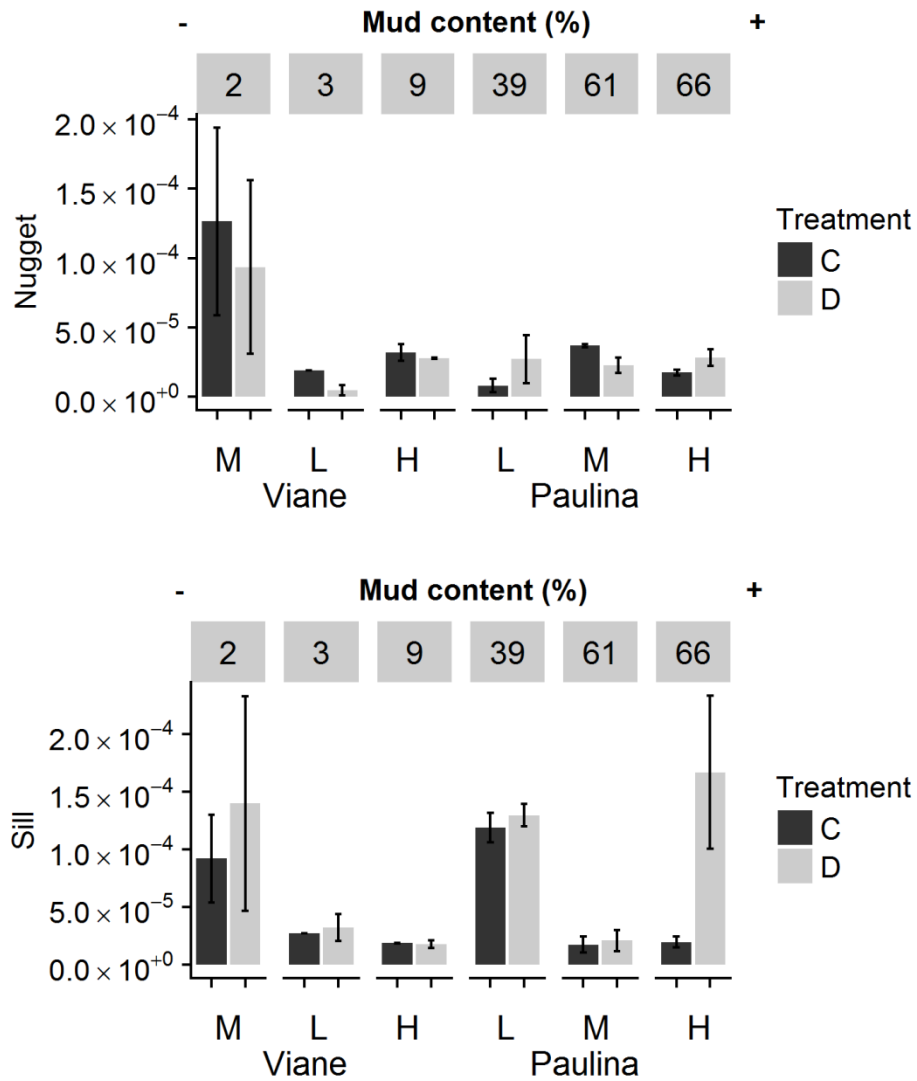
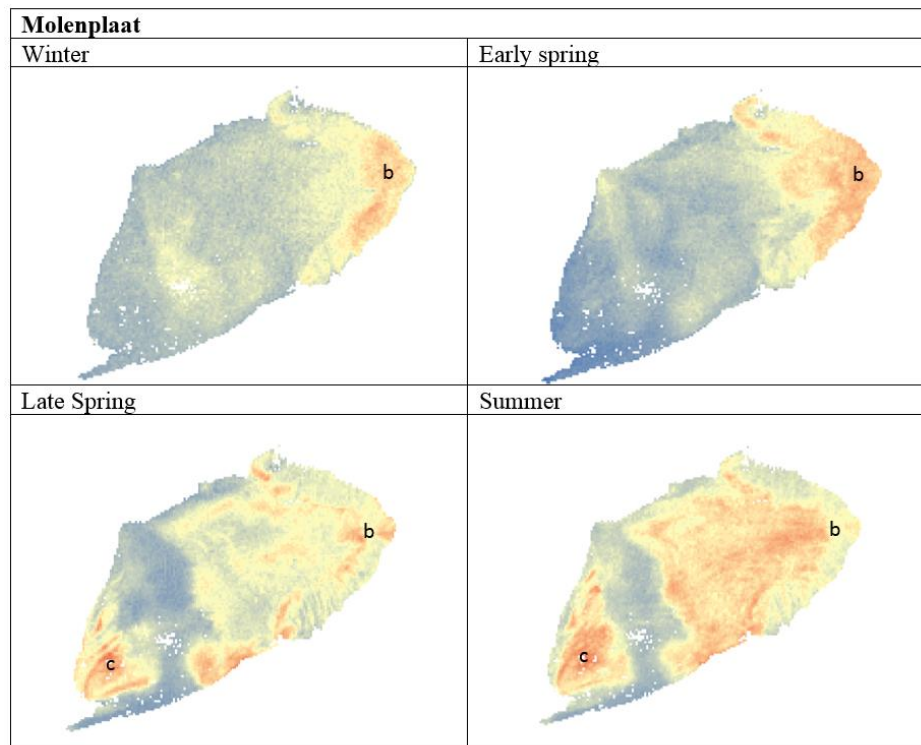
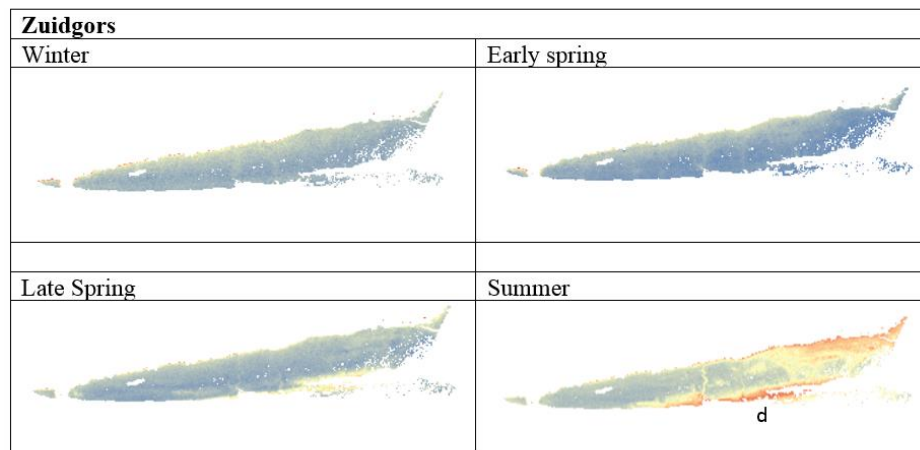
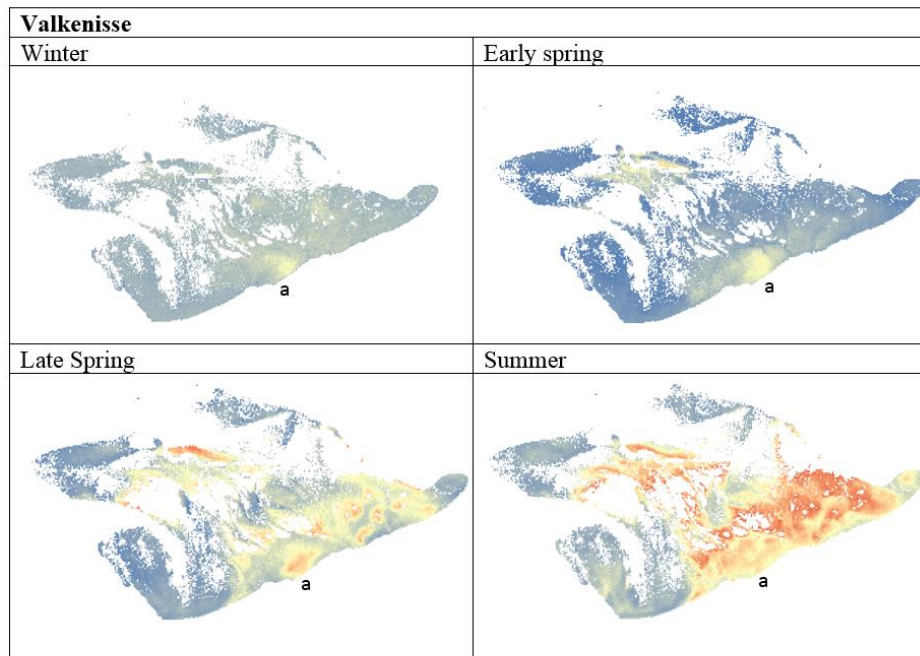


Figure S2. Nugget and sill at T2 in control and defaunated plots along a mud content gradient.

Supplementary material for: Seasonal and spatial variability in patchiness of microphytobenthos on intertidal flats from Sentinel-2 satellite imagery

STATUS: Published in *Frontiers in Marine Science*





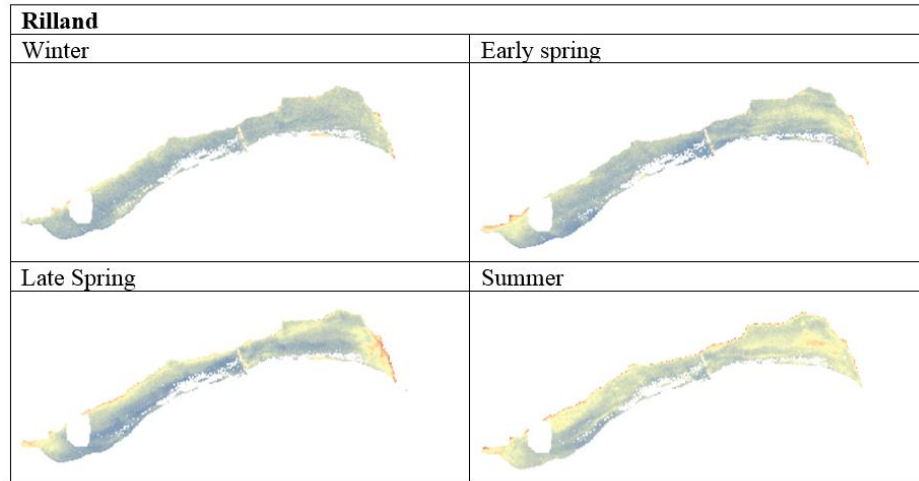


Figure S1. NDVI per season for Molenplaat, Valkenisse, Zuidgors and Rilland. The NDVI had a range of -0.05-0.27.

Table S1. Regression parameters and fit (R^2) of empirical line calibration of the Sentinel-2 imagery, using surface reflectances in an image of 16 March 2016 as reference. Surface reflectance values were multiplied by 10000 and, therefore, had a range of 0-10000.

	B4			B8		
	coefficient	intercept	R^2	coefficient	intercept	R^2
05-02-2018	1.1	163.0	0.9	1.0	104.7	0.9
12-12-2018	1.1	197.5	0.8	0.9	249.5	0.8
21-01-2019	1.1	118.5	0.9	0.9	70.8	0.8
11-04-2016	1.1	169.3	0.9	1.0	249.0	0.9
27-03-2017	1.0	11.8	0.9	1.0	48.2	0.9
06-04-2018	1.2	219.9	0.9	1.1	-364.9	0.9
26-05-2017	1.1	105.8	0.9	0.9	-216	0.9
06-05-2018	1.1	131.9	0.9	1.0	269.7	0.9
30-06-2018	1.0	133.5	0.9	1.0	231.4	0.9
20-07-2016	0.9	88.8	0.9	1.0	150.4	0.9
15-07-2018	1.1	223.7	0.9	1.1	340.9	0.9
05-07-2019	0.9	17.6	0.8	0.9	57.9	0.7

Table S2. Semi-variogram parameters calculated with a spherical model per tidal flat for each image.

Site	Season	Date	RMSE	Nugget (m)	Sill (m)	Major range (m)	NDVI (μ)
Lage Springer	Early spring	11-4-'16	$1.07 \cdot 10^{-7}$	0.00013	0.00042	315.8	0.044
	Early spring	27-3-'17	$1.45 \cdot 10^{-6}$	0.00022	0.00082	323.2	0.067
	Early spring	6-4-'18	$3.95 \cdot 10^{-7}$	0.00010	0.00078	379.4	0.051
	Late spring	6-5-'18	$6.19 \cdot 10^{-7}$	$6.16 \cdot 10^{-5}$	0.00193	398.1	0.069

Molen- plaat	Late spring	30-6-'18	$2.34 \cdot 10^{-6}$	0.00026	0.00130	353.0	0.040
	Late spring	26-5-'17	$8.51 \cdot 10^{-7}$	0.00014	0.00117	280.9	0.041
	Summer	20-7-'16	$4.10 \cdot 10^{-6}$	0.00028	0.00127	367.0	0.016
					$7.25 \cdot 10^{-5}$		
	Summer	5-7-'19	$1.69 \cdot 10^{-8}$	$9.6 \cdot 10^{-6}$		429.8	0.092
	Summer	15-7-'18	$1.23 \cdot 10^{-6}$	0.00022	0.00116	377.7	0.073
	Winter	12-12-'18	$7.90 \cdot 10^{-7}$	0.00014	0.00074	243.7	0.138
	Winter	21-1-'19	$1.01 \cdot 10^{-7}$	0.00016	0.00033	239.1	0.084
	Winter	5-2-'18	$9.44 \cdot 10^{-8}$	0.00011	0.00030	281.8	0.029
	Early spring	11-4-'16	$9.73 \cdot 10^{-7}$	0.00018	0.00055	482.6	0.056
	Early spring	27-3-'17	$1.51 \cdot 10^{-6}$	0.00019	0.00065	322.5	0.080
	Early spring	6-4-'18	$1.29 \cdot 10^{-6}$	0.00018	0.00064	466.5	0.061
	Late spring	6-5-'18	$9.91 \cdot 10^{-7}$	0.00015	0.00075	281.8	0.090
	Late spring	30-6-'18	$5.46 \cdot 10^{-7}$	$3.33 \cdot 10^{-5}$	0.00140	200.6	0.076
	Late spring	26-5-'17	$2.15 \cdot 10^{-6}$	0.00016	0.00212	302.8	0.101
	Summer	20-7-'16	$2.56 \cdot 10^{-5}$	$4.29 \cdot 10^{-5}$	0.00412	303.8	0.083
					$5.35 \cdot 10^{-5}$		
	Summer	5-7-'19	$2.28 \cdot 10^{-10}$	$7.33 \cdot 10^{-7}$		287.4	0.097
	Summer	15-7-'18	$2.03 \cdot 10^{-6}$	0.00013	0.00269	272.9	0.155
	Winter	12-12-'18	$1.42 \cdot 10^{-7}$	0.00023	0.00038	439.5	0.123
Paulina- polder	Winter	21-1-'19	$5.82 \cdot 10^{-7}$	0.00023	0.00041	311.9	0.073
	Winter	5-2-'18	$2.05 \cdot 10^{-7}$	0.00014	0.00066	605.1	0.024
	Early spring	11-4-'16	$1.33 \cdot 10^{-6}$	0.00064	0.00157	795.0	0.118
	Early spring	27-3-'17	$7.39 \cdot 10^{-7}$	0.00043	0.00063	400.6	0.064
	Early spring	6-4-'18	$4.26 \cdot 10^{-7}$	0.00032	0.00079	380.8	0.061
	Late spring	6-5-'18	$1.35 \cdot 10^{-6}$	0.00024	0.00200	360.8	0.102
	Late spring	30-6-'18	$1.31 \cdot 10^{-6}$	0.00050	0.00174	420.6	0.050
	Late spring	26-5-'17	$4.57 \cdot 10^{-7}$	0.00011	0.00169	305.4	0.076
	Summer	20-7-'16	$2.87 \cdot 10^{-6}$	0.00063	0.00189	190.6	0.076
					$3.38 \cdot 10^{-5}$		
Rilland	Summer	5-7-'19	$2.88 \cdot 10^{-10}$	$7.74 \cdot 10^{-6}$		509.7	0.095
	Summer	15-7-'18	$1.90 \cdot 10^{-7}$	0.00010	0.00220	298.5	0.117
	Winter	12-12-'18	$4.92 \cdot 10^{-7}$	0.00046	0.00063	277.7	0.133
	Winter	21-1-'19	$2.28 \cdot 10^{-8}$	0.00039	0.00041	365.3	0.078
	Winter	5-2-'18	$1.62 \cdot 10^{-8}$	0.00028	0.00031	500.9	0.013
	Early spring	11-4-'16	$2.70 \cdot 10^{-7}$	0.00013	0.00087	402.4	0.048
	Early spring	27-3-'17	$1.10 \cdot 10^{-6}$	0.00034	0.00102	613.0	0.069
	Early spring	6-4-'18	$4.28 \cdot 10^{-7}$	0.00021	0.00072	305.2	0.057
	Late spring	6-5-'18	$7.76 \cdot 10^{-7}$	0.00015	0.00091	390.4	0.070

Supplementary information

Valke- nisse	Late spring	30-6-'18	$1.33 \cdot 10^{-7}$	0.00023	0.00122	374.8	0.034
	Late spring	26-5-'17	$3.67 \cdot 10^{-6}$	0	0.00267	274.1	0.087
	Summer	20-7-'16	$1.46 \cdot 10^{-6}$	0.00014	0.00204	251.4	0.034
					$8.48 \cdot 10^{-5}$		
	Summer	5-7-'19	$1.37 \cdot 10^{-7}$	$1.04 \cdot 10^{-5}$		506.3	0.094
	Summer	15-7-'18	$5.21 \cdot 10^{-7}$	0.00041	0.00119	298.9	0.119
	Winter	12-12-'18	$8.17 \cdot 10^{-7}$	0.00026	0.00050	315.0	0.106
	Winter	21-1-'19	$2.90 \cdot 10^{-8}$	0.00025	0.00039	367.5	0.047
	Winter	5-2-'18	$4.17 \cdot 10^{-8}$	0.00019	0.00049	271.3	0.015
	Early spring	11-4-'16	$4.73 \cdot 10^{-7}$	0.00013	0.00100	891.9	-
	Early spring	27-3-'17	$4.02 \cdot 10^{-7}$	0.00020	0.00138	1006.6	0.001
	Early spring	6-4-'18	$8.04 \cdot 10^{-6}$	0.00015	0.00216	1187.6	0.016
	Late spring	6-5-'18	$3.21 \cdot 10^{-6}$	0.00024	0.00131	607.2	0.022
	Late spring	30-6-'18	$1.88 \cdot 10^{-5}$	0.00060	0.00380	803.8	0.058
	Late spring	26-5-'17	$4.46 \cdot 10^{-6}$	0.00041	0.00151	709.4	0.066
	Summer	20-7-'16	$1.23 \cdot 10^{-5}$	0.00076	0.00630	559.1	0.057
	Summer	5-7-'19	$9.61 \cdot 10^{-9}$	$1.37 \cdot 10^{-5}$	0.00016	1300.3	0.085
	Summer	15-7-'18	$1.28 \cdot 10^{-5}$	0.00057	0.00564	988.5	0.094
	Winter	12-12-'18	$2.24 \cdot 10^{-7}$	0.00020	0.00027	694.5	0.127
	Winter	21-1-'19	$2.86 \cdot 10^{-7}$	0.00019	0.00023	786.4	0.092
Zuid- gors							0.057
	Winter	5-2-'18	$2.72 \cdot 10^{-8}$	0.00011	0.00018	568.9	-
	Early spring	11-4-'16	$8.49 \cdot 10^{-8}$	0.00014	0.00029	321.6	0.021
	Early spring	27-3-'17	$3.92 \cdot 10^{-8}$	0.00013	0.00014	199.8	0.015
	Early spring	6-4-'18	$1.92 \cdot 10^{-7}$	0.00019	0.00052	395.1	0.019
	Late spring	6-5-'18	$6.72 \cdot 10^{-8}$	0.00011	0.00042	328.3	0.035
	Late spring	30-6-'18	$1.24 \cdot 10^{-6}$	0.00011	0.00250	322.5	0.056
	Late spring	26-5-'17	$7.71 \cdot 10^{-9}$	0.00013	0.00034	267.1	0.036
	Summer	20-7-'16	$2.33 \cdot 10^{-6}$	0.00029	0.00370	289.7	0.045
					$9.35 \cdot 10^{-5}$		0.072
	Summer	5-7-'19	$9.10 \cdot 10^{-10}$	$7.03 \cdot 10^{-6}$		445.0	-
	Summer	15-7-'18	$3.92 \cdot 10^{-7}$	0.00014	0.00274	353.1	0.088
	Winter	12-12-'18	$3.20 \cdot 10^{-8}$	0.00021	0.00037	399.2	0.124
	Winter	21-1-'19	$2.55 \cdot 10^{-8}$	0.00017	0.00018	284.8	0.091
							0.048
	Winter	5-2-'18	$3.28 \cdot 10^{-8}$	0.00013	0.00018	240.6	-
							0.011

Bibliography

Abrahams, M. & Kattenfeld, M., 1997. The role of turbidity as a constraint on predator-prey interactions in aquatic environments. *Behav Ecol Sociobiol* 40, 169-174.

Adam, S. et al., 2006. Sediment type unsupervised classification of the Molenplaat, Westerschelde estuary, the Netherlands. *EARSeL eProceedings* 5 (2), 146-160.

Adam, S. et al., 2011. Bio-physical characterization of sediment stability in mudflats using remote sensing: a laboratory experiment. *Cont. Shelf Res.* 31 (10), S26-S35.

Admiraal, W. et al., 1984. The seasonal succession patterns of diatom species on an intertidal mudflat: an experimental analysis. *Oikos* 42, 30-40.

Alcamo, J., 2003. Ecosystems and human well-being: a framework for assessment. Washington D. C., USA.

Alongi, D. M., 2014. Carbon Cycling and Storage in Mangrove Forests. *Annu Rev Mar Sci* 6, 195-219.

Andersen, T. J. et al., 2002. Enhanced erodibility of fine-grained marine sediments by *Hydrobia ulvae*. *J. Sea Res.* 48, 51-58.

Andersen, T.J. et al., 2010. Erodibility of a mixed mudflat dominated by microphytobenthos and *Cerastoderma edule*, East Frisian Wadden Sea, Germany. *Estuar Coast Shelf S* 87, 197-206.

Andrew, N.L., 1993. Spatial Heterogeneity, Sea-Urchin Grazing, and Habitat Structure on Reefs in Temperate Australia. *Ecology* 74, 292-302.

Armonies, W. et al., 2001. Effects of the severe winter 1995/96 on the benthic macrofauna of the Wadden Sea and the coastal North Sea near the island of Sylt. *Helgolander Mar Res* 55, 170-175.

Asmus, R.M. & Bauerfeind, E., 1994. The Microphytobenthos of Königshafen - Spatial and Seasonal Distribution on a Sandy Tidal Flat. *Helgolander Meeresun* 48, 257-276.

Azovsky, A.I. et al., 2000. Fractal properties of spatial distribution of intertidal benthic communities. *Marine Biology* 136, 581-590.

Baptist, M. J. et al., 2019. An ecotope map of the trilateral Wadden Sea. *J. Sea Res.* 152, 101761. <http://dx.doi.org/10.1016/j.seares.2019.05.003>

Barbier, E.B. et al., 2011. The value of estuarine and coastal ecosystem services. *Ecol. Monogr.* 81 (2), 169-193.

Barbier, E. B., 2017. Marine ecosystem services. *Curr Biol* 27, R507-R510.

Barille, L., et al., 2011. Spectral response of benthic diatoms with different sediment backgrounds. *Remote Sens. Environ* 115 (4), 1034-42.

Barranguet, C. & Kromkamp, J., 2000. Estimating primary production rates from photosynthetic electron transport in estuarine microphytobenthos.

Mar. Ecol. Prog. Ser. 204, 39-52. <http://dx.doi.org/10.3354/Meps204039>.

Barranguet, C. et al., 1997. Microphytobenthos biomass and community composition studied by pigment biomarkers: importance and fate in the carbon cycle of a tidal flat. *J. Sea Res.* 38, 59-70.

Barranguet, C. et al., 1998. Factors controlling primary production and photosynthetic characteristics of intertidal microphytobenthos. *Mar. Ecol. Prog. Ser.* 173, 117-126. <http://dx.doi.org/10.3354/Meps173117>.

Bartholoma, A. & Flemming, B. W., 2007. Progressive grain-size sorting along an intertidal energy gradient, Sediment. *Geol* 202 (3), 464-72.

Bates, B.C., et al., 2008. Climate change and Water, Technical Paper IPCC. Geneva: IPCC Secretariat.

Beukema, J.J. et al., 1999. A long-term study of the recovery of the macrozoobenthos on large defaunated plots on a tidal flat in the Wadden Sea. *J Sea Res* 42, 235-254.

Benyoucef, I. et al., 2014. Microphytobenthos interannual variations in a north-European estuary (Loire estuary, France) detected by visible-infrared multispectral remote sensing. *Estuar. Coast. Shelf Sci.* 136, 43-52. <http://dx.doi.org/10.1016/j.ecss.2013.11.007>

Bertness, M. D. & Leonard, G. H., 1997. The role of positive interactions in communities: Lessons from intertidal habitats. *Ecology* 78 (7), 1976-89.

Billerbeck, M. et al., 2007. Benthic photosynthesis in submerged Wadden Sea intertidal flats. *Estuar. Coast. Shelf Sci.* 71 (3-4), 704-716. <http://dx.doi.org/10.1016/j.ecss.2006.09.019>.

Birchenough, S. N. R. et al., 2015. Climate change and marine benthos: a review of existing research and future directions in the North Atlantic. *Wires Clim Change* 6, 203-223.

Blackford, J.C., 2002. The influence of microphytobenthos on the northern Adriatic ecosystem: a modelling study. *Estuar. Coast. Shelf Sci.* 55 (1), 109-123. <http://dx.doi.org/10.1006/ecss.2001.0890>.

Blanchard, G.F. et al., 1996. Quantifying the short-term temperature effect on light-saturated photosynthesis of intertidal microphytobenthos. *Mar. Ecol. Prog. Ser.* 134 (1-3), 309-313. <http://dx.doi.org/10.3354/Meps134309>.

Blanchard, G.F. et al., 1997. Seasonal effect on the relationship between the photosynthetic capacity of intertidal microphytobenthos and temperature. *J. Phycol.* 33 (5), 723-728. <http://dx.doi.org/10.1111/j.0022-3646.1997.00723.x>.

Blanchard, G.F. et al., 2000. The effect of geomorphological structures on potential biostabilisation by microphytobenthos on intertidal mudflats. *Cont. Shelf Res.* 20 (10-11), 1243-1256.

Bibliography

- Blommaert, L. et al., 2018. Behavioural versus physiological photoprotection in epipelagic and epipsammic benthic diatoms. *Eur. J. Phycol* 53 (2), 146-55.
- Borja, A. et al., 2010. Medium- and long-term recovery of estuarine and coastal ecosystems: patterns, rates and restoration effectiveness. *Estuar Coast* 33, 1249-1260.
- Boschker, H. T. S. et al., 2005. Biomarker and carbon isotopic constraints on bacterial and algal community structure and functioning in a turbid, tidal estuary. *Limnol. Oceanogr.* 50(1), 70-80.
- Boschker, H. T. S. et al., 1999. The contribution of macrophyte derived organic matter in microbial biomass in salt marsh sediments: Stable carbon isotope analysis of microbial biomarkers. *Limnol. Oceanogr.* 44, 309-319.
- Bouma, H. et al., 2006. A Dutch ecotope system for coastal waters (ZES.1): to map the potential occurrence of ecological communities in Dutch coastal and transitional waters, Middelburg.
- Brito, A. C. et al., 2013. Seasonality of microphytobenthos revealed by remote-sensing in a South European estuary. *Cont. Shelf Res.* 66, 83-91. <http://dx.doi.org/10.1016/j.csr.2013.07.004>
- Brotas, V. et al., 1995. Spatio-temporal distribution of the microphytobenthic biomass in intertidal flats of Tagus Estuary (Portugal). *Hydrobiologia* 300-301 (1), 93-104. <http://dx.doi.org/10.1007/BF00024451>.
- Brotas, V. et al., 2003. In situ measurements of photosynthetic activity and respiration of intertidal benthic microalgal communities undergoing vertical migration. *Ophelia* 57 (1), 13-26.
- Brunier, G. et al., 2020. Assessing the relationship between macro-faunal burrowing activity and mudflat geomorphology from UAV-based Structure-from-Motion photogrammetry. *Remote Sens Environ* 241, 111717.
- Bryson, M. et al., 2013. Kite Aerial Photography for Low-Cost, Ultra-high Spatial Resolution Multi-Spectral Mapping of Intertidal Landscapes. *Plos One* 8, e73550.
- Cadée, G.C. & Hegeman, J., 1974. Primary production of the benthic microflora living on tidal flats in the Dutch Wadden Sea. *Neth. J. Sea Res.* 8 (2-3), 31.
- Cahoon, L.B., 1999. The role of benthic microalgae in neritic ecosystems. *Oceanogr. Mar. Biol.* 37, 47-86.
- Cartaxana, P. et al., 2015. Effects of elevated temperature and CO₂ on intertidal microphytobenthos. *Bmc Ecol* 15.
- Cartaxana, P. et al., 2016. Regulation of Intertidal Microphytobenthos Photosynthesis Over a Diel Emersion Period Is Strongly Affected by Diatom Migration Patterns. *Front Microbiol* 7
- Chanton, J. P. & Lewis, F. G., 1999. Plankton and dissolved inorganic carbon isotopic composition in a river-dominated estuary: Apalachicola bay, Florida. *Estuaries* 22, 575-583.
- Chennu, A. et al., 2013. Hyperspectral imaging of the microscale distribution and dynamics of microphytobenthos in intertidal sediments. *Limnol Oceanogr-Meth* 11, 511-528.
- Choy, E. J. et al., 2009. Quantifying the trophic base for benthic secondary production in the Nakdong River estuary of Korea using stable C and N isotopes. *J Exp Mar Biol Ecol* 382, 18-26.
- Christianen, M.J.A. et al., 2017. Benthic primary producers are key to sustain the Wadden Sea food web: stable carbon isotope analysis at landscape scale. *Ecology* 98 (6), 1498-1512.
- Coelho, H. et al., 2009. Effects of dessication on the photosynthetic activity of intertidal microphytobenthos biofilms as studied by optical methods. *J. Exp. Mar. Biol. Ecol.* 381, 98-104.
- Coelho, H. et al., 2011. Endogenous versus environmental control of vertical migration by intertidal benthic microalgae. *Eur. J. Phycol.* 46 (2), 271-281.
- Cohn, S.A. et al., 2003. The effect of temperature and mixed species composition on diatom motility and adhesion. *Diatom Res.* 18 (2), 225-243.
- Colijn, F., 1982. Light absorption in the waters of the Ems-Dollard estuary and its consequences for the growth of phytoplankton and microphytobenthos. *Neth. J. Sea Res.* 15 (2), 196-216.
- Colijn, F. & de Jonge, V.N., 1984. Primary production of microphytobenthos in the Ems-Dollard Estuary. *Mar. Ecol. Prog. Ser.* 14 (2-3), 185-196. <http://dx.doi.org/10.3354/Meps014185>.
- Combe, J. P. et al., 2005. Mapping microphytobenthos biomass by non-linear inversion of visible-infrared hyperspectral images. *Remote Sens Environ* 98, 371-387.
- Connor, M.S. et al., 1982. The Effect of Feeding by Mud Snails, *Ilyanassa-Obsoleta* (Say), on the Structure and Metabolism of a Laboratory Benthic Algal Community. *J Exp Mar Biol Ecol* 65, 29-45.
- Consalvey, M. et al., 2004. The ups and downs of life in a benthic biofilm: migration of benthic diatoms. *Diatom Res.* 19 (2), 181-202.
- Cook, P.L.M. & Roy, H., 2006. Advective relief of CO₂ limitation in microphytobenthos in highly productive sandy sediments. *Limnol. Oceanogr.* 51 (4), 1601-1954.
- Costanza, R., et al., 1997. The value of the world's ecosystem services and natural capital. *Nature* 387 (6630), 253-260.
- Cottenie, K., 2005. Integrating environmental and spatial processes in ecological community dynamics. *Ecol Lett* 8, 1175-1182.
- Cozzoli, F. et al., 2013. Application of non-linear quantile regression to macrozoobenthic species distribution modelling: comparing two contrasting basins. *Mar. Ecol. Prog. Ser.* 475, 119-133. <http://dx.doi.org/10.3354/Meps10112>
- Currin, C. A. et al., 1995. The role of standing dead *Spartina alterniflora* and benthic microalgae in salt marsh food webs: considerations based on multiple

- stable isotope analysis. *Mar. Ecol. Prog. Ser.* 121, 99-116.
- Daggers, T. D. et al., 2018. A model to assess microphytobenthic primary production in tidal systems using satellite remote sensing. *Remote Sens. Environ.* 211, 129-145.
- Daggers, T.D. et al., 2019. Corrigendum to "A model to assess microphytobenthic primary production in tidal systems using satellite remote sensing" [*Remote Sens. Environ.* 211 (2018) 129-145]. *Remote Sens. Environ.* 230, 111206.
- Daggers, T.D. et al., 2020. Spatial variability in macrofaunal diet composition and grazing pressure on microphytobenthos in intertidal areas. *Limnol. Oceanogr.* 65, 2819-2834.
- Dalrymple, R. W. et al., 1992. A conceptual model of estuarine sedimentation. *J. Sediment. Petrol.* 62, 113-1146.
- Day, J. D. et al., 1990. *Introduction to estuarine ecology*, Estuarine ecology (New York: Wiley).
- De Brouwer, J.F.C. et al., 2000. Interplay between biology and sedimentology in a mudflat (Biezelingse Ham, Westerschelde, The Netherlands). *Cont Shelf Res* 20, 1159-1177.
- De Brouwer, J.F.C. & Stal, L.J., 2001. Short-term dynamics in microphytobenthos distribution and associated extracellular carbohydrates in surface sediments of an intertidal mudflat. *Mar. Ecol. Prog. Ser.* 218, 33-44.
- De Deckere, E. M. G. T. et al., 2001. Destabilization of cohesive intertidal sediments by infauna. *Estuar. Coast. Shelf Sci.* 53, 665-669. <http://dx.doi.org/10.1006/ecss.2001.0811>
- De Vet, P.L.M. et al., 2017. The differences in morphological development between the intertidal flats of the Eastern and Western Scheldt. *Geomorphology* 281, 31-42.
- Dejonge, V.N. & Vanbeusekom, J.E.E., 1995. Wind-Induced and Tide-Induced Resuspension of Sediment and Microphytobenthos from Tidal Flats in the Ems Estuary. *Limnol Oceanogr* 40, 766-778.
- Dekker, R. & Van Moorsel, G. W. N. M., 1987. Effects of Different Oil Doses, Dispersant and Dispersed Oil on Macrofauna in Model Tidal Flat Ecosystems, in: J. Kuiper, W.J.V.D.B. (Ed.), the Conference on Oil Pollution Organized under the auspices of the International Association on Water Pollution Research and Control (IAWPRC) by the Netherlands Organization for Applied Scientific Research TNO Amsterdam, p. 121.
- Dijkman, N. A. & Kromkamp, J. C., 2006. Phospholipid-derived fatty acids as chemotaxonomic markers for phytoplankton: Application for inferring phytoplankton composition. *Mar. Ecol. Prog. Ser.* 324, 113-125.
- Dittel, A. I. et al., 1997. Carbon and nitrogen sources for shrimp postlarvae fed natural diets from a tropical mangrove system. *Estuar. Coast. Shelf S.* 45, 629-637.
- Edwards, G.R. et al., 1996. The spatial pattern of vegetation in cut and grazed grass white clover pastures. *Grass Forage Sci* 51, 219-231.
- Eilers, P.H.C. & Peeters, J.C.H., 1988. A model for the relationship between light-intensity and the rate of photosynthesis in phytoplankton. *Ecol. Model.* 42 (3-4), 199-215. [http://dx.doi.org/10.1016/0304-3800\(88\)90057-9](http://dx.doi.org/10.1016/0304-3800(88)90057-9).
- Ellis, J. et al., 2006. Predicting macrofaunal species distributions in estuarine gradients using logistic regression and classification systems. *Mar. Ecol. Prog. Ser.* 316, 69-83.
- Evrard, V. et al., 2010. Carbon and nitrogen flows through the benthic food web of a photic subtidal sandy sediment. *Mar Ecol Prog Ser* 416, 1-16.
- Falkowski, P. & Raven, J.A., 2007. *Aquatic Photosynthesis*, 2 ed. Princeton University Press, Oxford.
- Federer, R. N. et al., 2010. Stable carbon and nitrogen isotope discrimination factors from diet to blood plasma, cellular blood, feathers, and adipose tissue fatty acids in spectacled eiders (*Somateria fischeri*). *Can. J. Zool.* 88, 866-874.
- Folk, R.L., 1954. The distinction between grain size and mineral composition in sedimentary-rock nomenclature. *J. Geol.* 62 (4), 344-359.
- Forster, R.M. & Kromkamp, J.C., 2004. Modelling the effects of chlorophyll fluorescence from subsurface layers on photosynthetic efficiency measurements in microphytobenthic algae. *Mar. Ecol. Prog. Ser.* 284, 9-22. <http://dx.doi.org/10.3354/Meps284009>.
- Forster, R.M. & Kromkamp, J., 2006. Estimating benthic primary production: scaling up from point measurements to the whole estuary. Functioning of microphytobenthos in estuaries: Proceedings of the Colloquium, Amsterdam, 21-23 August 2003. Koninklijke Nederlandse Akademie van Wetenschappen Verhandeligen, Afd. Natuurkunde (Tweede Reeks) 103, 109-120.
- Forster, R.M. et al., 2006. Biodiversity-ecosystem function relationship in microphytobenthic diatoms of the Westerschelde estuary. *Mar. Ecol. Prog. Ser.* 311, 191-201. <http://dx.doi.org/10.3354/Meps311191>.
- Galbraith, H. et al., 2002. Global climate change and sea level rise: Potential losses of intertidal habitat for shorebirds. *Waterbirds* 25 (2), 173-83.
- Galván, K. et al., 2008. Stable isotope addition reveals dietary importance of phytoplankton and microphytobenthos to saltmarsh infauna. *Mar. Ecol. Prog. Ser.* 359, 37-49.
- Gattuso, J. P. et al., 2006. Light availability in the coastal ocean: impact on the distribution of benthic photosynthetic organisms and their contribution to primary production. *Biogeosciences* 3 (4), 489-513.
- Gerbersdorf, S. U. & Wieprecht, S., 2015. Biostabilization of cohesive sediments: revisiting the role of abiotic conditions, physiology and diversity of microbes, polymeric secretion, and biofilm architecture. *Geobiology* 13, 68-97.
- Graf, G. 1992. Benthic-pelagic coupling: a review. *Oceanogr. Mar. Biol. Ann. Rev.* 30, 149-90.
- Guarini, J.M. et al., 1997. Modelling the mud surface

Bibliography

- temperature on intertidal flats to investigate the spatio-temporal dynamics of the benthic microalgal photosynthetic capacity. *Mar. Ecol. Prog. Ser.* 153, 25–36.
- Guarini, J. M. et al., 1998. Dynamics of spatial patterns of microphytobenthic biomass: inferences from a geostatistical analysis of two comprehensive surveys in Marennes-Oleron bay (France). *Mar. Ecol. Prog. Ser.* 166, 131–141.
- Guarini, J.M. et al., 2000. Dynamic model of the short-term variability of microphytobenthic biomass on temperate intertidal mudflats. *Mar. Ecol. Prog. Ser.* 195, 291–303.
- Guarini, J.M. et al., 2002. Microphytobenthic potential productivity estimated in three tidal embayments of the San Francisco Bay: a comparative study. *Estuaries* 25 (3), 409–417. <http://dx.doi.org/10.1007/Bf02695983>.
- Guarini, J.M. et al., 2008. Can the intertidal benthic microalgal primary production account for the "missing carbon sink"? *J. Oceanogr.* 1, 13–19.
- Hagerthey, S.E. et al., 2002. Influence of *Corophium volutator* and *Hydrobia ulvae* on intertidal benthic diatom assemblages under different nutrient and temperature regimes. *Mar. Ecol. Prog. Ser.* 245, 47–59.
- Hakvoort, H. et al., 1997. In-situ optical measurements of sediment type and phytobenthos of tidal flats: a basis for imaging remote sensing spectroscopy. *Ger. J. Hydrograph.* 49, 367–373.
- Halsey, K. H. et al., 2010. Physiological optimization underlies growth rate-independent chlorophyll-specific gross and net primary production. *Photosynth. Res.* 103, 125–37.
- Harley, C. D. G. et al., 2006. The impacts of climate change in coastal marine systems. *Ecol. Lett.* 9 (4), 228–241.
- Harte, J. et al., 2005. A theory of spatial structure in ecological communities at multiple spatial scales. *Ecol. Monogr.* 75, 179–197.
- Heip, C.H.R. et al., 1995. Production and consumption of biological particles in temperate tidal estuaries. *Oceanogr. Mar. Biol. Annu. Rev.* 33 (33), 1–149.
- Herlory, O. et al., 2007. Methodology of light response curves: application of chlorophyll fluorescence to microphytobenthic biofilms. *Mar. Biol.* 153 (1), 91–101.
- Herman, P.M.J. et al., 1999. Ecology of Estuarine Macrobenthos. *Adv. Ecol. Res.* 29, 195–240.
- Herman, P. M. J. et al., 2000. Stable isotopes as trophic tracers: combining field sampling and manipulative labelling of food resources for macrobenthos. *Mar. Ecol. Prog. Ser.* 204, 79–92.
- Herman, P. M. J. et al., 2001. Benthic community structure and sediment processes on an intertidal flat: results from the ECOFLAT project. *Cont. Shelf Res.* 21 (18–19), 2055–71.
- Hicks, N. et al., 2011. Impact of biodiversity-climate futures on primary production and metabolism in a model benthic estuarine system. *Bmc Ecol.* 11.
- Hillebrand, H., 2008. Grazing regulates the spatial variability of periphyton biomass. *Ecology* 89 (1), 165–73.
- Holt, J.T. et al., 2005. Error quantification of a high-resolution coupled hydrodynamic-ecosystem coastal-ocean model: part 1 model overview and assessment of the hydrodynamics. *J. Mar. Syst.* 57 (1–2), 167–188.
- Hope, J. A. et al., 2019. The role of microphytobenthos in soft-sediment ecological networks and their contribution to the delivery of multiple ecosystem services. *J. Ecol.* 108, 815–830.
- Jesus, B. et al., 2006. Effect of sediment type on microphytobenthos vertical distribution: Modelling the productive biomass and improving ground truth measurements. *J. Exp. Mar. Biol. Ecol.* 332 (1), 60–74. <http://dx.doi.org/10.1016/j.jembe.2005.11.005>.
- Jesus, B. et al., 2008. Detection of diatom xanthophyll cycle using spectral reflectance. *J. Phycol.* 44 (5), 1349–59.
- Jorgensen, B. B., 2001. Life in the diffusive boundary layer. *The benthic boundary layer* (Oxford Univ. Press), 348–73.
- Kamp, A. et al., 2011. Diatoms respire nitrate to survive dark and anoxic conditions. *P Natl Acad Sci USA* 108, 5649–5654.
- Kanaya, G. et al., 2013. Temporal changes in carbon and nitrogen stable isotope ratios of macrozoobenthos on an artificial tidal flat facing a hypertrophic canal, inner Tokyo Bay. *Mar. Pollut. Bull.* 71 (1–2), 179–89.
- Kang, C. K. et al., 2003. Trophic importance of benthic microalgae to macrozoobenthos in coastal bay systems in Korea: dual stable C and N isotope analyses. *Mar. Ecol. Prog. Ser.* 259, 79–92.
- Kang, C. K. et al., 2006. Microphytobenthos seasonality determines growth and reproduction in intertidal bivalves. *Mar. Ecol. Prog. Ser.* 315, 113–127.
- Kazemipour, F. et al., 2012. Microphytobenthos biomass mapping using the optical model of diatom biofilms: application to hyperspectral images of Bourgneuf Bay. *Remote Sens. Environ.* 127, 1–13. <http://dx.doi.org/10.1016/j.rse.2012.08.016>.
- Kelly, J.A. et al., 2001. Microscale analysis of chlorophyll-a in cohesive, intertidal sediments: the implications of microphytobenthos distribution. *J. Mar. Biol. Assoc. U. K.* 81 (1), 151–162.
- Kendall, M. A. & Widdicombe, S., 1999. Small scale patterns in the structure of macrofaunal assemblages of shallow soft sediments. *J. Exp. Mar. Biol. Ecol.* 237, 127–140.
- Kennish, M. J., 2002. Environmental threats and environmental future of estuaries. *Environ. Conserv.* 29, 78–107.
- Kingston, M.B., 2002. Effect of subsurface nutrient supplies on the vertical migration of *Euglena proxima* (Euglenophyta). *J. Phycol.* 38 (5), 872–880.

- Koch, E. W. et al., 2009. Non-linearity in ecosystem services: temporal and spatial variability in coastal protection. *Front Ecol Environ* 7, 29-37.
- Kon, K. et al., 2015. Do allochthonous inputs represent an important food resource for benthic macroalgal communities in tropical estuarine mudflats? *Food Webs* 2, 10-17.
- Kowalski, N. et al., 2009. Trace metal dynamics in the water column and pore waters in a temperate tidal system: response to the fate of algae-derived organic matter. *Ocean Dynam* 59, 333-350.
- Kristensen, E. et al., 1992. Effects of Benthic Macrofauna and Temperature on Degradation of Macroalgal Detritus - the Fate of Organic-Carbon. *Limnol Oceanogr* 37, 1404-1419.
- Kromkamp, J. et al., 1995. Nutrients, light and primary production by phytoplankton and microphytobenthos in the eutrophic, turbid Westerschelde Estuary (the Netherlands). *Hydrobiologia* 311 (1-3), 9-19.
<http://dx.doi.org/10.1007/BF00008567>.
- Kromkamp, J. et al., 1998. Determination of microphytobenthos PSII quantum efficiency and photosynthetic activity by means of variable chlorophyll fluorescence. *Mar. Ecol. Prog. Ser.* 162, 45-55.
<http://dx.doi.org/10.3354/Meps162045>.
- Kromkamp, J. C. & Peene, J., 2005. Changes in phytoplankton biomass and primary production between 1991 and 2001 in the Westerschelde estuary (Belgium/The-Netherlands). *Hydrobiologia* 540, 117-126.
- Kromkamp, J.C. et al., 2006. Relationship of intertidal surface sediment chlorophyll concentration to hyperspectral reflectance and chlorophyll fluorescence. *Estuar. Coasts* 29 (2), 183-196.
<http://dx.doi.org/10.1007/BF02781988>.
- Kühl, M. & Jorgensen, B.B., 1992. Spectral light measurements in microbenthic phototrophic communities with a fiber-optic microprobe coupled to a sensitive diode array detector. *Limnol. Oceanogr.* 37 (8), 1813-1823.
- Kühl, M. & Jorgensen, B.B., 1994. The light-field of microbenthic communities - radiance distribution and microscale optics of sandy coastal sediments. *Limnol. Oceanogr.* 39 (6), 1368-1398.
- Kühl, M. et al., 1994. Light penetration and light-intensity in sandy marine-sediments measured with irradiance and scalar irradiance fiberoptic microprobes. *Mar. Ecol. Prog. Ser.* 105 (1-2), 139-148.
<http://dx.doi.org/10.3354/Meps105139>.
- Kuwaie, T. et al., 2012. Variable and complex food web structures revealed by exploring missing trophic links between birds and biofilm. *Ecol. Lett.* 15, 347-356.
- Landry, C. E., 2011. Coastal Erosion as a Natural Resource Management Problem: An Economic Perspective. *Coast Manage* 39, 259-281.
- Langdon, C., 1993. The significance of respiration in production measurements based on oxygen. *ICES Mar Sci Symp* 197, 69-78.
- Larson, F. & Sundback, K., 2008. Role of microphytobenthos in recovery of functions in a shallow-water sediment system after hypoxic events. *Mar Ecol Prog Ser* 357, 1-16.
- Launeau, P. et al., 2018. Microphytobenthos Biomass and Diversity Mapping at Different Spatial Scales with a Hyperspectral Optical Model. *Remote Sensing* 10 (5).
- Le Bris, A. et al., 2016. Hyperspectral remote sensing of wild oyster reefs. *Estuar Coast Shelf S* 172, 1-12.
- Le Hir, P. et al., 2007. Sediment erodability in sediment transport modelling: Can we account for biota effects? *Cont Shelf Res* 27, 1116-1142.
- Le Hir, P. et al., 2000. Characterization of intertidal flat hydrodynamics. *Cont. Shelf Res.* 20 (12-13), 1433-1459.
- Lee, S. Y., 2000. Carbon dynamics of Deep Bay, eastern Pearl River estuary, China. II: Trophic relationship based on carbon- and nitrogen-stable isotopes. *Mar Ecol Prog Ser* 205, 1-10.
- Lefebvre, S. et al., 2007. Comparison between fluorimetry and oximetry techniques to measure photosynthesis in the diatom *Skeletonema costatum* cultivated under simulated seasonal conditions. *J. Photochem. Photobiol. B* 86 (2), 131-139.
<http://dx.doi.org/10.1016/j.jphotobiol.2006.08.012>.
- Legendre, P. & Legendre, L., 2012. "Spatial analysis," in *Numerical Ecology*, (Oxford: Elsevier), 785-858.
- Leguerrier, D. et al., 2003. Numerical analysis of the food web of an intertidal mudflat ecosystem on the Atlantic coast of France. *Mar Ecol Prog Ser* 246, 17-37.
- Leibold, M.A. et al., 2004. The metacommunity concept: a framework for multi-scale community ecology. *Ecol Lett* 7, 601-613.
- Levine, J. M. et al., 1998. Nutrients, competition and plant zonation in a New England salt marsh. *J. Ecol.* 86 (2), 285-92.
- Levington, J.S. & Bianchi, T.S., 1981. Nutrition and food limitation of deposit-feeders. I. The role of microbes in the growth of mud snails (Hydrobiidae). *J. Mar. Res.* 39, 531-45.
- Li, W.B. et al., 2013. A comparison of land surface water mapping using the normalized difference water index from TM, ETM plus and ALI. *Remote Sens.* 5 (11), 5530-5549.
- Lomas, M.W. et al., 2002. Temporal and spatial dynamics of urea uptake and regeneration rates and concentrations in Chesapeake Bay. *Estuaries* 25 (3), 469-482.
- Lotze, H.K. et al., 2006. Depletion, degradation, and recovery potential of estuaries and coastal seas. *Science* 312 (5781), 1806-1809.
<http://dx.doi.org/10.1126/science.1128035>.
- Lubarsky, H. V. et al., 2010. The Stabilisation Potential of Individual and Mixed Assemblages of Natural Bacteria and Microalgae. *Plos One* 5(11), e13794.

Bibliography

- Lucas, C. H. & Holligan, P. M., 1999. Nature and ecological implications of algal pigment diversity on the molenplaat tidal flat (Westerschelde estuary, SW Netherlands). *Mar. Ecol. Prog. Ser.* 180, 51–64.
- Lucas, C. H. et al., 2000. Benthic-pelagic exchange of microalgae at a tidal flat. 1. Pigment analysis. *Mar. Ecol. Prog. Ser.* 196, 59–73.
- MacIntyre, H.L. et al., 1996. Microphytobenthos: the ecological role of the "secret garden" of unvegetated, shallow-water marine habitats .1. Distribution, abundance and primary production. *Estuaries* 19 (2A), 186–201.
- Macko, S. A. et al., 1982. Nitrogen and Carbon Isotope Fractionation by 2 Species of Marine Amphipods - Laboratory and Field Studies. *J. Exp. Mar. Biol. Ecol.* 63, 145–149.
- Mahaut, M. L. et al., 1995. Weight-Dependent Respiration Rates in Deep-Sea Organisms. *Deep-Sea Res. Pt. I.* 42, 1575–1582.
- Mariotti, A. et al., 1984. Natural isotopic composition of nitrogen as a tracer of origin for suspended organic matter in the Scheldt estuary. *Geochim. Cosmochim. Acta* 48, 549–555.
- Maron, J.L. & Harrison, S., 1997. Spatial pattern formation in an insect host-parasitoid system. *Science* 278, 1619–1621.
- McCutchan, J. H. et al., 2003. Variation in trophic shift for stable isotope ratios of carbon, nitrogen, and sulfur. *Oikos* 102, 378–390.
- McLusky, D.S., 1989. The estuarine ecosystem. 2nd edition (New York: Chapman & Hall) 215 pp.
- Meire, P. M. et al., 1994. Spatial and Temporal Patterns of Intertidal Macrobenthic Populations in the Oosterschelde - Are They Influenced by the Construction of the Storm-Surge Barrier. *Hydrobiologia* 283, 157–182.
- Meleder, V. et al., 2003a. Spectrometric constraint in analysis of benthic diatom biomass using monospecific cultures. *Remote Sens. Environ.* 88 (4), 386–400.
- Meleder, V. et al., 2003b. Microphytobenthos assemblage mapping by spatial visible-infrared remote sensing in a shellfish ecosystem. *C. R. Biol.* 326 (4), 377–389.
- Meleder, V. et al., 2007. Spatiotemporal changes in microphytobenthos assemblages in a macrotidal flat (Bourgneuf bay, France). *J. Phycol.* 43, 1177–1190. <http://dx.doi.org/10.1111/j.1529-8817.2007.00423.x>
- Mélédér, V. et al., 2010. Hyperspectral imaging for mapping microphytobenthos in coastal areas. In: Maanan, M.R.E. (Ed.), *Geomatic solutions for coastal environments*. Nova Science Publishers.
- Meleder, V., B. Jesus, A. Barnett, L. Barille, and J. Lavaud. 2018. Microphytobenthos primary production estimated by hyperspectral reflectance. *Plos One* 13(5), e0197093.
- Menge, B.A. et al., 1997. Benthic-pelagic links and rocky intertidal communities: Bottom-up effects on top-down control? *P Natl Acad Sci USA* 94, 14530–14535.
- Meziane, T. & Tsuchiya, M., 2000. Fatty acids as tracers of organic matter in the sediment and food web of a mangrove/intertidal flat ecosystem, Okinawa, Japan. *Mar Ecol Prog Ser* 200, 49–57.
- Middelburg, J. J., 2014. Stable isotopes dissect aquatic food webs from the top to the bottom. *Biogeosciences* 11, 2357–2371.
- Middelburg, J. J. et al., 2000. The fate of intertidal microphytobenthos carbon: An in situ C-13-labeling study. *Limnol. Oceanogr.* 45, 1224–1234.
- Mohammad, Z. et al., 2015. Allometry, condition index and secondary production in bivalve *Barbatia decussata* on rocky intertidal shores in the Northern Persian Gulf, Iran. *J Environ Biol* 36, 1185–1192.
- Morris, E.P. & Kromkamp, J.C., 2003. Influence of temperature on the relationship between oxygen- and fluorescence-based estimates of photosynthetic parameters in a marine benthic diatom (*Cylindrotheca closterium*). *Eur. J. Phycol.* 38 (2), 133–142. <http://dx.doi.org/10.1080/0967026031000085832>.
- Moens, T. et al., 2005. Dual stable isotopes unravel trophic position of estuarine nematodes. *J. Mar. Biol. Ass.* 85, 1401–1407.
- Moerdijk-Poortvliet, T. C. W. et al., 2018. Seasonal changes in the biochemical fate of carbon fixed by benthic diatoms in intertidal sediments. *Limnol. Oceanogr.* 63, 550–69.
- Molinari, E. et al., 2009. Relationships between hydrodynamic parameters and grain size in two contrasting transitional environments: The Lagoons of Venice and Cabras, Italy. *Sediment Geol* 219, 196–207.
- Montserrat, F. et al., 2008. Benthic community-mediated sediment dynamics. *Mar. Ecol. Prog. Ser.* 372, 43–59.
- Moreira, M. H. et al., 1993. Environmental gradients in a southern Europe estuarine system: Ria de Aveiro, Portugal. Implications for soft bottom macrofauna colonization. *Neth. J. Aquat. Ecol.* 27, 465–482.
- Murphy, R.J. et al., 2004. Estimation of surface chlorophyll on an exposed mudflat using digital colour-infrared (CIR) photography. *Estuar Coast Shelf S* 59, 625–638.
- Murray, N. J. et al., 2019. The global distribution and trajectory of tidal flats. *Nature* 565 (7738), 222–225.
- Morris, E. P., 2005. Quantifying Primary Production Of Microphytobenthos: Application Of Optical Methods. Ph. D thesis, University of Groningen, Groningen.
- Murphy, R.J. et al., 2005a. Estimation of surface chlorophyll-a on an emerged mudflat using field spectrometry: accuracy of ratios and derivative-based approaches. *Int. J. Remote Sens.* 26 (9), 1835–1859.
- Murphy, R.J. et al., 2005b. Remote-sensing of

- benthic chlorophyll: should ground-truth data be expressed in units of area or mass? *J. Exp. Mar. Biol. Ecol.* 316, 69–77.
- Murphy, R. J. et al., 2008. Spatial variation of chlorophyll on estuarine mudflats determined by field-based remote sensing. *Mar. Ecol. Prog. Ser.* 365, 45–55. <http://dx.doi.org/10.3354/Meps07456>
- Neumann, A. C. et al., 1970. Composition, Structure and Erodability of Subtidal Mats, Abaco, Bahamas. *J. Sediment Petrol* 40.
- Nienhuis, P.H., 1992. Eutrophication, water management, and the functioning of Dutch estuaries and coastal lagoons. *Estuaries* 15 (4), 538–548.
- Nienhuis, P.H. & Smaal, A.C., 1994. The Oosterschelde Estuary, a case-study of a changing ecosystem - an introduction. *Hydrobiologia* 283, 1–14.
- Nieuwenhuize, J. et al., 1994. Rapid analysis of organic carbon and nitrogen in particulate materials. *Mar. Chem.* 45, 217–224.
- Nilsson, C. & Sundback, K., 1991. Growth and Nutrient-Uptake Studied in Sand-Agar Microphytobenthic Communities. *J. Exp. Mar. Biol. Ecol.* 153, 207–226.
- Oakes, J.M. & Eyre, B.D., 2014. Transformation and fate of microphytobenthos carbon in subtropical, intertidal sediments: potential for long-term carbon retention revealed by ¹³C-labeling. *Biogeosciences* 11, 1927–1940.
- Olsen, Y. S. et al., 2011. delta N-15 and delta C-13 reveal differences in carbon flow through estuarine benthic food webs in response to the relative availability of macroalgae and eelgrass. *Mar. Ecol. Prog. Ser.* 421, 83–96.
- Orvain, F. et al., 2012. Spatial and temporal interaction between sediment and microphytobenthos in a temperate estuarine macro-intertidal bay. *Mar. Ecol. Prog. Ser.* 458, 53–68.
- Orvain, F. et al., 2004. Interacting effects of *Hydrobia ulvae* bioturbation and microphytobenthos on the erodibility of mudflat sediments. *Mar. Ecol. Prog. Ser.* 278, 205–223. <http://dx.doi.org/10.3354/Meps278205>
- Oxtoby, L. E. et al., 2016. Feeding ecologies of key bivalve and polychaete species in the Bering Sea as elucidated by fatty acid and compound-specific stable isotope analyses. *Mar. Ecol. Prog. Ser.* 557, 161–175.
- Page, H.M., 1997. Importance of vascular plant and algal production to macro-invertebrate consumers in a southern California Salt Marsh. *Estuar Coast Shelf S* 45, 823–834.
- Palmer, J.D. & Round, F.E., 1967. Persistent, vertical migration rhythms in benthic microflora. VI. The tidal and diurnal nature of the rhythm in the diatom *Hantzschia virgata*. *Biol. Bull.* 132, 44–55.
- Parnell, A.C. et al., 2013. Bayesian stable isotope mixing models. *Environmetrics* 24, 387–399.
- Pascual, U. et al., 2010. The economics of valuing ecosystem services and biodiversity. *The economics of ecosystems and biodiversity: Ecological and economic foundations*. Routledge.
- Passarelli, C. et al., 2018. Mudflat Ecosystem Engineers and Services, p. 243–269. *In* P. G. Beninger [ed.], *Mudflat Ecology*. Springer Nature.
- Paterson, D. M., 1989. Short-Term Changes in the Erodibility of Intertidal Cohesive Sediments Related to the Migratory Behavior of Epipellic Diatoms. *Limnol Oceanogr* 34, 223–234.
- Paterson, D.M. et al., 1998. Microbiological mediation of spectral reflectance from intertidal cohesive sediments. *Limnol. Oceanogr.* 43 (6), 1207–1221.
- Pebesma, E.J. & Wesseling, C.G., 1998. Gstat: A program for geostatistical modelling, prediction and simulation. *Comput. Geosci-Uk* 24, 17–31.
- Pebesma, E. J., 2004. Multivariable geostatistics in S: the gstat package. *Comput. Geosci.* 30, 683–691.
- Peres-Neto, P.R. & Legendre, P., 2010. Estimating and controlling for spatial structure in the study of ecological communities. *Global Ecol. Biogeogr.* 19, 174–184.
- Perkins, R.G. et al., 2011. Chlorophyll a Fluorescence in Aquatic Sciences: Methods and Applications. Chapter 12: The Application of Variable Chlorophyll Fluorescence to Microphytobenthic Biofilms (Springer Science+Business Media B.V.).
- Peterson, B. J. & Fry, B., 1987. Stable isotopes in ecosystem studies. *Ann. Rev. Ecol. Syst.* 18, 293–320.
- Pezij, M., 2015. Understanding and Modelling of the Oosterschelde Nourishment. University of Twente.
- Pinckney, J.L. & Zingmark, R.G., 1991. Effects of tidal stage and sun angles on intertidal benthic microalgal productivity. *Mar. Ecol. Prog. Ser.* 76, 81–89.
- Pinckney, J.L. & Zingmark, R.G., 1993. Modeling the annual production of intertidal benthic microalgae in estuarine ecosystems. *J. Phycol.* 29 (4), 396–407. <http://dx.doi.org/10.1111/j.1529-8817.1993.tb00140.x>.
- Pinckney, J. & Zingmark, R.G., 1993. Photophysiological Responses of Intertidal Benthic Microalgal Communities to in-Situ Light Environments - Methodological Considerations. *Limnol Oceanogr* 38, 1373–1383.
- Pinckney, J.L. et al., 1994. Short-term changes in the vertical distribution of benthic microalgal biomass in intertidal muddy sediments. *Diatom Res.* 9 (1), 143–153.
- Platt, T. et al., 1980. Photoinhibition of photosynthesis in natural assemblages of marine-phytoplankton. *J. Mar. Res.* 38 (4), 687–701.
- Pniewski, F.F. et al., 2015. Photoregulation in microphytobenthos from intertidal mudflats and non-tidal coastal shallows. *Estuar. Coast. Shelf Sci.* 152, 153–161.

Bibliography

- Pomeroy, L. R., 1959. Algal Productivity in Salt Marshes of Georgia', *Limnol Oceanogr* 4 (4), 386-97.
- Posey, M. et al., 1995. Top-down Vs Bottom up Control of Benthic Community Composition on an Intertidal Tideflat. *J Exp Mar Biol Ecol* 185, 19-31.
- Posey, M.H. et al., 1999. Interactive effects of nutrient additions and predation on infaunal communities. *Estuaries* 22, 785-792.
- Poulin, R. & Mouritsen, K. N., 2006. Climate change, parasitism and the structure of intertidal ecosystems. *J Helminthol* 80, 183-191.
- Pratt, D.R. et al., 2013. The effects of short-term increases in turbidity on sandflat microphytobenthic productivity and nutrient fluxes. *J. Sea Res.* 92, 170-177.
- Pratt, D.R. et al., 2015. Spatial Distributions of Grazing Activity and Microphytobenthos Reveal Scale-Dependent Relationships Across a Sedimentary Gradient. *Estuaries Coasts* 38, 722-734.
- Pritchard, D. W., 1967. What is an estuary: physical viewpoint', in G. H. Lauff (ed.), *Estuaries* (83; Washington: American Association for the Advancement of Science), 3-5.
- Queiros, A. M. et al., 2013. A bioturbation classification of European marine infaunal invertebrates. *Ecol Evol* 3, 3958-3985.
- Rainey, M.P. et al., 2003. Mapping intertidal estuarine sediment grain size distributions through airborne remote sensing. *Remote Sens. Environ.* 86 (4), 480-490. [http://dx.doi.org/10.1016/S0034-4257\(03\)00126-3](http://dx.doi.org/10.1016/S0034-4257(03)00126-3).
- Riera, P. et al., 2004. Utilization of food sources by invertebrates in a man-made intertidal ecosystem (Westerschelde, The Netherlands): a $\delta^{13}\text{C}$ and $\delta^{15}\text{N}$ study. *J. Mar. Biol. Ass.* 84: 323-326.
- Riera, P. et al., 2000. Heavy delta N-15 in intertidal benthic algae and invertebrates in the Scheldt Estuary (The Netherlands): Effect of river nitrogen inputs. *Estuar. Coast. Shelf S.* 51: 365-372.
- Riera, P. et al., 2002. delta C-13 versus delta N-15 of co-occurring molluscs within a community dominated by *Crassostrea gigas* and *Crepidula fornicata* (Oosterschelde, The Netherlands). *Mar. Ecol. Prog. Ser.* 240, 291-295.
- Rijkswaterstaat, 2017. Toelichting op de zoute ecotopenkaart Westerschelde 2016: biologische monitoring zoute rijkswateren. Delft: Rijkswaterstaat – Centrale Informatievoorziening.
- Rijkswaterstaat, 2017. Waterbase. http://live.waterbase.nl/waterbase_locaties.cfm?whichform=1&wbwns1=1%7CWaterhoogte+in+cm+t.o.v.+normaal+amsterdams+peil+in+oppervlakte+water&wbthemas=&search, Accessed date: 18 September 2017.
- Ritchie, R.J., 2006. Consistent sets of spectrophotometric chlorophyll equations for acetone, methanol and ethanol solvents. *Photosynth. Res.* 89 (1), 27-41. <http://dx.doi.org/10.1007/s1120-006-9065-9>.
- Rossi, R. E. et al., 1992. Geostatistical tools for modeling and interpreting ecological spatial dependence. *Ecol. Monogr.* 62, 277-314. <http://dx.doi.org/10.2307/2937096>
- Rossi, F. 2006. Small-scale burial of macroalgal detritus in marine sediments: effects of *Ulva* spp. on the spatial distribution of macrofauna assemblages. *J. Exp. Mar. Biol. Ecol.* 332, 84-95.
- Rossi, F. et al., 2004. Interspecific and intraspecific variation of delta C-13 and delta N-15 in deposit- and suspension-feeding bivalves (*Macoma balthica* and *Cerastoderma edule*): Evidence of ontogenetic changes in feeding mode of *Macoma balthica*. *Limnol. Oceanogr.* 49, 408-414.
- Rouse, J.W. et al., 1973. Monitoring vegetation systems in the Great Plains with ERTS. *Proceedings of the Third ERTS Symposium*, NASA 1.pp. 309-317.
- Rysgaard, S. et al., 1995. Seasonal variation in nitrification and denitrification in estuarine sediment colonized by benthic microalgae and bioturbating infauna. *Mar. Ecol. Prog. Ser.* 126, 111-121.
- Ryu, J.H. et al., 2004. A critical grain size for Landsat ETM+ investigations into intertidal sediments: a case study of the Gomso tidal flats, Korea. *Estuar. Coast. Shelf Sci.* 60 (3), 491-502.
- Ryu, J. H. et al., 2014. Potential of remote sensing in management of tidal flats: a case study of thematic mapping in the Korean tidal flats. *Ocean Coast.Manag.* 102, 458-470. <http://dx.doi.org/10.1016/j.ocecoaman.2014.03.003>
- Sabbe, K., 1993. Short-term fluctuations in benthic diatom numbers on an intertidal sandflat in the Westerschelde estuary (Zeeland, The Netherlands). *Hydrobiologia* 26, 275-284.
- Sabbe, K. & Vyverman, W., 1991. Distribution of benthic diatom assemblages in the Westerschelde (Zeeland, The Netherlands). *Belg. Journ. Bot.* 124 (2), 91-101.
- Saburova, M.A. et al., 1995. Spatial structure of an intertidal sandflat microphytobenthic community as related to different spatial scales. *Mar. Ecol. Prog. Ser.* 129 (1-3), 229-239. <http://dx.doi.org/10.3354/Meps129229>.
- Saburova, M.A. & Polikarpov, I.G., 2003. Diatom activity within soft sediments: behavioural and physiological processes. *Mar Ecol Prog Ser* 251, 115-126.
- Sahan, E. et al., 2007. Community structure and seasonal dynamics of diatom biofilms and associated grazers in intertidal mudflats. *Aquat. Microb. Ecol.* 47, 253-266.
- Sandwell, D.R. et al., 2009. Density dependent effects of an infaunal suspension-feeding bivalve (*Austrovenus stutchburyi*) on sandflat nutrient fluxes and microphytobenthic productivity. *J Exp Mar Biol Ecol* 373, 16-25.
- Santos, P.J.P. et al., 1997. Spatial distribution and dynamics of microphytobenthos biomass in the Gironde estuary (France). *Oceanol. Acta* 20 (3), 549-556.

- Savelli, R. et al., 2018. On biotic and abiotic drivers of the microphytobenthos seasonal cycle in a temperate intertidal mudflat: a modelling study. *Biogeosciences* 15, 7243-7271.
- Savelli, R. et al., 2019. Impact of chronic and massive resuspension mechanisms on the microphytobenthos dynamics in a temperate intertidal mudflat. *J. Geophys. Res.: Biogeosciences* 124, 3752-3777.
- Schelske, C.L. & Odum, E.P., 1962. Mechanisms maintaining high productivity in Georgia estuaries. *Proc. Gulf Carrib. Fish Inst.* 14, 75-80.
- Schouten, S. et al., 1998. Biosynthetic effects on the stable carbon isotopic compositions of agal lipids: Implications for deciphering the carbon isotopic biomarker record. *Geochim. Cosmochim. Acta* 62, 1397-1406.
- Schuckel, U. & Kroncke, I., 2013. Temporal changes in intertidal macrofauna communities over eight decades: A result of eutrophication and climate change. *Estuar Coast Shelf S* 117, 210-218.
- Seabloom, E. W. et al., 2005. Spatial signature of environmental heterogeneity, dispersal, and competition in successional grasslands. *Ecol. Monogr.* 75 (2), 199-214.
- Serôdio, J., 2004. Analysis of variable chlorophyll fluorescence in microphytobenthos assemblages: implications of the use of depth-integrated measurements. *Aquat. Microb. Ecol.* 36 (2), 137-152. <http://dx.doi.org/10.3354/Ame036137>.
- Serôdio, J. & Catarino, F., 1999. Fortnightly light and temperature variability in estuarine intertidal sediments and implications for microphytobenthos primary productivity. *Aquat. Ecol.* 33, 235-241.
- Serôdio, J. & Catarino, F., 2000. Modelling the primary productivity of intertidal microphytobenthos: time scales of variability and effects of migratory rhythms. *Mar. Ecol. Prog. Ser.* 192, 13-30. <http://dx.doi.org/10.3354/Meps192013>.
- Serôdio, J. et al., 1997. Nondestructive tracing of migratory rhythms of intertidal benthic microalgae using in vivo chlorophyll a fluorescence. *J. Phycol.* 33 (3), 542-553. <http://dx.doi.org/10.1111/j.0022-3646.1997.00542.x>.
- Serôdio, J. et al., 2005. Short-term variability in the photosynthetic activity of microphytobenthos as detected by measuring rapid light curves using variable fluorescence. *Mar. Biol.* 146, 903-914.
- Serôdio, J. et al., 2006. Rapid light-response curves of chlorophyll fluorescence in microalgae: relationship to steady-state light curves and nonphotochemical quenching in benthic diatom-dominated assemblages. *Photosynth. Res.* 90 (1), 29-43.
- Serôdio, J. et al., 2008. Photosynthetic activity, photoprotection and photoinhibition in intertidal microphytobenthos as studied in situ using variable chlorophyll fluorescence. *Cont. Shelf Res.* 28, 1363-1375.
- Serôdio, J. et al., 2009. Effects of chlorophyll fluorescence on the estimation of microphytobenthos biomass using spectral reflectance indices. *Remote Sens. Environ.* 113 (8), 1760-1768.
- Seuront, L. & Spilmont, N., 2002. Self-organized criticality in intertidal microphytobenthos patch patterns. *Physica A* 313, 513-539.
- Silvertown, J., 2004. Plant coexistence and the niche. *Trends Ecol. Evol.* 19 (11), 605-11.
- Simonini, R. et al., 2007. Recolonization and recovery dynamics of the macrozoobenthos after sand extraction in relict sand bottoms of the Northern Adriatic Sea. *Mar Environ Res* 64, 574-589.
- Smaal, A. C. et al., 2013. Decrease of the carrying capacity of the Oosterschelde estuary (SW Delta, NL) for bivalve filter feeders due to overgrazing? *Aquaculture* 404, 28-34.
- Smith, D. et al., 1996. Predation of epipelagic diatoms by the amphipod *Corophium volutator* and the polychaete *Nereis diversicolor*. *Mar Ecol Prog Ser* 145, 53-61.
- Soetaert, K. & Van Oevelen, D., 2009. Modeling food web interactions in benthic deep sea ecosystems: a practical guide. *Oceanography* 22(1), 128-143.
- Solan, M. et al., 2003. Towards a greater understanding of pattern, scale and process in marine benthic systems: a picture is worth a thousand worms. *J. Exp. Mar. Biol. Ecol.* 285, 313-338.
- Spilmont, N. et al., 2007. Short-term variability of intertidal benthic community production during emersion and the implication in annual budget calculation. *Mar. Ecol. Prog. Ser.* 333, 95-101.
- Spilmont, N. et al., 2011. There's more to the picture than meets the eye: sampling microphytobenthos in a heterogeneous environment. *Estuar. Coast. Shelf Sci.* 95 (4), 470-476. <http://dx.doi.org/10.1016/j.ecss.2011.10.021>.
- Stock, B.C. & Semmens, B. X., 2013. MixSIAR GUI User Manual. Version 3.1.
- Stratmann, T., 2018. Benthic ecosystem response to polymetallic nodule extraction in the deep sea. PhD-Thesis. Ghent University
- Suggett, D.J. et al., 2004. Evaluation of biophysical and optical determinations of light absorption by photosystem II in phytoplankton. *Limnol. Oceanogr. Methods* 2, 316-332.
- Sundbäck, K. et al., 2000. Nitrogen fluxes, denitrification and the role of microphytobenthos in microtidal shallow-water sediments: an annual study. *Mar. Ecol. Prog. Ser.* 200, 59-76.
- Sutherland, T. F., J. et al., 1998. The effect of carbohydrate production by the diatom *Nitzschia curvilineata* on the erodibility of sediment. *Limnol. Oceanogr.* 43, 65-72.
- Thompson, R. C. et al., 2004. Physical stress and biological control regulate the producer-consumer balance in intertidal biofilms. *Ecology* 85 (5), 1372-82.

Bibliography

- Thornton, D. C. O. et al., 2002. Factors affecting microphytobenthic biomass, species composition and production in the Colne Estuary (UK). *Aquat. Microb. Ecol.* 27, 285-300.
- Thrush, S.F. et al., 1996. Scale-dependent recolonization: The role of sediment stability in a dynamic sandflat habitat. *Ecology* 77, 2472-2487.
- Thrush, S.F. et al., 2003. Habitat change in estuaries: predicting broad-scale responses of intertidal macrofauna to sediment mud content. *Mar Ecol Prog Ser* 263, 101-112.
- Thrush, S. F. et al., 2005. Multi-scale analysis of species-environment relationships. *Mar. Ecol. Prog. Ser.* 302, 13-26.
- Thrush, S. F. et al., 2012. Interaction networks in coastal soft-sediments highlight the potential for change in ecological resilience. *Ecol Appl* 22, 1213-1223. <http://dx.doi.org/10.1890/11-1403.1>
- Thrush, S. F. et al., 2013. The many uses and values of estuarine ecosystems., p. 226-237. *In* J. Dymond [ed.], *Ecosystem services in New Zealand - Conditions and trends*. Manaaki Whenua Press.
- Ubertini, M. et al., 2012. Spatial variability of benthic-pelagic coupling in an estuary ecosystem: consequences for microphytobenthos resuspension phenomenon. *PLoS One* 7, e44155. <http://dx.doi.org/10.1371/journal.pone.0044155>
- Ubertini, M. et al., 2015. Impact of sediment grain-size and biofilm age on epipellic microphytobenthos resuspension. *J. Exp. Mar. Biol. Ecol.* 467, 52-64.
- Underwood, G.J.C., 1994. Seasonal and spatial variation in epipellic diatom assemblages in the Severn estuary. *Diatom Res* 9, 451-472.
- Underwood, G.J.C. & Kromkamp, J., 1999. Primary production by phytoplankton and microphytobenthos in estuaries. *Adv. Ecol. Res.* 29 (29), 93-153. <http://dx.doi.org/10.1016/j.scitotenv.2017.12.184>
- Uthicke, S., 2006. Photosynthetic efficiency and rapid light curves of sediment-biofilms along a water quality gradient in the Great Barrier Reef, Australia. *Mar. Ecol. Prog. Ser.* 322, 61-73.
- Van Colen, C. et al., 2008. Macrobenthic recovery from hypoxia in an estuarine tidal mudflat. *Mar. Ecol. Prog. Ser.* 372, 31-42.
- Van Colen, C. et al., 2009. Settlement of *Macoma balthica* larvae in response to benthic diatom films. *Mar. Biol.* 156 (10), 2161-71.
- Van De Koppel, J. et al., 2001. Do alternate stable states occur in natural ecosystems? Evidence from a tidal flat. *Ecology* 82, 3449-3461.
- Van de Vijssel, R.C. et al., 2020. Estuarine biofilm patterns: Modern analogues for Precambrian self-organization. *Earth Surf Proc Land* 45, 1141-1154.
- Van der Meer, J. et al., 2003. Large spatial variability in lifetime egg production in an intertidal Baltic tellin (*Macoma balthica*) population. *Helgoland Mar Res* 56, 274-278.
- Van den Meersche, K. et al., 2009. Autochthonous and allochthonous contributions to mesozooplankton diet in a tidal river and estuary: Integrating carbon isotope and fatty acid constraints. *Limnol Oceanogr* 54(1), 62-74.
- Van der Wal, D. & Herman, P.M.J., 2007. Regression-based synergy of optical, shortwave infrared and microwave remote sensing for monitoring the grain-size of intertidal sediments. *Remote Sens. Environ.* 111 (1), 89-106.
- Van der Wal, D. et al., 2008. Distribution and dynamics of intertidal macrobenthos predicted from remote sensing: response to microphytobenthos and environment. *Mar. Ecol. Prog. Ser.* 367, 57-72.
- Van der Wal, D. Et al., 2010. Spatial synchrony in intertidal benthic algal biomass in temperate coastal and estuarine ecosystems. *Ecosystems* 13 (2), 338-351. <http://dx.doi.org/10.1007/s10021-010-9322-9>.
- Van der Wal, D. et al., 2010a. Spatial heterogeneity in estuarine mud dynamics. *Ocean Dyn.* 60, 519-533. <http://dx.doi.org/10.1007/s10236-010-0271-9>
- Van der Wal, D. et al., 2017. Hydrodynamic conditioning of diversity and functional traits in subtidal estuarine macrozoobenthic communities. *Est., Coast. and Shelf Sci.* 197, 80-92.
- Van der Wal, D. et al., 2017. Response of intertidal benthic macrofauna to migrating megaripples and hydrodynamics. *Mar. Ecol. Prog. Ser.* 585, 17-30. <http://dx.doi.org/10.3354/meps12374>
- Van der Werf, J. et al., 2015. Modeling the morphodynamics of the mouth of the Scheldt estuary, E-proceedings of the 36th IAHR World Congress, pp. 80-86.
- Van Maren, D. S. et al., 2015. The impact of channel deepening and dredging on estuarine sediment concentration. *Cont Shelf Res* 95, 1-14.
- Van Oevelen, D. et al., 2006. Carbon flows through a benthic food web: integrating biomass, isotope and tracer data. *J. Mar. Res.* 64, 453-482.
- Varela, M. & Penas, E. 1985. Primary Production of Benthic Microalgae in an Intertidal Sand Flat of the Ria-De-Arosa, Nw Spain. *Mar Ecol Prog Ser* 25, 111-119.
- Vieira, S. et al., 2013. Effects of short-term changes in sediment temperature on the photosynthesis of two intertidal microphytobenthos communities. *Estuar. Coast. Shelf Sci.* 119, 112-18.
- Vogt, J. et al., 2014. The importance of conspecific facilitation during recruitment and regeneration: A case study in degraded mangroves. *Basic Appl Ecol* 15 (8), 651-60.
- Volkenborn, N. et al., 2007. Effects of bioturbation and bioirrigation by lugworms (*Arenicola marina*) on physical and chemical sediment properties and implications for intertidal habitat succession. *Estuar Coast Shelf S* 74, 331-343.
- Wang, X.M.W. et al., 2015. Extraction of vegetation information from visible unmanned aerial vehicle images. *Nongye Gongcheng Xuebao/Transactions of the Chinese Society of Agricultural Engineering* 31, 152-159.

Weerman, E.J. et al., 2010. Spatial Self-Organization on Intertidal Mudflats through Biophysical Stress Divergence. *Am Nat* 176, E15-E32.

Weerman, E. J. et al., 2011. Top-down control inhibits spatial self-organization of a patterned landscape. *Ecology* 9, 487-495.
<http://dx.doi.org/10.1890/10-0270.1>

Weerman, E.J. et al., 2011. Macrobenthos abundance and distribution on a spatially patterned intertidal flat. *Mar Ecol Prog Ser* 440, 95-103.

Weerman, E. J. et al., 2012. Changes in diatom patch-size distribution and degradation in a spatially self-organized intertidal mudflat ecosystem. *Ecology* 93, 608-618.
<http://dx.doi.org/10.1890/11-0625.1>

Wetsteyn, L. P. M. J., & Kromkamp, J. C., 1994. Turbidity, Nutrients and Phytoplankton Primary Production in the Oosterschelde (the Netherlands) before, during and after a Large-Scale Coastal Engineering Project (1980-1990). *Hydrobiologia* 283, 61-78.

Whitney, D. & Darley, W., 1983. Effect of light intensity upon salt marsh benthic microalgal photosynthesis. *Mar. Biol.* 75, 249-52.

Wolf, N. et al., 2009. Ten years of experimental animal isotopic ecology. *Funct. Ecol.* 23, 17-26.

Worm, B. et al., 2006. Impacts of biodiversity loss on ocean ecosystem services. *Science*, 314 (5800), 787-90.

Yallop, M.L. et al., 1994. Comparative structure, primary production and biogenic stabilization of cohesive and noncohesive marine-sediments

inhabited by microphytobenthos. *Estuar. Coast. Shelf Sci.* 39 (6), 565-582.
[http://dx.doi.org/10.1016/S0272-7714\(06\)80010-7](http://dx.doi.org/10.1016/S0272-7714(06)80010-7).

Yallop, M. L. et al., 2000. Interrelationships between rates of microbial production, exopolymer production, microbial biomass, and sediment stability in biofilms of intertidal sediments. *Microb Ecol* 39, 116-127.

Yamaguchi, H. et al., 2007. Dynamics of microphytobenthic biomass in a coastal area of western Seto Inland Sea, Japan. *Estuar. Coast. Shelf Sci.* 75, 423-432.

Yokoyama, H. & Ishihi, Y., 2003. Feeding of the bivalve *Theora lubrica* on benthic microalgae: isotopic evidence. *Mar. Ecol. Prog. Ser.* 255, 303-309.

Ysebaert, T. & Herman, P. M. J., 2002. Spatial and temporal variation in macrofauna and relationships with environmental variables in an estuarine, intertidal soft-sediment environment. *Mar. Ecol. Prog. Ser.* 244, 105-124.

Ysebaert, T. et al., 2002. Macrobenthic species response surfaces along estuarine gradients: prediction by logistic regression. *Mar. Ecol. Prog. Ser.* 225, 79-95.

Ysebaert, T. et al., 2003. Large-scale spatial patterns in estuaries: estuarine macrobenthic communities in the Schelde estuary, NW Europe. *Estuar. Coast. Shelf. Sci.* 57, 335-55.

Zajac, R.N., R.B. Whitlatch and S.F. Thrush (1998). Recruitment, Colonization and Physical-Chemical Forcing in Marine Biological Systems. *Hydrobiologia* 375/376: 227-240.

Bibliography

Summary

Estuaries are semi-enclosed coastal water bodies situated where rivers flow into seas or oceans. Depending on local environmental factors such as tides, waves and fluvial processes, sediment may accrete and form sand and mud flats that emerge during low tide. The sediment of these mud and sand flats contains an enormous diversity of microalgae and cyanobacteria, which form the so called 'microphytobenthos' (MPB). MPB constitute an important food source for benthic macrofauna, such as worms and shellfish, which are in turn eaten by (flat)fish and waders.

To assess impacts of anthropogenic stressors and to sustainably manage intertidal systems, it is necessary to better understand the functional and structuring role of MPB in the intertidal ecosystem at the estuary level.

This thesis aimed to quantify the functional and structuring role of MPB on estuarine tidal flats in the estuarine ecosystem. A generic method was developed to retrieve MPB primary production rates from a combination of remotely sensed information, that allows the assessment of MPB on the estuary scale, ambient temperature measurements, field measurements of photosynthetic parameters and a tide model (Chapter 2). Furthermore, spatio-temporal variability in MPB biomass was studied in relation to tidal flat type, salinity and ecotopes using remotely sensed information (Chapter 5). The importance of MPB in the diet of macrofauna was compared to other available food sources and it was investigated how the diet composition of macrofauna may vary spatially, i.e. as function of elevation and estuary. In addition, the extent to which spatial variation in MPB production in spring may be used as proxy for macrofaunal grazing in summer/ autumn was tested (Chapter 3). The effect of macrofaunal presence on the total biomass and spatial variability of MPB was studied under varying hydrodynamic conditions (Chapter 4).

Remote sensing of MPB and sediment characteristics

In this thesis, passive optical satellite remote sensing was used to quantify sediment grain size (mud content), MPB biomass and production in the top layer of the sediment of estuarine intertidal flats. In passive optical remote sensing, images are made from radiation of the visible, near-infrared and short-wave infrared electromagnetic wavelengths that is reflected and emitted from the earth's surface and atmosphere. Materials may reflect and absorb radiation at specific wavelengths and may, therefore, be distinguished by their spectral reflectance signatures. The quality of images depends on the availability of solar irradiation and cloud presence, among other factors. In this

thesis, the suitability of the Landsat 8 OLI multispectral sensor to quantify the mud content and total MPB biomass in the upper 2 mm of the sediment was tested. MPB biomass (expressed as chl-*a* concentration) was predicted from the Normalized Differential Vegetation Index (NDVI), which is based on reflectance in the red band (absorbed by photosynthesizing organisms, including MPB) and infrared band. A regression model was used where sampled chl-*a* concentrations were regressed against a field radiometer-derived NDVI. A satellite-based (Landsat 8 OLI) regression model that included reflectance in the blue and near-infrared wavelengths was used to predict the mud content of the sediment (Chapter 2). The multispectral sensor Sentinel-2 MSI was used to compare meso-scale MPB patch sizes and degree of patchiness among seasons, salinity zones, tidal flat types and ecotopes using the NDVI (Chapter 5). It was demonstrated that MPB patch size (range derived from a semi-variogram) remains constant throughout the year, while the degree of patchiness (sill derived from a semi-variogram) increases from winter to summer. The MPB patch size and degree of patchiness was higher on relatively sandy mid-channel tidal flats than on the relatively silt rich fringing tidal flats.

Microphytobenthos as food source and ecosystem engineer

The development of techniques to spatially estimate the quantity of MPB can support the assessment of MPB availability as food source for higher trophic levels. It was demonstrated in this thesis that MPB primary production can accurately be quantified using remotely sensed information (Landsat 8 OLI satellite images) of MPB biomass and mud content. In addition, ambient temperature measurements, which are used as indicator for the photosynthetic capacity, and a tide model are required (Chapter 2). Modelled primary production rates ($\text{mg C m}^{-2} \text{ h}^{-1}$) matched well with an independent dataset of fluorometry-based primary production rates measured *in situ* (Oosterschelde: RMSE = 66.8; Westerschelde: RMSE = 89.8). A sensitivity analysis showed that emersion duration and the mud content were most important in determining variability in MPB primary production. The developed method can be applied to other estuaries, after calibration at the site of interest.

The importance of MPB in the diet of benthic macrofauna was confirmed in this thesis in two tidal systems in the Netherlands with contrasting salinities and macrofaunal communities (Chapter 3). Therefore, it is concluded that MPB on intertidal flats are an essential part of the temperate estuarine food web. We showed that the importance of MPB in the diet of macrofauna may somewhat differ between estuaries, which was the case for the mud snail *Peringia*, the sand digger shrimp *Bathyporeia* sp. and the Baltic tellin (*Limecola balthica*) (Chapter 3). This may be associated with the composition of deposited organic material or the availability of phytoplankton in the water column in an estuary.

The diet composition of macrofauna did not vary as function of elevation. Turnover rates of MPB are generally high, which may partly be explained by 1) high resuspension rates into the water column and 2) macrofaunal grazing which was in the same order of magnitude as MPB production (Chapter 3).

MPB also act as ecosystem engineer by reducing the erodibility of the sediment. Earlier studies showed that benthic diatoms, which often dominate MPB communities in temperate systems, produce extracellular polymeric substances that 'glue' the sediment together, resulting in less removal of silt and clay particles. In addition, hydrodynamically calm conditions, limiting resuspension, may be favourable for MPB growth. Thus, fine, silt rich sediment often contain higher MPB concentrations than sandy sediments. In this thesis, it was observed that the location of MPB patches varies among seasons, which suggests that food availability for higher trophic levels may vary spatially over time (Chapter 5). Visually, the observed seasonality in spatial variation of MPB appeared closely related to seasonal changes in the silt content of the studied intertidal flats.

Areas with a similar MPB biomass ('patches') occupy smaller surfaces in the presence of macrofauna than in sediments where macrofauna was experimentally removed (Chapter 4). This indicates that macrofauna may not only increase the erodibility of the sediment by bioturbation, but may also prevent the formation of continuous biofilms that increase the stability of the sediment.

The structuring role of microphytobenthos for the macrofaunal community

We investigated to what extent the spatial distribution of MPB production is indicative for the distribution of macrofauna that graze on MPB. As MPB biomass is the net result of MPB production and loss processes such as grazing and resuspension into the water column, MPB production may be a better indicator for food availability than MPB biomass. We tested whether MPB production in early spring, when macrofaunal biomass is still relatively low and spatial variability in MPB production is assumed to be mainly determined by abiotic parameters, can be used as proxy for macrofaunal grazing pressure on MPB in summer/autumn. No relationship between MPB production and grazing of the total macrofaunal community or surface deposit feeders was found (Chapter 3). As the location of MPB patches varied from winter to summer (Chapter 5), MPB production in summer/ autumn may be a better indicator for macrofaunal grazing. A defaunation experiment showed that macrofauna do not lower the MPB biomass standing stock (Chapter 4), which supports the use of remotely sensed information to quantify spatial variation in MPB food availability for higher trophic levels.

Management implications

Optical satellite remote sensing provides the opportunity to monitor MPB biomass and production on the estuary scale and to detect long term trends as consequence of anthropogenic stressors. Our MPB primary production model based on MPB biomass and mud content derived from satellite remote sensing, ambient temperature measurements and a tide model can be used as a tool to evaluate the effects of, e.g., a decrease in emersion duration and tidal flat area on MPB production (Chapter 2). The model may, for example, be included in predictive models of macrofaunal distributions. The spatio-temporal information on MPB biomass and production may also be included in food web models, which may support management of estuarine ecosystems. Our work confirms the essential role of MPB living in intertidal areas in the estuarine food web, which underlines the urgent need to preserve these intertidal flats.

Samenvatting

Estuaria zijn semi-ingesloten kustwaterlichamen die zich bevinden op locaties waar rivieren de zeeën of oceanen in stromen. Afhankelijk van omgevingsfactoren zoals getijden, golven en fluviale processen, kan sediment er aanslibben en platen en slikken vormen die droogvallen tijdens laagtij. Het sediment van deze platen en slikken bevatten een enorme diversiteit aan microalgen en cyanobacteriën, die het zogenaamde 'microfytobenthos' (MPB) vormen. MPB vormen een belangrijke voedselbron voor benthische macrofauna zoals wormen en schelpdieren, die op hun beurt gegeten worden door (plat)vissen en steltlopers.

Om de gevolgen van antropogene stressoren vast te stellen en om intergetijdesystemen duurzaam te beheren is het nodig om de functionele en structurerende rol van MPB in het intergetijdesysteem beter te begrijpen op estuariumniveau.

Dit proefschrift had als doel om the functionele en structurerende rol van MPB op estuariene platen en slikken in het estuariene ecosysteem te kwantificeren. Een generieke methode is ontwikkeld om de primaire productie van MPB te bepalen uit een combinatie van satellietbeelden, waarmee MPB op de estuariumschaal waargenomen kan worden, metingen van de omgevingstemperatuur, veldmetingen van de fotosynthesecapaciteit en een getijdemodel (Hoofdstuk 2).

Verder is de spatio-temporele variabiliteit in de biomassa van MPB bestudeerd in relatie tot het type intergetijdeplaat, het zoutgehalte en het ecotoop met behulp van satellietbeelden (Hoofdstuk 5). Het aandeel van MPB in het dieet van macrofauna is vergeleken met het aandeel van andere beschikbare voedselbronnen, en er werd onderzocht hoe de dieetsamenstelling van macrofauna ruimtelijk kan variëren, d.w.z. als functie van hoogte en estuarium. Daarnaast is onderzocht in hoeverre de ruimtelijke variatie in de productie van MPB in het voorjaar kan worden gebruikt als proxy voor begrazing door macrofauna in de zomer/herfst (Hoofdstuk 3). Het effect van de aanwezigheid van macrofauna op de totale biomassa en ruimtelijke variabiliteit van MPB werd onderzocht onder variërende hydrodynamische condities (Hoofdstuk 4).

Remote sensing van MPB en sedimentkarakteristieken

In dit proefschrift zijn passieve optische satellietsensoren gebruikt om de korrelgrootte van het sediment (i.e. het slibgehalte), biomassa en primaire productie van MPB in de toplaag van het sediment van estuariene

intergetijdeplaten te kwantificeren. Bij passieve optische remote sensing worden beelden gemaakt van straling afkomstig van zichtbare, nabij-infrarode en kortgolvig infrarode elektromagnetische golflengten, dat wordt gereflecteerd en uitgestraald vanuit het aardoppervlak en de atmosfeer. Materialen kunnen straling van specifieke golflengten reflecteren en absorberen en kunnen daarom onderscheiden worden aan de hand van hun spectrale signaturen. De kwaliteit van beelden hangt onder andere af van de hoeveelheid instraling van zonlicht en de aanwezigheid van bewolking. In dit proefschrift is getest of de multispectrale sensor Landsat 8 OLI geschikt is om het slibgehalte en de totale biomassa van MPB in de bovenste 2 mm van het sediment te kwantificeren. De biomassa van MPB (uitgedrukt als concentratie chl-*a*) is voorspeld aan de hand van de *Normalized Difference Vegetation Index* (NDVI), welke is gebaseerd op reflectie in de rode band (geabsorbeerd door fotosynthetiserende organismen, inclusief MPB) en infrarode band. Hiervoor is een regressiemodel gebruikt waarbij bemonsterde chl-*a* concentraties in sediment afhangen van de NDVI die bepaald is met een veldradiometer. Een regressiemodel gebaseerd op de blauwe en nabij-infrarode banden van Landsat 8 OLI is gebruikt om het slibgehalte van het sediment te voorspellen (Hoofdstuk 2). De multispectrale sensor Sentinel-2 MSI is gebruikt om met behulp van de NDVI de grootte van *patches* MPB en mate van fragmentatie van *patches* op de mesoschaal te vergelijken tussen seizoenen, mengzones met verschillende zoutgehalten, typen intergetijdeplaten en ecotopen (Hoofdstuk 5). Hieruit blijkt dat de grootte van *patches* (de *range* afgeleid van een semi-variogram) constant blijft van de winter tot aan de zomer, terwijl de mate van fragmentatie van *patches* (de *sill* afgeleid van een semi-variogram) toeneemt. De grootte van *patches* en fragmentatie van *patches* was hoger op relatief zanderige intergetijdeplaten dan op de relatief slibrijke slikken.

Microfytobenthos als voedselbron en biobouwer

De ontwikkeling van technieken om de hoeveelheid MPB ruimtelijk te schatten kan het vaststellen van de beschikbaarheid van MPB als voedselbron voor hogere trofische niveaus ondersteunen. In dit proefschrift is aangetoond dat de primaire productie van MPB nauwkeurig gekwantificeerd kan worden met behulp van remote sensing informatie (satellietbeelden afkomstig van Landsat 8 OLI) van de biomassa van MPB en het slibgehalte. Daarnaast zijn metingen van de omgevingstemperatuur, die gebruikt zijn als indicator voor de fotosynthesecapaciteit, en een getijdemodel vereist (Hoofdstuk 2). De gemodelleerde primaire productiesnelheden ($\text{mg C m}^{-2} \text{ u}^{-1}$) kwamen goed overeen met een onafhankelijke dataset van *in situ* met een fluorometer gemeten primaire productiesnelheden (Oosterschelde: RMSE = 66.8; Westerschelde: RMSE = 89.8). Een gevoeligheidsanalyse liet zien dat de droogvalduur en het slibgehalte de belangrijkste factoren waren in het bepalen van de aanwezige variabiliteit in primaire productie van MPB. De

ontwikkelde methode kan toegepast worden in andere estuaria na kalibratie in het betreffende estuarium.

Het grote aandeel van MPB in het dieet van benthische macrofauna werd bevestigd in dit proefschrift in twee intergetijdesystemen met contrasterende zoutgehalten en macrofaunagemeenschappen in Nederland (Hoofdstuk 3). Daarom wordt geconcludeerd dat MPB op intergetijdeplaten een essentieel onderdeel uitmaken van het estuariene voedselweb in een gematigd klimaat. We hebben aangetoond dat het aandeel van MPB in het dieet van macrofauna enigszins kan verschillen tussen estuaria, wat het geval was bij de wadslak *Peringia*, de vlokreeft *Bathyporeia* sp. en het nonnetje (*Limecola balthica*) (Hoofdstuk 3). Dit kan samenhangen met de samenstelling van het bezonken organisch materiaal of de beschikbaarheid van fytoplankton in de waterkolom in een estuarium. De dieetsamenstelling van het macrofauna varieerde niet als functie van de hoogte van de platen. De omzettingssnelheden van MPB zijn over het algemeen hoog, wat deels verklaard kan worden door 1) hoge resuspensiesnelheden naar de waterkolom en 2) begrazing door macrofauna wat in dezelfde orde van grootte was als de primaire productie van MPB (Hoofdstuk 3).

MPB functioneren ook als biobouwers doordat ze de erodeerbaarheid van het sediment kunnen reduceren. Eerder studies tonen aan dat benthische diatomeeën, die vaak MPB gemeenschappen domineren in estuaria in een gematigd klimaat, extracellulaire polymeren produceren die het sediment als het ware 'vastlijmen', wat erosie van klei- en slibdeeltjes tegengaat. Ook kunnen hydrodynamisch kalme condities, waarbij resuspensie gelimiteerd wordt, gunstig zijn voor de groei van MPB. Daarom bevat slibrijk sediment vaak hogere concentraties MPB dan zanderig sediment. In dit proefschrift is geobserveerd dat de locaties van *patches* van MPB variëren met de seizoenen, wat suggereert dat de voedselbeschikbaarheid voor hogere trofische niveaus in de loop der tijd ruimtelijk kan variëren (Hoofdstuk 5). Visuele observaties lieten zien dat de seizoenaliteit in ruimtelijke variatie van MPB sterk gerelateerd lijkt te zijn aan seizoenale veranderingen in het slibgehalte van de bestudeerde intergetijdeplaten.

Gebieden met een vergelijkbare biomassa aan MPB ('*patches*') beslaan kleinere oppervlaktes in de aanwezigheid van macrofauna dan in sedimenten waar macrofauna experimenteel verwijderd was (Hoofdstuk 4). Dit duidt erop dat macrofauna niet alleen de erodeerbaarheid van het sediment kunnen verhogen, maar dat ze ook de vorming van continue biofilms die de stabiliteit van het sediment verhogen verhinderen.

De structurerende rol van microfytobenthos voor macrofaunagemeenschappen

In dit proefschrift is onderzocht in hoeverre de ruimtelijke variatie in primaire productie van MPB indicatief is voor de ruimtelijke verdeling van begrazing door macrofauna op MPB. Aangezien de biomassa van MPB het netto resultaat is van primaire productie van MPB en verliesprocessen zoals begrazing en resuspensie naar de waterkolom, zou productie van MPB een betere indicator voor voedselbeschikbaarheid kunnen zijn dan de biomassa van MPB. We hebben getest of de productie van MPB in de vroege lente, wanneer de biomassa van het macrofauna nog relatief laag is en aangenomen wordt dat de ruimtelijke variatie in productie van MPB met name wordt bepaald door abiotische factoren, gebruikt kan worden als proxy voor de graasdruk van macrofauna op het MPB in de zomer/herfst. Er werd geen relatie gevonden tussen de productie van MPB en de graasdruk van de totale macrofaunagemeenschap of de graasdruk van oppervlakte *deposit feeders* (Hoofdstuk 3). Aangezien de locaties van *patches* van MPB varieerden van de winter tot de zomer (Hoofdstuk 5), zou de productie van MPB in de zomer/herfst een betere proxy kunnen zijn voor de graasdruk van macrofauna op MPB. Een defaunatie-experiment heeft aangetoond dat macrofauna de staande voorraad aan biomassa van MPB niet verlaagt (Hoofdstuk 4), wat het gebruik remote sensing informatie om ruimtelijke variatie in de beschikbaarheid van MPB als voedselbron voor hogere trofische niveaus te kwantificeren ondersteunt.

Management implicaties

Optische satelliet remote sensingtechnieken bieden de mogelijkheid om de biomassa en primaire productie van MPB te monitoren op de schaal van een estuarium en om trends op de lange termijn als gevolg van antropogene stressoren te detecteren. Ons MPB primaire productiemodel, wat gebaseerd is op satellietinformatie over de biomassa van MPB en het slibgehalte, metingen van de omgevingstemperatuur en een getijdemodel, kan als tool gebruikt worden om de effecten van bijvoorbeeld een afname in droogvalduur en oppervlakte van intergetijdeplaten op de productie van MPB te evalueren (Hoofdstuk 2). Het model kan bijvoorbeeld ook gebruikt worden in voorspellende modellen van de ruimtelijke verdeling van macrofauna. De spatio-temporele informatie over de biomassa en productie van MPB kan ook geïncorporeerd worden in voedselwebmodellen, wat het beheer van estuariene ecosystemen kan ondersteunen. Het huidige werk bevestigt de essentiële rol van MPB op intergetijdeplaten in het estuariene voedselweb, wat de dringende noodzaak onderstreept om deze intergetijdeplaten te behouden.

Curriculum Vitae

The author

Tisja Dagers was born on the 13th of June 1990 in Leersum, The Netherlands. Although she always had a very broad interest, a fascination for coasts already started in primary school by writing an essay on different types of coasts and what types of flora and fauna may be found there. She attended the 'Stedelijk Gymnasium' in Nijmegen, The Netherlands, from 2002 to 2008 and studied Biology at Utrecht University, The Netherlands, from 2008-2011, which included courses in marine sciences and ecology. She wrote her bachelor thesis at the Environmental Change Research Centre of University College London, United Kingdom, on the potential impacts of climate change on lake ecosystems. She holds a joint Msc degree in Sustainable Development (2011-2013) from Utrecht University and Ca' Foscari University of Venice, Italy, with a specialization in integrated coastal zone management. The master program included ecological modelling and marine ecology courses, which she partly followed in the beautiful Venice lagoon. Her major thesis was titled 'Validation of a marine primary production model using in situ measurements: First steps towards recalibration of the ecological model GEM' and sparked her interest in interactions between abiotic and biotic processes that act on the macro scale. Between 2013 and 2018, she carried out her PhD research at NIOZ Yerseke (The Netherlands) on quantification of the role of microphytobenthos in intertidal ecosystems using optical remote sensing. During this period, she gained experience with spatial analyses of satellite and drone imagery, working with Arcmap and programming languages such as R and Matlab, and performing field experiments and lab work. Afterwards, she started working as soil and remote sensing advisor and, from 2020 onwards, as data ecologist at the engineering consultancy firm TAUW.

Publications

- Dagers, T.D.; Van Oevelen, D.; Herman, P.M.J.; Boschker, H.T.S.; Van der Wal, D. (2020), Spatial variability in macrofaunal diet composition and grazing pressure on microphytobenthos in intertidal areas. *Limnology and Oceanology* 65: 2819-2834.

Curriculum Vitae

- Daggery, T.D.; Herman, P.M.J.; Van der Wal, D. (2020), Seasonal and spatial variability in patchiness of microphytobenthos on intertidal flats from Sentinel-2 satellite imagery. *Frontiers in Marine Science* 7: 392.
- Daggery, T.D.; Kromkamp, J.C.; Herman, P.M.J.; van der Wal, D. (2018). A model to assess microphytobenthic primary production in tidal systems using satellite remote sensing. *Remote Sens. Environ.* 211: 129-145.
- Daggery, T.D.; Kromkamp, J.C.; Herman, P.M.J.; van der Wal, D. (2019). Corrigendum to "A model to assess microphytobenthic primary production in tidal systems using satellite remote sensing" [Remote Sens. Environ. 211 (2018) 129–145]. *Remote Sens. Environ.* 230: 111206.
- Zhu, Q.; Van Prooijen, B.C.; Maan, D.C.; Wang, Z.B.; Yao, P.; Daggery, T.; Yang, S.L. (2019). The heterogeneity of mudflat erodibility. *Geomorphology (Amst.)* 345: 106834.

Courses

- NCK Summer School Estuarine and Coastal Processes in relation to Coastal Zone Management, Texel, The Netherlands, 2015
- Adobe Illustrator Beginners, NIOZ, The Netherlands, 2015
- Adobe Illustrator Level 2, NIOZ, The Netherlands, 2015
- Photoshop beginners, NIOZ, The Netherlands, 2015
- How to write a scientific paper, NIOZ, The Netherlands, 2014
- Introduction to R for statistical analysis, Wageningen, The Netherlands, 2014
- Spatial Ecology, Wageningen, The Netherlands, 2014
- Hand-on GIS for Earth Scientists, Utrecht, The Netherlands, 2014

Teaching and supervision

- BSc thesis Lenneke Ruissen, Utrecht University, The Netherlands, 2016
Thesis: Invloed van macrozoobenthos op biomassa en patroonvorming van microphytobenthos.
- MBO traineeship Joeri Minderhoud, Scalda Vlissingen, The Netherlands, 2016
Analyses of chlorophyll-a content and grain size distribution of sediment samples.
- MSc thesis Joost Hamoen, Wageningen University, The Netherlands, 2015
Thesis: Spatial variability of macrobenthic grazing pressure on microphytobenthos in intertidal areas.
- Co-supervision of case study: bioturbation and primary productivity of microalgae, NCK Summer School Estuarine and Coastal Processes in relation to Coastal Zone Management, Texel, 2017
- Co-supervision of case study "Using stable isotopes to unravel the Wadden Sea foodweb" at NIOZ Marine Masters's Summer Course, Texel, 2017

Presentations

- Oral presentation at NAEM 2016: "A model to assess benthic primary production in intertidal ecosystems at the macro scale", Netherlands Annual Ecology Meeting, Congrescentrum De Werelt, Lunteren
- Oral presentation at NCK days 2016, "A model to assess benthic primary production in intertidal ecosystems at the macro scale", Ouddorp
- Oral presentation Vergunningshoudersdag 2016 "Kiezelwieren als indicator voor de structuur van het ecosystem op platen en slikken", on Outreach/information day for estuarine managers, NIOZ, Yerseke
- Poster presentation at NAEM, 2014, Netherlands Annual Ecology Meeting, Lunteren
- Poster presentation at NCK Days 2014, UNESCO-IHE, Delft

Curriculum Vitae

- Poster presentation at NAEM 2015: Netherlands Annual Ecology Meeting, Lunteren
- Poster presentation Earth Observation for Science and Society Symposium 2015, NSO, The Hague
- Poster presentation at NAEM days, 2017, Netherlands Annual Ecology Meeting, Lunteren, 2017
- Poster presentation "A model to assess microphytobenthic primary production in tidal systems using satellite remote sensing" for SEP, 2017, NIOZ, Yerseke

Organisational activities

- Co-organizer of symposium "Yerseke Young Scientist Day", 2016
- Convener of the session "Spatial ecology: connectivity and functioning" at the NAEM Netherlands Annual Ecology Meeting, Lunteren, 2016